Loughborough University

This item was submitted to Loughborough University as a PhD thesis by the author and is made available in the Institutional Repository (https://dspace.lboro.ac.uk/) under the following Creative Commons Licence conditions.

creative commons

COMMONS DEED

Attribution-NonCommercial-NoDerivs 2.5

You are free:

- to copy, distribute, display, and perform the work

Under the following conditions:

Attribution. You must attribute the work in the manner specified by the author or licensor.

Noncommercial. You may not use this work for commercial purposes.

No Derivative Works. You may not alter, transform, or build upon this work.

- For any reuse or distribution, you must make clear to others the license terms of this work.
- Any of these conditions can be waived if you get permission from the copyright holder.

Your fair use and other rights are in no way affected by the above.

This is a human-readable summary of the Legal Code (the full license).

Disclaimer

For the full text of this licence, please go to:
http://creativecommons.org/licenses/by-nc-nd/2.5/

Loughborough University

Pilkington Library

Author/Filing Title . .....LEE.....

....

Vol No ..... . Class Mark .. T . . ..

Please note that fines are charged on ALL overdue items.

FOR REFERENCE ONLY

0402806298

Viscoelastic Behaviour of Poly(methyl methacrylate) and Polystyrene

by

Siaw Foon Lee

A Doctoral Thesis

Submitted in partial fulfilment of the requirements for the award of degree of Doctor of Philosophy of Loughborough University

October, 2002

© by Siaw Foon Lee (2002)

Supervisor: Dr G M Swallowe
Department of Physics

Loughborough University
P[illegible]brary
Date Sept 03
Class
Acc No. 04028062 9

献给：

伟大的母亲，感谢您多年来的教导，让我完成这最高阶层的教育。

Acknowledgement

I would like to thank the Department of Physics, Loughborough University for the studentship.

I would like to express my sincere gratitude to my supervisor, Dr Gerry M Swallowe, for his help, comment, patience and giving me an opportunity to do my PhD here in Loughborough University.

I thank Dr D J Parry and Prof. D C Emmony for the discussions Thanks are also due to Mr R Pancholi, Mr John Oaklay, Mr Brian Dennis, Mr Derek Hemsley (from IPTME) and Mr R. P. Owens (from IPTME) for their technical help and advice Thanks must go to the secretarial staffs and all the people I know in the Department of Physics and Mathematics.

The company of CF for the last three years, encouragement from H S Dhillon and C Srıcheewin will never be forgotten

Lastly, warmest thanks to my family members for their support and to my special little friend, Carlos F Sanz-navarro for his endless care.

Siaw Foon Lee
October 2002

ABSTRACT

Poly(methyl methacrylate) (PMMA) and polystyrene (PS), which are fully amorphous polymers, have been extensively studied for over a decade to discover how their mechanical behaviours vary with temperatures and strain rates. In this study, Mechanical tests were carried out at a range of strain rates and temperatures using a Hounsfield H50KM Test Machine which provides quasi- static rates ($10^{-4} \sim 10^{-3}$ s^{-1}) and low strain rates ($10^{-2} \sim 10^{-1}$ s^{-1}), and an in-house built Dropweight Machine which provides high strain rates ($10^{2} \sim 10^{3}$ s^{-1}) Mechanical tests were also performed in a high-speed photographic system, which provides high strain rates (10^{3} s^{-1}), to visualise the deformation of the polymers at a range of temperatures. An aluminium-heating block was built to heat up the samples to the required temperature. Strain limited tests were carried out at a range of strain rates and temperatures. Differential Scanning Calorimetry (DSC) was employed to study the glass transition temperatures and the specific heats of the samples. Dynamic Mechanical Thermal Analysis (DMTA) was adopted to study the transitions in the samples and the change of moduli with temperature Densities of samples before and after high strain rate compression at certain strain were measured using a Six Column Density Apparatus The polarising microscope was used to study the orientation of the polymer chains at a range of temperatures, strains and strain rates. Eyring's theory of viscous flow was applied on yield point, 20% and 30% strain to relate the activation energy and volume with strain rate and temperature from the thermodynamic perspective. Temperature rise was calculated for high strain rate data to fit into the isothermal curve for the application of Eyring's theory and to obtain the actual sample temperature at which the deformation took place. PMMA and PS showed ductile behaviour when tested at quasi-static and low strain rates at temperatures below their ductile-brittle transition temperatures. The densities of samples were not found to increase at different strains. The orientations of polymer chains did not influence the increase at yield stress at high strain rates. The interpretation of activation energy and volume provided information of how the flows of chains took place at different temperatures and strain rates.

Table of Content

Chapter 1 Introduction to the Study of Polymer Viscoelasticity

1.1 Introduction 1

1.2 Amorphous and Semicrystalline Polymer 1

1 3 Effect of Temperature 3

1.4 Effect of Strain Rate 4

1.5 Investigation into the Increase of Flow Stress 5

1.6 The Objectives and the Layout of the Thesis 7

References 8

Chapter 2 Theory

2.1 The characteristics of Poly(methyl methacrylate) (PMMA) and Polystyrene (PS) 10

2.2 Types of Stress-Strain Curves 12

2.3 The Elastic, Yield and Plastic Behaviour of Glassy Polymers 13

2.4 Stress, Strain and Strain Rate 15

References 18

Chapter 3 Mechanical Tests

3.1 Introduction 20

3.2 Hounsfield H50KM Test Machine

3.2.1 Introduction 21

3.2.2 Data Recording Methods 22

3.2 3 Measurement of Sample Displacement 23

3.2.4 Calibration of the Displacement Transducer 24

3.2.5 Low Pass Filter Circuit 25

3.2.6 Data Acquisition 26

3.3 Dropweight Machine

3.3.1 Introduction 27

3.3.2 Stress and Strain Analysis 28

3.3.3 Calibration of Strain Gauge 30

3.3.4 Data Acquisition 31

3.4 Experimental
3.4.1 Elevated Temperature Tests 31
3.4 2 Strain Limited Tests 32
3.5 Data Analysis 33
3.6 Results 34
3.7 Discussion 34
3.8 Conclusion 37
Appendix 3.1 38
Appendix 3 2 39
Appendix 3 3 40
References 41

Chapter 4 High-Speed Photography

4.1 Introduction 43
4 2 High-speed Photographic System
4.2.1 A.W.R.E. C4 Camera 44
4.2.2 C4-Camera Dropweight 45
4 2.3 Transient Light Source Generated System 47
4 3 Synchronisation of the Flash and the Camera Speed 48
4.4 Accelerometer
4.4.1 The Operation of the Accelerometer 48
4 4.2 Physical Dimensions 49
4.4.3 Temperature Effect 50
4 5 Conditioning Amplifier 50
4.6 Data Recording and Filtering 50
4.7 Film Processing 51
4.8 Stress and Strain Analysis 51
4.9 Experimental Procedure 53
4 10 Results and Discussion 53
4 11 Conclusion 55
References 56

Chapter 5 Thermal Analysis

5.1 Introduction 58

5.2 Differential Scanning Calorimetry (DSC)

5.2.1 Theory 58

5.2.2 Thermal Measuring System 59

5.2.3 Experimental Method 60

5.3 Dynamic Mechanical Thermal Analysis (DMTA)

5.3.1 Theory 60

5.3.2 Experimental Method 61

5 4 Results and Discussion

5.4.1 Differential Scanning Calorimetry 62

5.4.2 Dynamic Mechanical Thermal Analysis 63

5.5 Conclusion 64

References 65

Chapter 6 Density Measurement

6.1 Introduction 66

6.2 The Accuracy of Density Measurement 66

6 3 Preparation of Solution 67

6 4 Preparation of the Density Gradient Column 67

6.5 Experimental Procedures 68

6 6 Result and Discussion 69

6.7 Conclusion 70

Appendix 6 1 71

Appendix 6.2 72

References 73

Chapter 7 Optical Birefringence

7.1 Introduction 74

7.2 Polarising Microscope and Compensator 74

7.3 The Orientation of the Polymer Chains – Isotropic, Uniaxial and Biaxial Indicatrix 75

7.4 Measurement of Birefringence 78

7.5 Experimental 78
7 6 Results and Discussion 79
7.7 Conclusion 82
References 83

Chapter 8 Application of Eyring's Theory

8.1 Introduction 84
8.2 Eyring's Model of Viscous Flow 85
8.3 Ree-Eyring's Model of Viscous Flow 87
8.4 Analysis on $\frac{\sigma}{T}$ versus Ln($\dot{\varepsilon}$) 89
8 5 Activation Energy and Activation Volume 91
8.6 Application of Eyring's Theory to Experimental Data 93
8.7 High Strain Rate Analysis 95
8.8 Results and Discussion
8.8.1 Poly(methyl methacrylate) 96
8.8 2 High Strain Rate Analysis on Poly(methyl methacrylate) 98
8.8.3 Polystyrene 98
8.9 Conclusion 99
Appendix 8.1 100
References 101

Chapter 9 Discussion, Conclusion and Suggestion for Future Work

9.1 Discussion
9.1.1 Introduction 103
9.1.2 Low Strain Rate Test 104
9.1.3 High Strain Rate Test 105
9.1.4 Temperature Test 106
9.1.5 Strain Limited Test and Density Measurement 107
9.1 6 Dependence of Birefringence on Temperature, Strain Rate and Strain 108
9.1.7 High Strain Rate Deformation 110

9.1.8 Activation Enthalpy, Entropy, Energy and Activation Volume with Strain Rate and Temperature 111
9.2 Conclusion 113
9.3 Suggestion for Future Work 116

Chapter 1

Introduction to the Study of Polymer Viscoelasticity

1.1 Introduction

Polymers consist of repeating units called monomers The monomers are normally bonded together covalently in the form of long chains. The long chains can be linear, grafted or cross-linked The different structures of the polymer chains give rise to the diversity of the functions of polymers. However, the mechanical properties of polymers are greatly affected by temperature and strain rate Because of this, a lot of research has been carried out on polymers by subjecting them to different testing conditions to study their mechanical behaviour before putting them into application However, most of the research that has been carried out is in the low strain rate region. In the current project, two types of fully amorphous polymers - poly(methyl methacrylate) (PMMA) and polystyrene (PS) were adopted and subjected to a wide range of strain rates from low to high rate and a range of temperatures up to below the glass transition to study the change in yield and flow stress as a function of strain rate and temperature.

1.2 Amorphous and Semicrystalline Polymer

Amorphous Polymer

Amorphous polymers can be obtained by rapid cooling from the melt so that the chains do not have sufficient time to arrange into a regular structure in the form of a crystal. Hence, the chains in amorphous polymers are normally randomly oriented or oriented without long-range order. Polymers with bulky side-groups and irregular tacticity are likely to be amorphous, for example, atactic polystyrene and poly(methyl methacrylate) Polymers such as PET with a slow rate of crystallisation are easily obtained in an almost amorphous form by normal quenching techniques. However, polymers with very high rates of crystallisation such as PE or PMP41 can be obtained

in almost completely amorphous state by an ultraquenching technique developed by Hsu et al.[1]

Amorphous polymers are usually transparent due to the absence of crystallites or other inhomogeneities on the length scale of the wavelength of light. At sufficiently low temperatures, they are brittle solids. They behave plastically when the testing temperature is close to the glass transition or the deformation speed is slow. Cross-linked amorphous polymers behave as elastomers when they are at a temperature above the glass transition.

The viscoelastic behaviours of amorphous polymers show more distinct changes with frequency than crystalline polymers. The presence or absence of chemical cross-links or physical cross-links in the amorphous polymer chains causes the large changes in their viscoelastic behaviour. At low frequency, chemical cross-links prevent irreversible molecular flow and hence produce the rubbery plateau region. Physical cross-links due to entanglements form temporary networks and thus restrict molecular flow. With time, the physical entanglements lead to some irreversible flow.

Semicrystalline Polymer

Semicrystalline polymers are mixtures of crystalline and amorphous phases and can be obtained by slow cooling from the melt or subsequent heat-crystallization treatments. The crystallisation normally starts at temperatures between the glass transition temperature and the melting point and the rate of crystal formation depends on the temperature. Polymers with stereo regularity and a low degree of branching and cross-linking will crystallise. In addition, they should have enough chain mobility at the melting point for the crystallisation process to take place. During the crystallisation, most of the polymer chains fold forth and back to produce single crystals in the form of lamellae with thickness of the order of 100 Å. The lamellae thickness is regardless of the polymer chain length which could be in the order of 10^5 Å. The lamellas are imbedded in the amorphous matrix.

The crystalline content in polymers may affect the mechanical behaviour. The tensile modulus and strength of semicrystalline polymers increases with increasing degree of

crystallinity. The increase in the degree of crystallinity normally enhances the interchain force. The fall in modulus for crystalline polymers throughout the glass-transition region is much smaller than that of amorphous polymers, generally only involving a fall from 10^9 Nm^{-2} to 10^8 or 10^7 Nm^{-2}. Annealing undeformed semicrystalline polymers generally increases the degree of crystallinity in the polymers.[2]

1.3 Effect of Temperature

Temperature has strong effects on the mechanical properties of polymers such as modulus, yield strength, tensile strength and elongation to break. Linear amorphous or crystalline polymers are more sensitive to temperature compared to highly cross-linked polymers.

The modulus of amorphous polymers drops by a factor of a thousand when the temperature only increases a few degrees in the glass transition region. Below the glass transition temperature, the modulus of amorphous polymers remains fairly constant. The appearance of the crystalline content in the polymers reduces the degree of decrease of modulus in the glass transition region. For polymers with about 50 % crystallinity, the moduli decrease by a factor of about ten through the glass transition region. After the glass transition region, the modulus decreases gradually with temperature until the melting point At the melting point the modulus decreases tremendously.

It has been reported that, the elongations to break for amorphous polymers are small at temperatures below the glass transition temperatures. Approaching the glass transition temperature, the elongation becomes very large as the temperature is raised The elongation to break goes through a maximum and then decrease with further increasing temperature.[3,4,5]

The tensile strengths of amorphous polymers seldom change by a factor of more than ten. For amorphous polymers that have glass temperatures, the tensile strengths give sigmoidally shaped curves when plotted against temperature. Truss et al.[6] found that

tensile tests on two different molecular weight polyethylenes at strain rates from 10^{-5} to 10^{-2} s^{-1} showed a decrease of yield stress with temperature from 120 to 320 K. Lee et al.[7] found that PEEK showed a great drop in yield stress when tested at temperatures close to T_g compared to the yield stress when tested at room temperature. Helmckx et al.[8] reported the yield stress of PVDF decreased with temperature at a constant strain rate.

1.4 Effect of Strain Rate

Similarly to the case of temperature, strain rate also causes changes in the mechanical properties of polymers. The yield stress and the moduli of polymers increase when the strain rate increases. A lot of research has been carried out to investigate the reason that causes an increase in yield stress and modulus due to the increase in strain rate, until now the mechanism that causes the increase in yield stress and modulus still remains unknown. In addition, other properties such as elongation to break are also affected by strain rate. For rigid polymers such as poly(methyl methacrylate), the elongation to break decreases when the strain rate increases.

Strella[9] carried out tests on polymers with the testing speed up to 5000 inches per minute by observing force-time curves on an oscilloscope. He found that the yield stress and the modulus increase, and the elongation decreases as the strain rate increases. The yield point of polyethylene was more pronounced at very high speeds than at low speeds. He also found that polystyrene gave an ultimate elongation of about 2% at a testing speed of 1800 inches per minute.

Nanzai[10] and Zhu et al.[11] found that the yield stress at a particular temperature increased in a non linear manner with the logarithm of strain rate in the low rate region. Walley et al.[12] found that the flow stress of some polymers dropped at very high strain rates with no proven explanation.

1.5 Investigation into the Increase of Flow Stress

There have been many studies of the relationship between the flow stress of a material and the applied strain rate. An unusual and controversial phenomenon is a rapid increase in the flow stress at the strain rate region of $10^2 \sim 10^3$ s^{-1}. Some workers attribute the increase to instrumental effects arising from friction, inertia etc rather than the material effects. In the case of metals, some workers attribute the increase in flow stress to the multiplication and drag of dislocations and have proposed a theoretical model to fit the result.

Walley et al.[13] carried out uniaxial compressive tests on seventeen different polymers at room temperature over the strain rate region of $10^{-2} \sim 3x10^4$ s^{-1}. The purpose of studying such a large number was to identify the specific groupings of the behaviour of polymers. They found that six of the polymers (acetal, HDPE, dry nylon 6, moist nylon 6, moist nylon 66 and PBT) displayed a linear relationship between stress and strain rate. ABS, PET, PP, PVC, PVDF showed a sharp increase in flow stress at the rate of 10^3 s^{-1} while noryl, dry nylon 66, PC, PEEK and PES showed a decrease in flow stress at the rate of 10^3 s^{-1}. They did not attribute the changes to experimental error as all of the polymers were tested under the same equipment and test conditions. Furthermore, several repeated measurements had been carried out to examine the unexpected observations. However, the reason for the rapid increase in flow stress was not mentioned in the paper.

Al-Maliky et al.[14] proposed the reason for the rapid increase in flow stress at strain rate 10^3 s^{-1} was due to the increase in crystallinity of the tested samples. The samples studied by the authors were polyetheretherketone (PEEK) and nylatron (a nylon 6-6 derivative) and these polymers were tested in compression in the strain rate region of $10^{-3} \sim 10^4$ s^{-1}. Both of the polymers studied were semicrystalline. The crystal structure and the crystallinity of the tested polymers were examined using X-ray Diffraction and Differential Scanning Calorimetry (DSC). All the experiments were carried out at room temperature (~ 20 °C) A modest increase in flow stress at rate of $10^2 \sim 10^3$ s^{-1} and a rapid increase thereafter were observed. As the rate increased beyond 10^4 s^{-1}, both polymers showed a rapid decrease in flow stress. Comparison

between the PEEK crystallinity and the Nylatron heat of fusion with the schematic diagram of flow stress against strain rate was made. The authors attributed the rapid increase and decrease thereafter in the flow stress to the increase and decrease in the crystallinity and the heat of fusion of PEEK and Nylatron respectively. However, the authors deducted that the process causes the increase at rates > 10^3 s^{-1} and will not operate at rate beyond 10^4 s^{-1}. The explanation is then supported by the X-ray diffractograms of PEEK and Nylatron.

Fernandez et al.[15] carried out experiments on PET to determine whether the rapid increase in flow stress at high strain rate can be in fact attributed to the increase in crystallinity of the polymer. They investigated the development of crystallinity in PET as a function of strain, strain rate and temperature. PET was chosen as it consists of a mixture of amorphous and crystalline material with the crystalline fraction normally in the range of 10~50% In mechanical tests, they compressed the samples at a range of strain rates subjected to room temperature 298K. They also limited the strains by means of metal rings placed around the samples. The aim was to examine the development of crystallinity in samples at different stages of strain subjected to the same strain rate. They observed that the crystallinity only increases after a high strain > 0.7 has been achieved. However, at 0.2 strain and temperature 298 K the flow stress shows an increase at the high strain rate region. Therefore, the increase in crystallinity cannot be the cause of the increase in yield stress.

From the literature reviews, it can be seen that no clear explanation has been found to relate the increase in flow stress with the increase in strain rate. The samples studied in the literatures above were semicrystalline, hence, in this study two fully amorphous polymers were used to study the effect of the amorphous region on the increase in flow stress.

1.6 The Objectives and the Layout of the Thesis

The objectives in the current project are:

(i) to study the effect of temperature and strain rate on the two fully amorphous polymers: poly(methyl methacrylate) and polystyrene by relating the effect to the density and orientation of the samples after compression at limited strains.

(ii) to visualise the fracture of PMMA and PS using the high-speed photographic system and relate it to the temperature rise at each testing temperature.

(iii) to study the activation volume and energy of PMMA and PS by applying Eyring theory to the stress-strain curves and relate them to the increase in flow stress.

Chapter 2 describes the theories that were applicable in this study. Chapter 3 describes the mechanical testing on PMMA and PS. In Chapter 3, two types of machines (Hounsfield H50KM Machine and in-house built Dropweight Machine) were used to compress the samples at a wide range of strain rates and temperatures below the glass transition. The specifications of the machines are widely explained in this chapter. The fracture of PMMA and PS subjected to high strain rate deformation studied using the high-speed photographic system is described in Chapter 4. In Chapter 5, thermal analysis on PMMA and PS using DSC and DMTA to study properties such as the change of the specific heat and the modulus with temperature is described. The density of PMMA at different strains and the orientation of the samples after compression were studied and are described in Chapter 6 and Chapter 7 respectively Chapter 8 describes the application of Eyring theory in order to study the activation volume and energy at yield point, 20% and 30% strain and relates them to the increase in flow stress. Chapter 9 contains the discussion, conclusion and the suggestions for future work.

References

1. **C. C. Hsu and P. H. Geil,** Journal of Macromolecular Science - Physics, **B25**(4) (1986) 433~466

2. **I. M. Ward and D. W. Hadley,** "An Introduction to the Mechanical Properties of Solid Polymers", John Wiley & Sons, 1993

3. **G. Fromandi, R. Ecker and W. Heidemann,** "Proc. Intern. Rubber Conf.," p. 177, Washington, D C , Nov , 1959

4. **T. L. Smith,** Journal of Polymer Science **32** (1958) 99

5. **T. L. Smith and P. J. Stedry,** Journal of Applied Physics **31** (1960) 1892

6. **R. W. Truss, P. L. Clarke, R. A. Duckett and I. M. Ward,** Journal of Polymer Science **22** (1984) 191~209

7. **L. H. Lee, J. J. Vanselow and N. S. Schneider,** Polymer Engineering and Science **28** (1988) 181~187

8. **S. Hellinckx and J. C. Bauwens,** Colloid & Polymer Science **273** (1995) 219~226

9. **S. Stella,** "High Speed Testing", Vol. 1, A. G. H. Deitz, and F. R. Eirich, Interscience Publishers, Inc., New York, 1960

10. **Y. Nanzai,** Polymer Engineering and Science **30** (1990) 96~107

11. **X. X. Zhu and G. R. Zhu,** Polymer **33** (1992) 4968~4976

12. **S. M. Walley, J. E. Field, P. H. Pope and N. A. Safford,** Journal de Physique III **1** (1991) 1889~1925

13. **S. M. Walley and J. E. Field,** Dymat Journal **1** (1994) 211~227

14. **N. Al-Maliky, J. O. Fernandez, D. J. Parry and G. M. Swallowe,** Journal of Materials Science Letters **17** (1998) 1141~1143

15 **G. M. Swallowe and J. O. Fernandez,** Journal de Physique IV France **10** (2000) 311~316

Chapter 2

Theory

2.1 The characteristics of Poly(methyl methacrylate) (PMMA) and Polystyrene (PS)

Poly(methyl methacrylate) (PMMA)

PMMA is a vinyl polymer and made from the monomer methyl methacrylate by free radical vinyl polymerisation in an exothermic process. The monomer is a colourless liquid, boiling at 101 °C.

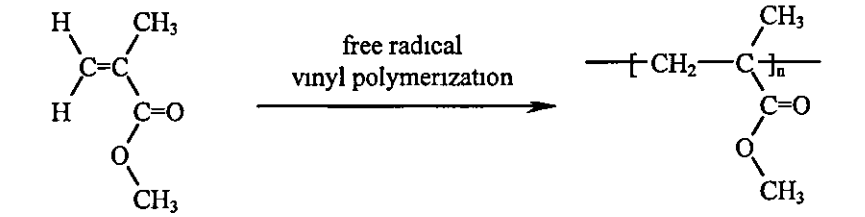

methyl methacrylate poly(methyl methacrylate)

PMMA is an atactic amorphous thermoplastic. This molecular chain is relatively large and is in a coiled configuration. The chains are asymmetric with the $-CH_3$ and $-COOCH_3$ groups arranged randomly above and below the chain. The randomness and steric effects of the ester groups make the molecular chains difficult to be arranged in orderly sequences Due to this, PMMA is completely non-crystalline and is optically transparent as there are no crystal interfaces to give light scattering.[1]

PMMA has high strength but is brittle and fails at low elongation. The ductile-brittle transition temperature for PMMA is 45°C. Its glass transition temperature is in the range 102~120 °C.[2&3] It has a hard surface and thus is scratch resistant. PMMA doesn't dissolve in water and is resistant to highly polar solvents (e g. ethanol), but is soluble in less-polar solvent (e g. toluene). It is flammable, resistant to UV radiation and to weathering. At room temperature, PMMA is resistant to non-oxidizing acids, alkalis, and salts but its resistance decreases at elevated temperature. At ordinary temperature, it is attacked by oxidizing acids.

Polystyrene (PS)

Polystyrene is a vinyl polymer with bulky pendant groups (benzene ring or phenyl groups) attached to backbone carbon atoms. It is formed from the monomer styrene ($C_6H_5CH=CH_2$) by free radical vinyl polymerisation in an exothermic process. The monomer is a colourless liquid boiling at 145 °C

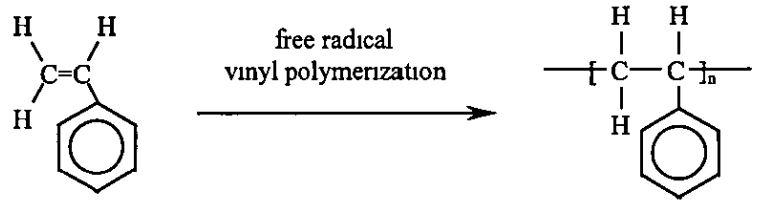

styrene polystyrene

Atactic polystyrene (at-PS) is an amorphous thermoplastic. The polymerisation of styrene is head-to-tail addition of monomer molecules. A benzene ring is attached to one of the carbons in every polystyrene monomer. This causes an asymmetric arrangement in the polymer chains and thus prevents crystallisation occuring.[1] It is optically transparent, brittle, hard and is unaffected by water, however, it is attacked by UV radiation, weathering and is permeable to water vapour as well as to most other gases. It is flammable, has excellent electrical properties, soluble in aromatic solvents (e.g. acetone) and is resistant to non-oxidising acids, alkalis and salts. However, it is attacked by chlorine and oxidising acids It has refractive index of 1.592 with the glass transition temperature T_g at 100 °C. The ductile-brittle transition temperature for PS is 90°C.

The brittleness of PS can be overcome by grafting styrene monomers with butadiene monomers to form high-impact polystyrene (HIPS). Compared to PS, HIPS can take harder impacts without cracking. Another kind of polystyrene is called syndiotactic polymer (it-PS) It is a brittle crystalline polymer with a specific gravity of 1.12 and a melting point T_m at 230 °C.[3]

2.2 Types of Stress-Strain Curves

The stress-strain curves of polymers can be divided into five classes (Figure 2.1):[4&5]

(1) soft, weak

Soft and weak polymers have low moduli, low tensile strengths and break at moderate strain. For example: soft polymer gels.

(2) hard, brittle

Hard and brittle polymers have high moduli, moderate tensile strengths and break at small strain (~2%) without any yield point. For example: polystyrene, poly(methyl methacrylate).

(3) hard, strong

Hard and strong polymers have high Young's modulus, high tensile strengths and break at strain of ~ 5%. The curves appear as though the material broke about where a yield point might be expected. For example: some rigid polyvinyl chloride formulations.

(4) soft, tough

Soft and tough polymers have low moduli, yield points, and break at high strain (20 to 1000 %) but with moderately high breaking strengths. For example. rubbers and plasticised polyvinyl chloride.

(5) hard, tough

Hard and tough polymers (e.g. cellulose acetate or nitrate and nylons) have high moduli, yield points, high tensile strengths and large strain. Most polymers of this group show cold-drawing or "necking" during the stretching process.[6&7]

The area under the stress-strain curve is equivalent to the energy required to break a polymer. Toughness is defined by the energy required to break a polymer The higher the energy required to break a polymer, the tougher the polymer is. It is calculated as $\int_0^{\varepsilon_b} \sigma d\varepsilon$.

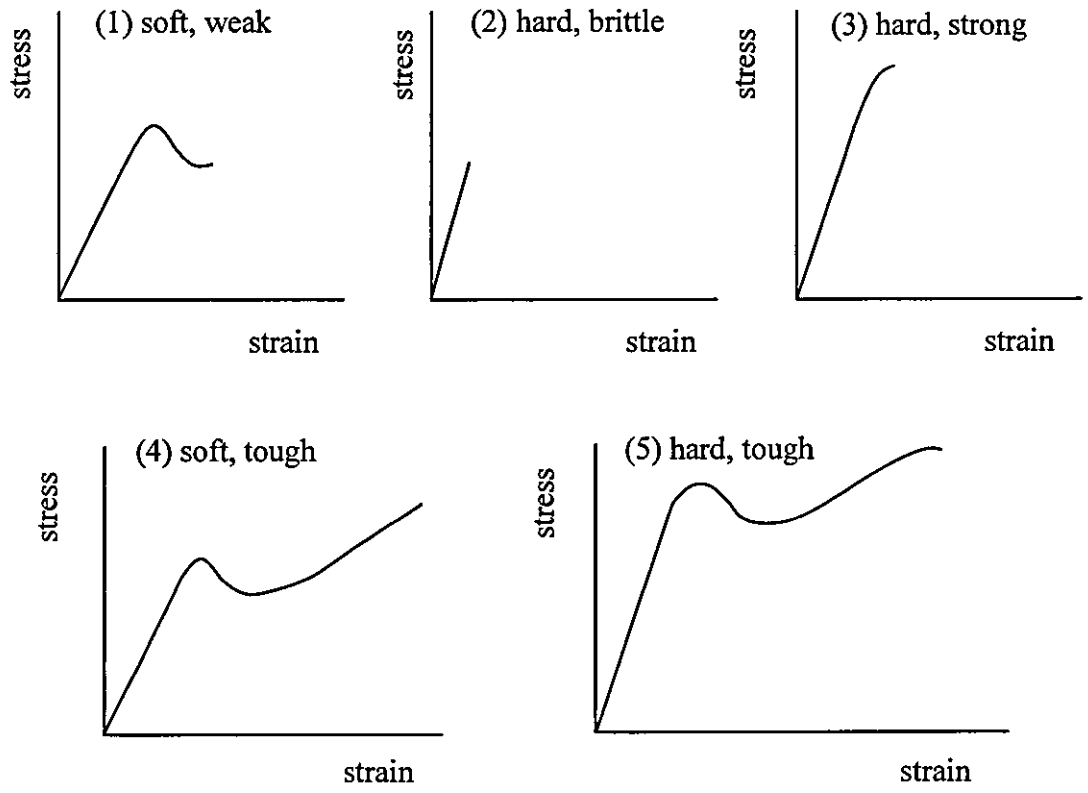

Figure 2 1: Types of stress-strain curves.

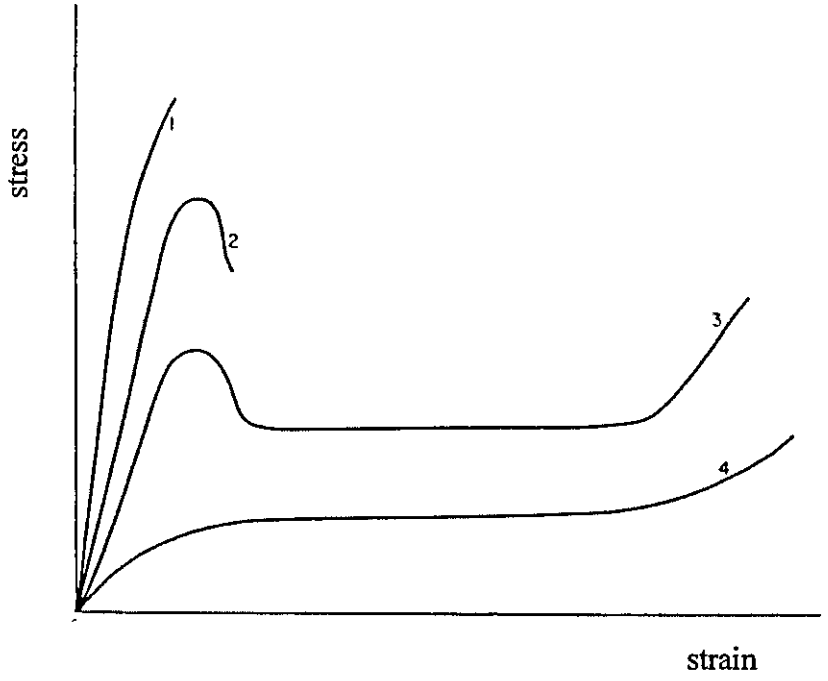

Figure 2.2: Stress-strain curves for a brittle polymer tested at four temperatures showing different mechanical behaviour. (1) Brittle fracture (2) Ductile failure (3) Cold drawing and necking (4) Rubber-like behaviour.[8]

The temperature of testing sometimes effects the shape of the stress-strain curves of polymers that are brittle at room temperature (Figure 2.2). For example: polymethyl methacrylate and polystyrene. At temperature higher than the room temperature, the polymers undergo a ductile-brittle transition and break after the yield point. At temperature below T_g, the cold drawing behaviour is shown on the stress-strain curve. At temperature above T_g, the polymers behave like a rubber and show homogeneous deformation at all strain up to the very high strain (~500 %) before breaking occurs.[8]

2.3 The Elastic, Yield and Plastic Behaviour of Glassy Polymers

Elastic Behaviour

When a material is deformed under an applied stress, a strain is induced On removing the applied stress the material returns to its original shape; the deformation is said to be elastic deformation. Materials that have this property and regain their original shape after the applied stress is removed are elastic.

In the elastic deformation, the increase in stress is linearly proportional with the increase in strain. This relationship is known as Hooke's Law: $\sigma = E\varepsilon$, where σ is the applied stress, ε the strain and E the Young's modulus. Young's modulus describes the stiffness of a material or how easily the material deforms. For most metals, the Young's modulus is approximately constant; however, for polymers it depends on the strain rate and temperature to which the polymers are subjected [9]

Hooke's Law is only valid in the region where the applied stress does not exceed the limit of proportionality 'a' in Figure 2.3. Young's modulus can be calculated from the slope of the stress-strain curve from initial stress to the limit of proportionality. Beyond 'a', stress is no longer proportional with strain and continues to 'b' where the elastic limit is reached. However, for many materials it is difficult to detect the difference between the limit of proportionality and the elastic limit. When polymers are stressed beyond the elastic limit, the physical properties of the material change and a residual strain exists on removal of the stress.

Yield Behaviour

The deformation of a material is recoverable on removing the stress provided that the deformation does not exceed the elastic limit. For some materials the applied stress reaches its maximum after the elastic limit and further application of stress causes materials to start to deform plastically. At this maximum point, the material is said to have yielded. The yield point can then be defined as this maximum point. It is the point where the elastic deformation ceases and where the onset of permanent plastic deformation occurs. The yield stress and yield strain, hence, correspond to the values at this maximum.[10]

For some cases where the stress-strain curve does not show any maximum stress, the yield point can be defined as the intersection point of two tangent lines on the stress-strain curve (Figure 2.5).[11] However, there is generally no sharp distinction between the elastic and plastic deformation on the stress-strain curves obtained experimentally. For the ductile materials such as aluminium where the stress-strain curves do not have a clear yield stress, a 0.1% proof stress method is adopted to define the yield point (Figure 2.4). 0.1% proof stress is the stress needed to produce a permanent strain of 0.001 on removal of the applied stress.[12]

Plastic Behaviour

Plastic deformation is a non-recoverable deformation on removal of the applied stress. In this region, the change in the structure of materials occurs permanently. It is the deformation shown by materials before breaking. For some materials (e g polystyrene, mild steel, etc.), the phenomena such as strain softening, followed by a roughly constant increase of stress and strain hardening when the strain increases are normally observed in the plastic region. However, strain softening does not occur in some materials such as rubber and aluminium when stressed in the plastic region.

In the plastic deformation of a metal, atoms slip on specific planes of a crystal. The slipping of atoms does not occur over the entire crystal at any one time. It takes place by the movements of dislocations across slip planes in a crystal.[13] Metals that have easy-move dislocations tend to be soft while hard and strong metals have dislocations

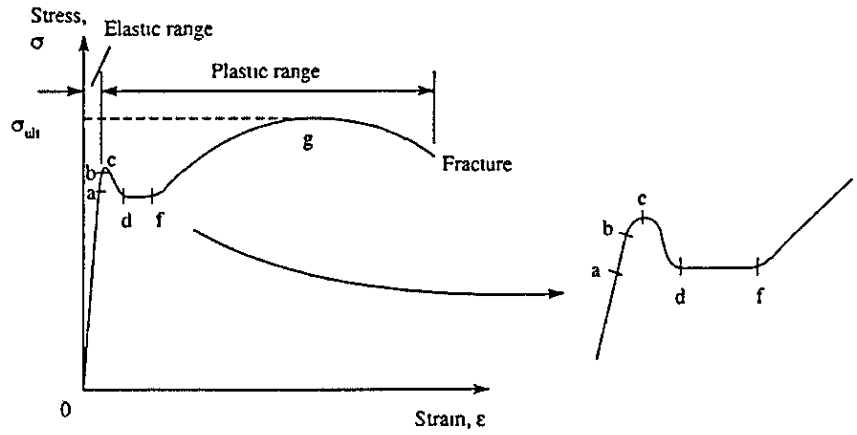

Figure 2.3: Stress-strain curve for materials which show a maximum stress after elastic limit; the yield point is defined as this maximum stress. (a) the limit of proportionality (b) elastic limit (c) yield point (d) lower yield point (f) the onset of strain hardening (g) ultimate stress.[12]

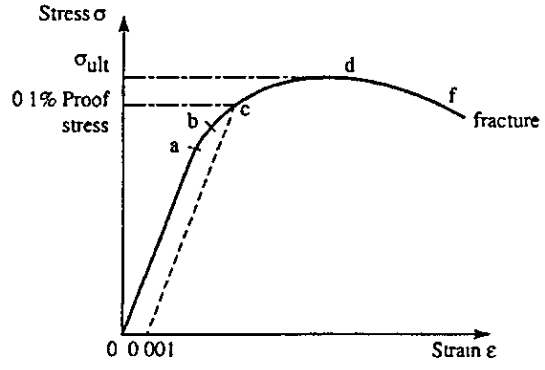

Figure 2.4: Stress-strain curve for materials which do not have distinct maximum stress; 0.1% proof stress method was used to determine the yield point (a) the limit of proportionality (b) elastic limit (c) yield point (d) ultimate stress.[12]

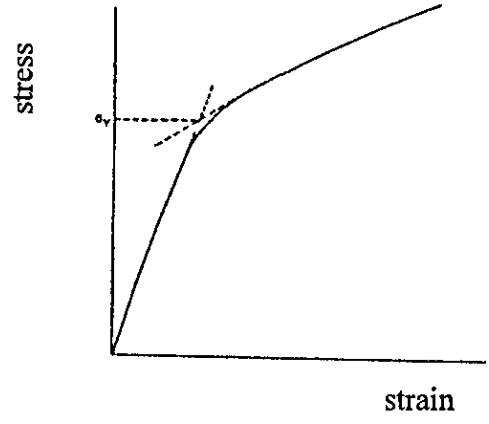

Figure 2.5: Stress-strain curve for materials without distinct maximum stress. The yield point is defined as the intersection point of two tangent lines on the stress-strain curve [11]

that are difficult to move. As plastic deformation proceeds, many dislocations are generated and react with each other. The dislocations accumulate in a crystal and finally prevent further movements of atoms. Hence, they cause strain hardening in the metals when plastic deformation continues The accumulated dislocations can be made to disappear when the hardened metals are heated in an annealing process.

However, the movement of molecules in polymers in plastic deformation is not well defined. Many authors[14,15&16] have come out with their suggestions about the processes occurring in the plastic deformation of polymers. Polymers can be semicrystalline or fully amorphous. Hence, the deforming processes that occur in the plastic region of polymers might involve the interaction between the polymer chains in the crystalline phase and amorphous phase. It was reported that plastic deformation could involve pulling chains out of crystalline phase or be caused by irreversible chain rupture of a weak point in the polymer chains.[14] Another alternative theory of plastic deformation is due to the formation of molecular kinks.[15] Some authors reported that two mechanisms are involved in stretching a linear polymer. In the first, the polymer chains slip past each other and the slips are relative movements of their centres of gravity. This movement is non-recoverable on releasing the stress. In principle, it is a viscous strain and is described by Newton viscosity. In the second, the randomly coiled chains straighten out in the direction of stress. This movement is recoverable on removing the stress. This is rubber-like strain and is described by Hooke's law.[16]

2.4 Stress, Strain and Strain Rate

Stress and strain can be defined in two ways, that is engineering stress and engineering strain or true stress and true strain. Consider a cylindrical sample of cross-sectional area A_0, diameter d_0 and height h_0 is subjected to a uniaxial force F_t and changed to A_t, d_t and h_t after time t. The engineering stress is defined as the force divided by the original cross-sectional area:

$$\sigma_e = \frac{F_t}{A_0} \tag{2.1}$$

and the engineering strain is the change in length divided by the original length:

$$\varepsilon_e = \frac{dh}{h_0} = \frac{h_t - h_0}{h_0} \qquad (2\,2)$$

However, the engineering stress shows a decrease when the strain continues beyond the maximum point. In the calculation of the engineering stress, the original cross-sectional area A_0 is used and this is actually not precise as the area decreases (for tensile tests) or increases (for compression tests) when the strain increases.

For a more accurate way of calculating stress and strain, true stress and true strain are defined by taking into consideration the changes of the cross-sectional area and the length with time t. The true stress and true strain are defined as below:

$$\sigma_t = \frac{F_t}{A_t} \qquad (2\,3)$$

$$\text{and } \varepsilon_t = \int_{h_0}^{h_t} \frac{dh}{h} = \ell n\left[\frac{h_t}{h_0}\right] \qquad (2.4)$$

However, the relationship of the engineering strain and true strain can be constructed by putting Equation (2.2) into Equation (2 4) as below:

$$\varepsilon_t = \ell n\left[\frac{h_t}{h_0}\right]$$

$$= \ell n\left(\frac{h_t - h_0 + h_0}{h_0}\right)$$

$$= \ell n(1 + \varepsilon_e) \qquad (2.5)$$

The calculation of the true stress σ_t can be simplified by assuming the volume of the tested sample in the plastic deformation remains constant during the whole experiment Therefore, with the law of volume conservation:

$$V_t = V_0 \qquad (2\,6)$$

$$A_t h_t = A_0 h_0$$

$$A_t = \frac{A_0 h_0}{h_t} \qquad (2.7)$$

Submitting Equation (2 7) into Equation (2.3), the true stress becomes:

$$\sigma_t = \frac{F_t h_t}{A_0 h_0} \tag{2.8}$$

In an ideal test, uniform deformation under a velocity v will give the strain rate:

$$\dot{\varepsilon} = \frac{v}{h_t} \tag{2.9}$$

In the experiments carried out in this work, the strain rate was estimated from the slope of the true strain versus time as below:

$$\dot{\varepsilon} = \frac{d\varepsilon}{dt} \tag{2.10}$$

The velocity of the impact changes with time as the sample is compressed and the sample then recovers after compression Hence, the final height measured using the micrometer is not same as the height just after compression.

References

1 **G. F. Kinney,** "Engineering Properties and Applications of Plastics", John Wiley & Sons, INC., New York, 1957

2. **R. B. Seymour and C. E. Carraher, Jr.,** "Structure-Property Relationships in Polymers", Plenum Press, New York, 1984

3. **D. R. Askeland,** "The Science and Engineering of Materials", third edition, Chapman & Hall, 1996 page 503

4 **T. S. Carswell and H. K. Nason,** "Symposium on Plastics", Sec. Tech. Publ No 59, p 22, Philadelphia, Pa., Am. Soc. Testing Materials, Feb , 1944

5. **T. S. Carswell and H. K. Nason,** Modern Plastics, 21 (June, 1944) 121

6. **I. Marshall and A. B. Thompson,** Proceedings. Royal Society of London A **221** (1954) 541~562

7 **P. I. Vincent,** Polymer **1** (1960) 7~19

8. **I. M. Ward,** "Mechanical Properties of Solid Polymers", second edition, Wiley-Interscience, 1983

9. **P. D. Ritchie,** "Physics Of Plastics", Iliffe Books Ltd , London, 196

10. **R. N. Haward,** "The Physics of Glassy Polymers", Applied Science Publishers Ltd., London, 1973

11. **I. M. Ward,** Journal of Materials Science **6** (1971) 1397~1417

12. **T. H. G. Megson,** "Structural and Stress Analysis", Arnold, 1996

13. **T. S. Hutchison & D. C. Bair,** "The Physics of Engineering Solids", Wiley, 1968

14. **R. W. Truss, P. L. Clarke, R. A. Duckett and I. M. Ward,** Journal of Polymer Science **22** (1984) 191~209

15. **S. Argon,** Journal of Macromolecular Science. Part B: Science **8**(3~4) (1973) 573~596

16. **B. Thompson,** Journal of Polymer Science **35** (1959) 741~760

Chapter 3

Mechanical Tests

3.1 Introduction

The aim of the current study is to relate mechanical properties to other characteristics of polymers The characteristics of poly(methyl methacrylate) (PMMA) and polystyrene (PS) were given in Chapter 2.1. Most studies on polymers have been carried out in the quasi static (10^{-4}~10^{-2} s^{-1}) and low strain rate regions (10^{-2}~1 s^{-1}), however, relatively few have been done in the high strain rate region (10^{2}~10^{3} s^{-1}). In order to study the mechanical behaviour of PMMA and PS in a more explicit way, a wide range of strain rate tests from the quasi static to high strain rate were performed on PMMA and PS and the results are described in this chapter In addition, elevated temperature tests were also performed on PMMA and PS from room temperature to a temperature 20 °C below their glass transition temperatures as determined using the Differential Scanning Calorimetry (DSC) method described in Chapter 6.

For the mechanical tests, a conventional Hounsfield H50KM Machine and an in-house built Dropweight Machine were adopted to perform compressive tests on PMMA and PS. The Hounsfield Machine provides strain rates from quasi static to low strain rates, while the Dropweight Machine provides strain rates in the high strain rate region An aluminium-heating block was built in the current study to be incorporated in the Hounsfield and Dropweight system in order to perform the elevated temperature tests on PMMA and PS.

There are a few methods in determining the yield stress of polymers from the stress-strain curves obtained in the experiments as explained in Chapter 2.2. In the current study, PMMA and PS showed a maximum stress after their elastic limit. Hence, the maximum stress shown on the stress-strain curves of PMMA and PS was chosen as yield stress for the analysis which follows in this thesis

The objectives of this chapter were to investigate the effect of the temperatures and strain rates on the flow stress and the point where strain hardening occurred in the samples of PMMA and PS. Strain limited tests were also performed on PMMA and PS in the Hounsfield and Dropweight system to view the relationship between the morphology of polymers with the stress-strain curves produced. Eyring theory was also applied to the stress-strain curves of PMMA and PS in order to study their activation volume, energy and entropy at the yield point, 20 % and 30 % strain This is explained in Chapter 8.

3.2 Hounsfield H50KM Test Machine

3.2.1 Introduction

The Hounsfield Test Equipment, H50KM, has been designed to test a wide range of materials in compression and tension with forces of up to 50 kN maximum There are five different force recorder ranges defined by % of 50 kN and thus the equipment can be set to get 5 different maximum force outputs (Table 3.1). During compression or tension, the mechanical force was converted to an electronic signal by the use of a cantilever load cell. This signal was fed to the force amplifier and then converted from analogue form to digital form to be shown on the force display LED in kilo Newton. The output voltage for each recorder range of force is 1 volt. However, the maximum permissible output voltage for each recorder range is 1 05 volts (that is 5% above the maximum permissible force for that recorder range)

In addition there are 5 extension recorder ranges with 5 different maximum crosshead movements (Table 3.2). The ultimate output voltage is 1 volt for each maximum movement The signal generated from the crosshead movement is shown on the extension display LED in a digital form that has been converted from analogue form.

The range of the crosshead speeds is from 0 1 to 500 mm/min. It can be set to any speed required within the range but with the interval 0.1 mm/min between one and another.[1] The diagram of the Hounsfield Machine and how the sample is placed for compression in the system is shown in Figure 3.1

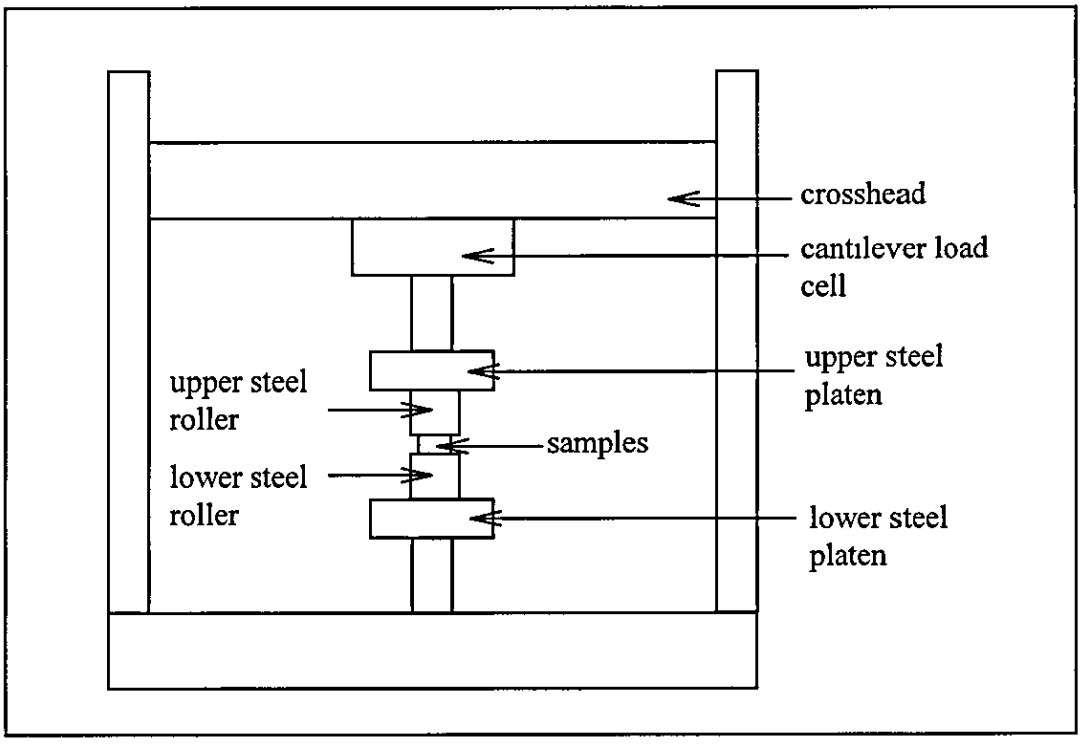

Figure 3.1: Diagram of the Hounsfield H50KM Machine.

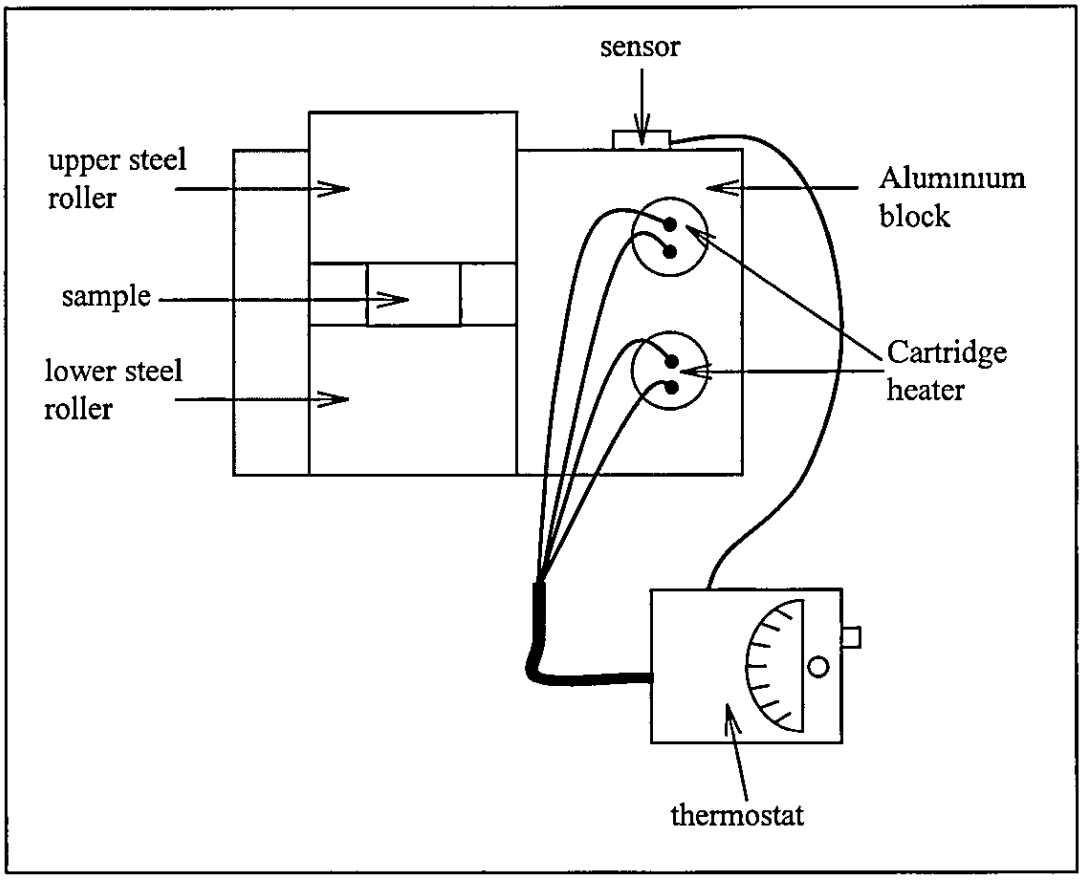

Figure 3.2: Diagram of the heating system in the Hounsfield Machine for elevated temperature tests.

Table 3.1: Five different Force Recorder Ranges.

Force Recorder Range (%)	Force Display (kN)	Applied Force (N)
100	50.00	50 000
50	25.00	25 000
20	10 00	10 000
10	5.000	5 000
5	2.500	2 500

Table 3.2: Five different Extension Recorder Ranges

Extension Recorder Range (mm)	Extension Display	Crosshead Movement (mm)
1000	1000	1000
500	500.0	500
100	100.0	100
50	50 00	50
10	10 00	10

3.2.2 Data Recording Methods

The Hounsfield Machine displays the signals obtained from the cantilever load cell and the crosshead in two ways – digital form and analogue form. The digital forms are shown on the LED displays. For the lowest speeds, it is possible to record the digital signals manually, however, for higher speed they change too fast to do that. The analogue signals can be channelled to the recording equipment through co-axial cables for further analysis. The methods used in this work for recording the output of the force and displacement from the Hounsfield Machine are listed below:

(i) A Thurbly DSA 524 digital storage adaptor was used to collect analogue signals from two channels A personal computer was connected to the DSA. The signals were then displayed through the personal computer installed with DS-PC link software and were saved under the file with extension " DSA". This file is in ASCII format. A program called DSA.BAS was used to transfer the ASCII format to digital in real time and voltage so that the data could be viewed through Microsoft Excel. This program is written in Basic2 and is in extension ".ZXW". It was developed by Z.XinWu This recording method was used by Hamdan[2] when studying PEEK, PEK and PES using the Dartec Hydraulic Machine. This method also used by Fernandez[3] when studying PET and Nylon 11 using the Hounsfield Machine.

(ii) The analogue signals can be viewed directly from the TDS360 Digital Real Time Oscilloscope using either YT display or XY display. The range of the timebase is from 4 ns to 10 s and the data can be saved on the oscilloscope internal floppy drive under spreadsheet file format. The maximum recording time on the oscilloscope is 100 s and the minimum recording time is 40 ns. The memory for the maximum recording time is not big enough to record the whole event of one-centimetre compression when the speed is set at 0.1 up to 0.6 mm/min. However, for testing carried out at 500 mm/min, the timebase is fast enough to catch the signals generated and the memory is big enough to record the whole events.

(iii) The analogue signals can also be viewed from the Picolog software installed on a PC. The installation of the software can be referred to Reference 4. Both analogue output voltages from the Hounsfield were converted into digital signal via PICO ADC-100 and recorded by the Picolog software. The PICO ADC-100 is a high-speed analogue to digital converter with two input channels and its specification is in Appendix A. Appendix B and C are summaries of how to record and display data using the Picolog software. The parameters for recording data using the Picolog software were set manually The speed of recording is determined by the sampling interval that can be in milliseconds, seconds, minutes, hours and days The sampling interval must be greater than the total sampling time, which is the total time required to collect the readings from the channels of the PICO ADC-100, in the 'Edit Channel'. The measurement mode is scaled in volts.

In the experiments, method (II) and (III) were used to record the output voltages from the Hounsfield Machine. The choice of method depended on the time required to finish the whole compression in a single experiment.

3.2.3 Measurement of the Sample Displacement

The digital reading shown on the extension display and the analogue signal collected with the oscilloscope or Picolog software actually contain the displacement of the tested sample together with the machine compliance. In order to obtain the actual displacement of sample, two methods have been worked out.

(i) A steel roller (ø12.69mm x H12.69mm) was compressed between two steel platens with the force of 50 kN. The displacement against time curve obtained is due to the machine compliance together with the elastic response of the steel roller. The Young modulus E for the steel is 20.14×10^{10} Nm^{-2}. The stress σ caused by 50 kN onto the steel was 395 MPa. This induced the strain of 3×10^{-3} onto the steel roller. The value for the strain was small and thus could be ignored. When a sample is compressed between two platens, the displacement against time curve obtained is the sample deformation together with the machine compliance The data of the force against displacement for the steel

roller and the compressed sample were plotted in the same axes To obtain the real sample displacement, the machine compliance curve was subtracted from the sample + machine curve as shown in Figure 3.3.[5]

(ii) The displacement of sample being tested was measured directly by placing a displacement transducer under the crosshead. The transducer used was bought from Tokyo Sokki Kenkyujo Co., Ltd and its characteristic is stated in Figure 3.4. It works on the full bridge method with the input and output resistance of 350 Ω and produce 5440 x 10^{-6} volts per mm. It has four wires with two for input (red and black) and another two for output (green and white). The output voltage from the transducer is positive if the white wire is connected to the positive connection of recording equipment; is negative if the green wire is connected The transducer was powered with 10 V from a Thurlby LB15 power supply. It functions well at 23 °C but the output voltage fluctuates when the transducer is operated at higher temperature. Hence, during the experiment it was put under the crosshead so that it was far away from the aluminium-heating block used to heat the samples in elevated temperature tests This method was adopted in the experiments as it involved direct measurement of the sample displacement and will give higher accuracy than method (i).

3.2.4 Calibration of the Displacement Transducer

The transducer was calibrated by compressing and decompressing it between two steel platens at speeds of 0 6, 6, 60, 200 and 500 mm/min without a sample. The Hounsfield extension output voltage and the transducer displacement output voltage were recorded using the Picolog software via the PICO ADC-100. The Hounsfield extension output voltage was then converted into the Hounsfield displacement by multiplying the output voltage with the maximum value of the extension recorder range chosen. Graphs with displacement versus transducer output voltage were plotted for each condition and speed. Figure 3.5 is an example of the graphs obtained. Equation was calculated for each graph using 'Fit Linear' in the Analysis menu of Microcal Origin software (Table 3.3). The transducer calibration equation was

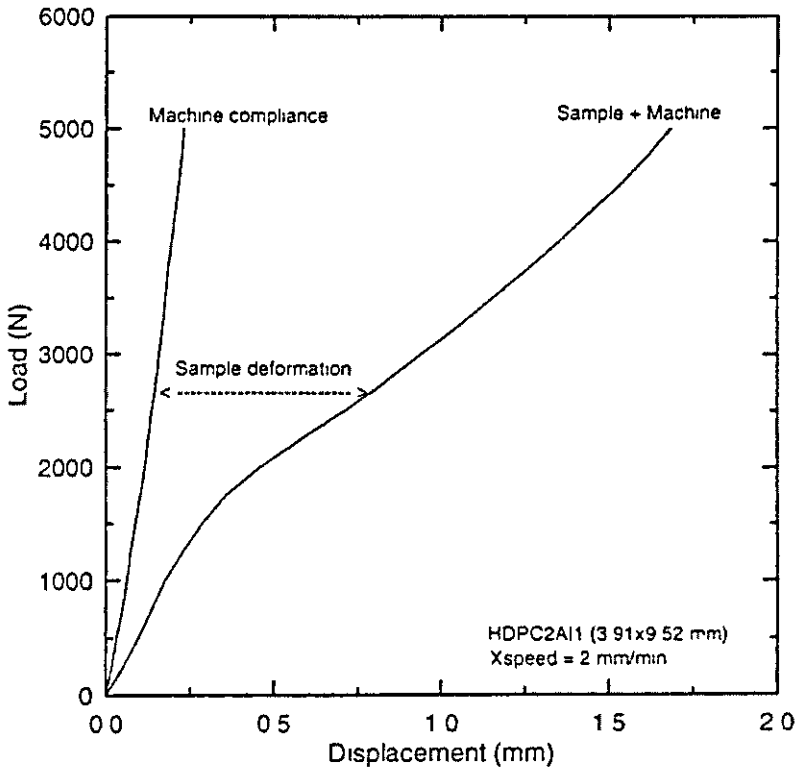

Figure 3.3: Graph of compressive test of HDPE using the Hounsfield Machine.[5]

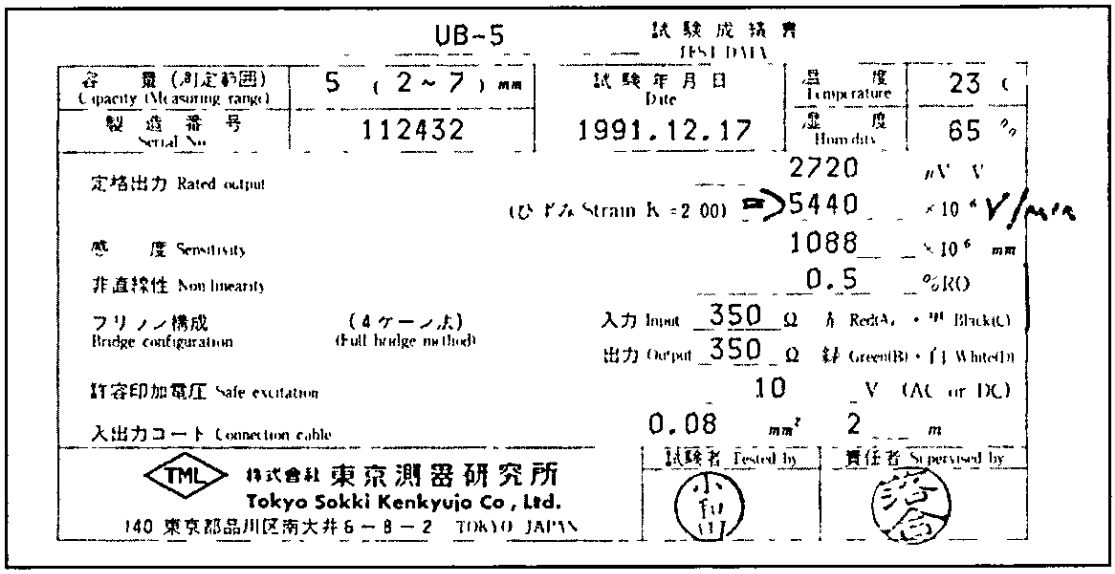

UB-5 試験成績書 TEST DATA

容量 (測定範囲) Capacity (Measuring range)	5 (2~7) mm	試験年月日 Date		温度 Temperature	23 ℃
製造番号 Serial No.	112432		1991.12.17	湿度 Humidity	65 %

定格出力 Rated output		2720	μV/V
	(ひずみ Strain K=2.00)	5440	×10⁻⁶ V/mm
感度 Sensitivity		1088	×10⁻⁶ mm
非直線性 Non linearity		0.5	%RO
ブリッジ構成 Bridge configuration	(4ゲージ法) (Full bridge method)	入力 Input 350 Ω	赤 Red(A)・黒 Black(C)
		出力 Output 350 Ω	緑 Green(B)・白 White(D)
許容印加電圧 Safe excitation		10	V (AC or DC)
入出力コード Connection cable		0.08 mm²	2 m

TML 株式会社 東京測器研究所
Tokyo Sokki Kenkyujo Co., Ltd.
140 東京都品川区南大井6－8－2 TOKYO JAPAN

試験者 Tested by 小川

責任者 Supervised by

Figure 3.4: Characteristic of the Displacement Transducer.

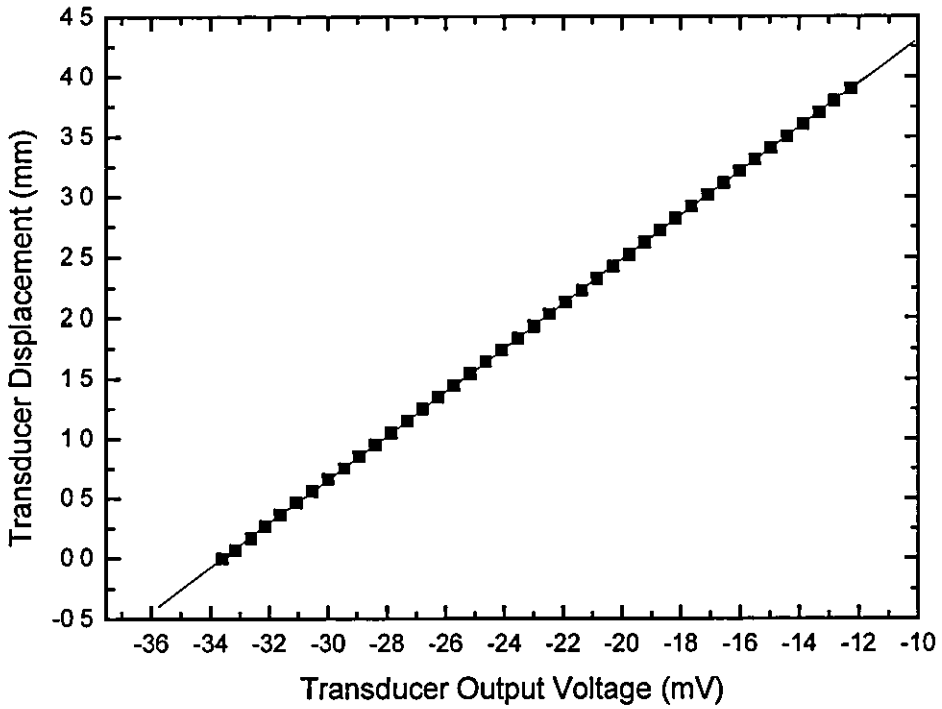

Figure 3.5: Example of the graph for the displacement transducer tested at each condition and speed using the Hounsfield Machine.

Compressing (mm/min)	Decompressing (mm/min)	Equation
0.6	[illegible]	y = 6.322 + 0.1831x
[illegible]	0.6	y = 6.23711 + 0.18343x
6	[illegible]	y = 6.26062 + 0.18313x
[illegible]	6	y = 6.14232 + 0.17781x
60	[illegible]	y = 6.14251 + 0.18279x
[illegible]	60	y = 6.04775 + 0.18197x
200	[illegible]	y = 5.92336 + 0.18411x
[illegible]	200	y = 5.96594 + 0.18249x
500	[illegible]	y = 5.88867 + 0.18468x
[illegible]	500	y = 5.88583 + 0.18541x
	Average	y = 6 08161 + 0.18289x

Table 3.3: Equations of the displacement transducer tested under different conditions and speeds.

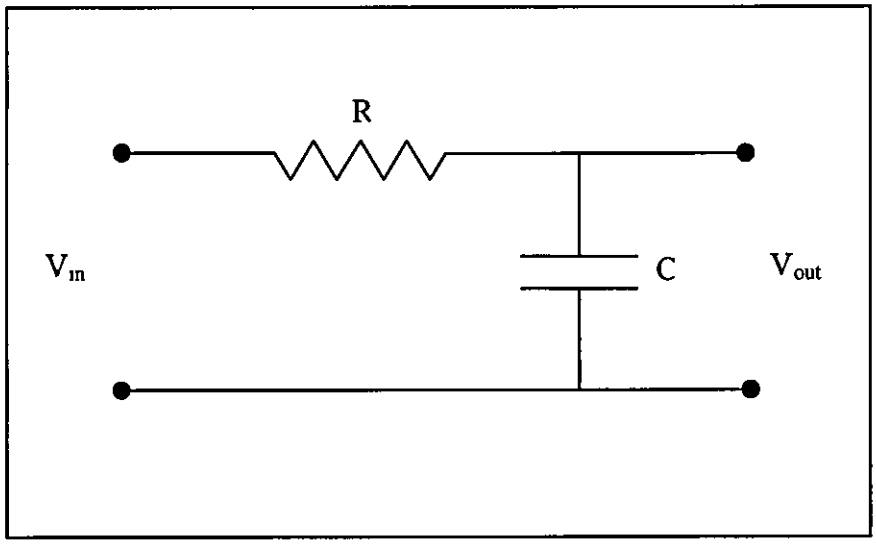

Figure 3.6: Low Pass Filter Circuit.

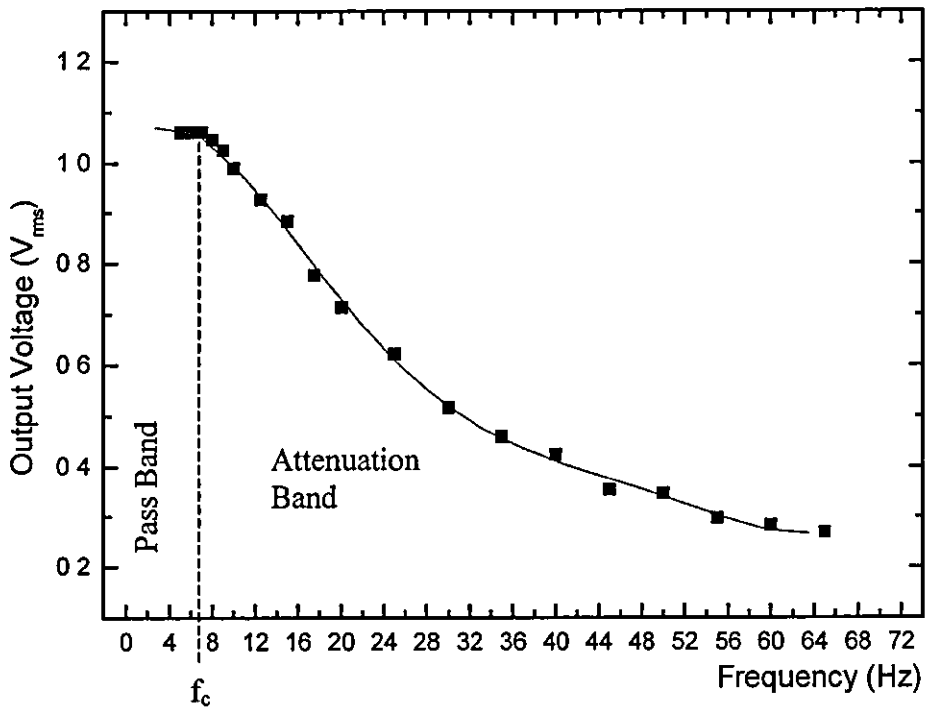

Figure 3.7a: Frequency-attenuation diagram of the low pass filter circuit used for filtering the frequency after 7 Hz coupled on the transducer signal.

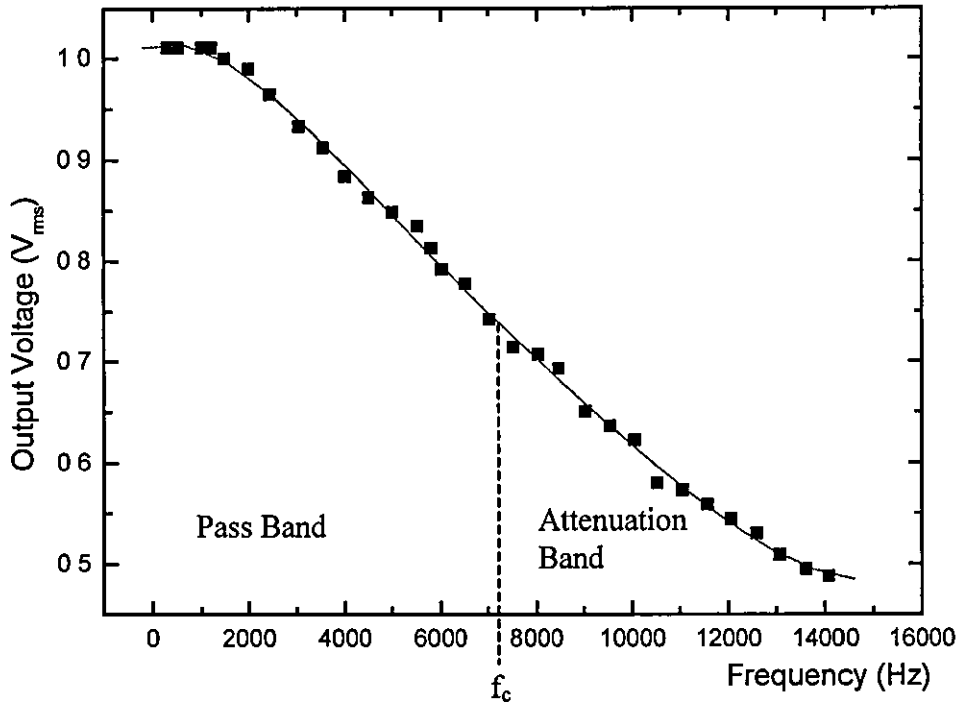

Figure 3 7b: Frequency-attenuation diagram of the low pass filter circuit used for filtering the frequency after 7234 Hz coupled on the Hounsfield force output signal.

obtained by averaging the gradient and intercept of all equations. From the slope of the calibration curve, it is found that 1-mm displacement of transducer produces 5468 x 10^{-6} volts The given standard value is 5440 x 10^{-6} volts/mm. From the comparison between 5468 x 10^{-6} volts/mm and 5440 x 10^{-6} volts/mm, the deviation is +0.51%. The transducer is still usable when compared to the technical data sheet that is ±0 5%. The force used to compress the transducer up to 3 5 mm was 0.007 kN, shown on the force display LED, was small enough not to cause any machine compliance effects on the Hounsfield extension output voltage data collected. Hence, the Hounsfield displacement calculated was equivalent to the transducer displacement.

3.2.5 Low Pass Filter Circuit

During compression or tensile tests, the movement of the crosshead produces some high frequency noise. This high frequency noise is normally coupled with the force output signal. In order to filter out the high frequency noises, a low pass filter was constructed as shown in Figure 3.6. The low pass filter was put between the output of the Hounsfield and the recording equipment.

Figure 3.7a & 3.7b showed the frequency-attenuation diagrams for the low pass filter circuits used for filtering the unwanted frequencies that coupled with the transducer and the Hounsfield force output signals, where f_c is the cut-off frequency. The diagram was obtained by measuring the amplitude of the voltage of each frequency signal that passed through the filtering circuit using the oscilloscope. The V_{rms} was then calculated from the amplitude of the voltage of each signal. The input frequency signals were generated from the AF frequency generator with the V_{rms} of each signal maintained at 1 volt. The frequencies that are above f_c after pass through the filtering circuits will be attenuated At f_c, the capacitive reactance of the capacitor C is equal to the resistance of the resistor R.

$$X_c = R$$

$$\frac{1}{2\pi f_c C} = R$$

$$\therefore f_c = \frac{1}{2\pi RC} \qquad (3.1)$$

At frequency well below f_c, the capacitive reactance of the capacitor C is much higher than the resistance of the resistor R, therefore the output voltage is practically equal to the input voltage and vice versa. In the experiments, two low pass filters were constructed with f_c = 7234 Hz (C = 0.022 μF, R = 1 kΩ) and f_c = 7 Hz (C = 22μF, R = 1 kΩ). The low pass filter with f_c = 7234 Hz was used to filter the noise coupled with the force output voltage, while with f_c = 7 Hz was used to filter the noise coupled with the transducer output voltage.

In order not to lose the information on the material stress-strain curve, the filtering frequency is set at more than thousand Hz so that the recording time could be set to the minimum timebase of 1 ms (2000 Hz). For experiments carried out at 500 mm/min timebase of 100 ms was used. Therefore, the choice of the frequency at 7234 Hz allows the complete information to be obtained without being filtered out.

The transducer output voltage obtained refers to the displacement of the sample being compressed. For compression up to four millimetre with 500 mm/min speed, the time required are 480 ms and this produced 2 08 Hz In addition, the displacement of the sample shows almost a straight line and no sinusoidal curve. Hence, the chosen cut-off frequency at 7 Hz will not effect the displacement signal obtained.

3.2.6 Data Acquisition

Samples were compressed at a range of speed from 0.1 to 500 mm/min using the Hounsfield H50KM Machine at different temperatures. Picolog software was used to record the data for the tests carried out at the speeds from 0 1 to roughly 8 or 10 mm/min. The sampling interval was set from around 80 ms to 4 s depended on how many data needed to be collected after calculating the compression time. The recording voltage was set at ± 2 V for the Hounsfield force output voltage and ± 50 mV for the transducer output voltage.

For samples tested at the speeds from 10 mm/min onwards, TDS360 Digital Real Time Oscilloscope was used. The oscilloscope was set at the 'stop after single acquisition' sequence with DC coupling. There are ten graticules in this oscilloscope

and the timebase was set according to the time required to compress the sample to the specific height. For samples compressed at speed 500 mm/min, the timebase 100 ms was set to record the Hounsfield force output data.

3.3 Dropweight Machine

3.3.1 Introduction

The in-house built Dropweight machine, used to produce strain rate of 500 ~ 3000 s^{-1}, was initially built by Dawson[6] in1993 and had similar functions to that used by Field et al.[7] Dawson[6] used the machine to investigate the response of polymers at room temperature to uniaxial compressive loading at high rates of strain. This machine was later used by Hamdan[2] and Fernandez[3] to investigate the effect of the strain rates on the yield stress of polymers over a range of strain rates and temperatures.

Figure 3.8 shows the diagram of the in-house built Dropweight Machine. The machine characteristic is extensively explained in Dawson's[6] and Hamdan's[2] thesis. During the present works, small modifications were made to the machine order to achieve more accurate results and ensure that the impact force was exerted evenly onto the sample. The three guide rods that position the free fall weight were cut short to make the whole system more rigid. Two hardened steel rollers of same length as previously were modified to different length. The upper steel roller, the roller holder and the position holder were made longer in order to prevent the hardened steel roller from bouncing out when the weight was dropped on it. Three brass rings with smooth surfaces were inserted into the 3-guide holes of the weight so that the weight falls down steadily avoiding sideways vibrations and hits the upper steel roller at right angles. Oil was regularly brushed on the rods to reduce the friction between the weight and the rods. The flag attached to the weight was fastened with two bolts to prevent the flag from slanting while impacting onto the sample.

The lower steel roller has its two opposite surfaces ground to form a 4-mm wide flat along the length of the cylinder. Two semiconductor strain gauges were stuck to the flats with strain gauge cement. They were connected in series so that the change of

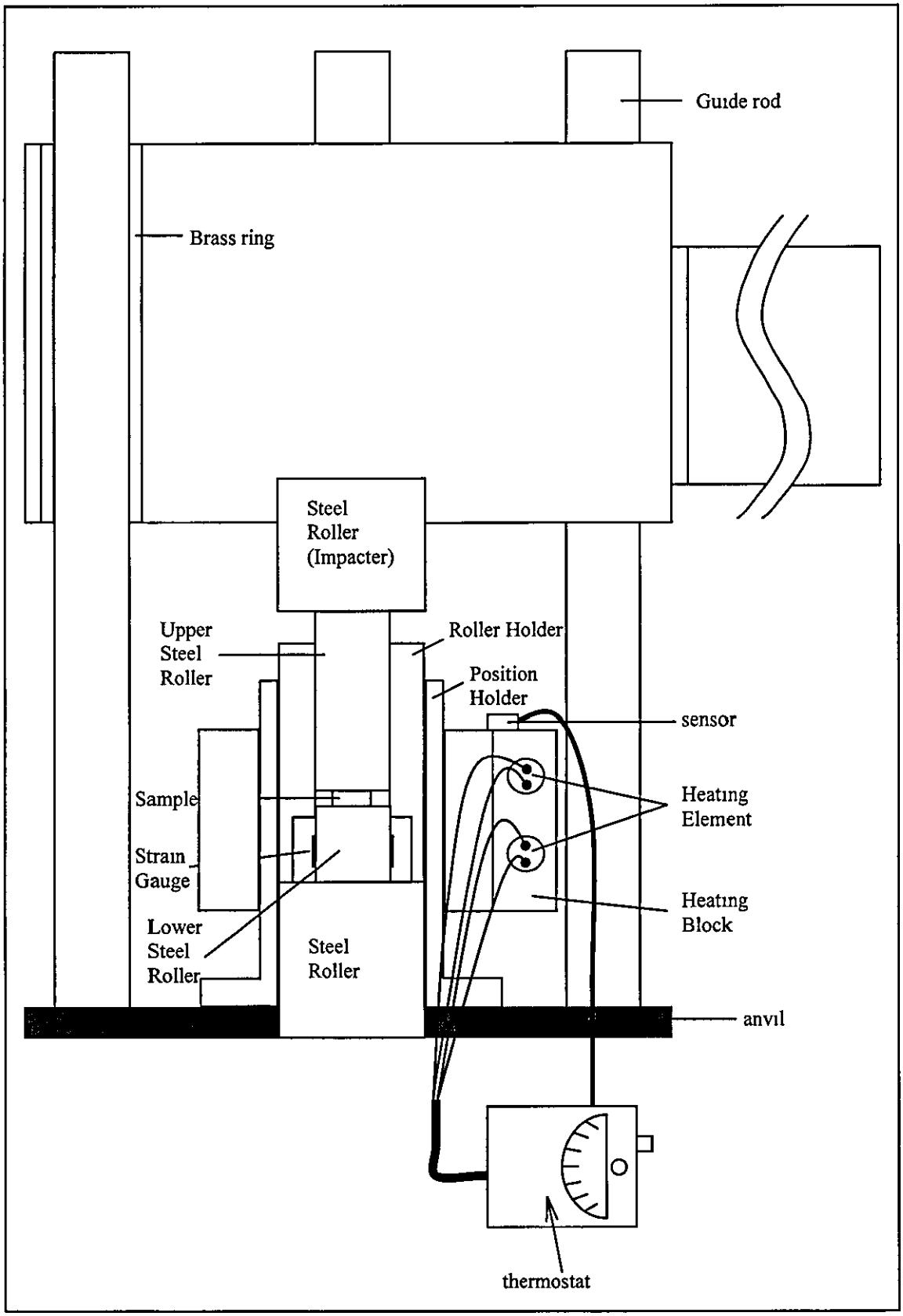

Figure 3.8: Diagram of the Dropweight Machine together with the heating system

the resistance induced in the gauges was due to the compressive stress alone. Any bending forces that cause an increase in the resistance of one of the gauges will be compensated by a decrease in resistance of the diametrical opposite gauge. High temperature resistance wires were used to connect the gauges for the purpose of elevated temperature tests. The gauges were made by Kulite Sensors Ltd type S/UCP-120-090 with each having a resistance of 120 ohm and a gauge factor of 100 ± 5% at 75°F. Semiconductor gauges were chosen because of their small size and because they produce a large output with small-induced strain and so are less prone to EM interference.

In use, the sample was put between the two steel rollers. The weight was dropped from selected heights and the impact force was transferred through the upper roller and compressed the sample. A stress pulse was produced and travelled down to the lower roller that has two gauges attached to it. The magnitude of the stress pulse produced depends upon the physical properties of the specimen. The stress pulse caused a resistance change in the gauges, which resulted in a change in the potential across the 330 Ω series resistor (Figure 3 9). The digital oscilloscope was triggered by this change in the potential. The resulting trace shown on the oscilloscope represented the variation in voltage across the resistor with time throughout the process

The whole system rests on a base consisting of a cast iron anvil weighing 80 kg, which in turn rests on the concrete floor. The system acts very effectively to disperse stress waves and reduce the amplitude of the reflected pulse.

3.3.2 Stress and Strain Analysis

Dawson[6] in 1993 determined the true stress and strain of tested samples from the strain gauge output voltage-time pulse during impact. The voltage was first converted to force and then to velocity by integrating the acceleration-time data The resulting array is subtracted from the impact velocity to give a velocity-time trace for the dropweight. Integration on the velocity-time data gave the displacement of the weight. The impact velocity is defined as the velocity just before impact occurs. In order to measure the impact velocity, a laser beam was split into two parallel beams by reflection from two 45° aligned parallel glass slides vertically displaced from each

other. The beams were shone into two BPX 65 photodiodes 0.9 cm apart. A Gould (DSO) 400 Dual Beam Storage oscilloscope was used to measure the time taken for the weight to drop between two diodes. The impact velocity was calculated as the distance between two diodes divided by the time taken to fall between them. The results were analysed using programs written in BBC Basic.

Hamdan[2] in 1994 used a modified form of the same equipment and calculated the true stress from the strain gauge output voltage. He calculated the true strain from the photodiode output voltage that was generated when a 'flag' attached to the weight passed through a laser beam targeted to a large area photodiode He calibrated the photodiode dynamically by passing the dropweight through the laser beam. The output voltage generated is a trace of voltage against time. He converted the time axis of the output voltage to the displacement axis by multiplying with the velocity of the dropweight while crossing the laser beam. Since the displacement within the photodiode is small, he assumed that the dropweight velocity is constant while crossing the laser beam. He determined the dropweight velocity using Dawson's impact velocity measurement method. However, the dynamic calibrated displacement curve obtained was not linear at the beginning and at the end of the trace but is sufficient to incorporate strain measurement up to 60%. For each experiment, the system was arranged so that the sample displacement was within the linear part of the curve.

Fernandez[3] in 1999 calculated the true stress from the strain gauge output voltage and the true strain from the photodiode signal. He illuminated the photodiode with a laser beam powered with a stabilised 5 V supply. On impact, the flag attached to the weight cut the laser beam and thus induced voltage generated from the photodiode. The photodiode used was a Centronic Large Area 100 mm^2 supplied by RS and the laser was Imatronic LDM 135 Laser Diode Module. He calibrated the photodiode signal by cutting the laser beam with the blade of a digital Mitutoyo calliper and recorded the voltage generated using a digital voltmeter The calibration curve for displacement versus voltage plotted was fitted to a fourth order polynomial that is $y = -1.434x^4 + 6.0151x^3 - 8.2001x^2 + 6.3009x + 0.9408$.

In the current experiments, the true stress and strain were determined from the strain gauge output voltage during impact. It is similar to the Dawson's double integration method except for the impact velocity measurement method. The voltage was converted to force using the strain gauge calibration curve. From Newtons Second Law, F = ma, where m is the weight mass and the acceleration, a, was calculated by dividing F by m. The acceleration was converted to velocity (v) by integrating the acceleration-time data. The impact velocity (v_o) is determined from the array of the velocity (v) at which the applied force is maximum. Subtracting the resulting velocity (v) from the impact velocity (v_o) give a velocity-time trace (v_o-v) for the dropweight. A second integration over the velocity-time (v_o-v) data gives the dropweight displacement that is equivalent to the displacement of the sample being compressed This method avoids direct calculation of the impact velocity from $v = \sqrt{2gH_d}$, where $g = 9.8\ ms^{-2}$ and H_d is the height of the weight from the base as it suffers from a lack of accuracy as the friction between the weight and guided rods is not negligible.

In the current study, the device of laser beam targeted onto the photodiode was adopted in order to monitor the consistency of the functionality of the Dropweight system. In addition, the photodiode signal was also used as an indicator to show the point at which the maximum force took place (Figure 3.10a & 3.10b) For polymers which fractured before yield point (Figure 3.10c), it was used to calculate the impact velocity by converting the voltage into displacement using the calibration curve shown in Fernandez's thesis.

3.3.3 Calibration of Strain Gauge

The strain gauges were calibrated statically by compressing the steel roller onto which the gauges were attached using the Hounsfield H50KM machine up to a force of 50 kN. The gauges were connected in series with a 330-ohm resistor (R1) in a simple measuring circuit. A 15V constant voltage was supplied and stabilised through the voltage stabiliser in the circuit. When the steel roller was compressed, the compressive strain caused a contraction of the gauges As a result, the resistance of the gauges reduced and caused an increase of the voltage across R1. The calibration was carried out at 20 °C, 50 °C and 70 °C. The output voltage across R1 was

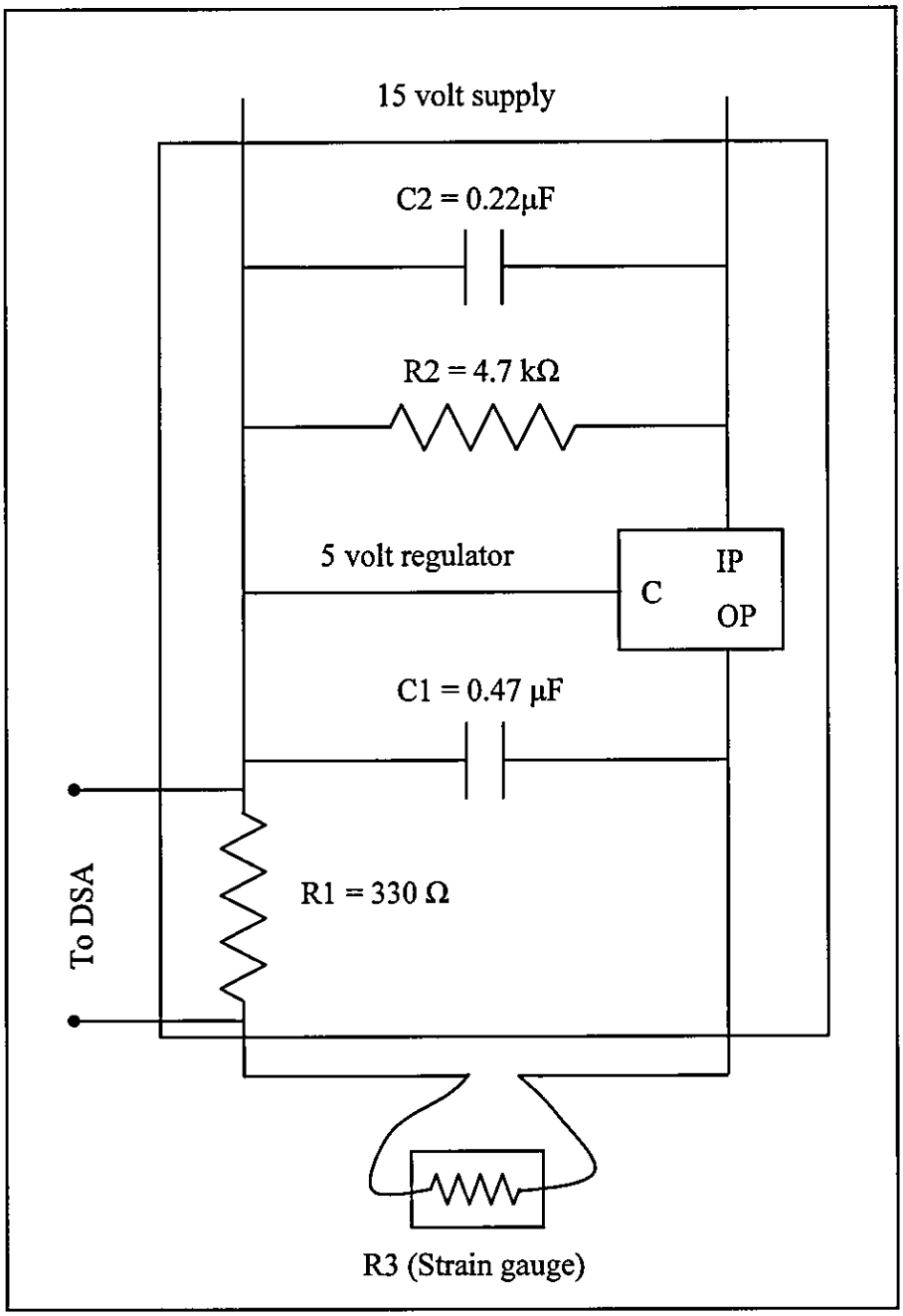

Figure 3.9: Circuit diagram for voltage stabiliser.

(a) Higher strain rate impact

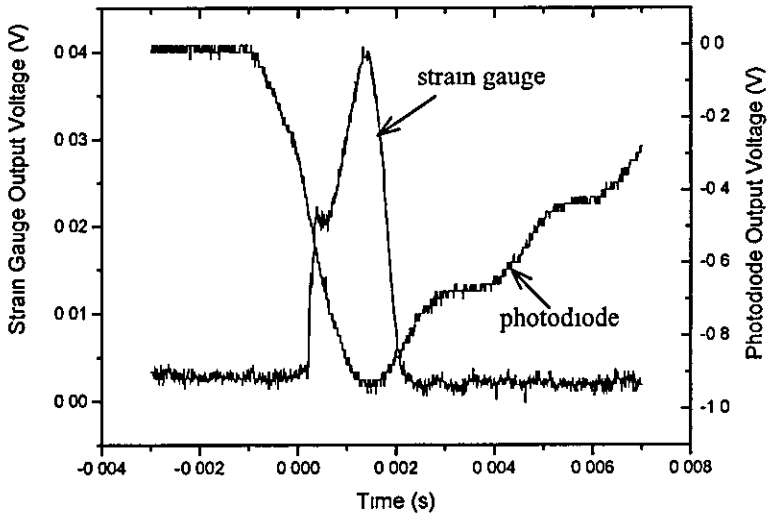

(b) Lower strain rate impact

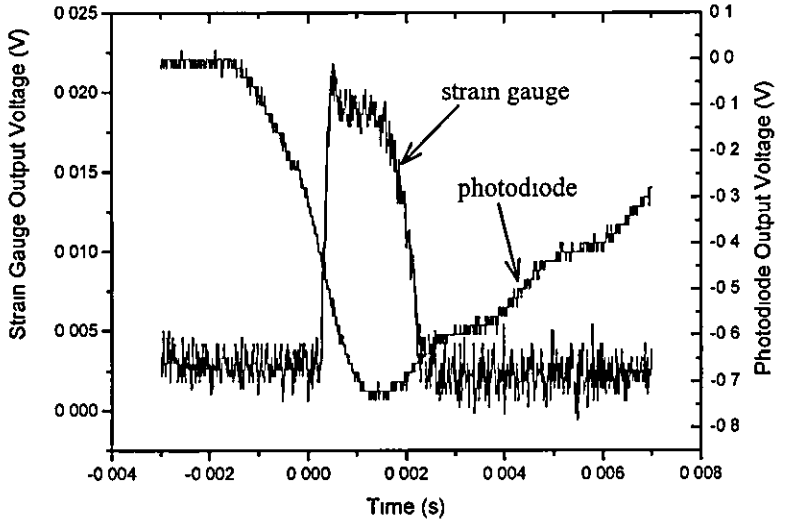

(c) Fracture before yield point

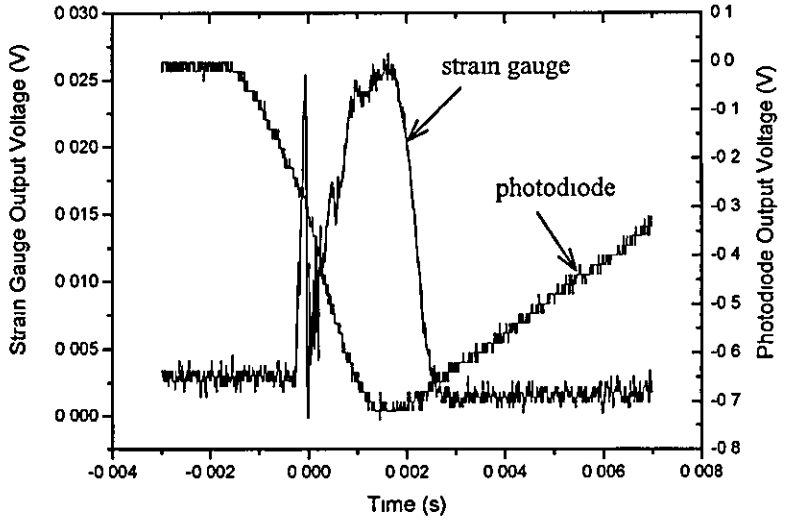

Figure 3.10: Typical curves shown in the Dropweight system due to the different impact condition and the characteristic of the polymer tested.

(a) T = 20 °C (293 K)

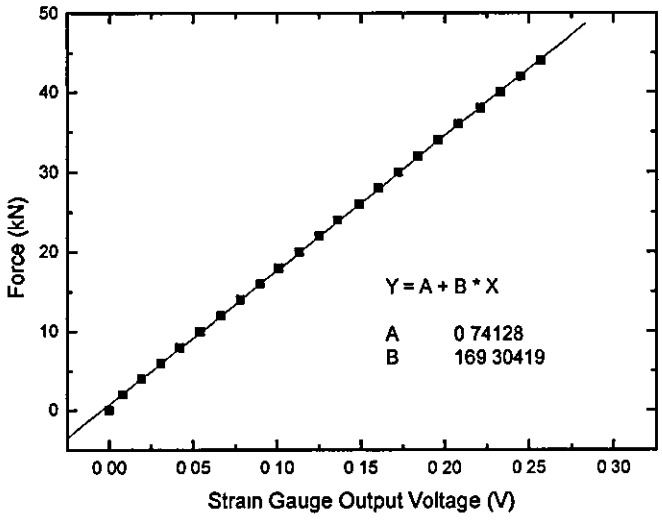

(b) T = 50 °C (323 K)

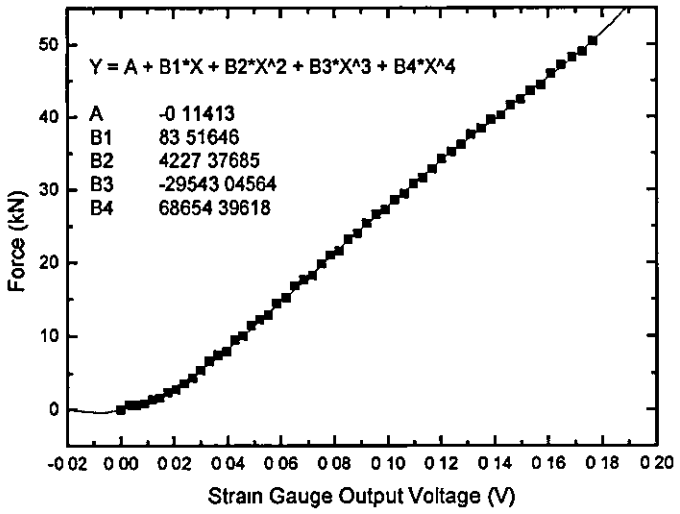

(c) T = 70 °C (343 K)

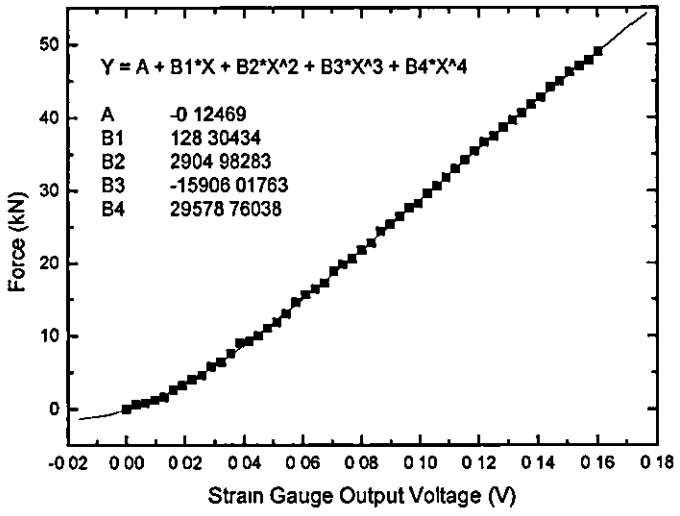

Figure 3.11. Calibration curves for the strain gauge tested at (a) 20 °C (293 K), (b) 50 °C (323 K) and (c) 70°C (343 K).

measured with a digital voltmeter when calibrated at 20 °C and measured with the oscilloscope when calibrated at 50 °C and 70 °C The calibration curves of force versus voltage are plotted in Figure 3.11.

3.3.4 Data Acquisition

The TDS 360 Digital Real Time Oscilloscope was used to record the signals generated from the photodiode and strain gauge. 'Stop after single acquisition' method was used in capturing the signals produced during impact. The trigger point was set on the photodiode channel since the voltage produced from this channel was consistent regardless the height from where the weight was dropped Hence, this assures that the trigger point will not be set out of the signal produced. Normally, the timebase was set at 500 μs, the photodiode channel at 500 mV/div and the strain gauge channel at 10 mV/div during the experiments. The setting of the timebase and the strain gauge channel varied depended on the height the dropweight was dropped.

3.4 Experimental

Two fully amorphous polymers were studied in the current experiments – poly(methyl methacrylate) (PMMA) and polystyrene (PS). Both polymers were purchased from Goodfellow Cambridge Limited. PS was in the form of sheet with thickness 4 mm and PMMA was in the rod with diameter 6 mm. PS was then cut into cylindrical shaped samples with diameter 8 mm and height 3.7 mm and PMMA with diameter 6 mm and height 3 mm. For each experiment, a layer of petroleum jelly as lubricant was applied onto the surface between the sample and the lower and upper steel roller in order to reduce friction during compression.

3.4.1 Elevated Temperature Tests

Samples were tested at the quasi-static rate using the Hounsfield Machine and high strain rate using the Dropweight Machine. For quasi-static tests, PMMA was tested at temperatures of 20 °C (293 K), 38 °C (311 K), 50 °C (323 K), 70 °C (343 K) and 90 °C (363 K), while PS was tested at temperatures of 20 °C (293 K), 50 °C (323 K) and 80 °C (353 K). For each temperature, samples were tested at a range of speeds for the

purpose of the application of Eyring theory and to study the effect of strain rates on the stress-strain curves. At high strain tests, samples of PMMA were tested at 20 °C (293 K), 50°C (323 K), 70 °C (343 K) and 90 °C (363 K); PS at 20 °C (293 K), 50 °C (323 K) and 80 °C (353 K). The dropweight was dropped at different heights in order to obtain a range of strain rates.

For the elevated temperature tests, an aluminium block with two embedded cartridge heaters (400W output power each) was used to heat up the samples to the required temperature. A thermostat that has a range of temperature from 0 to 100 °C was used to adjust the testing temperature to the required one. The input voltage for the thermostat is 240 V. A thermocouple sensor was stuck on the aluminium block to control the required testing temperature. A thermocouple thermometer was used to check the testing temperature set by the thermostat. In all elevated-temperature experiments, the sample was heated for 30 minutes in order to reach thermal equilibrium before testing.

For elevated-temperature tests carried out using the Hounsfield Machine, two steel rollers together with the sample in between were put into the aluminium block and heated simultaneously before testing. The whole heating system was rested on the lower steel platen (Figure 3.2). As for the Dropweight Machine, the aluminium block was put in such a way to enclose the position holder, the roller holder and two steel rollers with a sample in between (Figure 3.8). Thus, the whole unit could be heated simultaneously before testing.

3.4.2 Strain Limited Tests

Strain limited tests were carried out to study how the stress-strain curves and the microstructure of PMMA and PS vary with the strain. They were carried out with the aid of metal rings.

In the Hounsfield system, the tests were limited to four strains, which are 0.2, 0 4, 0.6 and 0.8. Since the thickness of PMMA and PS were 3 and 4 mm respectively, metal rings with eight different thickness were constructed. The thickness of the rings for PMMA were 2.45, 2.00, 1.64 and 1 34; for PS were 3, 2.5, 2.03 and 1.65 in order to

attain the required strain. The rings were placed on the lower steel roller with the sample in the middle. On compression, the upper steel roller would be halted from travelling down by the metal ring when the required strain was reached

In the Dropweight system, the diameter of the lower steel roller to which the strain gauge was glued on is 12.69 mm. On compression, the sample expanded radially. The diameter of the PMMA sample is 6 mm and of the PS 8 mm. Thus, the strain could only be limited to around 30%.

3.5 Data Analysis

The stress and strain are calculated using the spreadsheet in Microsoft Excel. The force output voltages obtained were changed into units of Newtons and then the formulas stated in the Chapter 2 4 were used to work out the stress applied onto the sample during the experiment. The stress and strain data were then transferred to Microcal Origin for plotting.

The force output voltages from the Hounsfield Machine were changed to Newtons by multiplying the maximum force for the range chosen. The displacement of the sample was calculated by putting the voltage obtained into the equation obtained in the displacement transducer calibration curve.

The force output voltages from the Dropweight Machine were changed to Newtons by putting the voltage obtained into the calibration equation obtained. The displacement of the sample was then calculated using the method mentioned in the stress-strain analysis

Fourier Domain Filtering in Jandel PeakFit v4 software was used to filter the signals obtained from the Dropweight Machine. It was also used to filter the signals obtained from the Hounsfield Machine when necessary.

3.6 Results

Graph 3.1(a)-3.1(d) and Graph 3.2(a)-3.2(d) show the stress-strain curves for PMMA and PS tested at strain rates of 0 0006, 0.006, 0.05 and 0.5 s^{-1} respectively using the Hounsfield Machine The tests were carried out at three different temperatures, for PMMA they were 20 °C (293 K), 50 °C (323 K) and 70 °C (343 K) while for PS were 20 °C (293 K), 50 °C (323 K) and 80 °C (353 K).

Graph 3.3(a)-3.3(c) and Graph 3.4(a)-3.4(c) show the stress-strain curves for PMMA and PS compressed to four different strains (0 8, 0.6, 0.4 and 0.2) using the Hounsfield Machine. The tests were carried out at the strain rates and temperatures mentioned above.

Graph 3.5(a)-3.5(c) and Graph 3.6(a)-3.6(b) show the combination of the stress-strain curves of PMMA and PS compressed at quasi-static and low strain rates using the Hounsfield Machine and at high strain rates using the Dropweight Machine at the temperatures mentioned above.

The stress-strain curves for PMMA and PS carried out in a range of strain rates for the purpose of the application of Eyring theory are not shown here. However, the stress at the yield point, 20% and 30% strains are shown in the Chapter 8.

3.7 Discussion

The use of lubricant in reducing the friction between platen and sample is very important Walley et al.[16] carried out dynamic friction measurements between anvil and sample with and without lubricant. They found out that the stress-strain curves were greatly influenced by the present of lubricant. In this study, petroleum jelly was chosen as lubricant to reduce the friction between platen and sample.

From the stress-strain curves, it can be seen that PMMA and PS showed elastic deformation before the yield point. The increase in stress is linearly proportional to the increase in strain except for the initial 1% strain. It is found that the nonlinear

slope shown in the 1% strain region only occurred when the samples were tested at quasi-static rates. The surface of the sample obtained during machining was not exactly flat. During compression, the squashing of the uneven surface and the initial resistance of flow of the whole polymer chains in the radial direction might contribute to the nonlinear slope found at the beginning of the compression. The squashing of the uneven surface causes increase in the applied stress and the initial resistance to flow acted as a dashpot and causes nonlinear increase in the applied stress. At higher rate tests, the speed of compression was fast enough that the effect of the uneven surface and the initial resistance of polymer chains to flow became negligible.

In the elevated temperature experiments, PMMA and PS were tested at a range of temperatures from 20 °C (293 K) to the temperature 20 K below their glass transition temperatures. It was found that PMMA and PS deformed prior to testing when they were tested at a temperature 10 K below their glass transition temperatures. From the DSC tests, the glass transition temperatures for PMMA and PS were found to be 117 °C and 100 °C respectively.

PMMA and PS behaved like ductile polymers when they were tested under quasi-static and low strain rates. At high strain rates, PMMA fractured before the yield point when tested at 20 °C but behaved in a ductile manner when tested at 50 °C and 70 °C. However, PS fractured before the yield point when tested at 20 °C, 50 °C and 80 °C at high strain rates. From the transition temperature tests which had been carried out, it was found that the ductile-brittle transition temperature for PMMA is 45 °C and for PS is 90 °C.[17] Due to this, PMMA showed ductile behaviour when tested at the temperatures 50 °C and above and PS showed brittle behaviour when tested at the temperatures below 90 °C under high strain rates.

For quasi-static and low strain rate tests, the stress-strain curves of PMMA and PS displayed yield point, strain softening and strain hardening before fracture. However, PS showed a sharp drop after the yield point compared to PMMA. This phenomenon is well known for many polymers such as polyethylene, nylon, polytetrafluoroethylene and poly(ethylene terephthalate) when tested in tensile tests. Marshall et al.[8] and Muller et al.[9] suggested that the yield drop might due to softening caused by localised heating during stretching. Vincent[10] suggested that the fall in stress is a geometrical

effect due to the fact that the fall in cross-sectional area during stretching is not compensated by an adequate degree of strain hardening. Brown et al.[11] attributed the drop in the yield point to an intrinsic yield process in the case of compression and shear deformation. They said that the upper yield stress initiated the yielding and the propagation of yielding causes an intrinsic drop in the stress rather than the geometrical effect. Bryant[15] proposed that the increase of a free volume under stress caused yielding.

After the strain softening, the continuous application of stress caused the polymer chains to become oriented towards the direction of flow and induced samples underwent strain hardening. In strain hardening region, the stretching of polymer chains not only involves overcoming Van der Waal's bonds between adjacent chains but also the covalent bonds between the atoms. This caused the flow stress became increasingly greater than the yield stress when strain hardening started to take place in the polymer.

Graph 3.1 and 3.2 shows the stress-strain curves of PMMA and PS tested at three different temperatures. The yield and flow stress decreased when the testing temperatures increased. This effect of temperature on the flow and yield stress of polymers is quite common.[12,13,14]

Graph 3 3 and 3 4 shows that the yield stress of PMMA and PS increased when the strain rate increased. Samples were compressed to four different strains (0.8, 0.6, 0 4 & 0.2) for each strain rate It could be seen that compression at different strains did not affect the stress-strain curves produced Although there was small deviation for the curves compressed at different strains at the same strain rate, it could be due to the temperature variation when compressing the sample. For high strain rate tests, temperature rise obviously occurs in the samples and this causes the actual sample temperatures to differ from the testing temperatures. This is discussed in Chapter 8.

Graph 3 5 and 3 6 are the combination stress-strain curves of high strain rate with quasi-static and low strain rate for PMMA and PS. At high strain rates, it can be seen that PMMA and PS displayed brittle behaviours when tested at temperatures below their ductile-brittle transition temperatures. However, PMMA displayed ductile

behaviour when tested at temperatures above its ductile-brittle transition temperature at high strain rates. For high strain rate tests carried out on PS, the testing temperatures were below its ductile-brittle transition temperature 90 °C. For temperatures above 90 °C, PS deformed after heated for 30 minutes before compression. Hence, experiment was not carried out on PS at temperatures above 90 °C.

The samples tested at 50 °C at 242 s^{-1} and at 70 °C at 318 s^{-1} deformed before strain hardening In order to obtain strain hardening, higher strain rates were required.

3.8 Conclusion

PMMA and PS are fully amorphous. PMMA and PS underwent ductile behaviour when they were tested at quasi-static and low strain rates using the Hounsfield H50KM Machine. However, PMMA and PS fractured before yield when they were tested at high strain rates and at temperatures below their ductile-brittle transition temperature. The ductile-brittle transition temperature for PMMA is 45 °C and for PS is 90 °C.

Similarly to the case of semicrystalline polymers, the yield stress of fully amorphous PMMA and PS increased when the strain rate increased and decreased when the temperature increased. The point where the strain hardening started seemed to be influenced by the strain rate but not by the testing temperature. For samples tested in the Hounsfield Machine, the strain hardening occurred at higher strain when tested at the higher strain rate, however, this phenomena was not consistent when compared with the high strain rate results.

(a) strain rate 0.0006 s^{-1}

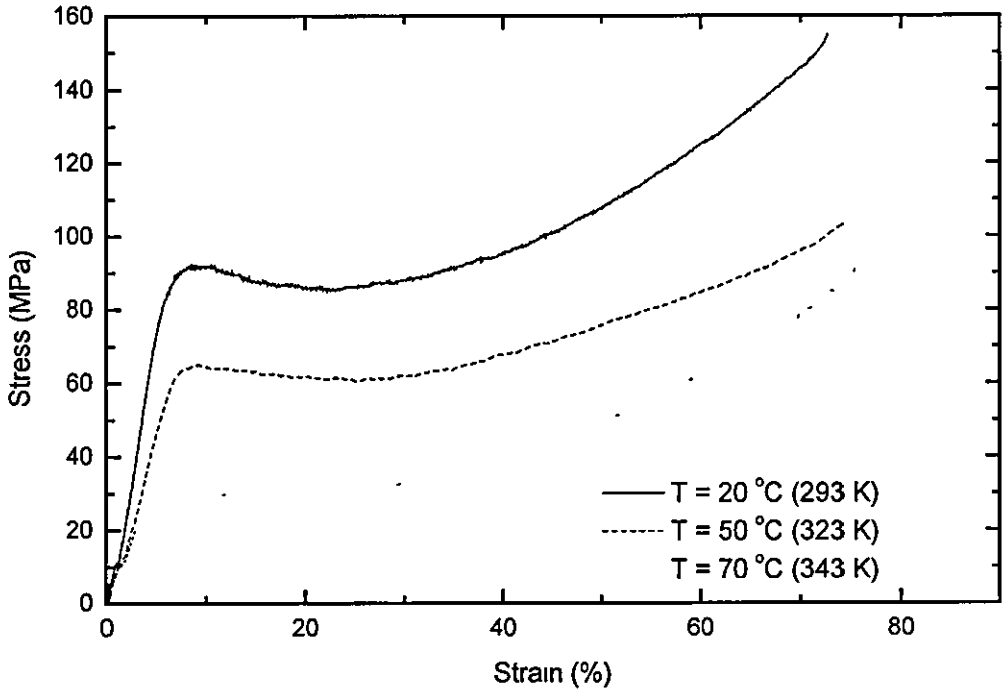

(b) strain rate 0.006 s^{-1}

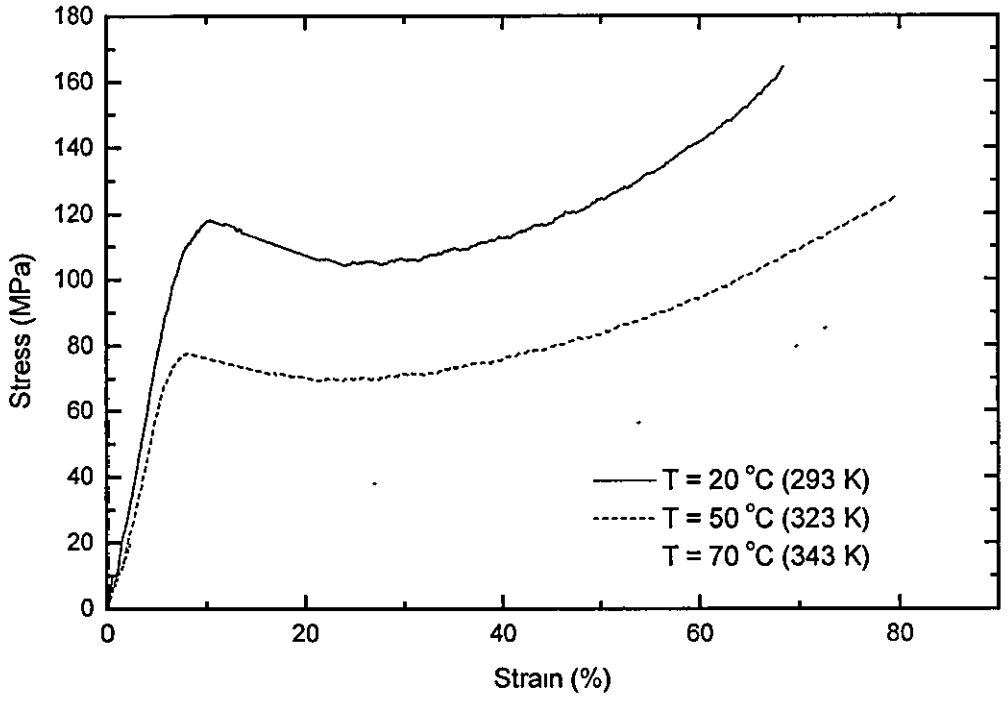

(c) strain rate 0.05 s^{-1}

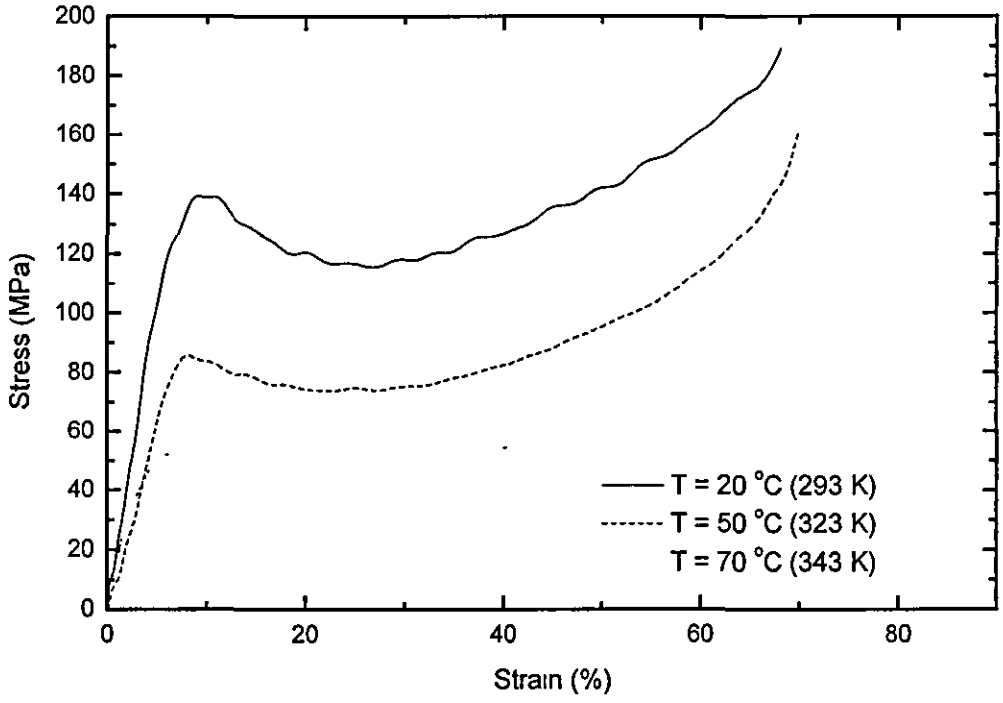

(d) strain rate 0.5 s^{-1}

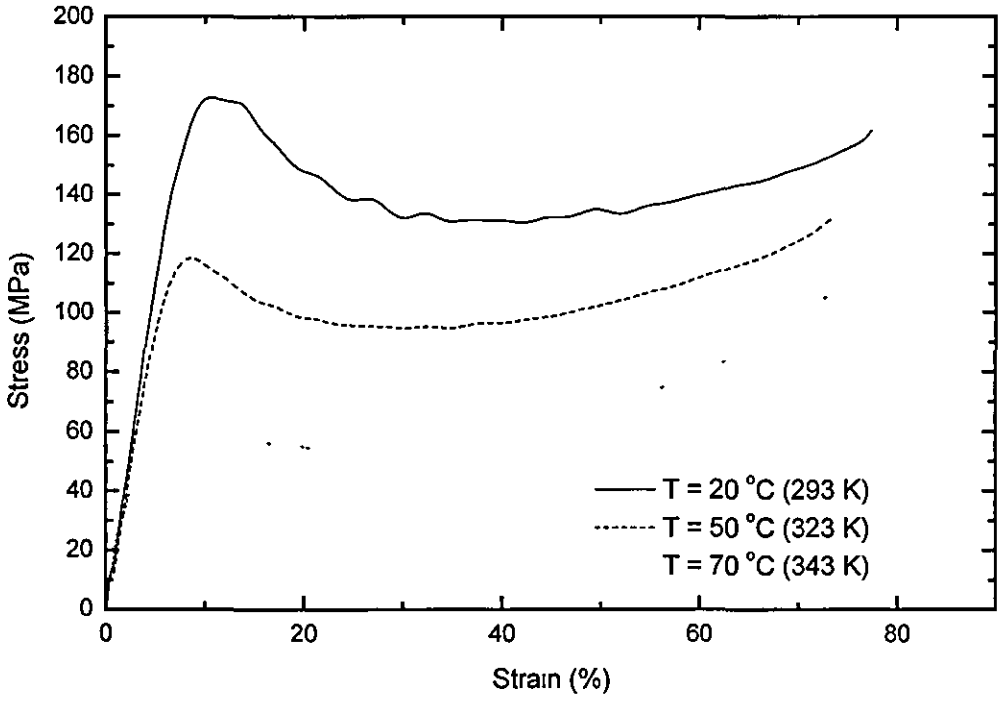

Graph 3.1: Stress-strain curves for PMMA tested at three different temperatures at the strain rates of (a) 0 0006, (b) 0.006, (c) 0.05 and (d) 0.5 s^{-1} using the Hounsfield Machine.

(a) strain rate 0.0006 s^{-1}

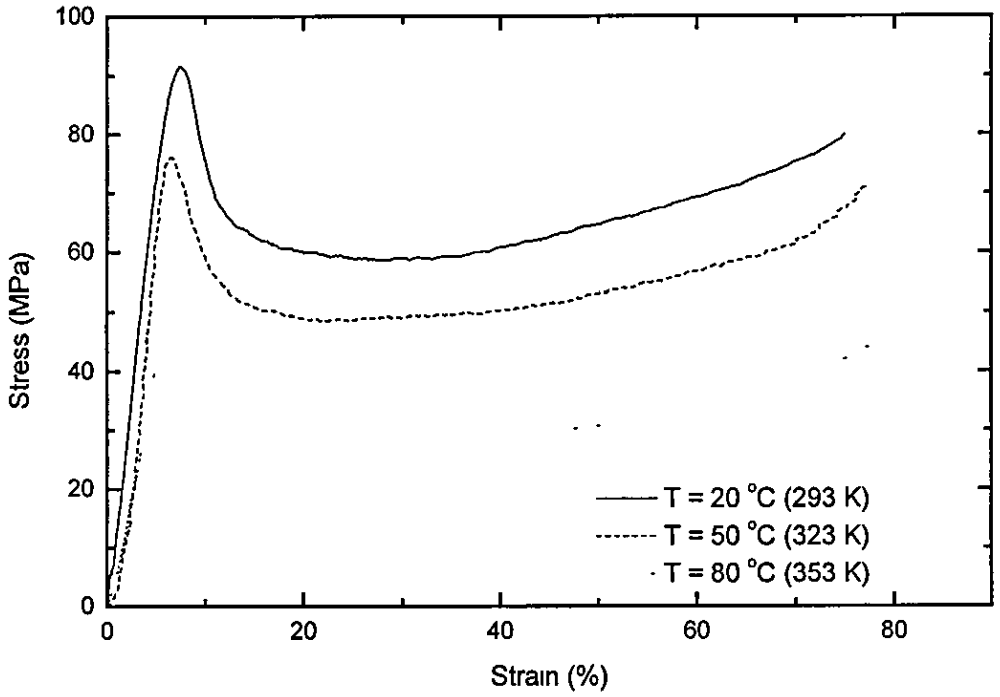

(b) strain rate 0.006 s^{-1}

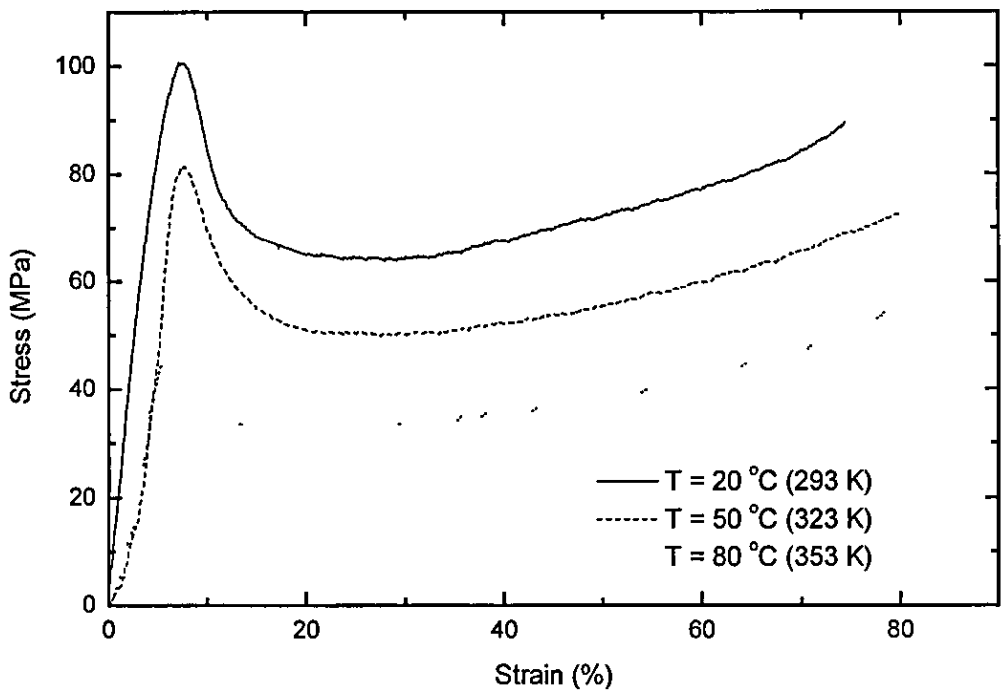

(c) strain rate 0 05 s^{-1}

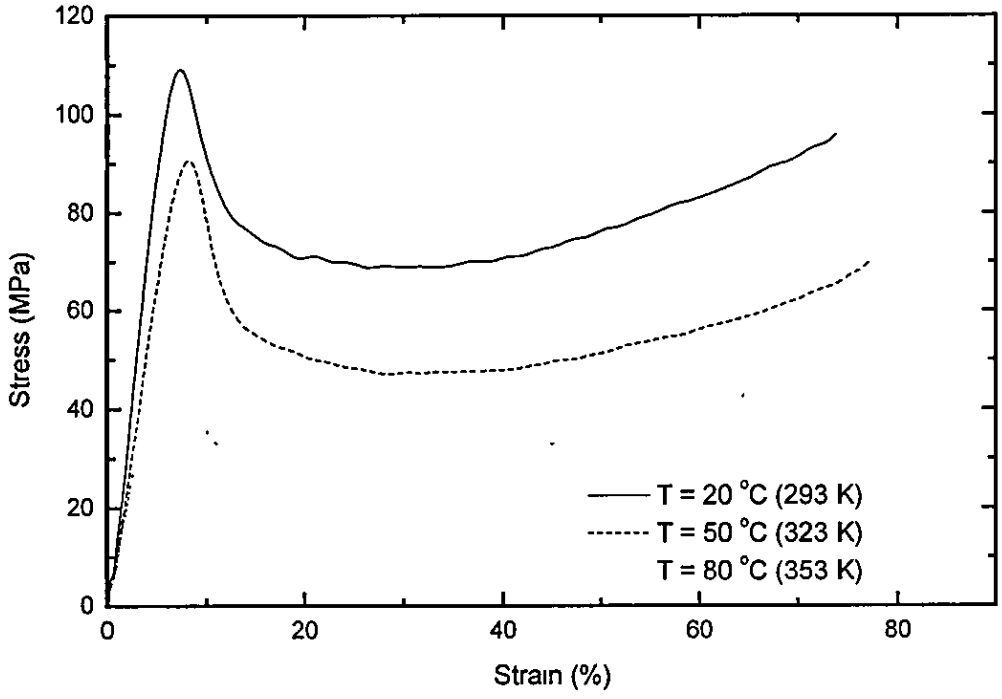

(d) strain rate 0 5 s^{-1}

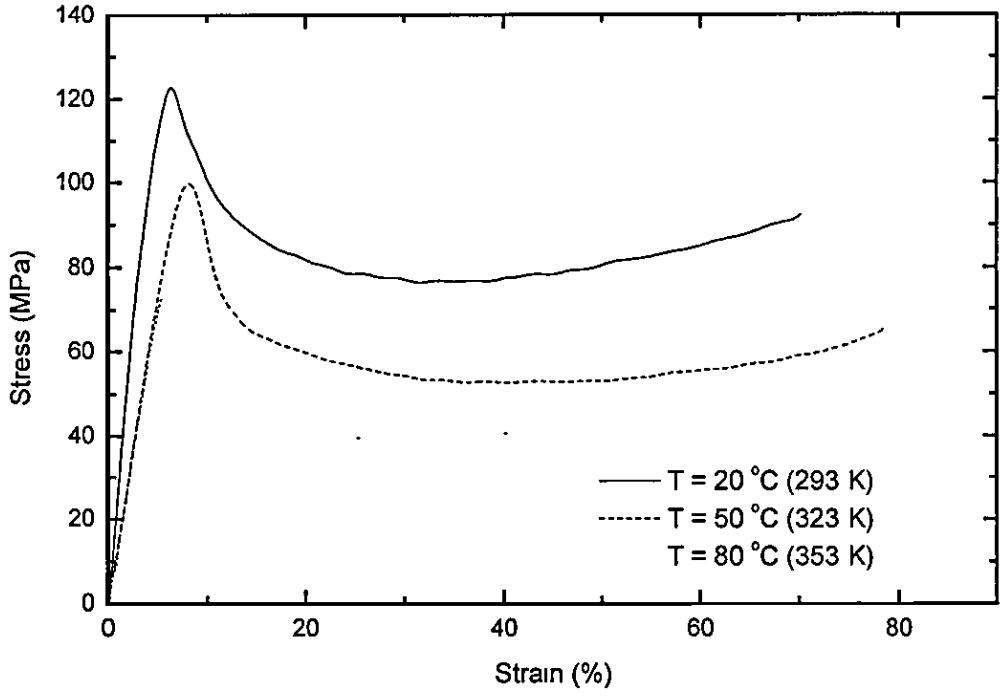

Graph 3.2: Stress-strain curves for PS tested at three different temperatures at the strain rates of (a) 0.0006, (b) 0 006, (c) 0.05 and (d) 0.5 s^{-1} using the Hounsfield Machine.

(a) T = 20 °C (293 K)

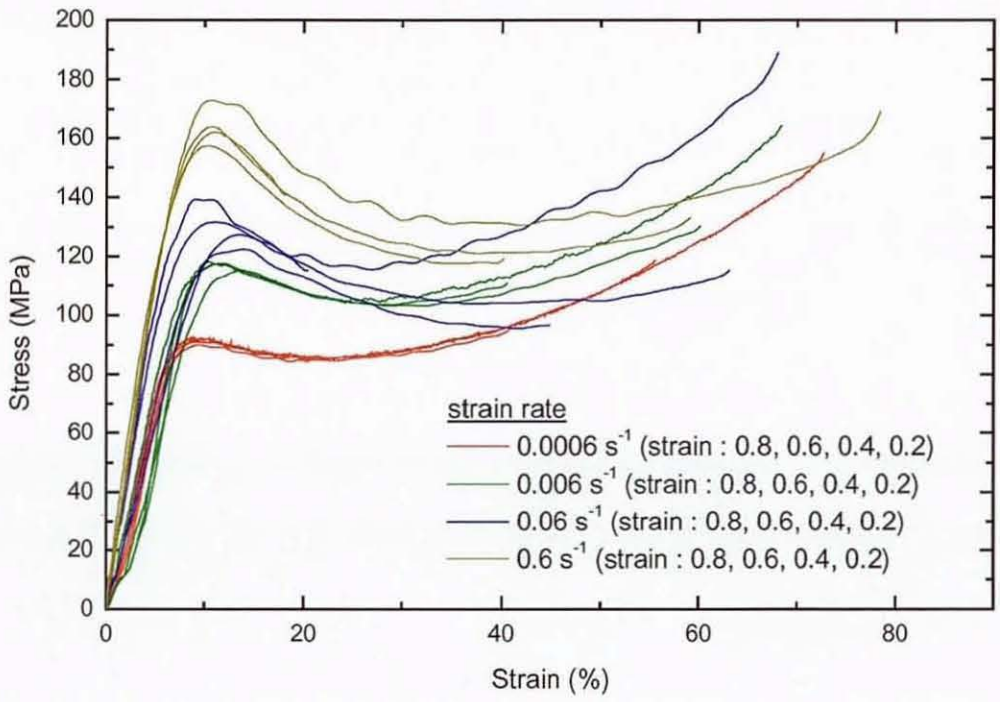

(b) T = 50 °C (323 K)

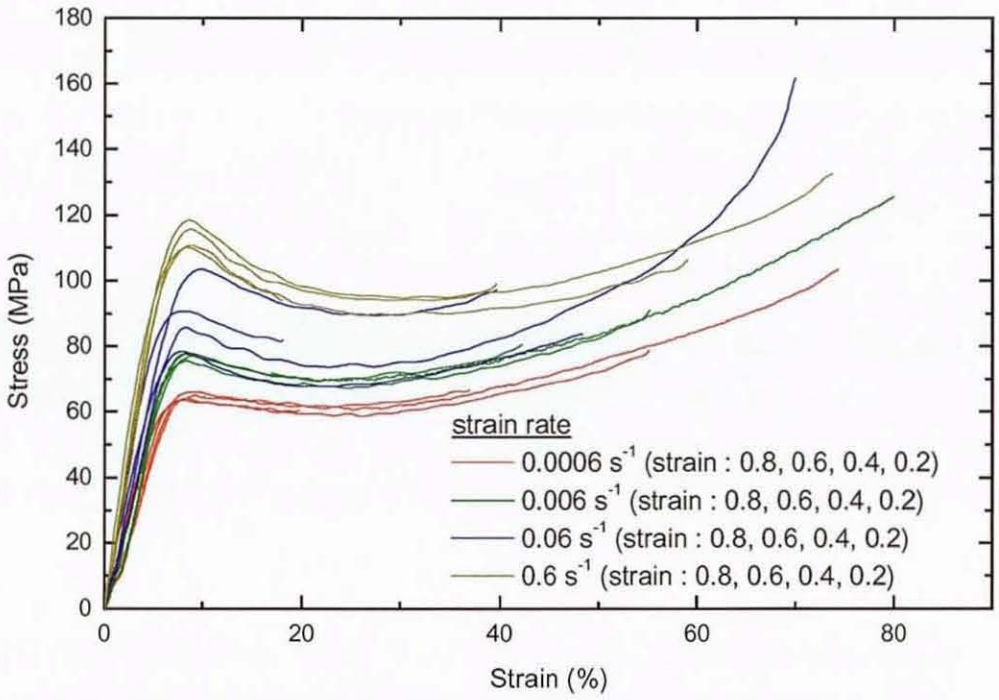

(c) T = 70 °C (343 K)

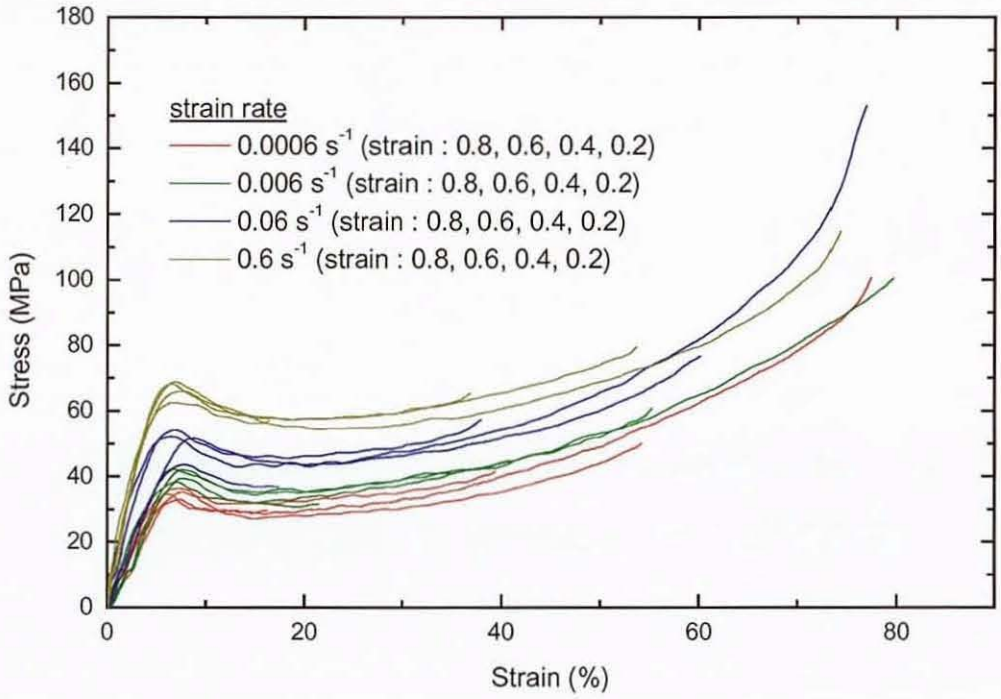

Graph 3.3: Stress-strain curves for PMMA tested at four different strain rates at the temperature of (a) 293, (b) 323 and (c) 343 K using the Hounsfield Machine at the limited strains of 0.8, 0.6, 0.4 and 0.2.

(a) T = 20 °C (293 K)

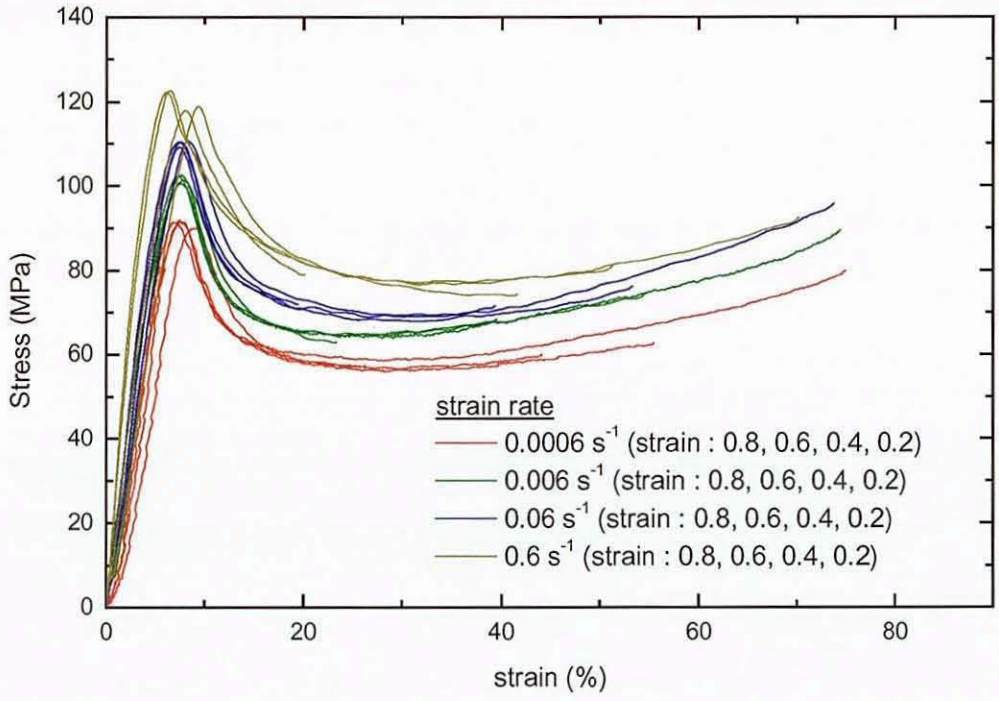

(b) T = 50 °C (323 K)

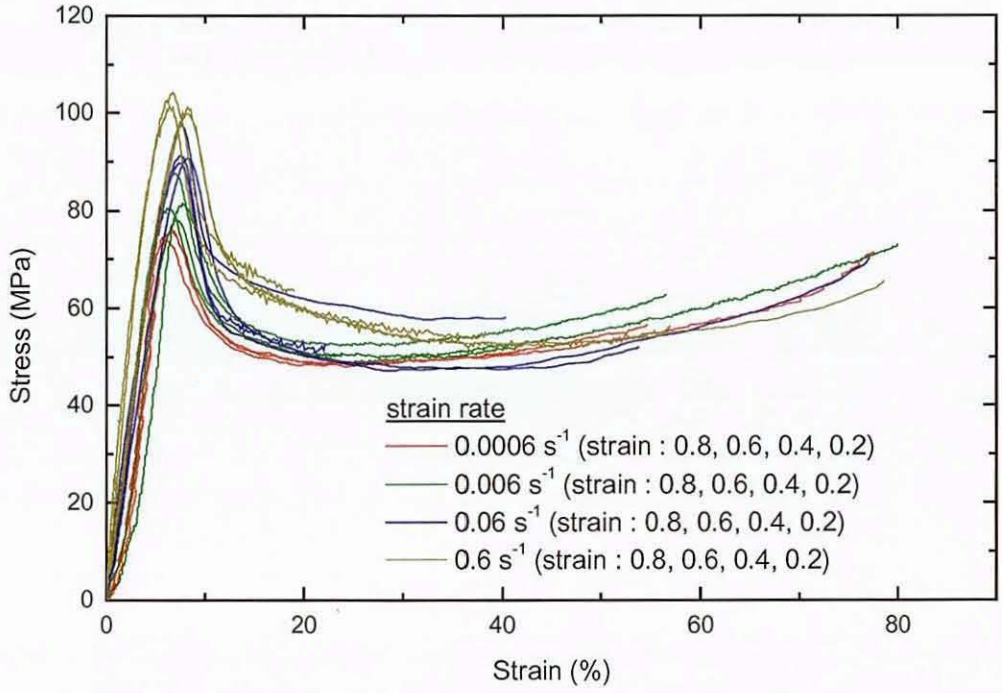

(c) T = 80 °C (353 K)

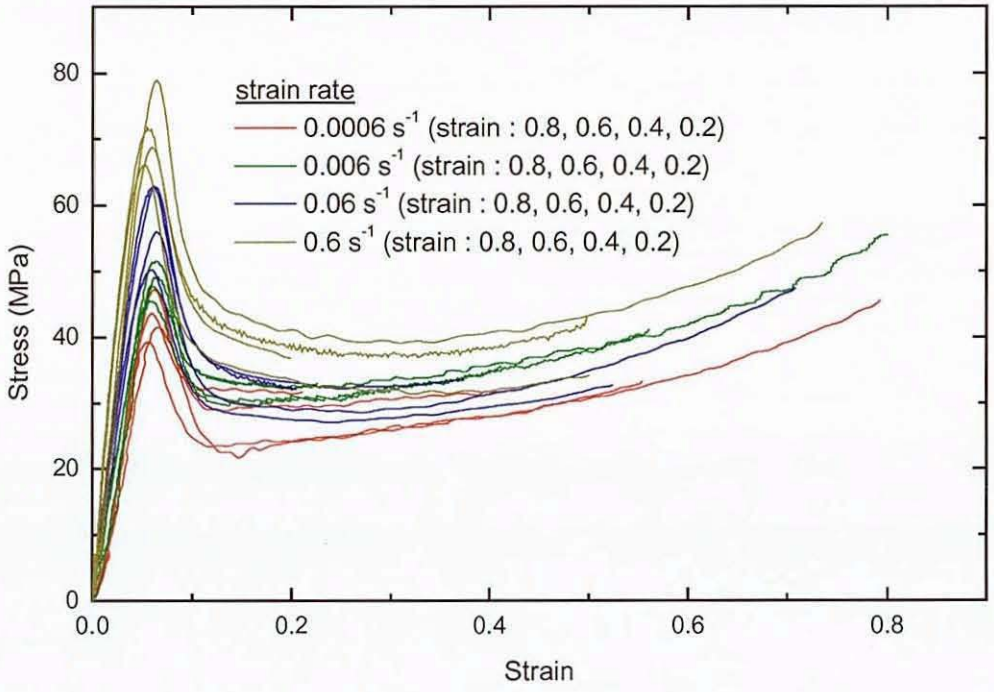

Graph 3.4: Stress-strain curves for PS tested at four different strain rates at the temperature of (a) 293, (b) 323 and (c) 343 K using the Hounsfield Machine at the limited strains of 0.8, 0.6, 0.4 and 0.2.

(a) T = 20 °C (293 K)

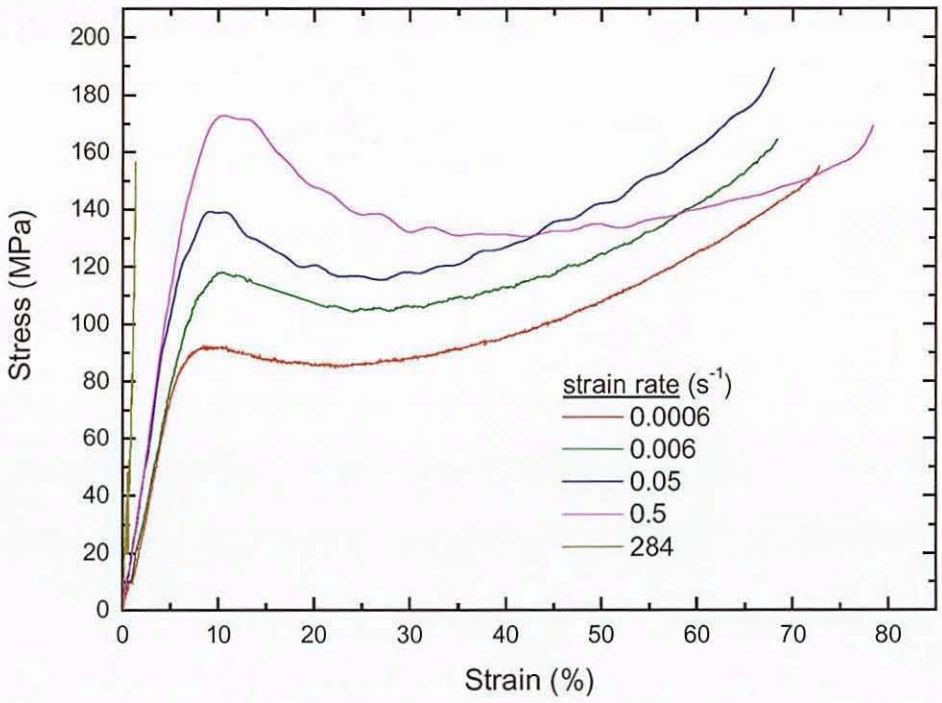

(b) T = 50 °C (323 K)

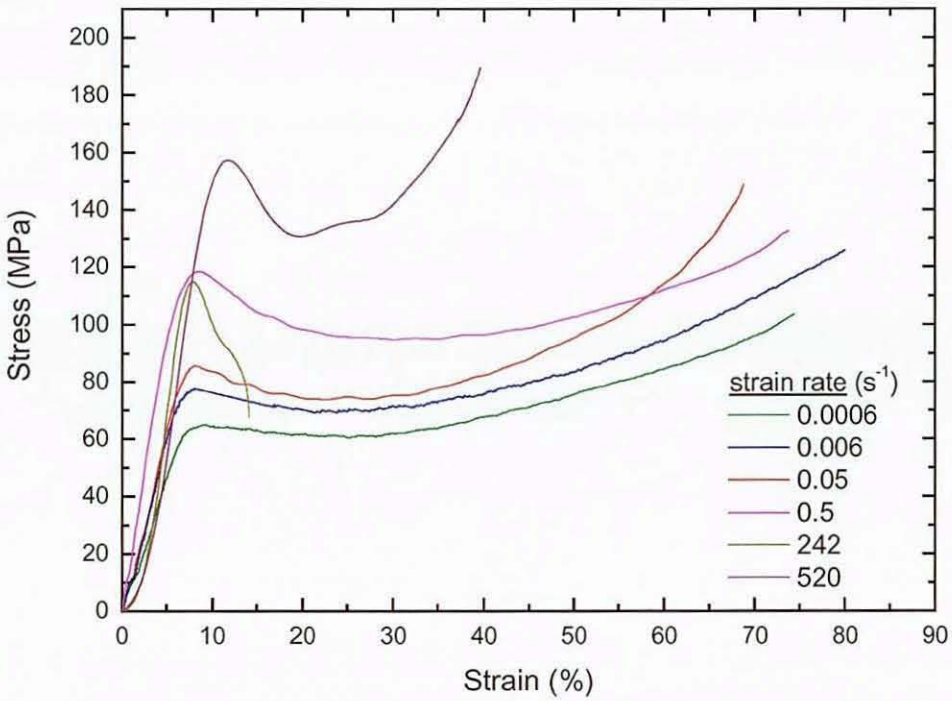

(c) T = 70 °C (343 K)

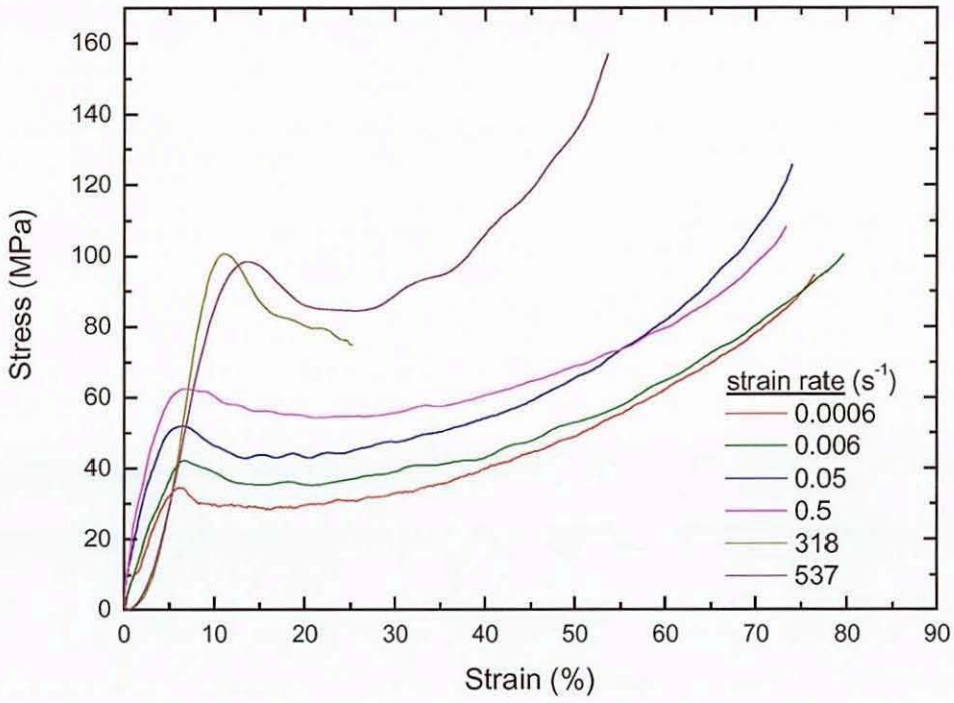

Graph 3.5: Stress-strain curves for PMMA tested using the Hounsfield Machine (strain rates : 0.0006, 0.006, 0.05, 0.5 s^{-1}) and the Dropweight Machine (strain rates : (a) 284, (b) 242, 520 and (c) 318, 537 s^{-1}) at the temperatures of (a) 293, (b) 323 and (c) 343 K.

(a) T = 20 °C (293 K)

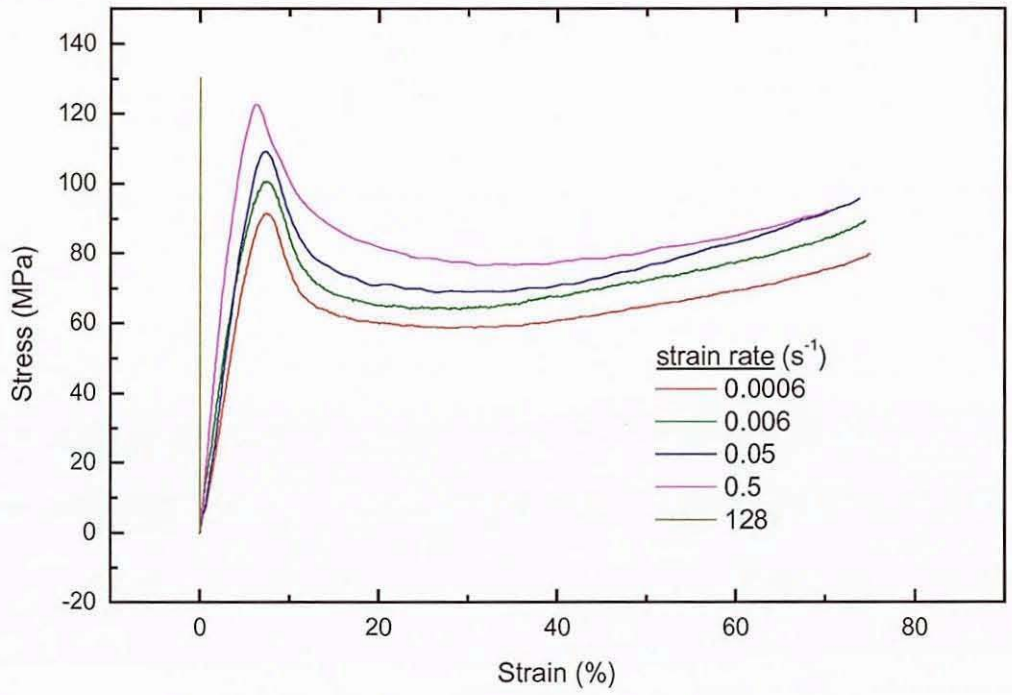

(b) T = 80 °C (353 K)

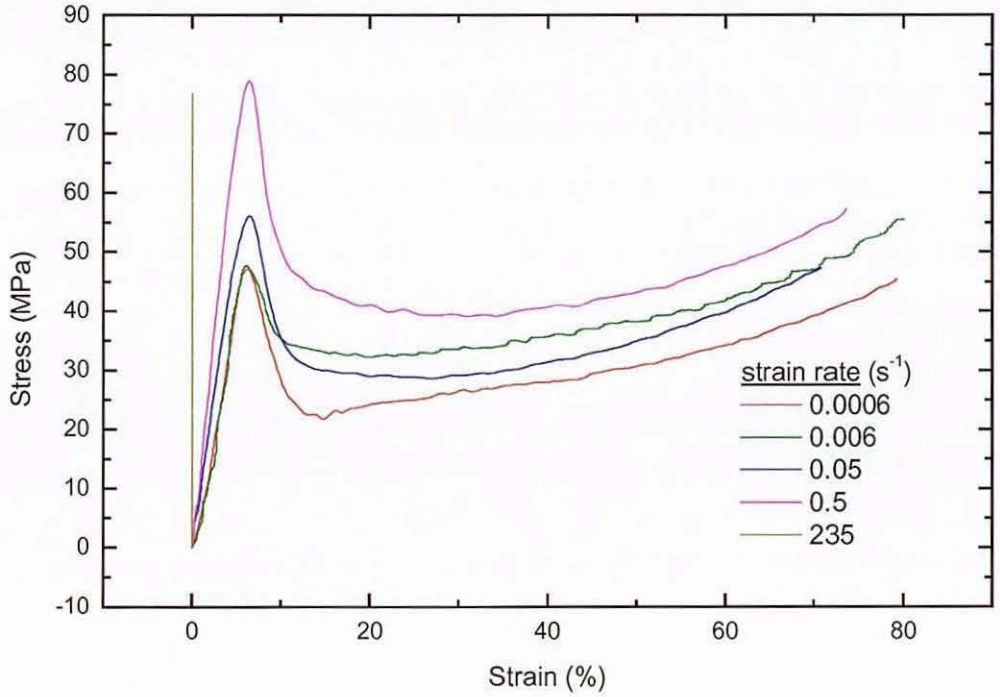

Graph 3.6: Stress-strain curves for PS tested using the Hounsfield Machine (strain rates : 0.0006, 0.006, 0.05, 0.5 s^{-1}) and the Dropweight Machine (strain rates : (a) 128 and (b) 235 s^{-1}) at the temperatures of (a) 293 and (b) 353 K.

Appendix 3.1: Specification of The Pico ADC-100.

Resolution	12 bits
Number of input channels	2
Input voltage ranges	software selectable: ±20V, ±10V, ±5V, ±2V, ±1V, ±500mV, ±200mV [±100mV, ±50mV accuracy not guaranteed] manually selectable: AC/DC
Maximum sampling rate	depends on computer: 120k samples per sec on 486/66 100k samples per sec on 386/33 30ksps on 8086/20
Repeatability	±4lsb at 25°C
Absolute accuracy	±1% typical at 25°C ±3% worst case over operating temperature range
Overvoltage protection	±200V
Input impedance	1MΩ
Input connectors	2xBNC
Output connector	25 way male D-type to computer printer port
Power requirements	No power supply required
Environmental conditions	0 to 70°C 0 to 95% humidity NOT water resistant

Appendix 3.2: How to Record Data using PICOLOG Software?

C \PICO> PICOLOG

↓

MAIN MENU

Collect data (new or repeat run) ↵

↓

COLLECT MENU

Define new run ↵

↓

DEFINE NEW RUN

Filename·

F10-Accept

↓

EDIT SAMPLING RATE

Sampling Interval:

Units:

Max samples·

F10-Accept

↓

EDIT CHANNEL

Channel A unused

Channel B unused

↓	↓
Edit Channel	Edit Channel
Channel A:	Channel B:
Channel name: Force	Channel name: Displacement
:	:
Measurement mode·	Measurement mode:
	:
Total sampling time	Total sampling time:

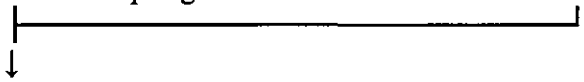

↓

EDIT CHANNEL

Force

Displacement

Esc

↓

COLLECT MENU

Start collecting ↵

Appendix 3.3: How to Display Data using PICOLOG Software?

COLLECT MENU

Add or Edit reports ↵

↓

EDIT REPORT

Name:

Format

F10-Accept

↓

EDIT Y VS TIME GRAPH

Title:

:

F10-Accept

↓

COLLECT MENU

Display report ↵

Format:

Monitor

Tabulation

Y vs time graph

X vs Y graph

References

1. Hounsfield Test Equipment H50KM Operating Instructions manual

2. **S. Hamdan,** PhD Thesis 1994, "The Thermomechanical Properties of Aromatic Polymers", Department of Physics, Loughborough University, Loughborough, UK.

3. **J. O. Fernandez Lorences,** PhD Thesis 1999, "Crystallinity Changes in PET and Nylon 11 with Strain, Strain Rate and Temperature", Department of Physics, Loughborough University, Loughborough, UK.

4. PICOLOG Data Logging Software User manual, Pico Technology Limited, Broadway House, 149-151 St Neots Road, Hardwick, Cambs CB3 7QJ United Kingdom.

5. **N. S. J. Al-Maliky,** PhD Thesis 1997, "Strain Rate Behaviour of Thermoplastic Polymers", Department of Physics, Loughborough University, Loughborough, UK

6. **P. C. Dawson,** PhD Thesis 1993, "The Mechanical and Thermal Behaviour of Polymers under High Strain Rate Compression", Department of Physics, Loughborough University, Loughborough, UK

7 **J. E. Field, G. M. Swallowe, P. H. Pope and S. J. P. Palmer,** Institute of Physics Conference, serial no. 70 (1984) 381~388

8 **I. Marshall and A. B. Thompson,** Proceedings. Royal Society of London A **221** (1954) 541~562

9. **F. H. Müller and K. Jäckel,** Kolloid Zeitschrift **129** (1952) 145

10. **P. I. Vincent,** Polymer **1** (1960) 7~19

11. **N. Brown and I. M. Ward,** Journal of Polymer Science: Part A-2, **6** (1968) 607~620

12. **R. W. Truss, P. L. Clarke, R. A. Duckett and I. M. Ward,** Journal of Polymer Science **22** (1984) 191~209

13. **L. H. Lee, J. J. Vanselow and N. S. Schneider,** Polymer Engineering and Science **28** (1988) 181~187

14. **S. Hellinckx and J. C. Bauwens,** Colloid & Polymer Science **273** (1995) 219~226

15. **G. M. Bryant,** Textile Research Journal **31** (1961) 399

16. **S. M. Walley, J. E. Field, P. H. Pope and N. A. Safford,** Philosophical Transactions. Royal Society of London **328A** (1989) 1~33

17. **H. F. Mark, N. M. Bikales, C. G. Menges and J. I. Kroschwitz,** "Encyclopedia of Polymer Science and Engineering", Second edition, Wiley, 1987

Chapter 4
High-Speed Photography

4.1 Introduction

High-speed photography, which has been developed since the 19th century, has been widely employed to study ballistic impact, dynamic fractures of materials subjected to forces, explosion initiation and many other transient events.

Paisley (1993) defined high-speed photography as " recording optical or electro-optic information fast enough for an event to be temporally evaluated with resolution that satisfies the experimenter".[2] The definition was then modified by Fuller (1994) as "recording optical or electro-optic information with adequately short exposures and fast enough framing rates for an event to be evaluated with a temporal and dimensional resolution which satisfies the experimenter" to cover resolution aspects.[3]

The first person who developed the method of high-speed photography was W. H. F. Talbot in 1852.[4] He used a short duration, high intensity light released from a Leyden jar, which was the predecessor of the capacitor, to illuminate moving objects. He carried out the photographic technique in a darkened room with the camera shutter open. By installing a page of newspaper on a drum which could be rotated at high speed, he managed to photograph a small area of the fast moving print when the page surface was illuminated by the spark. Since then, research into high-speed photography (e.g. high-speed cameras, photographic recording technique, light sources and types of films) had been extensively carried out by a lot of workers.

The outbreak of World War II in 1939 initiated the demand for high-speed cameras to record micro and nanosecond events happening in ballistics and detonics. At that times the cameras developed could only achieve the maximum speed of ~ 8000 pps (Fastax cameras) and did not provide fast enough exposures or fast enough framing rates and their long recording periods were not suitable for these kinds of applications Hence, new photographic techniques such as rapid rotating drum and rotating mirror

cameras were developed. The rapid rotating drums allowed framing rates up to 220 000 pps for a period of 250 μs. In a single rotation of the drum discrete successive images were recorded on the film attached to the peripheral surface of the drum. The rotating mirrors allowed framing rates up to 2 x 10^6 pps and were used to study nuclear explosions and could be used in streak and framing modes.

The advantage of the high-speed photography is that it provides detailed visual information about the whole deformation process of a sample under impact. Therefore, it was adopted in this work as one of the methods to study the energy of fracture, temperature rise and the fracture mode of poly(methyl methacrylate) (PMMA) and polystyrene (PS).

4.2 High-speed Photographic System

The high-speed photographic system consisting of the A W R E. C4 camera combined with a Dropweight and a transient light source generation system were adopted in the current study. The schematic diagram of the high-speed photographic system is shown in Figure 4.1.

4.2.1 A.W.R.E. C4 Camera

The operation of the Atomic Weapon Research Establishment (A W R E.) C4 camera is shown in Figure 4.2. On entering the camera, the parallel light from the C4-Camera Dropweight is focused by the focussing lens in front of the C4 camera The focused light is then split into two directions by a beam splitter onto a pair of plane mirrors that reflects the light onto the rotating mirror. The light from the rotating mirror is then focused onto the arc of the film by framing lenses Therefore, the deformation of the sample can be viewed as individual sharp dark images on the films in the C4 camera. There are two film tracks in the C4 camera with 70 frames in each track. For each experiment carried out, two rolls of films in curved strips were laid out in the two film tracks. The film has a radius of curvature of 5.3 m. Since the C4 camera operates with a rotating mirror to reflect the light onto the films, a proper selection of

the mirror rotation speed is essential to allow the whole events of an impact to be recorded into a series of 140 frames in one exposure.

The rotating mirror is driven by an electric motor via a belt with the rotation speed controlled by a variac. The mirror rotation speed was calibrated by shining a light beam from a torch onto a silvered portion of the shaft the rest of which was painted black. The reflected light pulse was then captured by a silicon photodiode with integrated amplifier that fed into a TDS 306 Digital Real Time oscilloscope (Figure 4.3). Figure 4.4 shows the light pulse signals of variac setting of 35. The duration for a full rotation is the time taken from one major peak to the next major peak, whereas the duration of half rotation, which is the duration of 140 frames, is from one major peak to the next minor peak. The same type of photodiode is also used to measure the flash duration at each experiment. Table 4.1 shows the calibrated rotation speed for each variac number.

Optic-Clean Polymer was used to clean the mirrors in the C4 camera. It is a denatured ethyl alcohol-based solution. It forms mechanical bonds with contaminants on the mirror surface. The polymer layer shrinks when it dries and mechanically picks up contaminants on the surface.

4.2.2 C4-Camera Dropweight

The C4-Camera Dropweight diagram is shown in Figure 4.5. The guided cylindrical dropweight can be adjusted to drop freely from a selected height. On hitting the sample, the impact energy is transferred to the sample. The deceleration of the weight during impact is measured with an accelerometer coupled to the weight. The deformation process of the sample is photographed in transmitted light.

The flash trigger switch consists of a simple contact system with its positive point connected to a spring steel strip screwed to a wooden spacer that is fastened onto the anvil. Its negative point is fixed to the anvil. The wooden spacer acts as an insulator between the positive and negative point A metal pin was screwed into the weight. On the falling of the weight, the metal pin touches the spring steel strip to complete

the electrical contact. The height of the spring steel strip is adjustable and was set such that the pin touches it before the weight strikes the sample.

The weight was hollowed out in an L shape. A mirror put at the corner of the hollow at 45° reflects the parallel horizontal light from the flash tube to a parallel vertical light. The parallel vertical light passes through the upper and lower glass cylinders. A prism in the cast iron anvil reflects the parallel vertical light to horizontal and into the C4 camera. The upper glass cylinder that acts as an impactor is held in the bottom recess of the weight. The sample is positioned on the lower glass cylinder.

Basically, there are two phenomena that effect the accelerometer signal:

(1) The dropweight vibrates when hitting the sample. The high frequency vibrations together with the dropweight deceleration are sensed by the accelerometer during the sample deformation Due to this, the signal recorded by oscilloscope is the coupling of the high frequency vibrations and the accelerometer signal (Figure 4.6). In order to reduce the coupling, a cylindrical steel block with half of the dropweight height was put on top of the dropweight with the idea to break the weight vibrations from reaching the accelerometer during impact. The steel block was stuck onto the dropweight with a layer of glue to prevent it from bouncing up and down in a large magnitude when the dropweight hits the sample. In this case, the force exerted on the sample will become uneven; one moment with the force from the steel block and the dropweight and another moment reduced to just from the dropweight. Hence, with a layer of glue, this effect could be reduced.

The height of the dropweight is 9 4 cm and the steel block is 5 cm. The sound speed in the steel is 5960 ms^{-1}. On hitting the sample, the vibrations transferred from the dropweight to the steel block. The steel block then vibrated on the top of the dropweight. For vibrations that bound back from the steel block to the dropweight would take around 64 μs (distance: 9.4 + 5 + 5 + 9.4 + 9.4cm) to reach the accelerometer. In addition, the layer of glue could act as a sponge to attenuate the amplitude of the vibrations. Figure 4 7 shows the signal recorded after putting the steel block on the top of the dropweight.

It can be seen that less coupling of the high frequency vibrations on the signal was found. The total weight of the dropweight together with the steel block is 8.25 kg.

(ii) The flash tube must be insulated properly from the earth. Any contact with the earth generates a spark in the air. The spark will be detected by the accelerometer channel as electrical signals and thus disturb the accelerometer signal recorded by the oscilloscope (see Figure 4.8).

Two RS Cartridge heaters connected to a RS thermostat were implanted in the anvil. The range of the thermostat is from 0 to 100°C. A sensor from the thermostat was stuck onto a glass plate to control the testing temperature.

4.2.3 Transient Light Source Generated System

A 12V100W projection lamp controlled by a variac (0-240 V, 2.5 A) through a transformer is used to aid focusing of sample images on the arc of the film in the C4 camera by simulating the light from the flash tube. This is achieved by using a plane-convex lens to image the lamp onto the flash tube. In the experiment, the lamp image was replaced by the flash tube.

An Elevam MFT 218 Xenon flash tube was used to produce light in the high-speed photographic experiments. The characteristic of the Xenon flash tube and the circuit diagram of the trigger box are stated in Hamdan's thesis.[1] Its rise time and light duration in the circuit used are 420 μs and 4520 μs respectively.

Figure 4 9 shows a simple circuit explaining the concept of how the flash tube is triggered. The transformer T represents the motor coil used in the experiment. The capacitor C in the simple circuit represents the capacitor box in Figure 4 1. The capacitor box consists of four capacitors with 125 μF each and can be charged up to a maximum of 2.5 kV. The maximum flash voltage for the Xenon flash tube is 1.05 kV. Hence, in the experiment the capacitor box is changed up to 1 kV voltage. Before it discharges between the flash tube electrodes to produce light, the tube is triggered with higher voltage to induce ionisation. By closing the switch S1, the capacitor CT

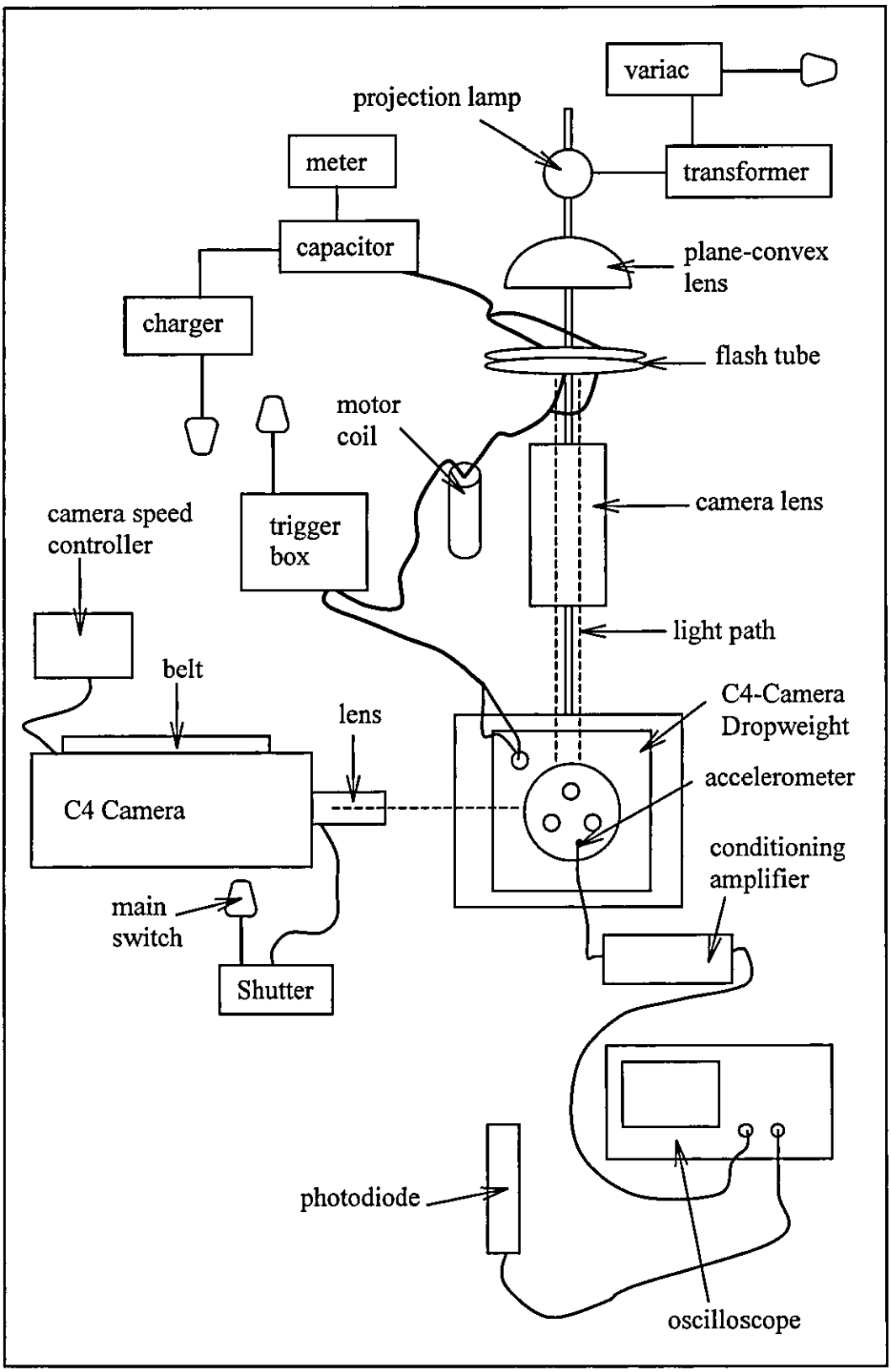

Figure 4.1: Schematic diagram of the high-speed photographic system

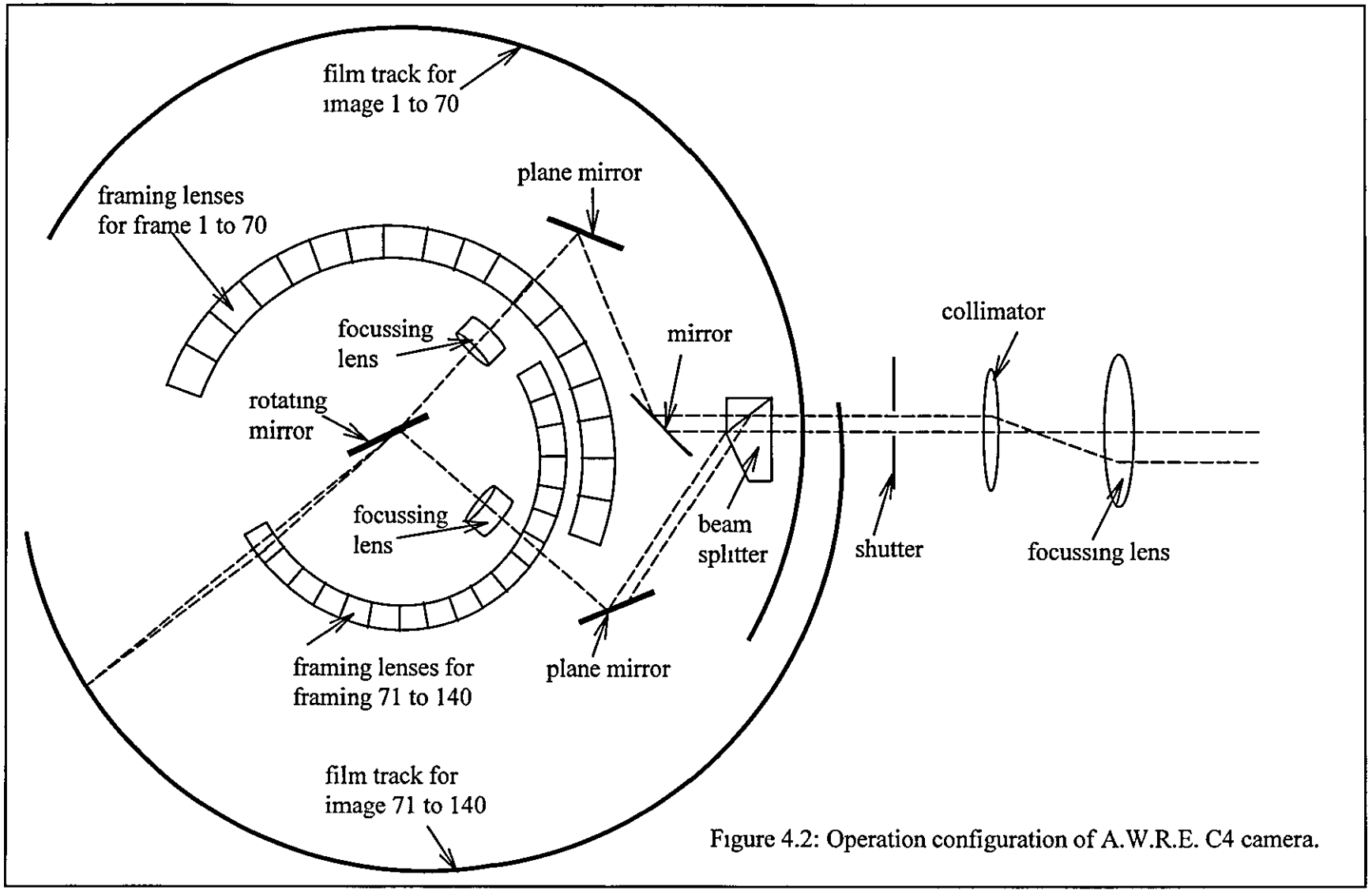

Figure 4.2: Operation configuration of A.W.R.E. C4 camera.

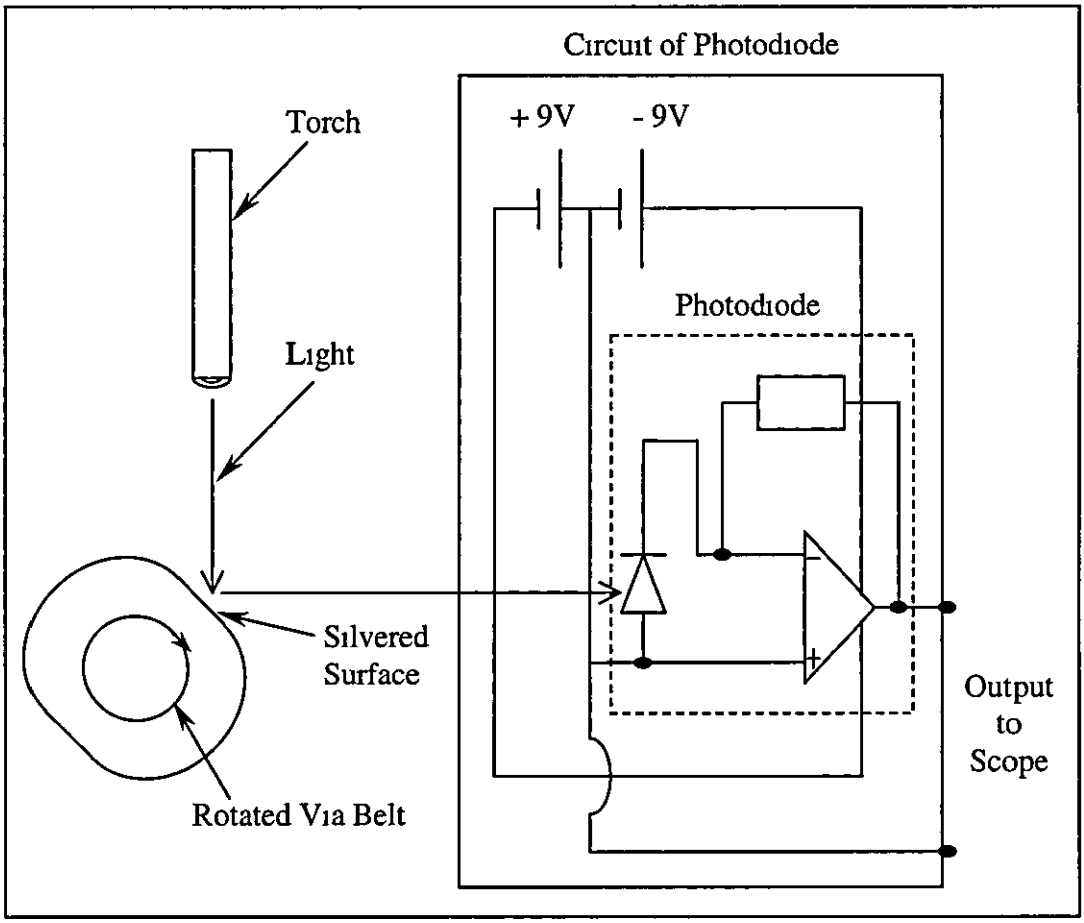

Figure 4.3: Configuration of the Rotation Speed Measuring Unit.

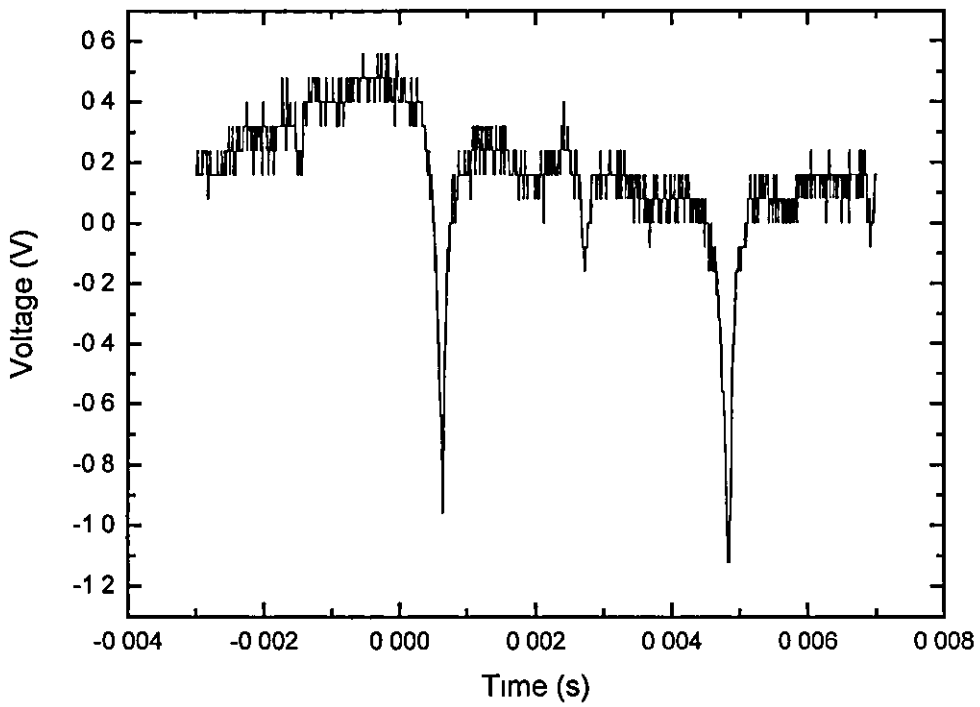

Figure 4.4: The reflected light pulse of C4 camera variac setting of 35.

Variac Setting	Duration for 140 frames (μs)	Duration for 1 frame (μs)	Camera Speed (pps)
30	2479.4	17.71	56 465
35	2100	15.0	66 666
40	1829.8	13.07	76 511
45	1635.2	11.68	85 616
50	1485.4	10.61	94 251
55	1365	9.75	102 564
60	1265.5	9.04	110 619

Table 4.1: Calibration table for the C4 camera variac setting.

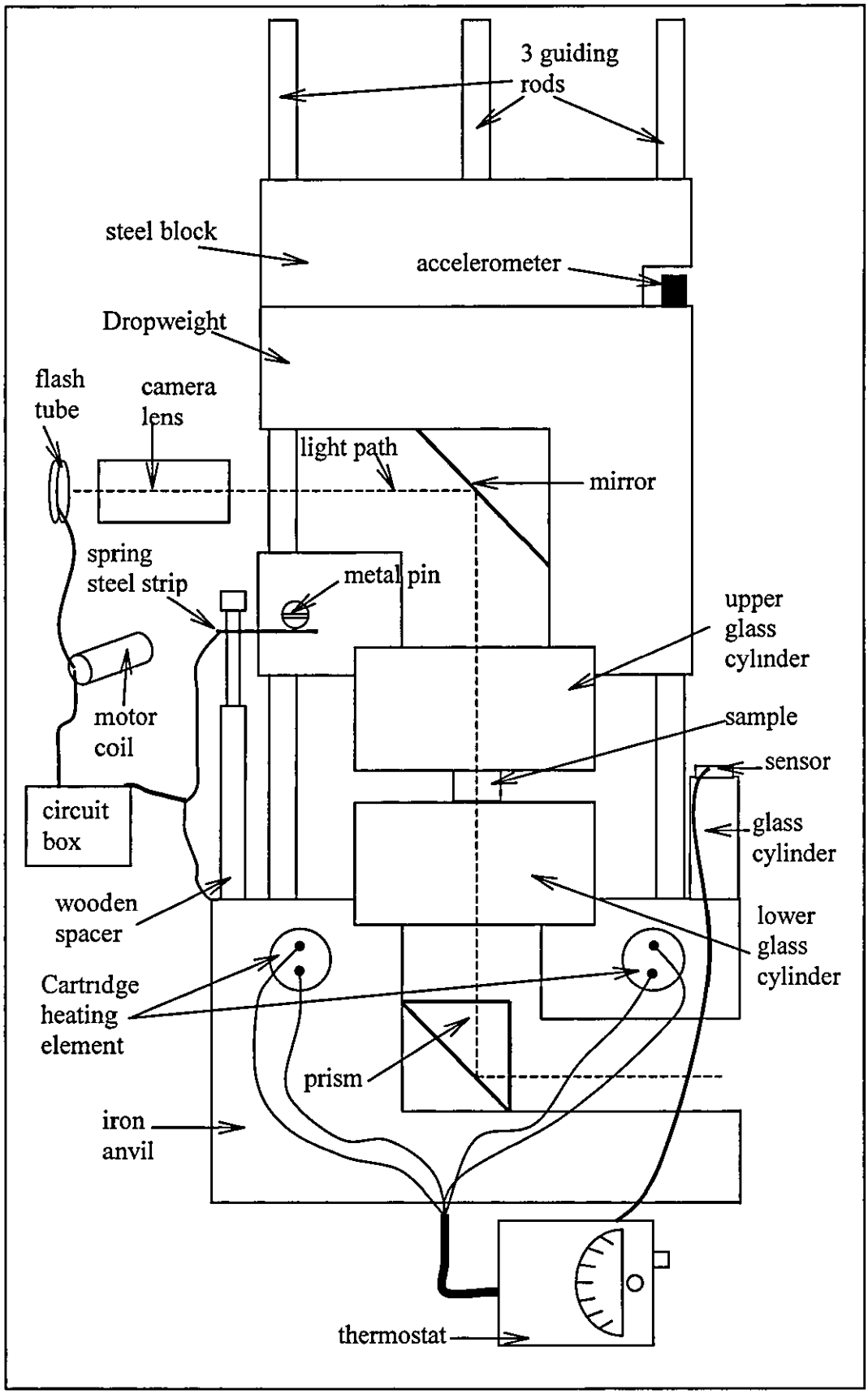

Figure 4.5: Diagram of the C4-Camera Dropweight together with the heating system.

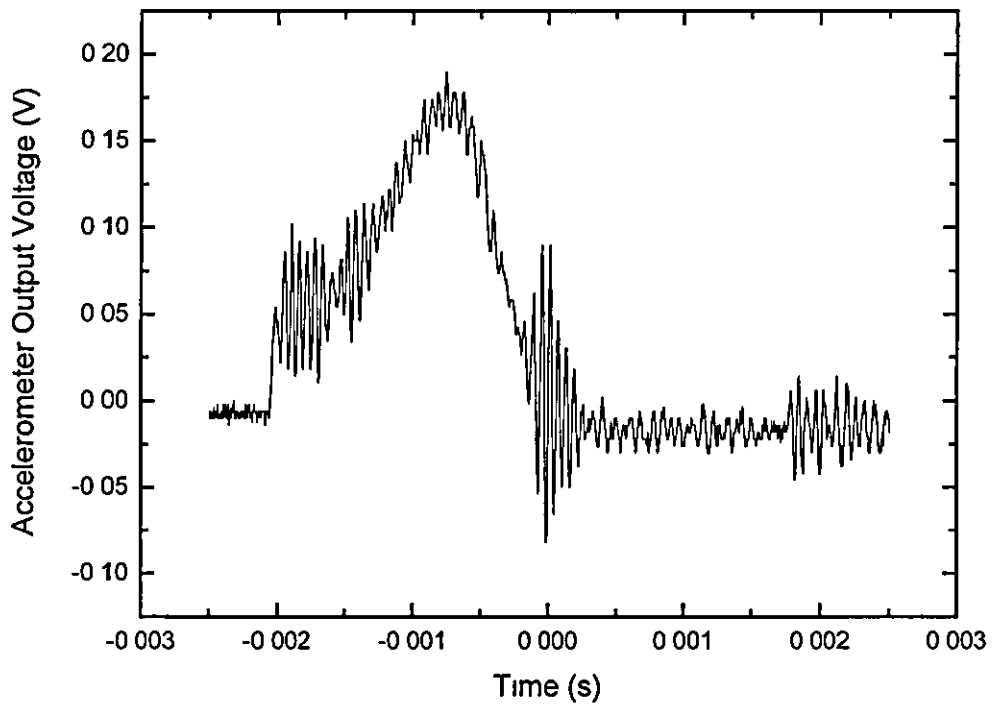

Figure 4.6: The accelerometer output voltage signal coupled with the high frequency dropweight vibrations.

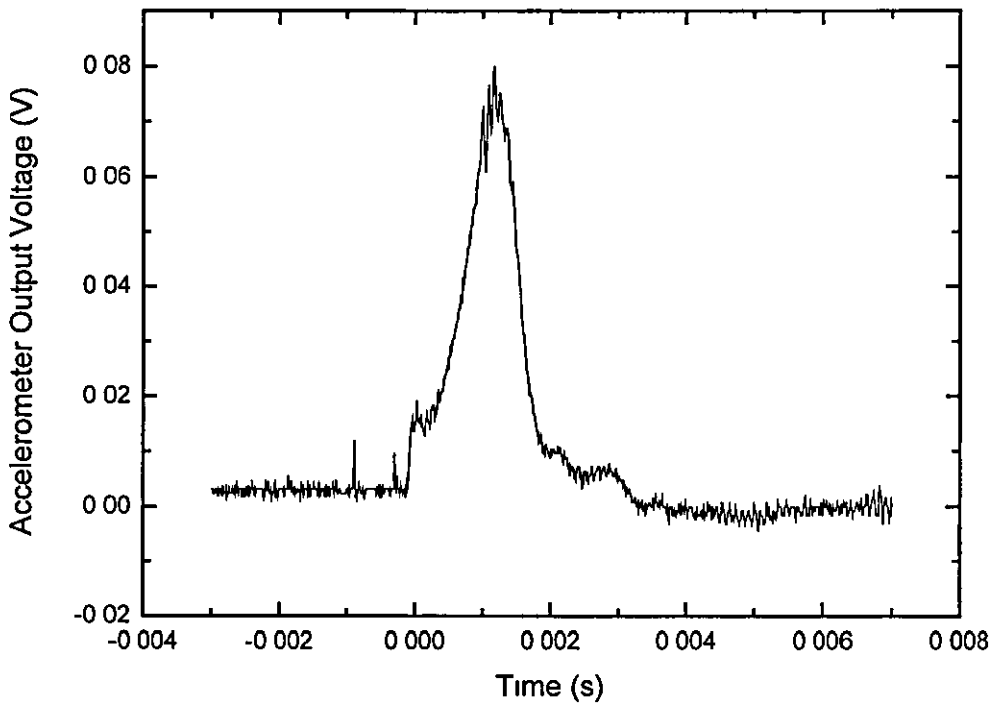

Figure 4.7: The accelerometer output signal after putting an additional weight on the top of the dropweight.

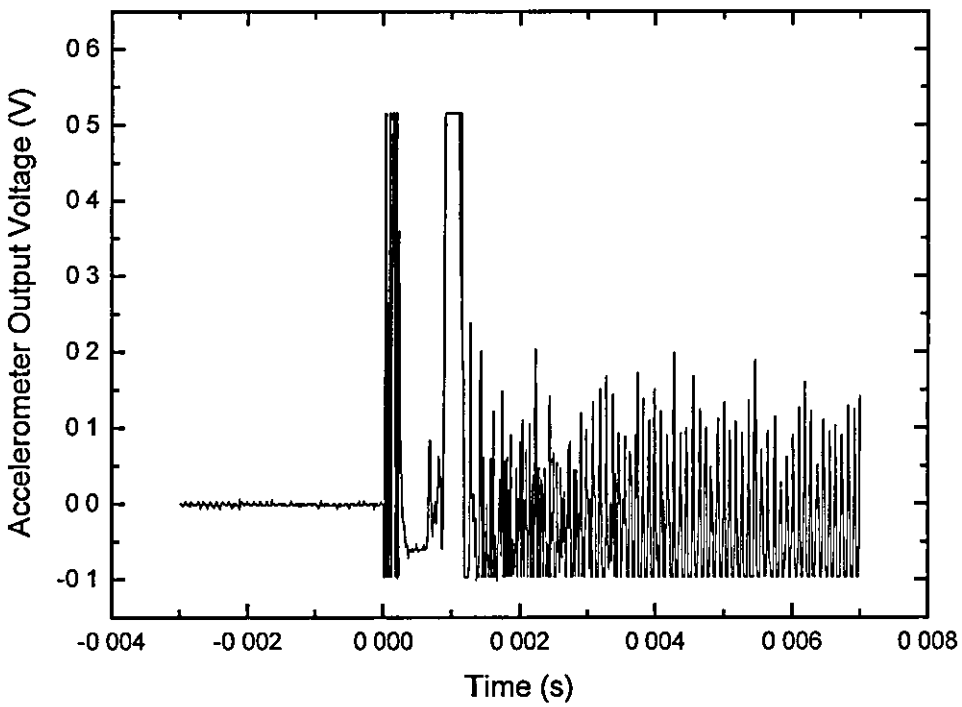

Figure 4.8: Accelerometer output signal coupled with electrical disturbance.

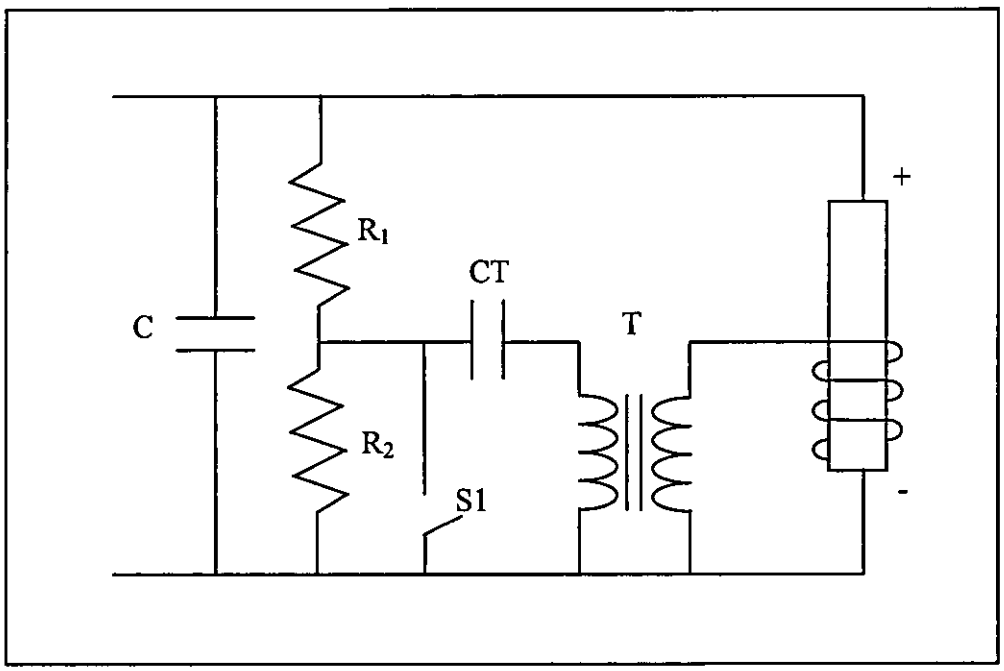

Figure 4.9: Simple circuit explaining how the flash tube is triggered.

will discharge through the primary winding of transformer T. A higher voltage will be induced across the secondary winding of transformer T onto the wire wound over the tube to ionise the gas. After the ionisation is induced, the resistance of the tube drops. This allows the high voltage from the capacitor C to discharge through the tube and produce light.

4.3 Synchronisation of the Flash and the Camera Speed

The most essential step in the photographic experiment in producing a dynamic stress-strain curve is being able to capture the whole impact events onto two rolls of films in one exposure. It is important that the flash tube is triggered slightly earlier than the impact so that the image before impact can be used in the enlargement factor when calculating strain. In addition, the flash duration (~4520 μs) should be long enough to illuminate the whole impact events (~1500 μs). The selection of the camera speed is also important in determining the success of the experiment The duration for 140 frames in one exposure should be long enough to cover the events start from just after the flash is triggered until the whole impact finishes. If the duration for 140 frames is shorter than the impact duration, the on-going events of the impact will be lost as the film cannot be used again to record images on the second exposure. Hence, information about the sample deformation could not be fully extracted from the film. In the experiments, a camera speed of 67 000 pps (15 μs/frame) was used.

4.4 Accelerometer

The accelerometer adopted in the experiments is the Brüel & Kjær type 4344 that is a piezoelectric compression transducer. The accelerometer produces an e m f proportional to the acceleration to which it is subjected. The output of the accelerometer is then fed directly to a Brüel & Kjær type 2626 conditioning amplifier.

4.4.1 The Operation of the Accelerometer

The diagram of accelerometer is shown in Figure 4.10 and its characteristic is in Figure 4.11. The mass is preloaded by a stiff spring and rests on top of two

piezoelectric discs, which acts as transducing elements The whole system is mounted in a housing, which is made of titanium with a thick base.

When the accelerometer is subjected to vibration, the mass will exert a variable force on the piezoelectric disc. Due to the piezoelectric effect, a variable voltage will be developed across the disc. The variable voltage is proportional to the force exerted and therefore to the acceleration of the mass. For frequencies much lower than the resonance frequency of the mass and the stiffness of the whole accelerometer system, the acceleration of the mass is virtually the same as the acceleration of the whole accelerometer. Therefore, the voltage produced will be proportional to the acceleration to which the transducer is subjected. The voltage can be picked up from the output terminals of the accelerometer. The type 4344 accelerometer has an undamped resonance frequency of 122 kHz. Several tests of the accelerometer over the frequency range 0.3 Hz to 30 kHz was carried out by Hamdan[1] and showed that the output voltage is linearly proportional to the acceleration in the frequency range.

4.4.2 Physical Dimensions

An accelerometer should be as light as possible in order not to influence the vibration frequency of the specimen on which it is mounted. For measurements on heavy specimens, the weight of the accelerometer will cause no problem. For lighter specimens (e g a thin metal plate), the accelerometer weight becomes important. For a vibrating system in a single degree of freedom, the resonance frequency is

$$f_0 = \frac{1}{2\pi}\sqrt{\frac{k}{m_0}} \tag{4.1}$$

where m_0 is effective mass and k is stiffness of the system. With additional mass, e g. accelerometer, will result a new resonance frequency

$$f_1 = \frac{1}{2\pi}\sqrt{\frac{k}{m_1 + m_0}} \tag{4.2}$$

where f_1 is the new resonance frequency and m_1 is the added mass

The accelerometer type 4344 used in the experiment is 2 grams excluding cable, therefore, compared to 8.25 kg weight it is negligible.

4.4.3 Temperature Effect

The voltage sensitivity of the accelerometer will be reduced at higher temperature. The sensitivity will revert to its normal value when the temperature is brought back to normal again. The Brüel and Kjær accelerometer type 4344 is designed to be used up to 250 °C (500 °F) However, beyond a certain temperature, the piezoelectric element is permanently damaged. For the B & K accelerometer, the damage temperature is 350 °C. Figure 4.12 shows the performance characteristics of the accelerometer for the temperature range –100 to 260 °C .[5] In the experiment, the testing temperature is from 20 °C to 80 °C .

4.5 Conditioning Amplifier

The Bruel & Kjær type 2626 conditioning amplifier was used to amplify the accelerometer output voltage. The amplifier charge sensitivity is set according to the accelerometer sensitivity i e. 2.46 pCg^{-1}. The voltage sensitivity is set at the lowest value i.e. 0 001 Vg^{-1}. The calibration of the voltage sensitivity accuracy was done by Hamdan[1] using two methods - the sinusoidal motion calibration method and the transient motion calibration method. The results showed that the conditioning amplifier was in the good condition and therefore the calibrated constant K could be calculated directly from the voltage sensitivity of the amplifier The calculated K constant is 9810 Vms^{-2}. The conditioning amplifier has filtering feature and the selected frequency range is from 0.3 Hz to 30kHz. This referred to the thesis of Hamdan[1] who had carried out several tests at different frequency ranges.

4.6 Data Recording and Filtering

It is necessary to ensure that the mounting of the accelerometer onto the dropweight is sufficiently stiff, so that the force vibration produced from the accelerometer is mainly due to the sample deformation. A TDS 306 Digital Real Time Oscilloscope with two input channels was used to record simultaneously the accelerometer output voltage

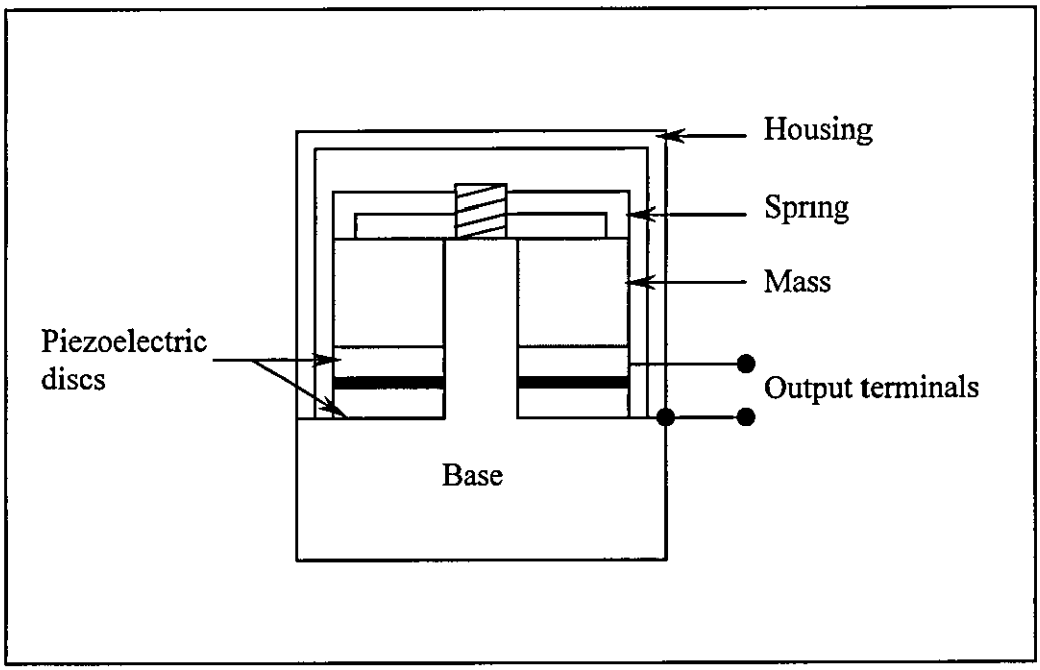

Figure 4.10: Schematic drawing of a piezoelectric accelerometer.

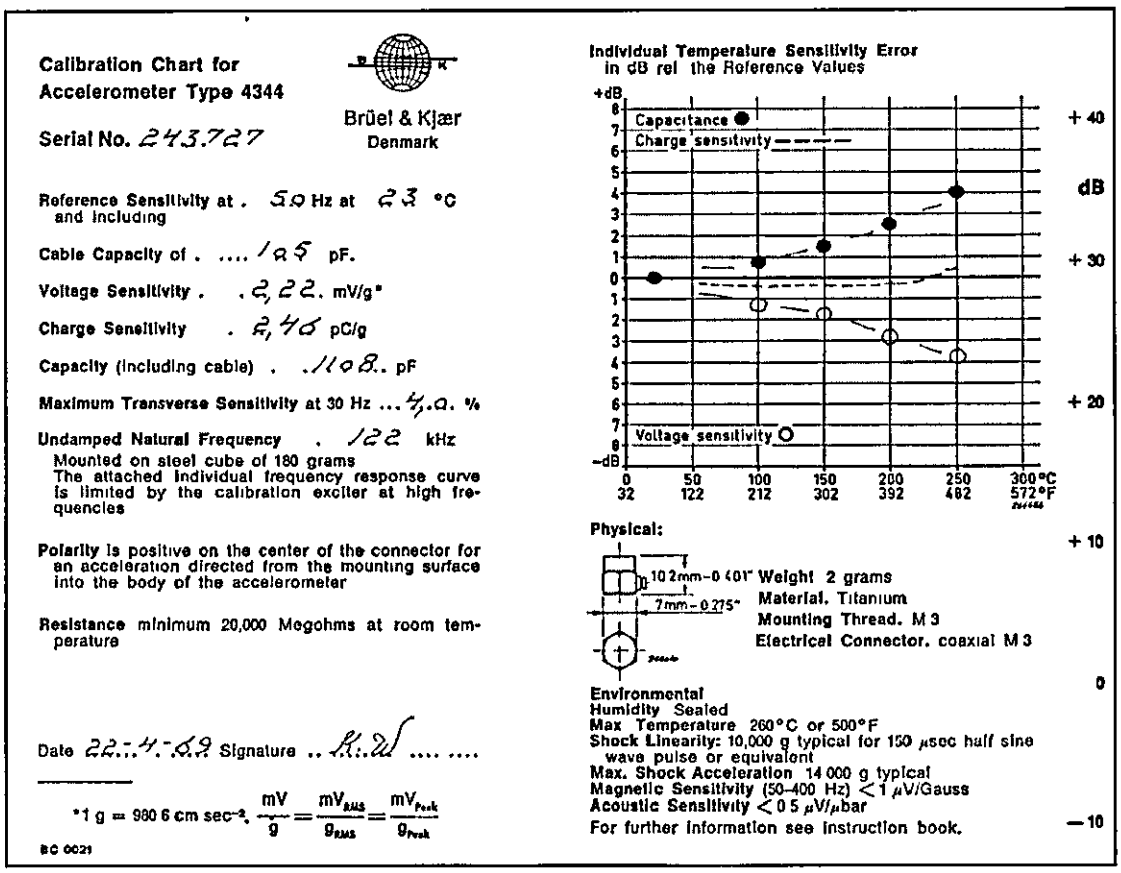

Figure 4.11: Characteristic of the accelerometer type 4344.

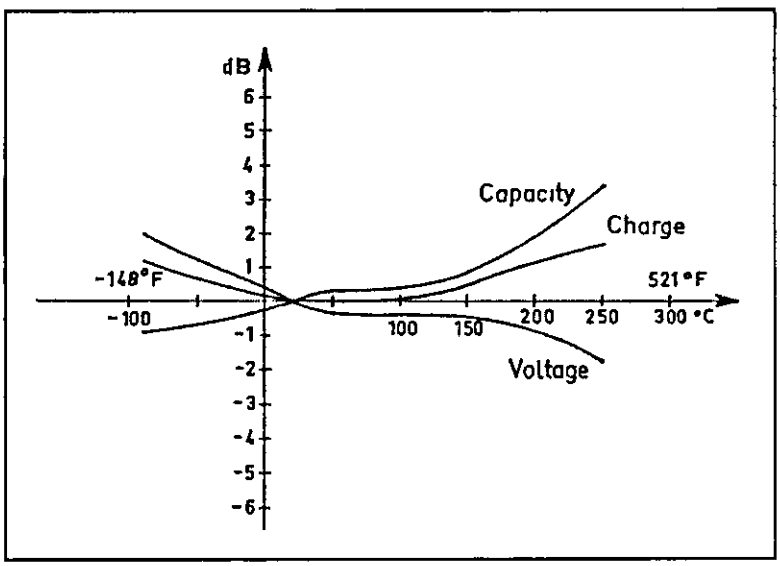

Figure 4.12: Performance characteristics of the accelerometer for the temperature range – 100 °C to 260 °C [5]

after being amplified via the conditioning amplifier and the flash signal from the photodiode.

The acquisition of the oscilloscope was set to "stop after single acquisition" sequence In order to ensure that the accelerometer output voltage was successfully recorded each time the experiment was run, the trigger was set on the flash channel because this receives constant magnitude voltage input. Because the accelerometer signal varies based on the force exerted on the sample it is difficult to set the trigger point in the oscilloscope from the accelerometer output.

The function of Fast Fourier Transform on the PeakFit 4 software was used to filter the accelerometer output voltage-time curve obtained. Due to the natural vibrational frequency of samples during deformation, the cut-off frequency used was from 20 kHz and higher. The typical impact duration was 1500μs corresponding to a frequency of ~ 700 Hz, the cut off was set at ~ 30 times this frequency. Therefore, the detailed shape of the signal will not be lost.

4.7 Film Processing

The film used in capturing the sample deformation images was Ilford HP5 aerial film The ILFord ID-11 or Jacobs Photo & Video developer was used in developing the film at 20 °C with the developing time similar to FP4 Plus. The developing time varies if the film is developed at the temperature other than 20 °C and can be worked out from Appendix A. ILFord Hypam Rapid Fixer was used in fixing the film The film was then dried in the heated cabinet at 50 °C for around 30 minutes.

4.8 Stress and Strain Analysis

The strain of the tested sample is calculated from the deformed sample images captured on the film. The film was cut into stripes with four images on each stripe. The stripes were scanned into a PC using a resolution of 1200 dpi set in HP Precision Scan software under extension of "bmp". The scanned images consisting of the

deforming sample diameter D_i at time t_i were then measured using MGI Photosuite software (Figure 4 13)

Since the accelerometer is mounted on the top of the dropweight, there is a significant time delay for the stress wave to travel from the impact point to the accelerometer. The sound velocity in the glass and steel are 5334 ms^{-1} and 5151 ms^{-1} respectively. Therefore, the travelling time in 2.5 cm of glass is 4.8 μs while in the 9.5 cm thickness of steel is 18 5 μs. The time delay is thus 23.3 μs. If Δt is the time difference between the flash and impact (Figure 4.15), dt the time delay and δt the interframe time, the first frame of impact is the n-th frame in the film and is calculated by

$$n = \frac{\Delta t - dt}{\delta t} \qquad (4\ 3)$$

By plotting the deformation data from the first frame to the last frame of impact using Microcal Origin, the equation of the deforming sample diameter as the function of time can be obtained (Figure 4.14). The equation is then used to reproduce the deforming sample diameter, D(t), at the same time interval as the accelerometer output voltage time interval.

The actual deforming sample diameter d(t) at time t can be measured as below:

$$d(t) = \frac{D(t)}{D(t_o)} \cdot d(t_o) \qquad (4\ 4)$$

with $D(t_o)$ is the scanned diameter of the sample before deformation and $d(t_o)$ is the original measured diameter of the sample before deformation. Therefore, the radial strain is

$$\varepsilon_r = \ln\frac{d(t)}{d(t_o)} \quad \text{or} \qquad (4.5)$$

$$\varepsilon_r = \ln\frac{D(t)}{D(t_o)} \qquad (4.6)$$

The true axial strain can be obtained using Poisson ratio ν

$$\varepsilon_a = -\frac{\varepsilon_r}{\nu} \qquad (4.7)$$

where ν=0 5 for polymeric materials undergoing plastic deformation.

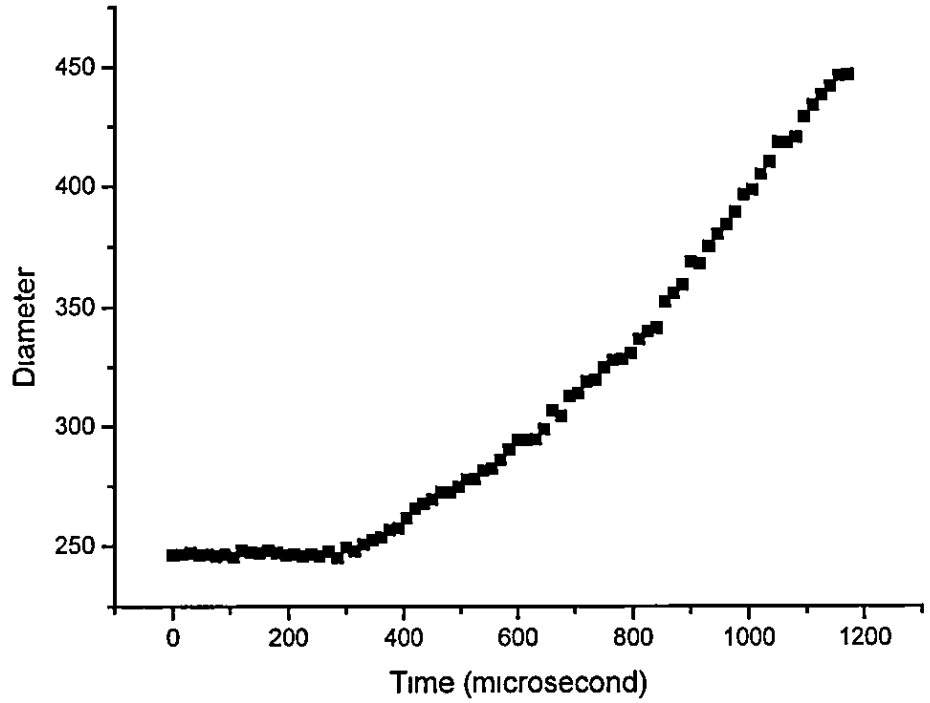

Figure 4.13: Graph showing data of the deforming sample diameter in 1200 dpi resolution measured using MGI Photosuite software and plotted against accumulated interframe time.

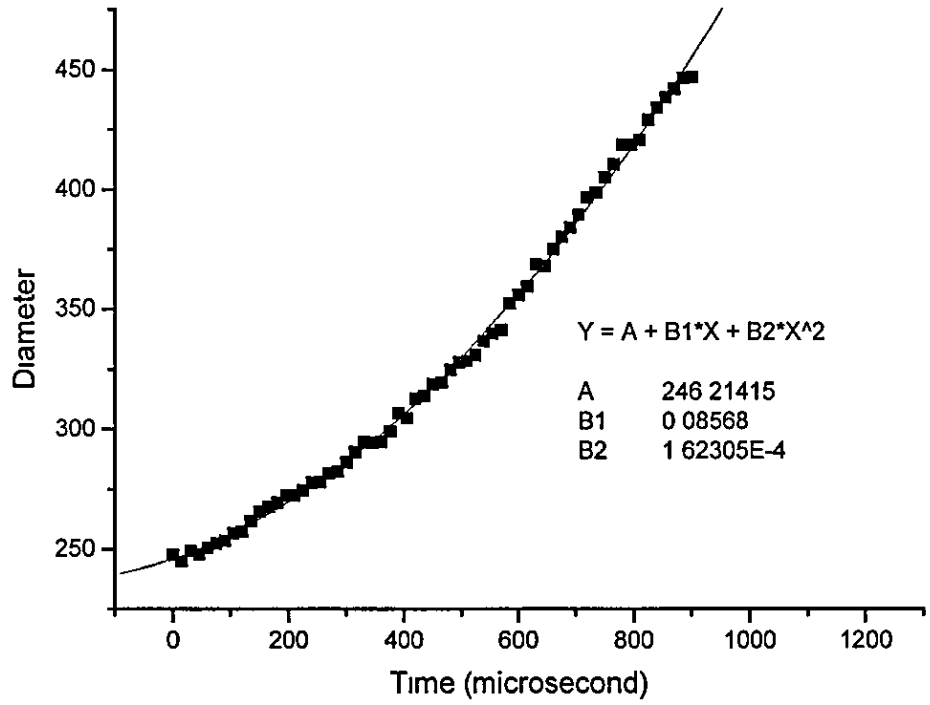

Figure 4.14: Equation of the deforming sample diameter as the function of time obtained using Microcal Origin.

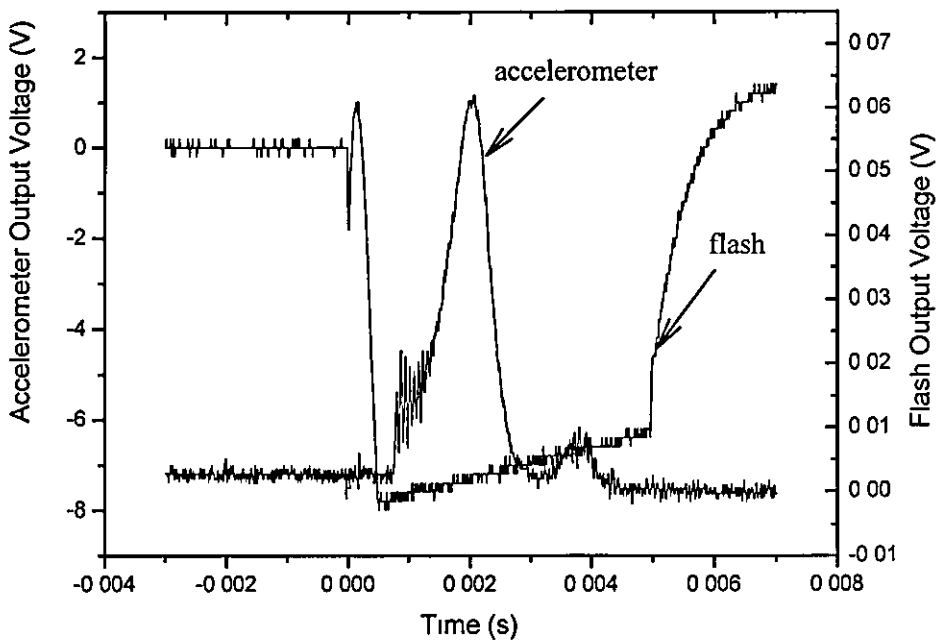

Figure 4.15: Signals of accelerometer and flash.

The true axial stress at time t is given as

$$\sigma(t) = \frac{F(t)}{A(t)} \tag{4.8}$$

where F(t) and A(t) is the impact force and the deforming sample area at time t.

F(t) is calculated by converting the filtered accelerometer output voltage V(t) into the impact acceleration a(t) using the following equation

$$a(t) = KV(t) \tag{4.9}$$

where the calibrated constant K is 9810 $V^{-1}ms^{-2}$ referring to the voltage sensitivity of the conditioning amplifier which is 0.001 Vg^{-1} or 0.001 $V/9.81ms^{-2}$. From $F(t) = ma(t)$ with the mass of the dropweight m 8.2 kg, the impact force at time t can be calculated and A(t) is given as

$$A(t) = \pi(\frac{d(t)}{2})^2 \tag{4 10}$$

4.9 Experimental Procedure

The experiments were carried out at three temperatures 20 °C, 50 °C and 70 °C. The test sample was put on the lower glass cylinder and the weight was pulled to a predetermined height and then released to hit the sample. The upper glass cylinder that was fixed to the bottom of the weight acts as an impactor. Samples were heated for 30 minutes on the lower glass cylinder and a thermocouple thermometer was used to check the sample temperature prior to testing. The upper glass cylinder was heated up to the test temperature with a hot-air blower prior to the impact.

4.10 Results and Discussion

High Speed Photography has been widely adopted not only to measure the strain in deforming a sample[7] but also to study the rapid deformation in polymers due to impact.[8] In the current study, the C4 camera incorporated with an instrumented

Dropweight was used to study the deformation until fracture occurred in PMMA and PS.

Photo 4.1 shows the deformation until fracture for PS tested at the temperatures below 80 °C. Photo 4.2, 4.3 and 4.4 show the deformation until fracture of PMMA tested at 20 °C, 50 °C and 70 °C. From Photo 4.1 and 4 2, it could be seen that the fracture was catastrophic failure. Photo 4.3 and 4.4 show adiabatic shear band in the deforming zone of PMMA tested at 50 °C and 70 °C.

Graph 4.1 shows the stress-strain curve for poly(methyl methacrylate) compressed using the high-speed photographic system. The stress-strain curve for PS tested was hard to obtain as PS fractured without deformation under the high strain rate (Photo 4.1). Table 4.2 shows the temperature rises for the fractures of poly(methyl methacrylate) occurred at 20 °C, 50 °C and 70 °C. The actual sample temperature (testing temperature + temperature rise) of PMMA at the testing temperature of 50 °C where the adiabatic shear band formed was around 235 °C. The actual sample temperature of PMMA at the testing temperature of 70 °C was around 300 °C. The temperature rise ΔT was calculated using the following equation:

$$\Delta T = \frac{\int \sigma d\varepsilon}{\rho C_p}$$

where the plastic work $\int \sigma d\varepsilon$ is calculated by measuring the area under the stress-strain curve. The density of PMMA (ρ) is taken to be 1190 kgm^{-3}. The specific heat capacity of PMMA (C_p) is found from the DSC data which is 710 $Jkg^{-1}K^{-1}$ at 20 °C (293 K), 840 $Jkg^{-1}K^{-1}$ at 50 °C (323 K) and 970 $Jkg^{-1}K^{-1}$ at 70 °C (343 K) respectively.

A few names have been given to the adiabatic shear band by different authors. Massey[11] and Johnson[12] called it thermal crosses or heat lines; Recht[13] catastrophic thermoplastic shear bands; Bedford et al.[14] white bands of streaks. Adiabatic shear bands are normally developed in dynamic processes and mainly due to the rapid local heating, resulting from the intense plastic shear deformation. Narrow bands of intense plastic shear strain are sometimes observed on the surfaces of loaded materials. There have been a number of researches revealing that adiabatic shear band not only occurring exclusively in metals but also in polymers.[9,10]

Adiabatic shear bands usually appear on planes of maximum shear stress. It is said that adiabatic shear bands can be the precursors to catastrophic failures. However, it is impossible to know the susceptibility of materials to adiabatic shear banding from mechanical data such as fracture toughness and strength. It generally follows the trajectories of slip-lines in the plastic deformation.

In the plastic deformation of polymers, most of the deformation energy is converted to heat. If the strain rate is high, the heat generated may not have enough time to dissipate into the surrounding from the deforming zone. This induces localised heating and leads to local thermal softening. If the localised plastic work in a time is greater than heat diffused away from the deforming zone, adiabatic shear banding occurs.

4.11 Conclusion

PS tested at the temperature below 80 °C shows catastrophic failure. PMMA tested at 20 °C shows catastrophic failure while tested at 50 °C and 70 °C reveals adiabatic shear band in the deforming zone.

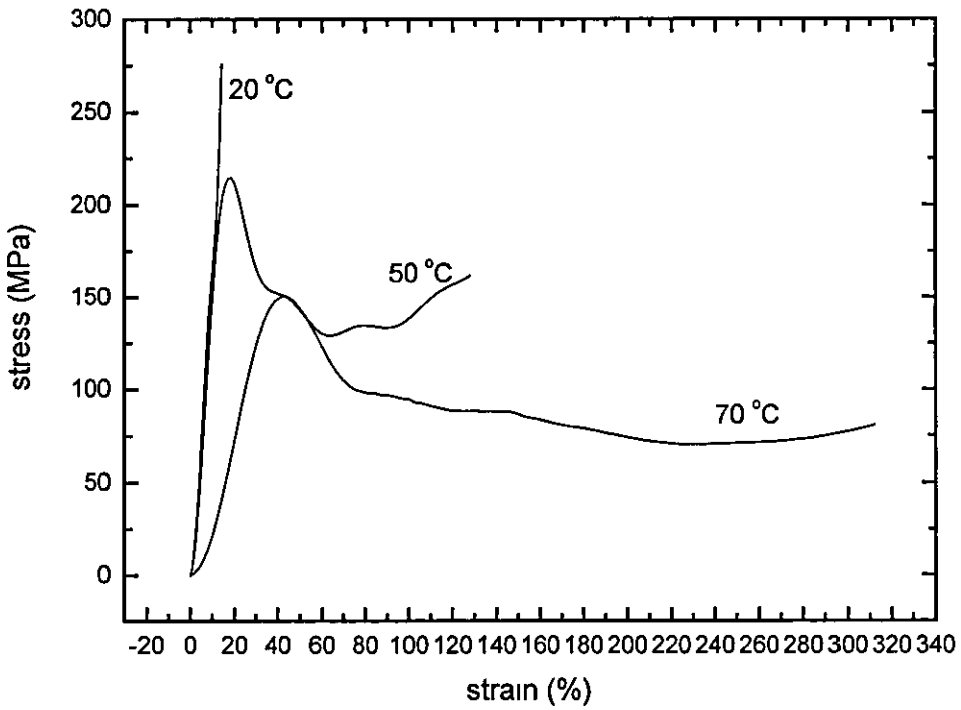

Graph 4.1: True stress-true strain curves for PMMA tested at 20 °C, 50 °C and 70 °C until fracture using the high-speed photographic system

Poly(methyl methacrylate) (PMMA)						
Testing temperature (°C)	Yield point			At fracture		
	Strain rate (s^{-1})	Energy (kJ/m^3)	Temperature rise, ΔT (°C)	Strain rate (s^{-1})	Energy (kJ/m^3)	Temperature rise, ΔT (°C)
20	-	-	-	424	16799	20
50	1211	23765	24	1804	185356	185
70	2640	36986	32	3460	265598	230

Table 4.2: Strain rate, energy and temperature rise at yield point and at fracture of PMMA tested at 20 °C, 50 °C and 70 °C using the high-speed photographic system.

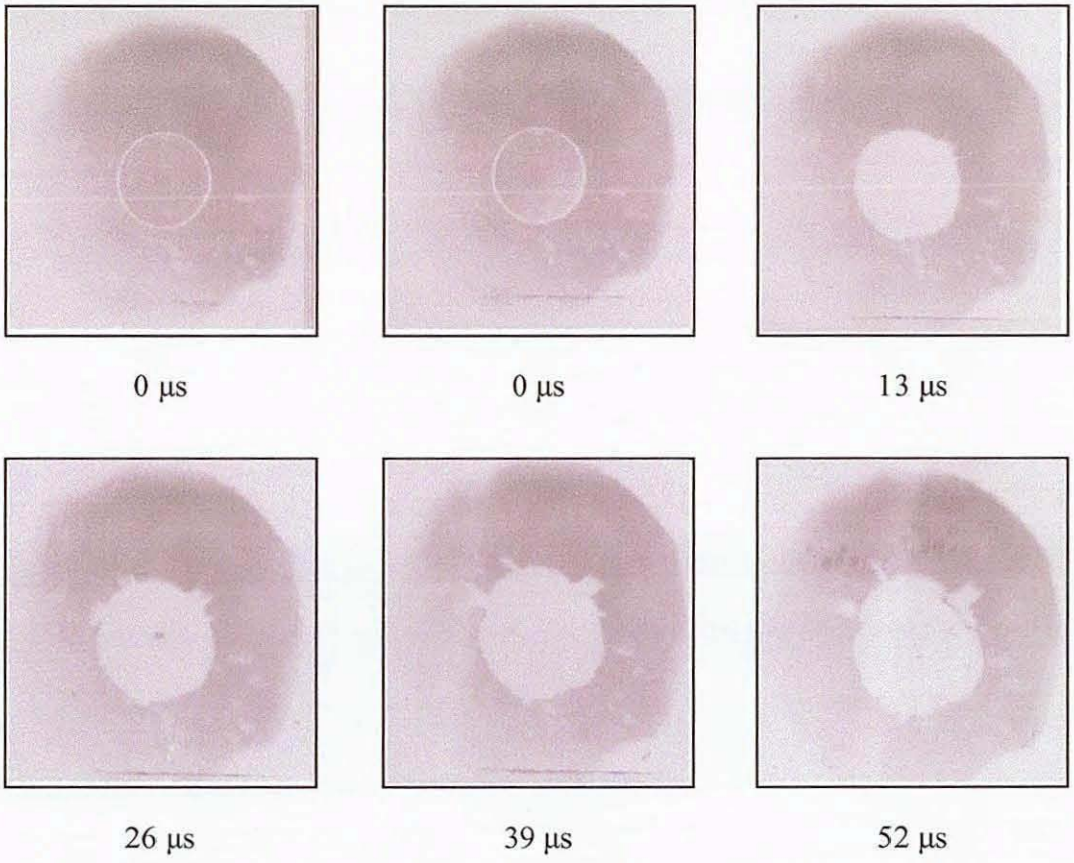

Photo 4.1: Deformation of polystyrene tested at the temperature below 80°C visualised using the high-speed photographic system.

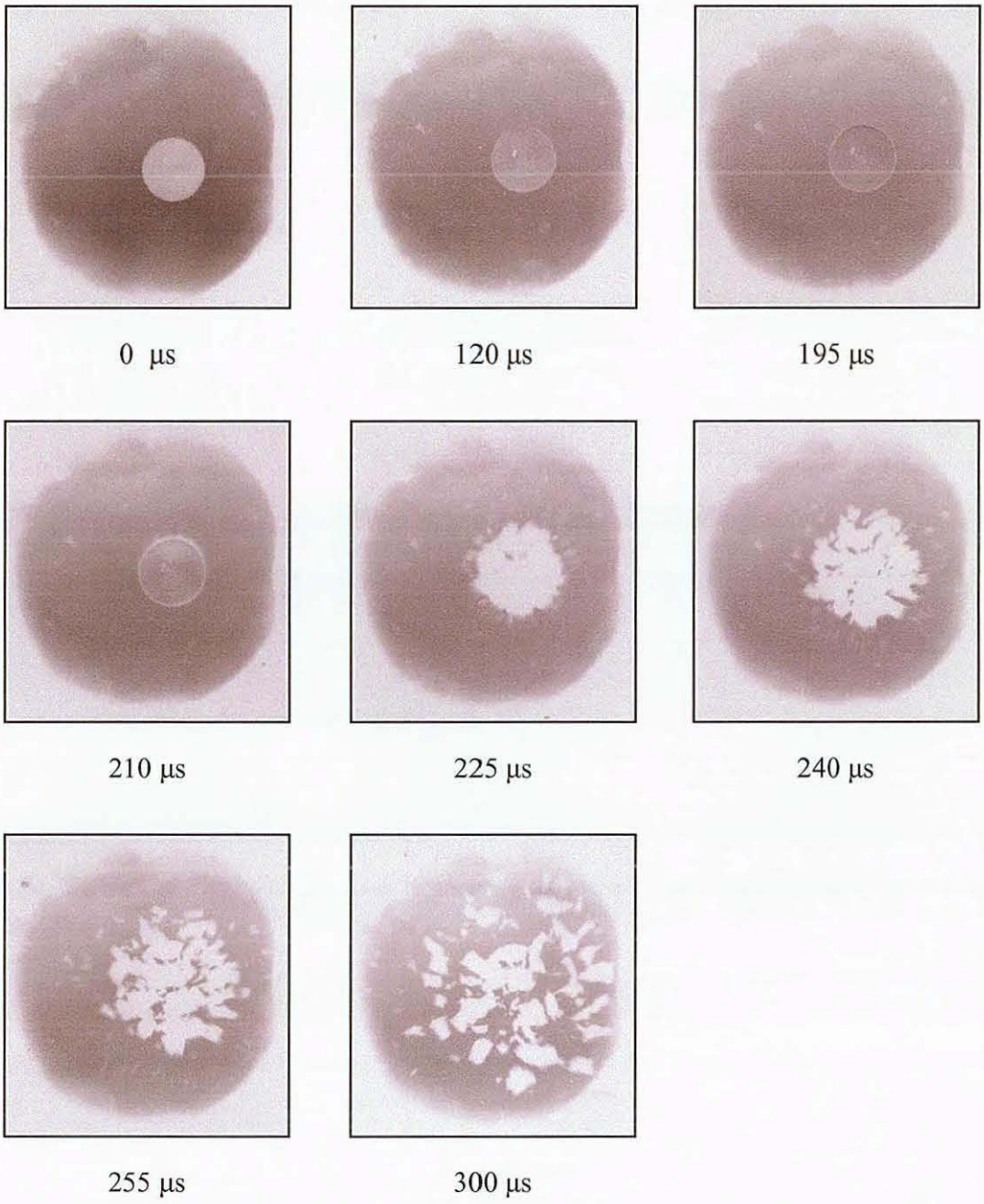

Photo 4.2: Deformation of poly(methyl methacrylate) at 20°C visualised using the high-speed photographic system.

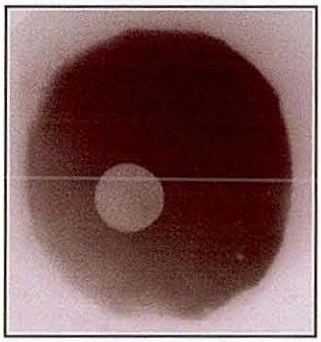

0 μs

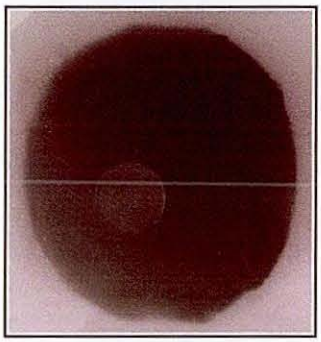

60 μs

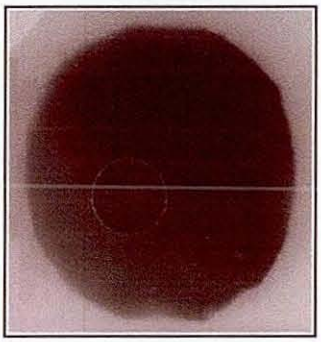

195 μs

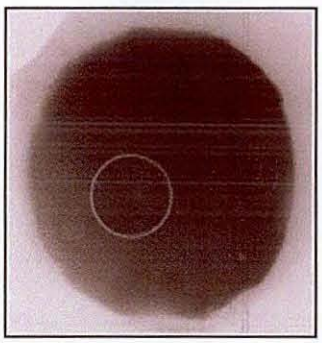

345 μs

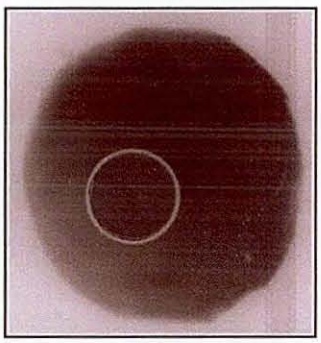

495 μs

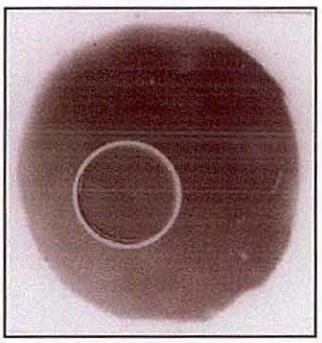

645 μs

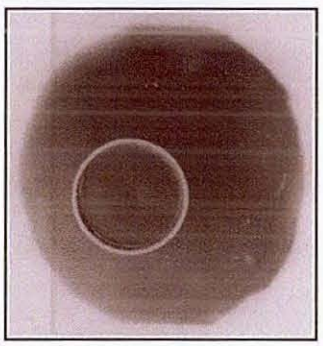

720 μs

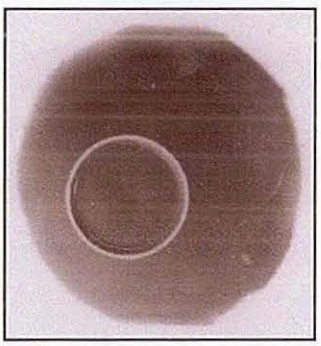

765 μs

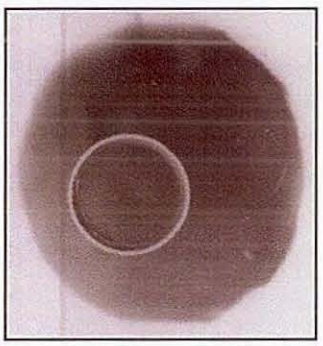

795 μs

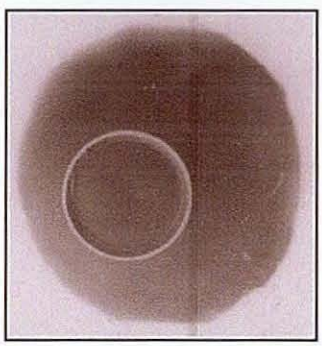

855 μs

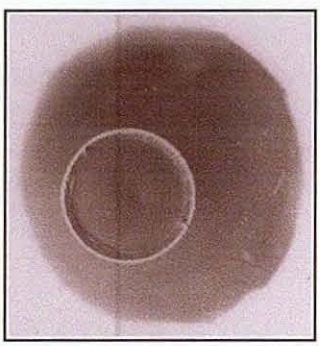

900 μs

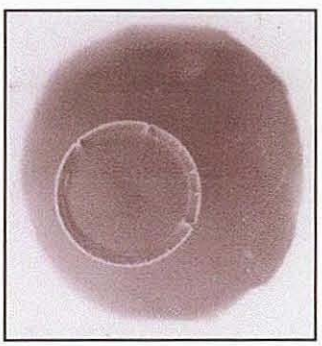

1005 μs

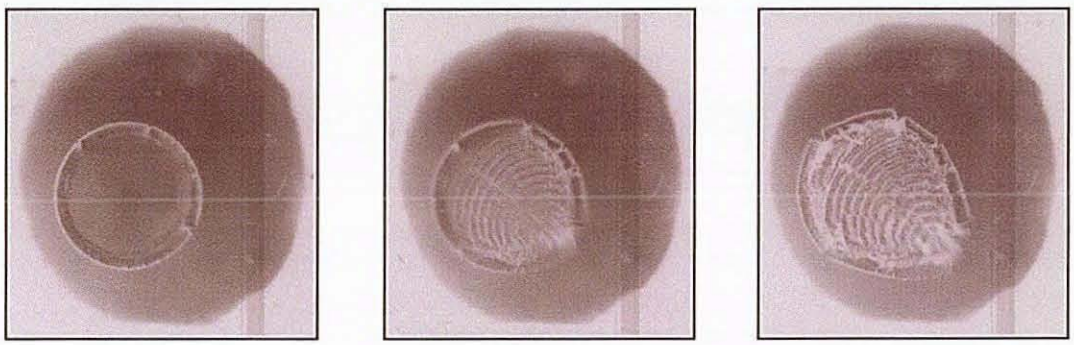

1020 μs 1035 μs 1050 μs

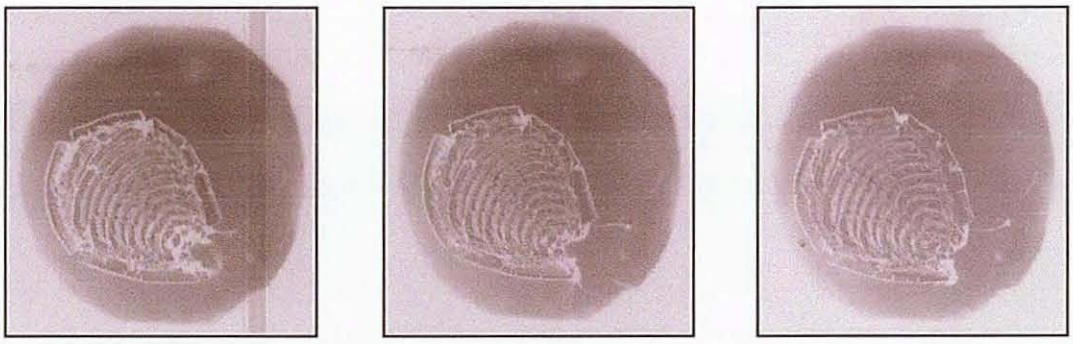

1065 μs 1095 μs 1125 μs

Photo 4.3: Deformation of poly(methyl methacrylate) at 50°C using the high-speed photographic system

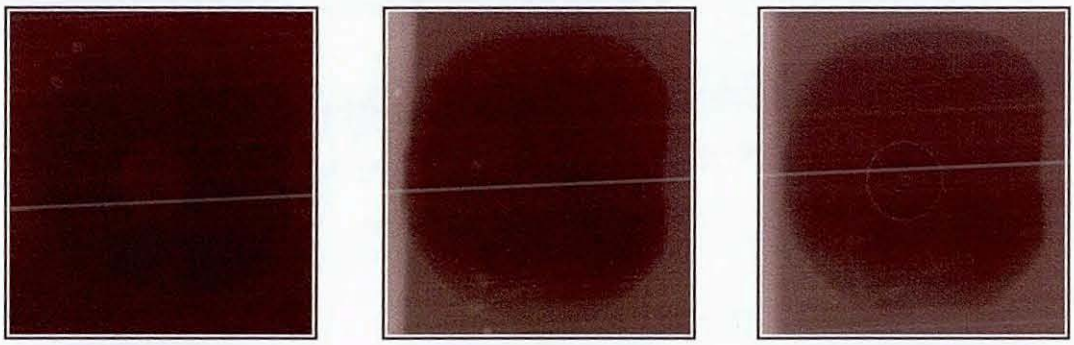

0 μs 105 μs 195 μs

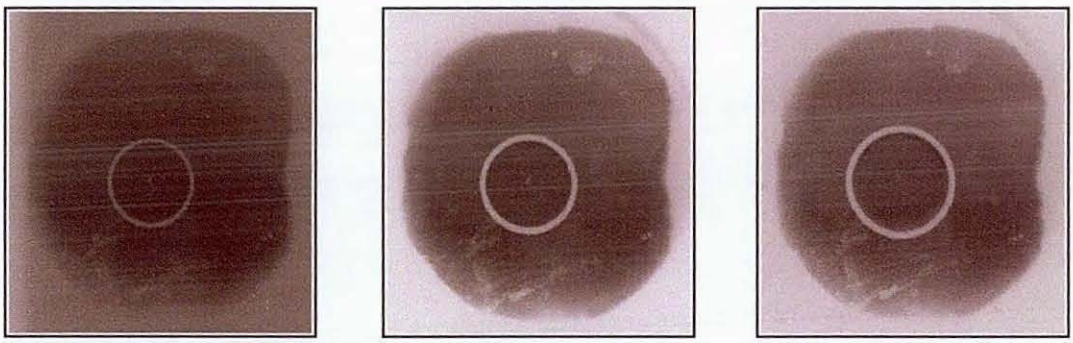

345 μs 495 μs 645 μs

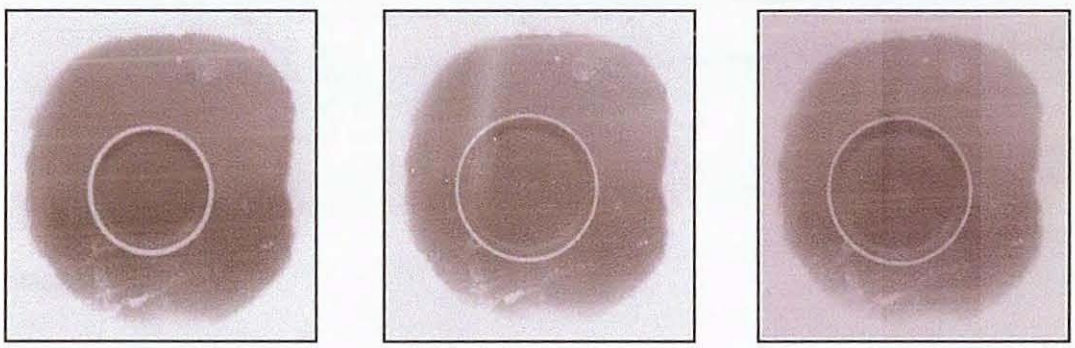

795 μs 945 μs 960 μs

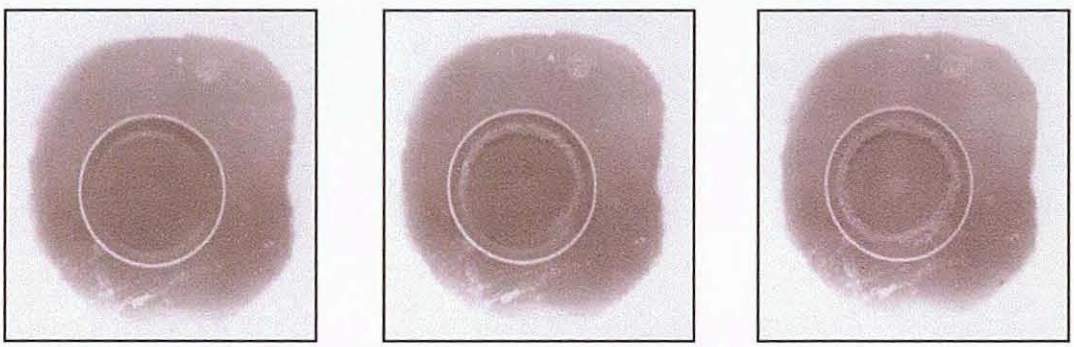

975 μs 990 μs 1005 μs

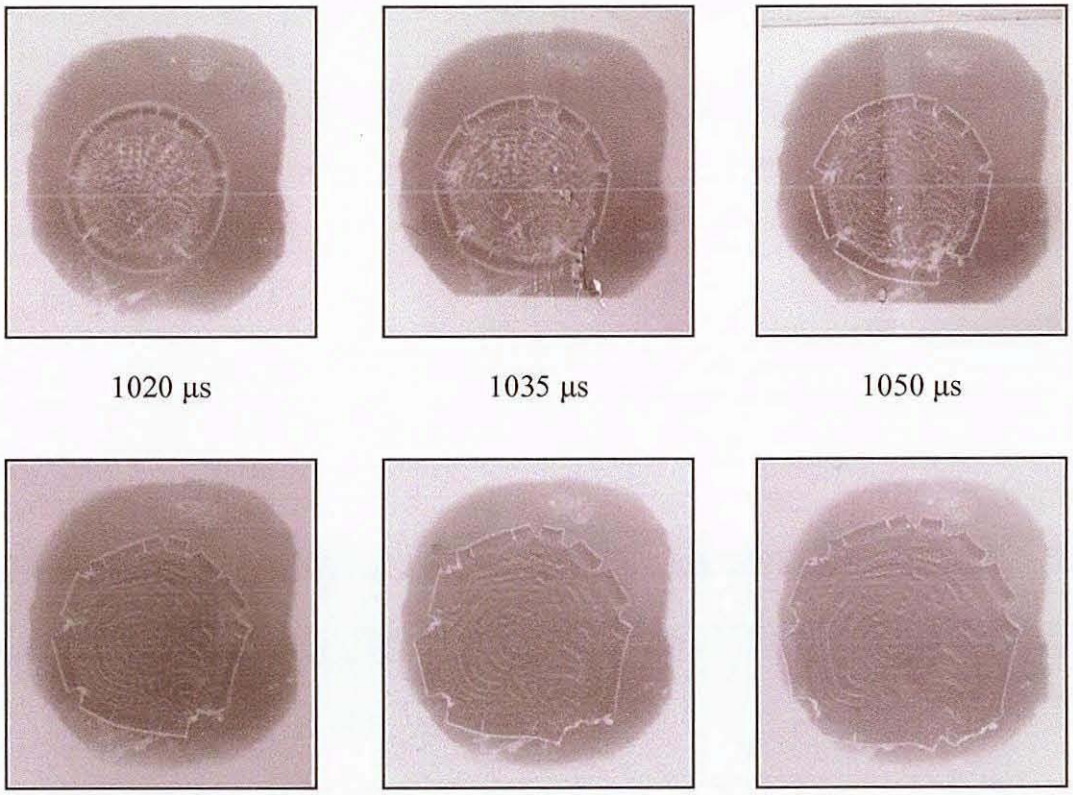

1020 μs 1035 μs 1050 μs

1125 μs 1200 μs 1335 μs

Photo 4.4: Deformation of Poly(methyl methacrylate) at 70°C visualised using the high-speed photographic system

References:

1. **S. Hamdan,** PhD Thesis 1994, "The Thermomechanical Properties of Aromatic Polymers", Department of Physics, Loughborough University, Loughborough.

2 **D. Paisley,** "What constitutes high speed photography", OE Reports, **Nov,** SPIE USA (1993)

3. **P.W. W. Fuller,** Journal of Photographic Science **42** (1994) 42-43

4. **W. H. F. Talbot,** "On the production of instantaneous photographic images", Phil Mag. (4^{th} series), January, (1852) 73-77

5. Instructions and Applications booklet of Conditioning Amplifier Type 2626 and Accelerometer Type 4324

6. **S. F. Ray,** "High Speed Photography and Photonics", Focal Press, 1997

7. **T. Kuboki, T, Mada and K. Takahashi,** Key Engineering Materials **183-187** (2000) 289~294

8. **J. M. Huntley and J. E. Field,** Optical Engineering **33** No 5 (1994) 1700~1706

9. **R. E. Winter,** Philosophical Magazine **31** (1975) 765~773

10. **S. M. Walley, J. E. Field, P. H. Pope and N. A. Safford,** Philosophical Transactions Royal Society of London **A 328** (1989) 1~33

11. **H. R. Massey,** Proc. Manchester Assoc Engineers (1921)

12. **W. Johnson,** "Impact Strength of Materials", Edward Arnold, London, 1972

13. **R. F. Recht,** Journal of Applied Mechanics **31** (1964) 189~193

14. **J. Bedford, A. L. Wingrove and K. R. L. Thompson,** Journal. Australian Institute of Metals **19** (1974) 61~73

Chapter 5
Thermal analysis

5.1 Introduction

The use of thermal analysis in studying the mechanical properties of a polymer has increased over the past ten to fifteen years It involves the measurement of changes in the physical properties of a sample compared to the same property of a reference material as a function of temperature whilst the sample being heated to some elevated temperature. There are several methods of thermal analysis available in studying the thermal and mechanical properties of polymers.[1] In the current study, Differential Scanning Calorimetry (DSC) which measures the difference in enthalpy was adopted to study the specific heat and the glass transition temperature of PMMA and PS Dynamic mechanical analysis (DMA) which measures the difference in mechanical properties, etc. was used to study the variation of modulus with temperature and the transition temperatures of PMMA and PS.

5.2 Differential Scanning Calorimetry (DSC)

5.2.1 Theory

DSC is a technique that measures the difference of the heat flow required to keep a sample of interest at the same temperature as the reference as a function of time or temperature. The difference in heat flow between the sample and reference in a calorimeter which is needed to keep both at the same temperature T, is given by

$$\frac{dq}{dt} = \frac{dT}{dt}(C_s - C_r) \qquad (5.1)$$

where q is the heat, t is the time and C_s and C_r are the heat capacity of the sample-pan and reference-pan systems respectively.

Hence, thermal events such as glass transition, melting, crystallization and degradation in the sample appear as deviations from the DSC baseline in either an

endothermic or exothermic direction, depending upon whether more or less energy has to be supplied to the sample relative to the reference The displacement of the baseline h of a sample studied in a DSC cell with heating rate Φ is given by

$$h = B\Phi mC_p \qquad (5.2)$$

where B is a calibration factor, m is the mass of the sample and C_p is the specific heat capacity[1].

5.2.2 Thermal Measuring System

In the current study, a Mettler TA3000 Thermal Analysis System[2] consisting of the TC10A TA Processor and of a DSC30 measuring cell was used to perform the Differential Scanning Calorimetry (DSC) technique on uncompressed samples of PMMA and PS. The TC10A TA processor is the central unit of the system It controls the temperature of the furnace in the measuring cell and analyses the measured curve using various evaluation methods and calculates the final numerical results.

In the measuring cell, there are two identical measuring holders - one for the sample and the other for the reference pan (Figure 5.1). Each holder has a hole surrounded by 5 thermocouples. The pans are placed in such a way that the central pin of the pans are in the hole. In general, the sample is measured against a reference pan in all DSC measurements. In these experiments, the reference pan is an empty pan with two holes pierced in its lid to differentiate it from the sample pan

For samples tested at temperature below 500 °C, aluminium pans are used. For temperatures above 500 °C, the use of aluminium pan will destroy the DSC sample holder. Therefore, for samples that react with aluminium pan or for temperatures above 500 °C, a gold or graphite pan is recommended. The pan is hermetically sealed off with a lid in these experiments. In the work described here, a hole is pierced in the lid to release the air trapped in the pan since no corrosive gases are produced and this prevents the pan distorting due to pressure changes caused during heating

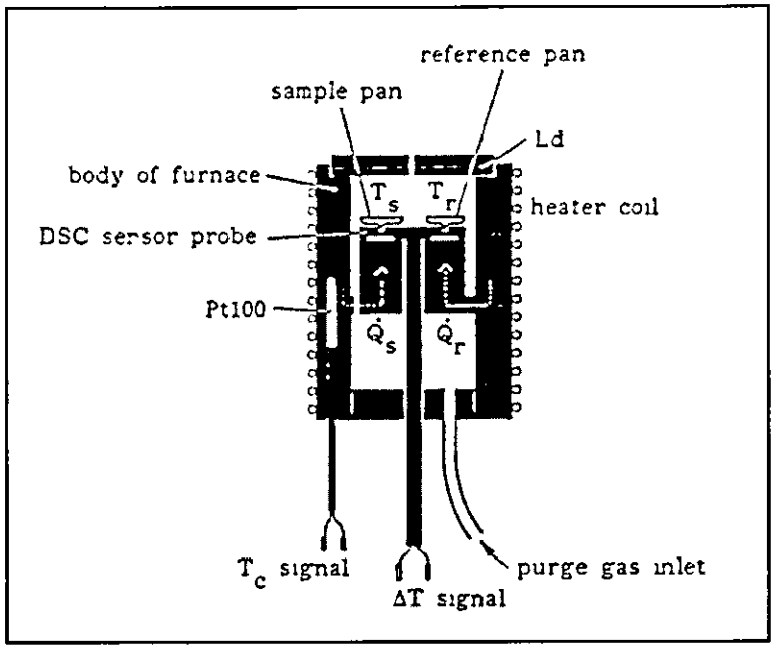

Figure 5.1: Diagram of measuring cell.[2]

Argon, an inert gas, is used to purge gas and vapour products produced during analysis from the measuring cell and thus protect it from corrosive gases The purge gas also removes atmospheric oxygen in order to avoid unwanted oxidation of the sample. After the sample pan is inserted into the measuring cell, it is purged at a high flow (50 ~ 200 ml/min) for a period of 2 to 5 minutes at the initial temperature.

5.2.3 Experimental Method

A sample of approximately 10 ~ 12 mg was cut from the uncompressed sample of PMMA or PS. It was weighed in a Sartorius balance, model R180D. In order to get the net weight of the sample, the weight of the pan and lid was tared before putting in the sample. The pan was then hermetically sealed off with the lid using a press. A hole was pierced in the lid to release the air trapped in the pan. The sample was then tested at the temperature range of 200 ~ 570 K at the heating rate of 10 K/min The cell was purged with argon, at a rate of approximately 80 cm^3/mm. Data obtained were in heat flow (mW) against temperature (°C). The specific heat at constant pressure and the glass transition were determined from the data obtained.

5.3 Dynamic Mechanical Thermal Analysis

5.3.1 Theory

Dynamic mechanical thermal analysis (DMTA) is useful in studying the effect of molecular structure and phase morphology on the mechanical properties (e g. transition temperatures, loss factor, storage and loss moduli) of polymers. It is reported to be one of the most sensitive techniques for characterising and interpreting the mechanical behaviour of materials. This technique measures the response or deformation of viscoelastic materials to periodic or varying forces. The applied force and the resulting deformation produced in the polymer generally vary sinusoidally with time.

When a sinusoidal stress is applied to a perfect elastic materials, the elastic strain produced is in phase with the applied stress (phase angle $\delta = 0$) and no mechanical damping occurs. For elastic materials, the applied stress is stored as potential energy when they are stretched and converted to kinetic energy when it is removed and the materials return back to their original dimensions. While for the viscous materials, the viscous strain lags behind the applied stress by $\delta = 90°$. Viscous materials do not store all the energy used in deforming them as potential energy. Part of the energy is instead dissipated as heat. The energy dissipated as heat manifests itself as mechanical damping In general, the potential energy stored in the elastic materials is reversible while in viscous materials is irreversible. For viscoelastic polymers that possess both viscous and elastic features, part of the energy is stored as potential energy and part is dissipated as heat. Therefore, the phase angle between strain and stress is between $0 < \delta < 90°$.

The elastic (or storage) modulus E' corresponds to the elastic response is the ratio of the elastic stress to strain and represents the stored elastic energy in the sample. While the viscous (or loss) modulus E'' is due to the viscous response is the ratio of the viscous stress to strain and corresponds to the amount of energy dissipated as heat during the deformation of the material. The elastic and viscous responses are related to the complex modulus E^* of the material that is a measure of the materials resistance to deformation by the following equations:

$$E^* = E' + iE'' \tag{5.3}$$

Tan δ or loss tangent indicates the relative damping ability in the material. It is a measure of the ratio of energy lost to energy stored in a cyclic deformation and is defined as loss modulus to storage modulus ($\tan \delta = E''/E'$). It is dimensionless. The peak shown in the tan δ in the glass transition region when tan δ is plotted against temperature refers to the rapid change of the material properties from a rigid phase to a rubbery phase [3]

5.3.2 Experimental Method

The Polymer Laboratories Dynamic Mechanical Thermal Analyser (PL-DMTA) was used to perform DMTA on rectangular bars of PMMA and PS with dimensions of

17.5 x 10.5 x 1.9 mm^3 in the single cantilever bending mode. The sample was firmly clamped at one end and held by a central clamp at other end. The central point of the bar was continuously vibrated sinusoidally by a drive shaft connected to an oscillator. The clamped samples were then cooled using liquid nitrogen, which was introduced into the chamber via a glass funnel. All measurements were carried out at 0 1 and 100 Hz frequency with a strain setting of x 4. The heating rate was set at 3 °C/min and specimens were tested over the temperature range from –100 °C to the temperature at which the specimens were found to have become excessively softened and could not be properly flexed. E' and E'' were continuously recorded.

5.4 Results and Discussion

5.4.1 Differential Scanning Calorimetry

Graph 5.1a and 5.1b showed the heat flow against temperature for PMMA and PS obtained from the Differential Scanning Calorimetry. PMMA and PS are fully amorphous, therefore no crystallinity peak was found on the curves.

The motions of polymer chains are governed by the temperature. In principle, the main modes of motion in polymers involve the motion of branch points, rotation of side groups, crankshaft motion involving 4-6 bonds, segmental motion and motion of crystallite. The polymer chains are immobile and effectively frozen in position at temperatures close to 0 K, as they possess too little thermal energy to move. As the temperature increases, the acquired thermal energy is divided between all the various possible modes of motion. However, the different modes require different amounts of energy to activate them and hence there exist threshold temperatures that can be detected as transitions for the unfreezing of each.

The glass transition is the most important thermal transition shown by amorphous polymers. It is usually known as α transition The secondary transitions β, γ...are observed in order of decreasing transition temperature ($T_\alpha > T_\beta > T_\gamma$). The discontinuity at T_g suggests a change in the availability of free volume between the molecules. Such volume must be present for the motions of long-range segmental

polymer chains to occur. The glass transition region therefore corresponds to the onset of long-range segmental motions that involve the movements of around 30 ~100 backbone atoms. As the polymer cools to the glass transition the free volume reduces to the critical value below which the long-range segmental motion is impossible, and only the three or five-bond crankshaft rotations of the main chain and rotations of side groups remain at temperatures below T_g.

From the DSC data, the glass transition temperatures of PMMA and PS were detected at around 117 °C (Graph 5.2a) and 100 °C (Graph 5.2b) respectively. However, the glass transition is sometimes considered as a range of temperatures that in this region the properties of polymers continuously changed from glassy to rubber. From Graph 5.2a and 5 2b, the baseline showed the discontinuity for the glass transition from 111 °C to 123 °C for PMMA and from 97 °C to 104 °C for PS. The specific heats of PMMA at 50 °C and 90 °C are 840 $Jkg^{-1}K^{-1}$ and 1110 $Jkg^{-1}K^{-1}$ (Graph 5.3a) and of PS are 530 $Jkg^{-1}K^{-1}$ at 50 °C and 680 $Jkg^{-1}K^{-1}$ at 80 °C respectively (Graph 5 3b).

5.4.2 Dynamic Mechanical Thermal Analysis

DMTA is capable of detecting the β transition in a sample, this cannot be done using DSC. From Graph 5.4a, 5 4b, 5.5a and 5.5b, it is observed that the storage moduli of PMMA and PS drop very strongly in the glass transition region. This is reasonable as PMMA and PS are fully amorphous polymers not semicrystalline polymers in which the decrease in storage modulus is less pronounced.

During mechanical experiments, the motions of the polymer chains give rise to energy dissipation and will appear as peaks on the loss factor curve at temperatures where the motions take place [7] For PMMA tested at 0.1 Hz, the broad peak of β relaxation is around –50 °C to 25 °C (Graph 5.4a), while at 100 Hz is around 35 °C to 70 °C (Graph 5.4b). The β relaxation in PMMA is generally due to the movement of the ester group in the polymer. A number of authors using dilatometric techniques have shown the existence of transition processes in the 20 °C ~ 70 °C range.[4,8,9,10,11]

In both dynamic mechanical loss spectrum and in dielectric loss measurements, the β relaxation peak of polystyrene appears just below the glass transition.[12] However, for

polystyrene tested by DMTA at 0.1 Hz, a very broad peak was observed at the temperature between –25 °C and 25 °C. It could be due to the β relaxation of polymer chains in PS. However, at 100 Hz, the peak disappeared. Illers[5] reported the β relaxation peak merges with the α relaxation at frequencies higher than 40 Hz. In the mechanical loss spectrum at 100 Hz, Takayanagi[6] observed that the β relaxation is apparent as a shoulder on the primary glass transition peak. This tendency, the merging of the α and β relaxation regions at higher frequencies, is noticed for several other polymers. Illers and Jenckel[7] said that the β relaxation is due to the rotation of some phenyl groups, which possess less steric hindrance than others.

5.5 Conclusion

PMMA has two transitions while PS has only one at 100 Hz The transition temperatures shown by PMMA were the glass transition at around 117 °C and the secondary transition at 70 °C at 100 Hz. While, the transition temperature shown by PS at 100 Hz was only the glass transition at 100 °C. At 0.1 Hz, both PMMA and PS showed two transitions – the glass transition and the secondary transition. However, the secondary transition temperature of PMMA shifted to around 0 °C and PS showed a broad peak, possibly due to the β transition, over a temperature range from –25 °C to 25 °C at 0.1 Hz.

The secondary (β) transition is due to the movement of side group in the polymer chains The transition temperatures are influenced by the excitation frequencies chosen in DMTA. Therefore, it is difficult to compare the transition temperatures when different excitation frequencies are used.[13]

The specific heat of PMMA and PS differed from temperature to temperature. For PMMA, the specific heat was 840 $Jkg^{-1}K^{-1}$ at 50 °C and 1110 $Jkg^{-1}K^{-1}$ at 90 °C. While for PS, the specific heat was 530 $Jkg^{-1}K^{-1}$ at 50 °C and 680 $Jkg^{-1}K^{-1}$ at 80 °C.

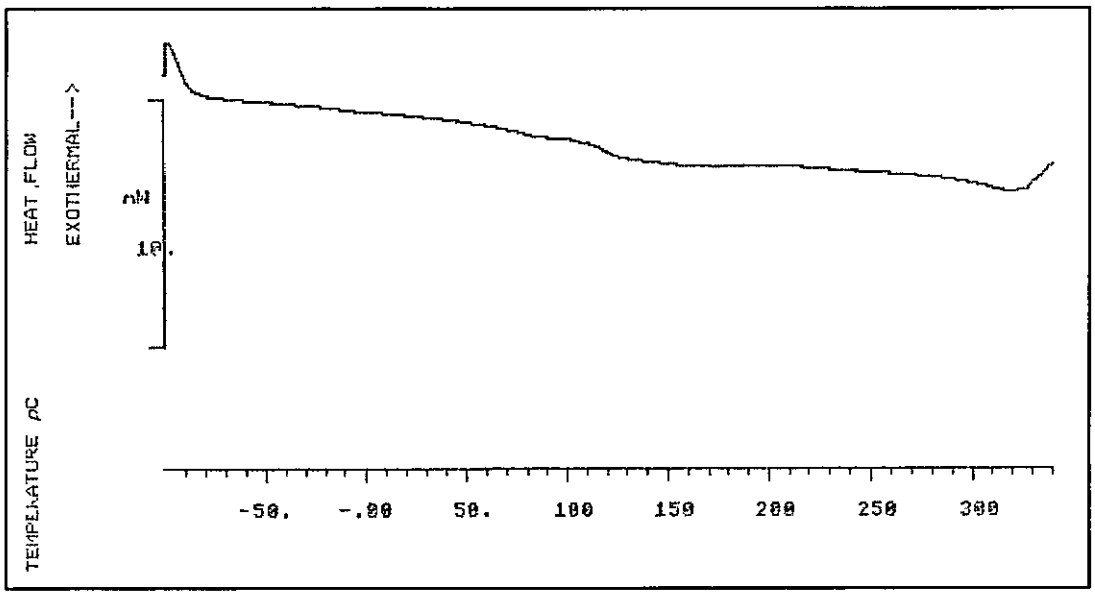

Graph 5.1a. Heat flow against temperature for poly(methyl methacrylate) obtained from DSC.

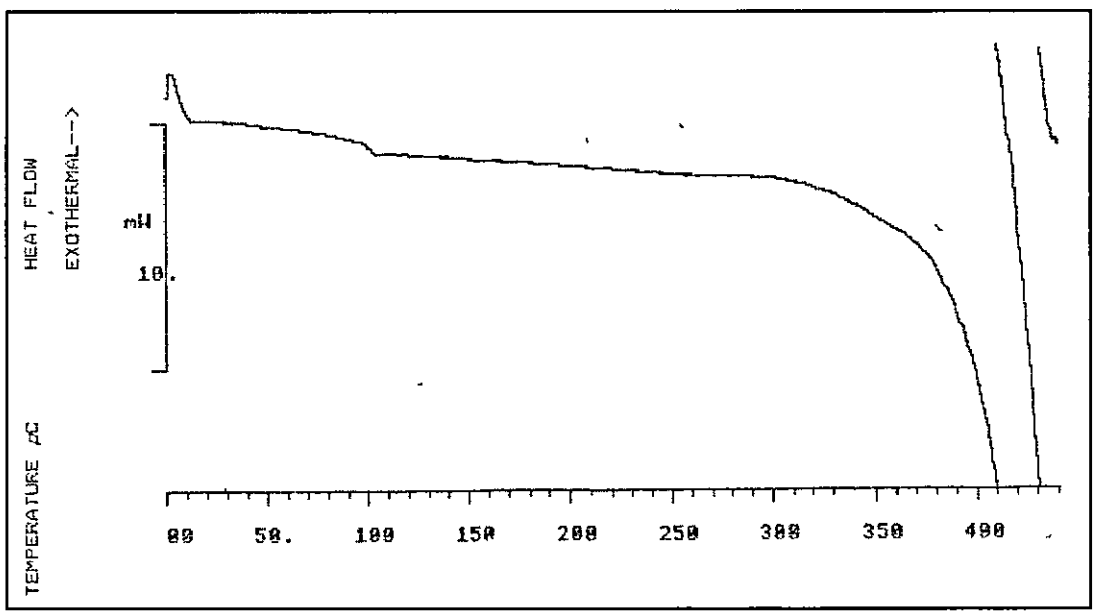

Graph 5.1b: Heat flow against temperature for polystyrene obtained from DSC.

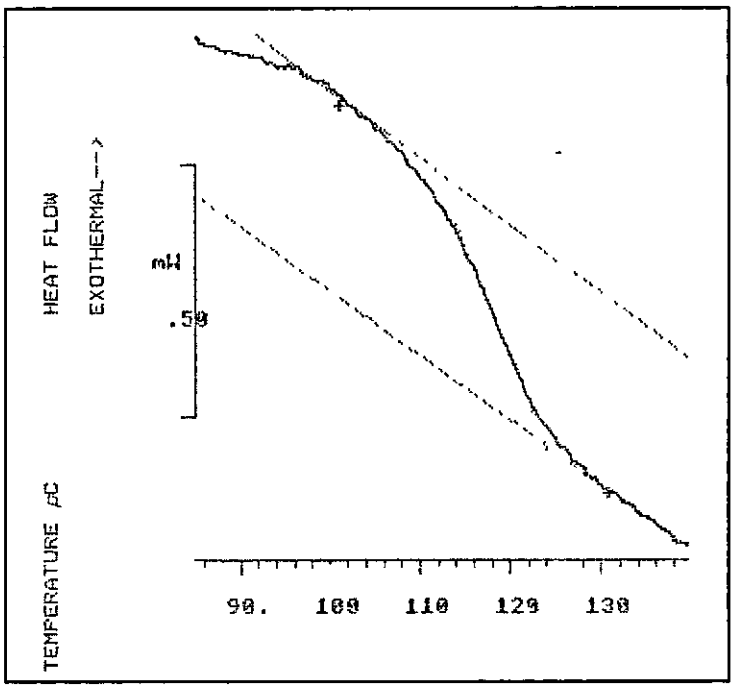

Graph 5 2a: Glass transition temperature for PMMA.

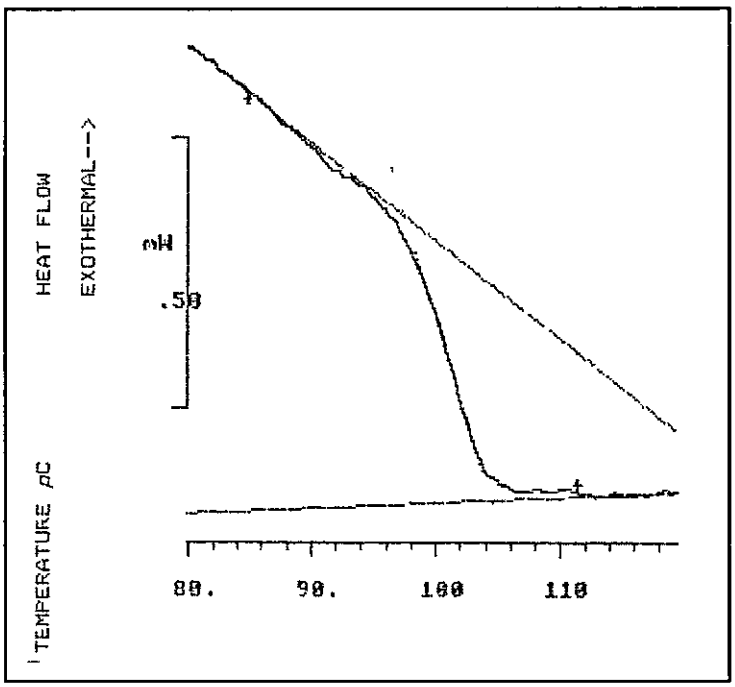

Graph 5.2b: Glass transition temperature for PS.

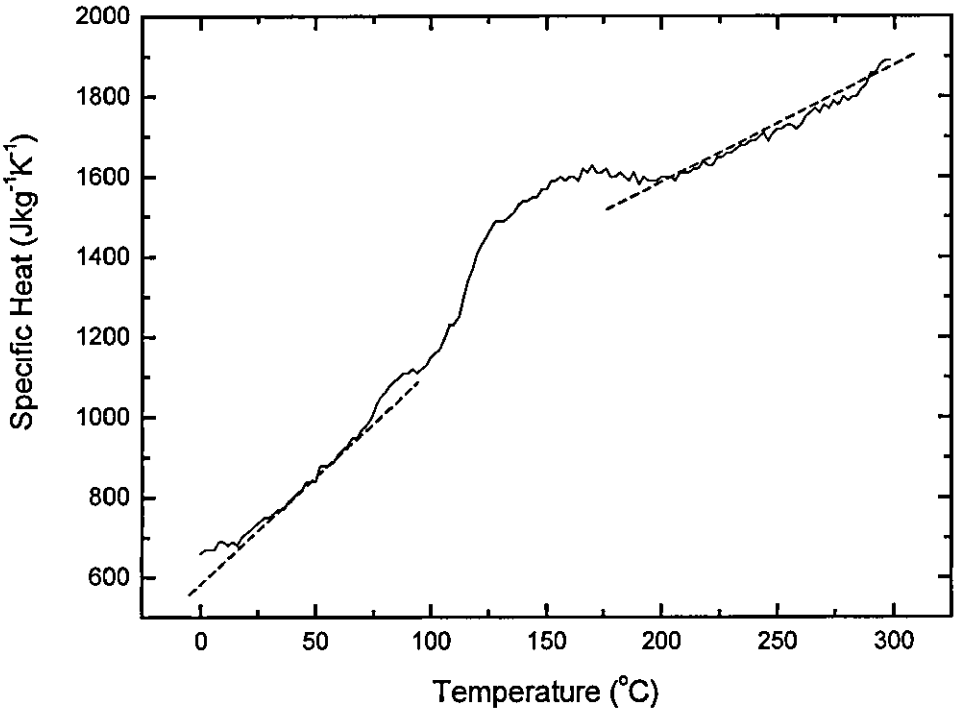

Graph 5.3a: Specific heat of Poly(methyl methacrylate) from 0 to 300 °C

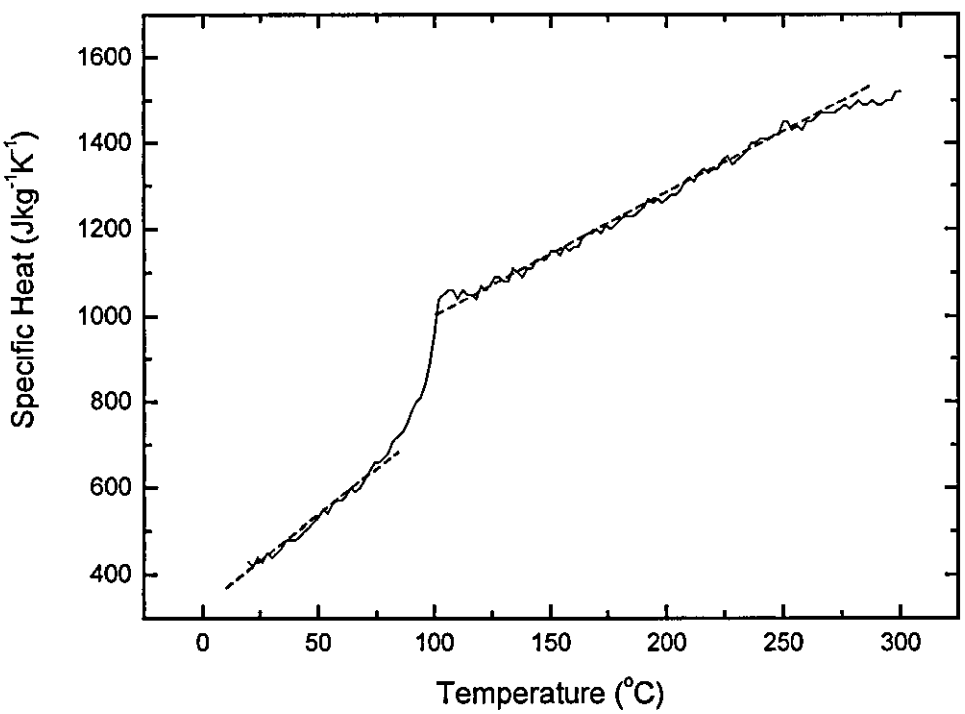

Graph 5 3b· Specific heat of Polystyrene from 0 to 300 °C.

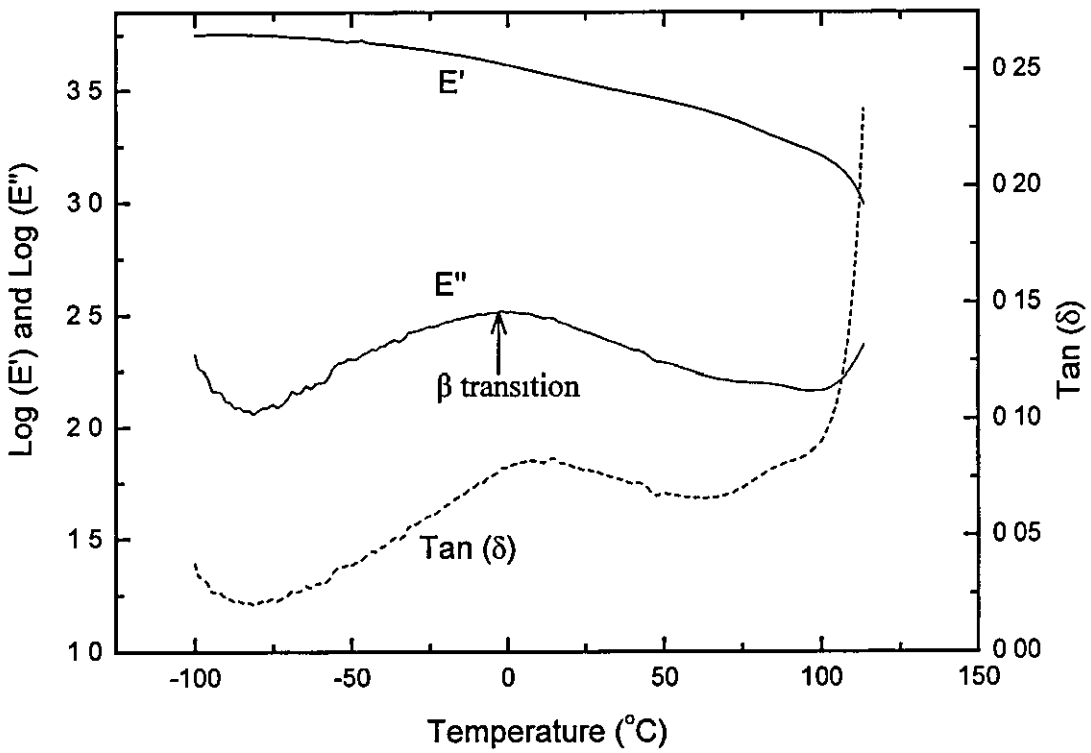

Graph 5.4a Diagram of the storage modulus (E'), loss modulus (E'') and loss tangent (tan (δ)) of Poly(methyl methacrylate) at 0.1 Hz.

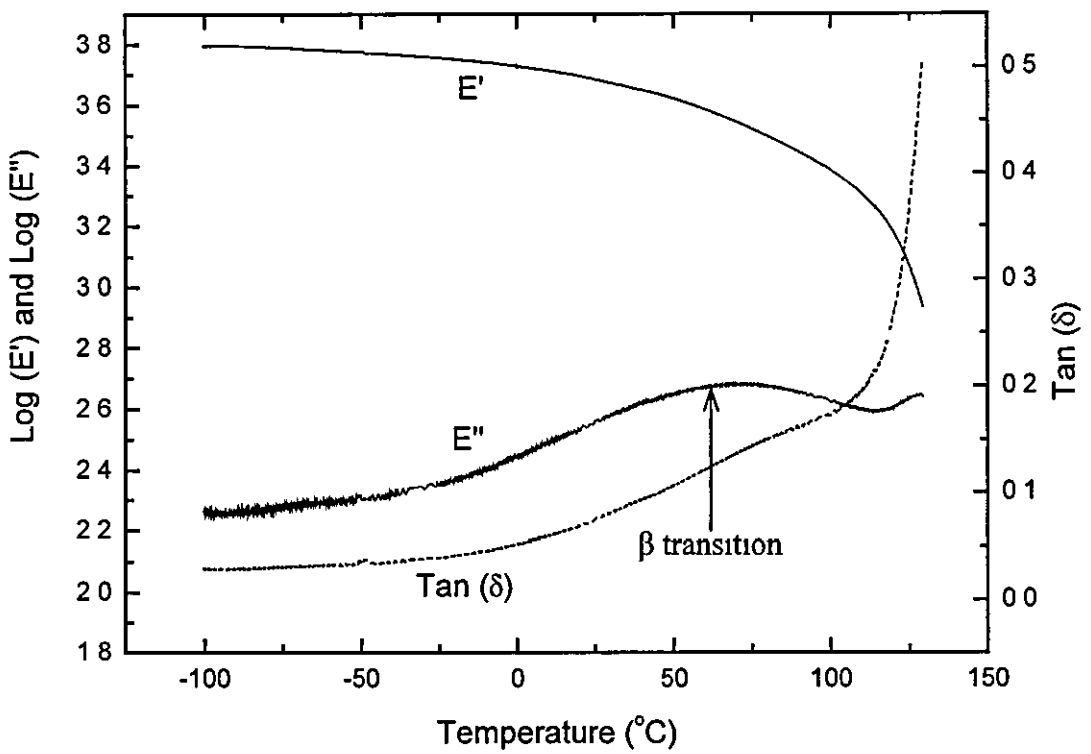

Graph 5.4b: Diagram of the storage modulus (E'), loss modulus (E'') and loss tangent (tan (δ)) of Poly(methyl methacrylate) at 100 Hz.

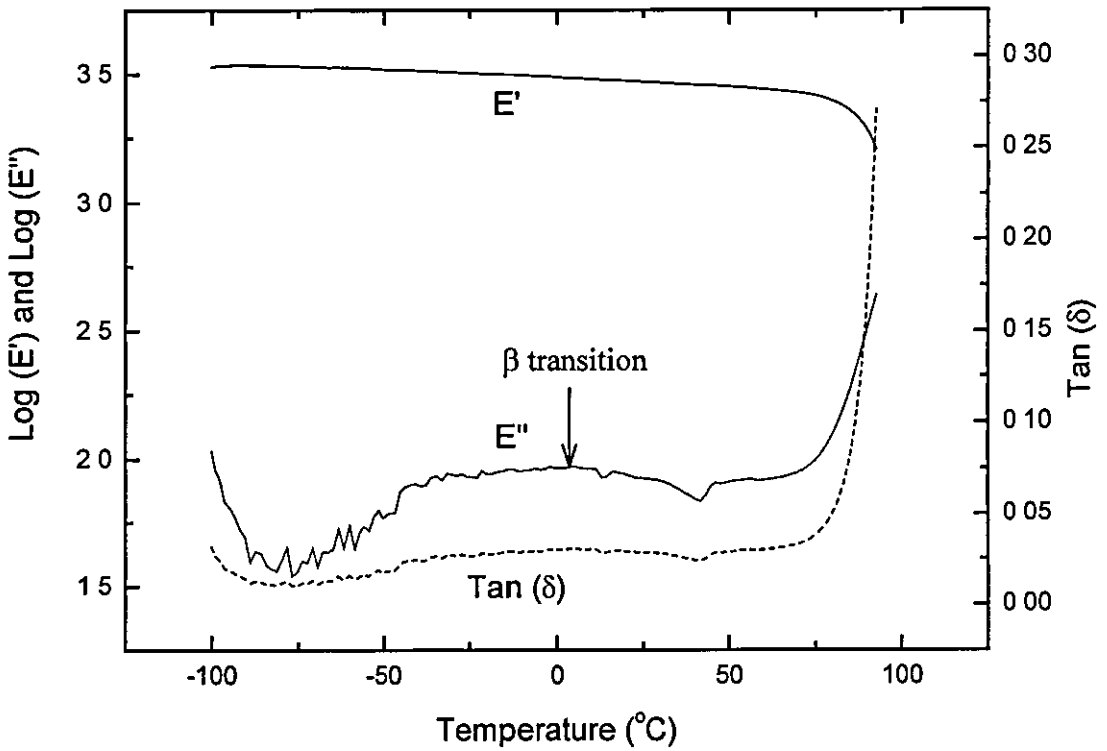

Graph 5.5a: Diagram of the storage modulus (E'), loss modulus (E'') and loss tangent (tan (δ)) of Polystyrene at 0.1 Hz.

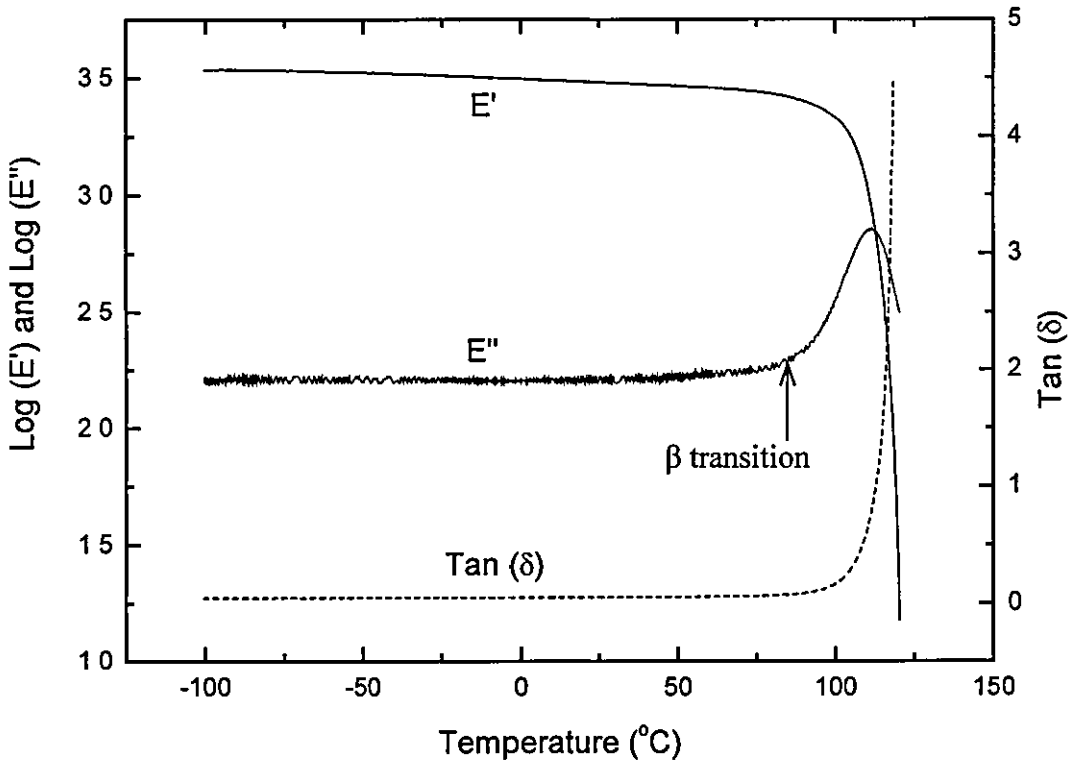

Graph 5.5b: Diagram of the storage modulus (E'), loss modulus (E'') and loss tangent (tan (δ)) of Polystyrene at 100 Hz.

References

1. **M. E. Brown,** "Introduction to Thermal Analysis : Techniques and Applications", Chapman & Hall, London, 1988

2. The operating instruction for TA3000 system

3. **J. D. Ferry,** "Viscoelastic Properties of Polymers", John Wiley & Sons, INC. London,1969

4 **O. D. Sherby and J. E. Dorn,** Journal of the Mechanics and Physics of Solids **6** (1958) 145

5 **K. H. Illers,** Zeitschrift fuer Elektrochemie **65** (1961) 679

6. **M. Takayanagi,** Reports on Progress in Polymer Physics (Japan) **6** (1963) 121

7. **K. H. Illers and E. Jenckel,** Journal of Polymer Science **41** (1959) 528~531

8. **Y. Wada and K. Yamamoto,** Journal of Physical Society of Japan **11** (1956) 887

9 **S. S. Rogers and L. Mandelkern,** Journal of Physical Chemistry **61** (1957) 985~990

10. **T. Holt and D. Edwards,** Journal of Applied Chemistry **15** (1965) 223~229

11. **E. V. Thompson,** Journal of Polymer Science **A-2 6** (1968) 433~449

12. **R. N. Haward,** "The Physics of Glassy Polymers", Applied Science Publishers Ltd., London, 1973

13. **R. J. Young and P. A. Lovell,** "Introduction to Polymers", Chapman & Hall, New York, 2nd Edition, 1991

Chapter 6

Density Measurement

6.1 Introduction

A Six Column Density Apparatus manufactured by DAVENPORT, was used to study the density of compressed polymer samples after testing using the C4 camera system. The apparatus consists of six column tubes made from precision bore glass tubing (borosilicate) and held in a water jacket which is made from cast acrylic tube (Figure 6.1).

The adoption of a proper sweeping method is essential in order to help to extend the life of a column. Sweeping is loading or unloading samples and floats into or out of the column. However, it is not necessary to sweep the column after every test but is essential to sweep it after a few specimens have been collected. Specimens and floats should be swept into the solution using the sweep basket. Since too many specimens and floats fill up the sweep basket, the whole unit will act like a solid piston and introduce turbulent flow conditions that will destroy the density gradient The sweeping speed is approximate 4 hours/m. The basket was descended/ascended vertically, not hitting the sides and pulling the line tight to avoid any disturbance to the density gradient.

The floats must be cleaned with acetone or chloroform to remove any greasy contamination. The preferred number of floats for a column is eight. Specimens are wet with the residue of high-density solution before being added to the column.

6.2 The Accuracy of Density Measurement

The preparation of density gradient columns depends on both the density gradient required and the samples themselves. The recommended range over one column gradient is 0.05 g/ml. The range of 0.1 g/ml is common. However, with increasing range, the accuracy of measurement will reduce. A range that exceeds 0 3 g/ml is not

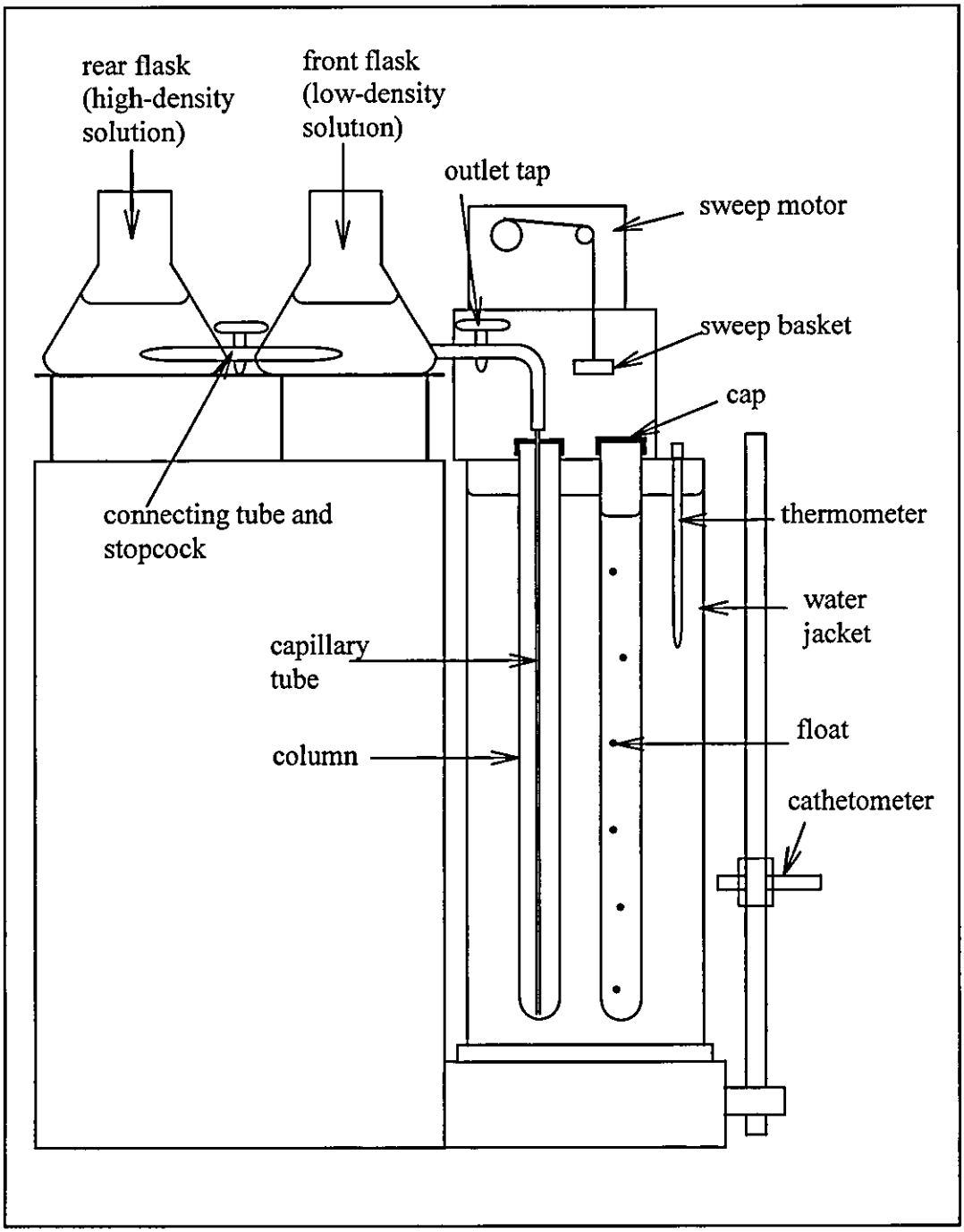

Figure 6.1: Diagram of the Six Column Density Apparatus.

recommended. The densities of floats used were calibrated at the temperature 23 °C to an accuracy of ± 0.00015 g/ml.

6.3 Preparation of the Solution

The commercial density of the purchased PMMA sample is 1.19 gcm^{-3}. Referring to Appendix 6.1, the combination of calcium nitrate and water that provides the density range from 1.00 to 1.60 gcm^{-3} is chosen as the medium to study the densities of the compressed samples.

A 1000 ml low-density solution was prepared by dissolving calcium nitrate hydrated, $Ca(NO_3)_2.4H_2O$, into distilled water in a beaker. The solution was heated to 70 °C on a hotplate equipped with a magnetic stirrer. After the chemical was fully dissolved, the solution was left to cool down to room temperature before its density was determined using a hydrometer. More $Ca(NO_3)_2.4H_2O$ was then added, heating up and cooling down the solution to the room temperature repeatedly until the required density was obtained. Another 1000 ml of high-density solution was prepared using the same method.

The most accurate reading of the solution density can be obtained when the temperatures of the hydrometer and the solution are equal to the room temperature. The low-density solution prepared was 1.12 g/ml and the high-density solution was 1.21 g/ml. Two hydrometers with range 1.000~1.200 g/ml and 1.200~1.400 g/ml available in the laboratory were used to measure the low-density and the high-density solutions prepared respectively. The minimum deviation for the scale is 0.002 g/mm.

6.4 Preparation of the Density Gradient Column

860 ml of the high-density solution was measured out and poured into the rear flask with the stopcock closed The stopcock was then opened carefully and slowly to fill the connecting tube with the solution After the connecting tube filled with the solution, the stopcock was then closed back again. Similarly, 860 ml of the low-density solution was measured out and poured into the front flask slowly so that the

connecting tube would be filled up with the solution. Air trapped in the connecting tube can be removed by tilting the assembly.

Turning on the stopcock on the connecting tube, a constant amount of the high-density solution was flowed to the low-density solution in the front flask. A magnetic stirrer was used to mix the solutions. The system was left for 10 minutes to achieve equilibrium before piping them to the column through the capillary tube connected to the front flask. The outlet tap was opened gradually until a continuous unbroken flow of mixed solutions through the capillary tube was observed. This must be achieved before around 5-cm height of solution had been run into the column. Any bubble formed during filling will alter the density gradient. The rate of flow through the capillary tube must be less than that between two flasks. A detailed procedure of filling the tube can be found in the Six Column Density Apparatus manual (Reference 1). After filling the column, it was left at least 2-3 hours or overnight to stabilise.

6.5 Experimental Procedures

Samples of PMMA with Ø6 4 mm and H3.00 mm and floats were swept into the column using the sweep basket provided. They were left for 48 hours to achieve equilibrium in this experiment The heights of the samples and the floats were measured using the cathetometer by sighting the crosshair on the centre of the float and the sample. After taking the measurements, samples were retrieved from the column and compressed at the temperature 50 °C (323 K) using the C4-Camera Dropweight system. Metal rings were used to limit the strain of the samples being compressed.

The compressed samples and the floats were then swept into the same column The heights of the floats and samples were measured after leaving for 48 hours to stabilise in this experiment The density of the sample (ρ) at the height of x is calculated using the formula below:

$$\rho = a + \frac{(x-y)(b-a)}{(z-y)} \tag{6.1}$$

where a and b are the densities of the standard floats (next to each other) which are at heights y and z, and the height of the sample x is located between y and z.

The density gradient of the column deteriorates with time The reliability of the gradient could be studied by plotting the float densities against their heights. If the graph is linear, the column can still be used to study the sample density. In order to monitor the reliability of the gradient, the heights of the floats together with the heights of the samples were measured each time the sweeping was carried out. The float densities against their heights were plotted and were fitted to a straight line using linear regression to check against the graph (Figure 6 2). If the modulus of the correlation coefficient is close to one, this indicates that the gradient is still reliable for measurement.

6.6 Result and Discussion

Density measurement was carried on PMMA with the objective to see if there was an increase in the sample density after being compressed. The compression was carried out in C4-Camera Dropweight system as it provided high-strain rate deformation information on the PMMA sample.

Swallowe et al.[2] carried out high rate testing on semicrystalline polymers PEK, PET and PEEK and discovered these polymers showed a great increase in crystallinity when tested at high rate of 10^3 s^{-1}. The density in the crystalline region is higher than that in the amorphous region. Thus, with a great increase in crystallinity the density of semicrystalline polymer after compression will definitely increase.

However, PMMA is an amorphous polymer with atactic regularity It was expected that high rate deformation might induce an arrangement of polymer chains that lead to an increase in density. Table 6.1 shows the data of the densities of PMMA samples before and after compression to different strains measured using the Six Column Density apparatus. The data is displayed in Graph 6 1 by plotting density versus strain. It can be seen that the densities of the PMMA samples did not increase after compression. The deviation in the density before and after compression was very

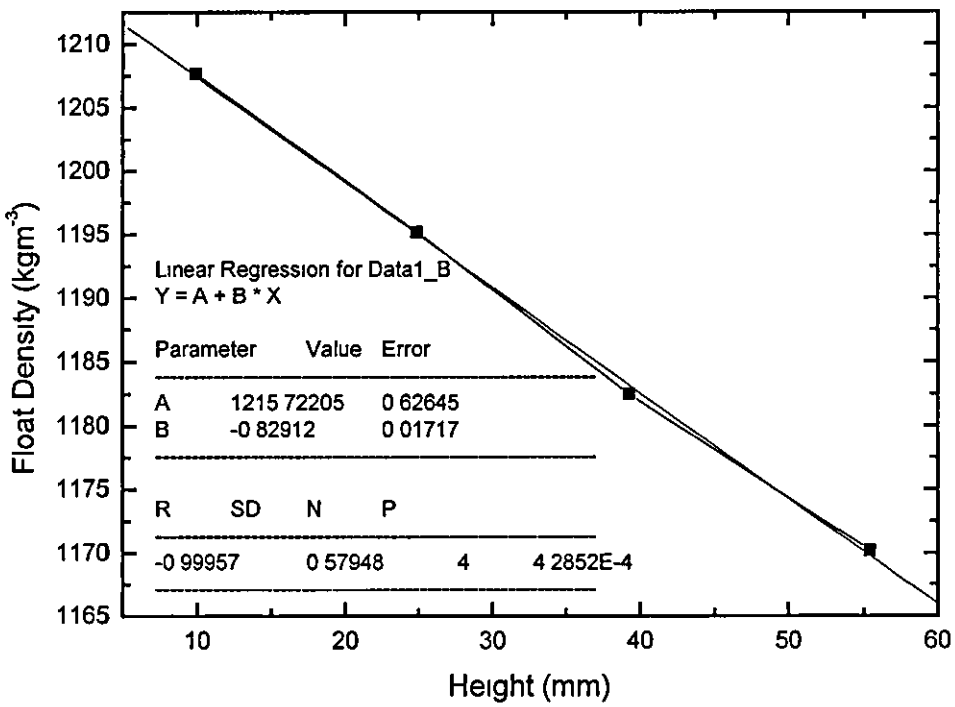

Figure 6.2: Plot of the float density versus height The plot was carried out each time the densities of the samples were measured to monitor the validity of the column.

small. It might due to the implantation of dirt onto the sample that caused an increase in the sample density or the sample fractured on the edge and caused a decrease in the sample density during impact. A detailed discussion about the increase and decrease in the sample density is found in Chapter 9.1 5

6.7 Conclusion

The density of the PMMA sample did not show any sign of increase with strain after the high strain rate deformation.

strain	density (kgm^{-3})		difference
	before compression	after compression	
0.45	1188.77	1188.23	-0 54
0.50	1186.44	1187.62	+1.18
0.63	1189 26	1186.44	-2.82

Table 6.1: Densities of PMMA samples before and after compression at different strains at 50 °C using the C4-Camera Dropweight system.

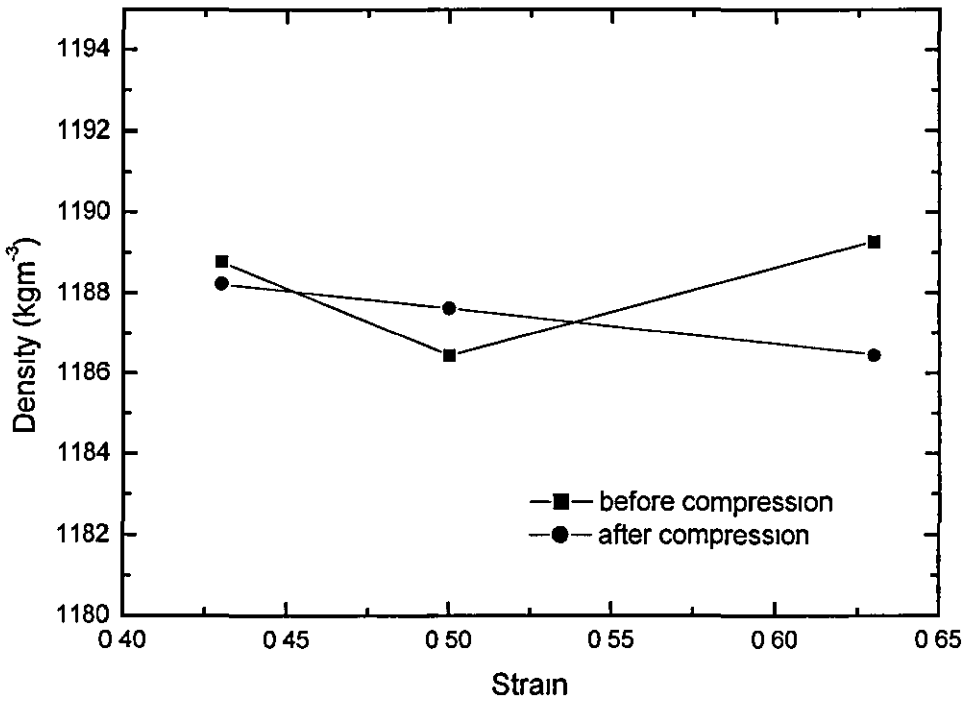

Graph 6 1: Density versus strain for PMMA samples, before and after compression at 50 °C (323 K) using the C4-Camera Dropweight system.

Appendix 6.1: Media for Density Gradient Columns

DENSITY	MEDIA 1	MEDIA 2
0.79-0 98	Isopropanol	Water
0.79-0.98	Ethanol	Water
0.79-1.11	Isopropanol	Di-ethyleneglycol
0.79-1.59	Ethanol	Carbon Tetrachloride
0.87-1.59	Toluene	Carbon Tetrachloride
0 98-1.00	Ethanol/water	Water/Pot Iodide
1 00-1.41	Water	Sodium Bromide
1.00-1.60	Water	Potassium Iodıde
1 00-1.60	Water	Calcium Nitrate
1 10-2.80	Tetra-Bromoethane	Triethylphosohate
1.60-1.99	Carbon Tetrachlorıde	Trimethylenedibromide
1.99-2 18	Trimethylenedibromide	Ethylenebromide
2.19-2.89	Ethylenebromide	Bromoform
2.80-3.30	Triethylphosohate	Diodomethane

Appendix 6.2: Density Error Calculation

The density of the sample (ρ) at the height of x is calculated as below:

$$\rho = a + \frac{(x-y)(b-a)}{(z-y)}$$

where a and b are the densities of the standard floats (next to each other) which are at heights y and z, and the height of the samples x is located between y and z.

Let the error for the float (δa or δb) is 0.15 kgm^{-3} and the error for the height (δx, δy or δz) is 0.05 cm.

Let $v = x - y$, $w = z - y$ and $s = b - a$, thus

$$\delta v = \delta x + \delta y$$

$$\delta w = \delta z + \delta y$$

$$\delta s = \delta b + \delta a$$

Let $f = \frac{v \times s}{w}$, the error of f can be calculated as below:

$$\left(\frac{\delta f}{f}\right)^2 = \left(\frac{\delta v}{v}\right)^2 + \left(\frac{\delta s}{s}\right)^2 + \left(\frac{\delta w}{w}\right)^2$$

Therefore, the error of the sample density is

$$\delta x = \delta a + \delta f$$

References

1. The Six Column Density Apparatus, user manual, Davenport, a division of ILOYD INSTRUMENTS LTD.

2. **G. M. Swallowe, J. O. Fernandez and S. Hamdan,** Journal de Physique IV France **7** (1997) C3-453~C3-458

Chapter 7
Optical Birefringence

7.1 Introduction

The phenomenon of double refraction or birefringence in plastic materials is a result of a polymer chain having different refractive indices along and across the main chain axis; such a chain is therefore said to be optically anisotropic. For materials having chains distributed randomly or unoriented, there is no resultant anisotropy, which means the refractive indices are same in all direction; such materials are said to be optically isotropic. The measurement of optical anisotropy is one of the methods used to study the orientation in polymers. Others include wide-angle X-ray diffraction, low-angle X-ray scattering and sonic techniques.[1]

Birefringence measures the orientation of both the crystalline and amorphous phases in semicrystalline polymers. However, the orientation of the crystallites in crystalline polymers can be measured by X-ray diffraction. Thus, by a combination of various experimental techniques, it is possible to determine the degree of orientation of the crystalline and amorphous phases in the semicrystalline polymer.

For polymers in the glassy state, the application of a stress makes polymers become birefringent because of changes in polarisability brought about by mechanisms such as deformation of bond angles, changes in bond lengths, and orientation of side groups [2]

7.2 Polarising Microscope and Compensator

The Carl Zeiss 431 polarising microscope was adopted to study the birefringence of samples. The arrangement of the main components in the Carl Zeiss polarising microscope is shown diagrammatically in Figure 7.1. White light source was used to illuminate the samples studied. The polariser is held under the microscope stage to constrain the incident light to vibrate in one plane only. The analyser is mounted in the body tube of the microscope and is above the objective lense. The polariser and

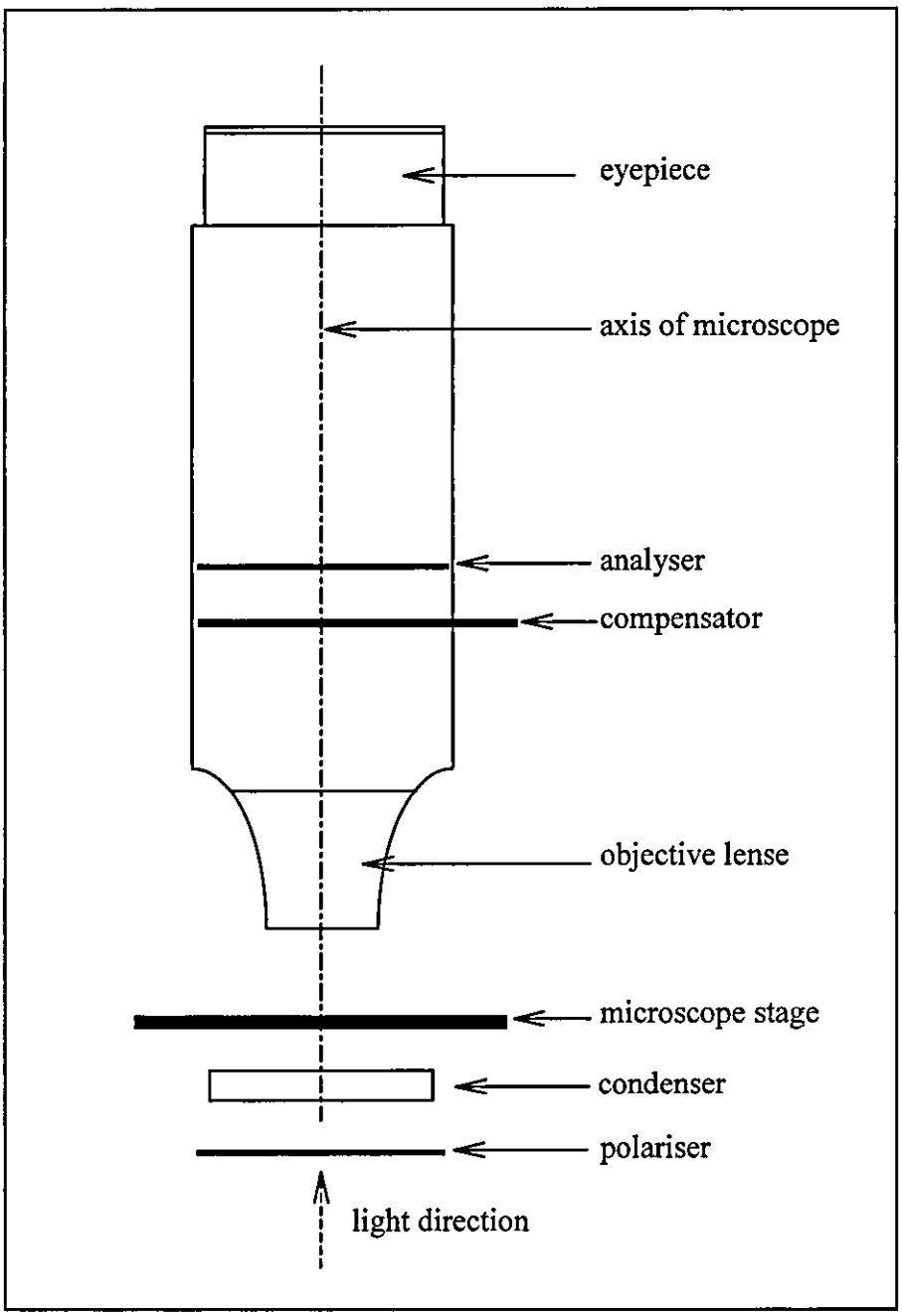

Figure 7.1: Diagram of the polarising microscope.

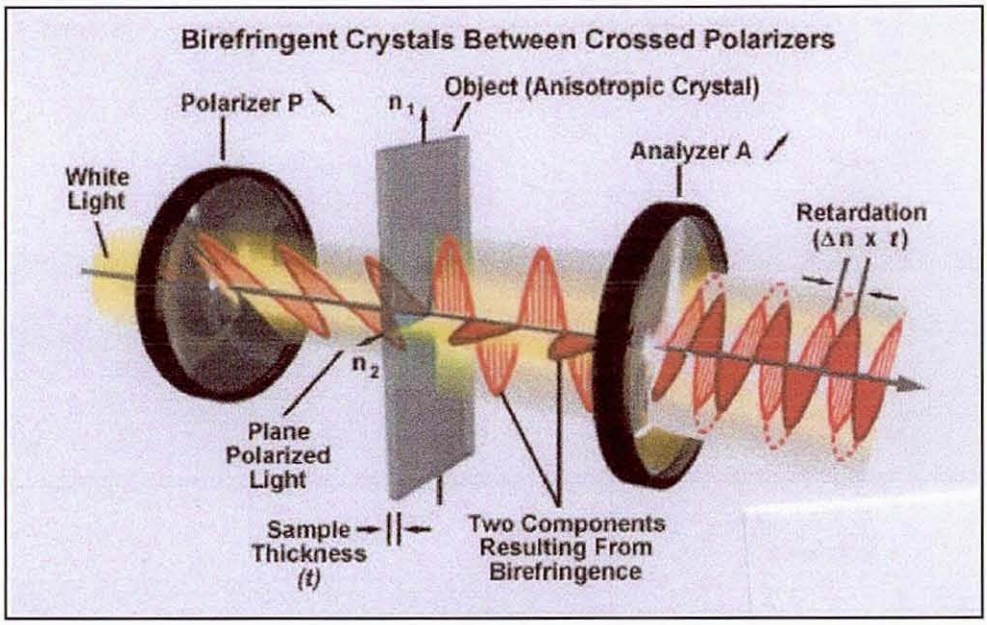

Figure 7.2: White light entering the polariser is constrained to vibrate in one plane with its direction parallel to the polarisation direction of the polariser. The polarised light after passing through the anisotropic crystal is refracted and separated into two components travelling with their planes perpendicular to each other and with two different velocities. The individual components of these two rays that are parallel to the polarisation direction of the analyser will pass through the analyser. The interference will then be formed due to the path differences of the individual components. Picture taken from Reference 9.

the analyser are in the crossed condition that is the polarisation direction of the polariser is oriented perpendicular to the polarisation direction of the analyser. If no birefringent sample is put on the microscope stage, the vibration plane of the emergent polarised light from the polariser will be perpendicular to the direction of the polariser. Hence, no light will pass through the analyser and the view will appear dark. When a birefringent sample is put on the microscope stage, the polarised light will be refracted into two components travelling with their vibration planes perpendicular to each other. The component that travels in the same velocity in every direction is called ordinary ray. While the component that travels with its velocity depends on the propagation direction is called extraordinary ray. Figure 7.2 shows the diagram of the light passing through the polariser and the analyser with a birefringent sample put on the path of the light.

The Carl Zeiss 4894000 Erhinghaus rotary compensator was used to measure the optical path differences of the emergent lights caused by the stress applied to the compressed samples. It consists of a calcite plate and a rotating drum calibrated in degree from 0° to 35°. The minimum scale is 0.05°. It is mounted on a horizontal axis to the microscope axis. The drum shows zero when the plate is horizontal. It is rotated when the drum is turned By rotating the plate, the path difference of the interference light is compensated when a dark band is seen moving across the interference field The drum can be turned to right and left to obtain compensations at two positions. By the use of the table supplied together with the compensator,[8] the path difference can be read off from the drume-scale reading.

For more detailed explanation about the microscopic examination of a sample can be found in Reference 3.

7.3 The Orientation of the Polymer chains – isotropic, uniaxial and biaxial indicatrix

The examination of a sample in polarised light between two crossed polarisers allows its structural orientation and birefringence to be revealed. Orientation in polymers refers to the alignment of the polymer chains, or the segments of the polymer chains,

or the crystalline regions in the polymer to some extent. The orientation of the stretched polymer can be retained permanently if it is cooled to below its glass-transition temperature before the molecules have had a chance to relax back to their random coiled configuration. The orientation of the materials can be optically divided into three indicatrices:[3]

a) isotropic
b) anisotropic uniaxial
c) anisotropic biaxial

Basically, an indicatrix is a geometric construct whose shape is determined by the refractive indices and the orientation of a crystal.

An isotropic indicatrix is a sphere with the lengths of the axes proportional to the refractive indices experienced by the light travelling through it (Figure 7 3) Since it is a sphere, the radii of all circles drawn through its center are equal to the radius of the sphere. Since all radii of the circles are equivalent, therefore, only one refractive index is found. Furthermore, the velocity of light in the isotropic materials (e.g isometric crystals) is the same in all direction and no constraint on the orientation of the vibration direction of the light due to the chemical bonds holding the molecules together are the same in all directions. Hence, all isotropic materials appear dark and stay dark on rotation of the microscope stage. If an isotropic material is strained, some of the chemical bonds will be stretched and others will be compressed This causes the materials become birefringent.

The uniaxial indicatrix is an ellipsoid with two unique axes. The lengths of the axes are proportional to the values of two unique refractive indices (n_ω and n_ε). There are two types of uniaxial indicatrix – positive when $n_\varepsilon > n_\omega$, negative when $n_\varepsilon < n_\omega$ (Figure 7.4) The axis of the indicatrix parallel to the optic axis is always proportional to n_ε while the axes perpendicular to the optic axis are proportional to n_ω The orientation of the optic axis of the uniaxial materials (e g. hexagonal and tetragonal crystals) greatly influences the interference pattern viewed under the polarised microscope.

(i) The optic axis of the materials is oriented vertically. When convergent light passes through the material, the vibration pattern is symmetrical about the melatope (the point where the optic axis emerge). Extraordinary rays with n_ε

vibrate along radial lines from the melatope and ordinary rays with n_ω vibrate tangentially to the circular lines. When the vibration directions of the extraordinary and ordinary rays are parallel to the polarisation directions the interference pattern appears black (Figure 7.5a)

(ii) The optic axis of the materials is oriented horizontally and parallel to the polarisation direction of the lower polariser. In this orientation the material exhibits its maximum birefringence and highest interference colour. The resulting dark cross is broad, fuzzy and nearly fills the field of view (Figure 7.5b).

(iii) The optic axis of the materials is oriented 45° horizontally. In this orientation the material not only exhibits its maximum birefringence and highest interference colour, the emergent light also shows its maximum brightness. However, the dark cross disappears (Figure 7.5c).

The biaxial indicatrix has three principal refractive indices (n_α, n_β and n_γ) along 3 mutually perpendicular axes (Figure 7.6). n_α is plotted along X, n_β along Y and n_γ along Z with $n_\alpha < n_\beta < n_\gamma$. The uniaxial indicatrix exhibits a single circular section, a biaxial indicatrix exhibits two circular sections with radius = n_β which intersect along the Y indicatrix axis (Figure 7.7). The optic axes are perpendicular to the circular sections and lie within the XZ plane of the indicatrix. The angle between the optic axis is the optic angle or 2V angle. Polarised light passing through biaxial materials (e.g. orthorhombic, monoclinic and triclinic crystals) is split into two rays – extraordinary and ordinary rays which vibrate at 90° to each other. By orientating the acute bisectrix (Bxa) vertically, the interference patterns with $2V < 40°$ (biaxial positive) and $2V > 40°$ (biaxial negative) are shown in Figure 7.8 and 7.9 respectively when the microscope stage is rotated. The retardation increases slowly from melatopes towards the acute bisectrix (Bxa).

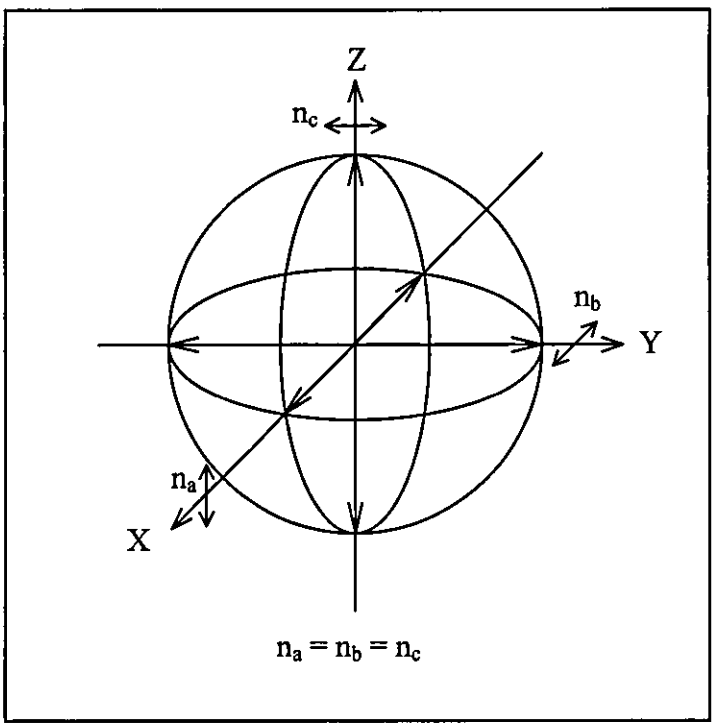

Figure 7.3: Isotropic Indicatrix.

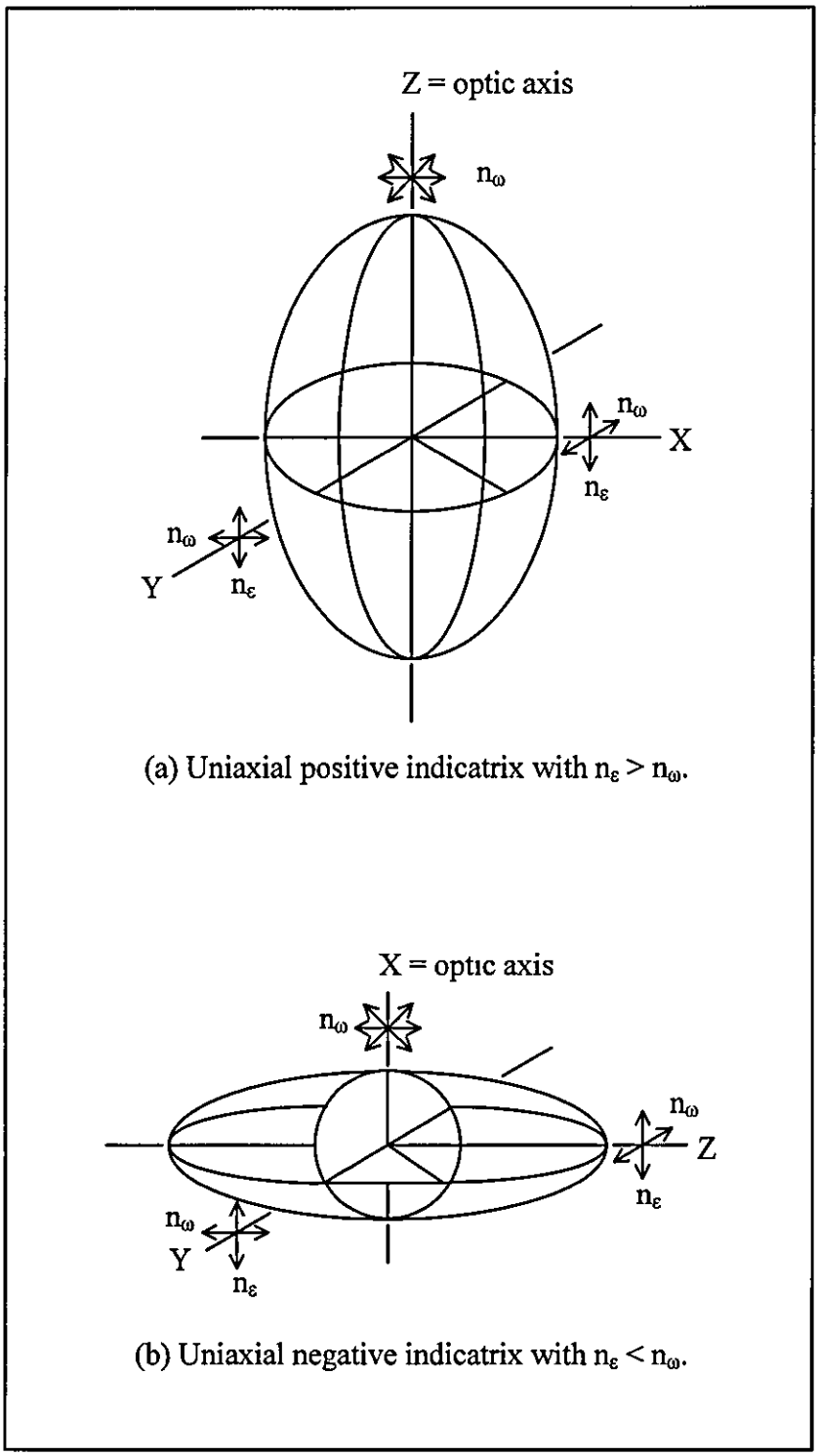

Figure 7.4: Uniaxial indicatrix.

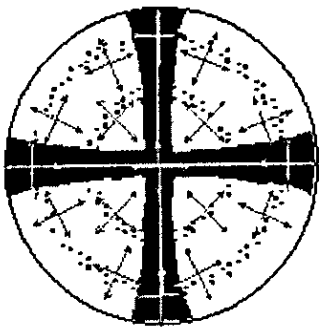

(a) The optic axis is vertical.

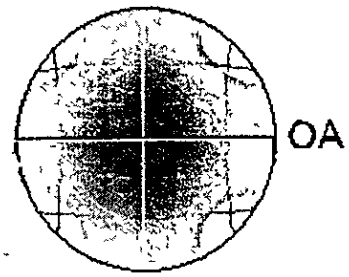

(b) The optic axis is horizontal and parallel to the polarisation direction of the polariser.

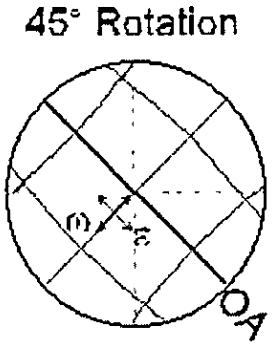

(c) The optic axis is horizontal and 45° to the polarisation direction of the polariser and analyser.

Figure 7.5: Interference patterns of a uniaxial material under the polarising microscope when its optic axis is vertical or horizontal or 45° horizontal to the polarisation direction of the polariser and the analyser. Picture taken from References 11 and 12.

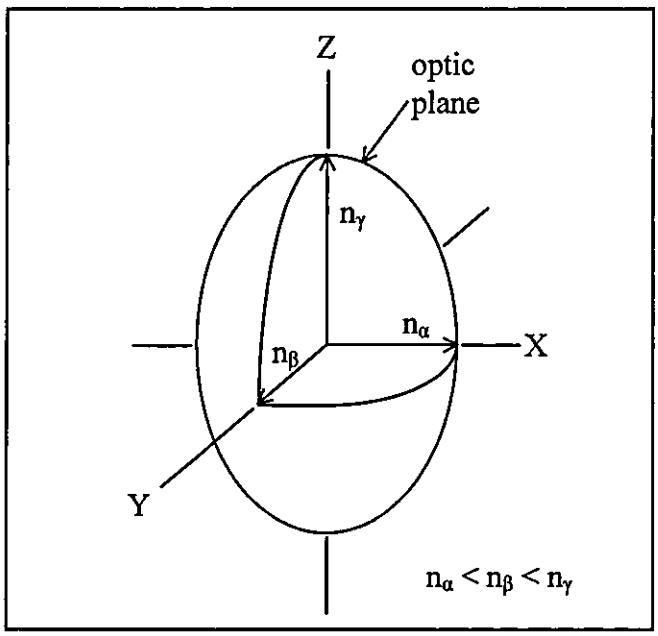

Figure 7.6: Biaxial indicatrix.

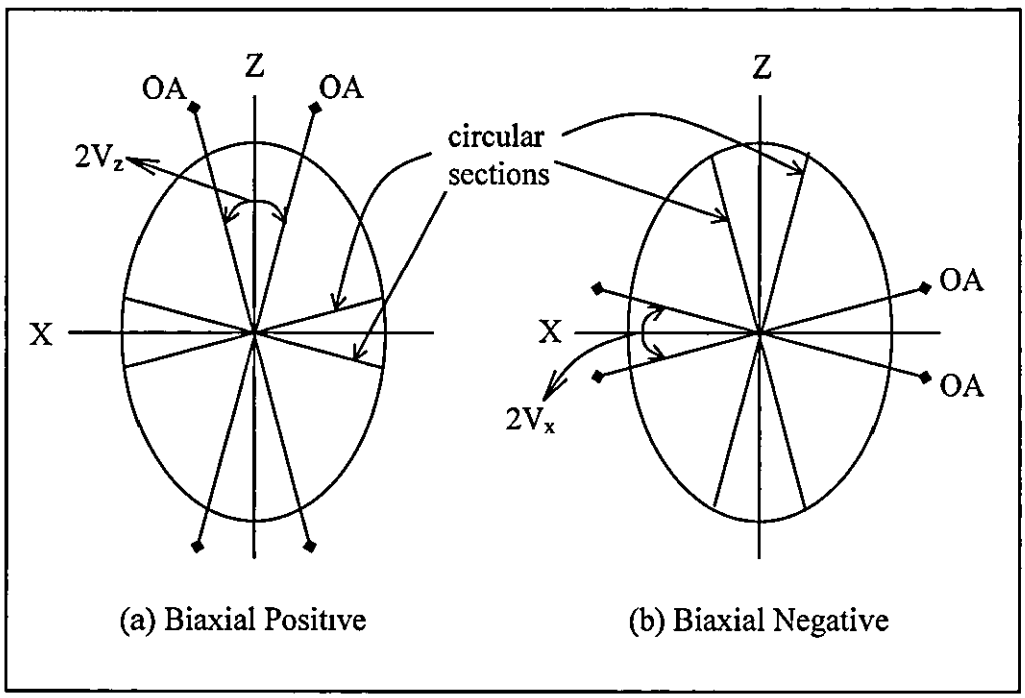

Figure 7.7: Materials are biaxial positive when the acute bisectrix is on Z axis and are biaxial negative when the acute bisectrix is on X axis.

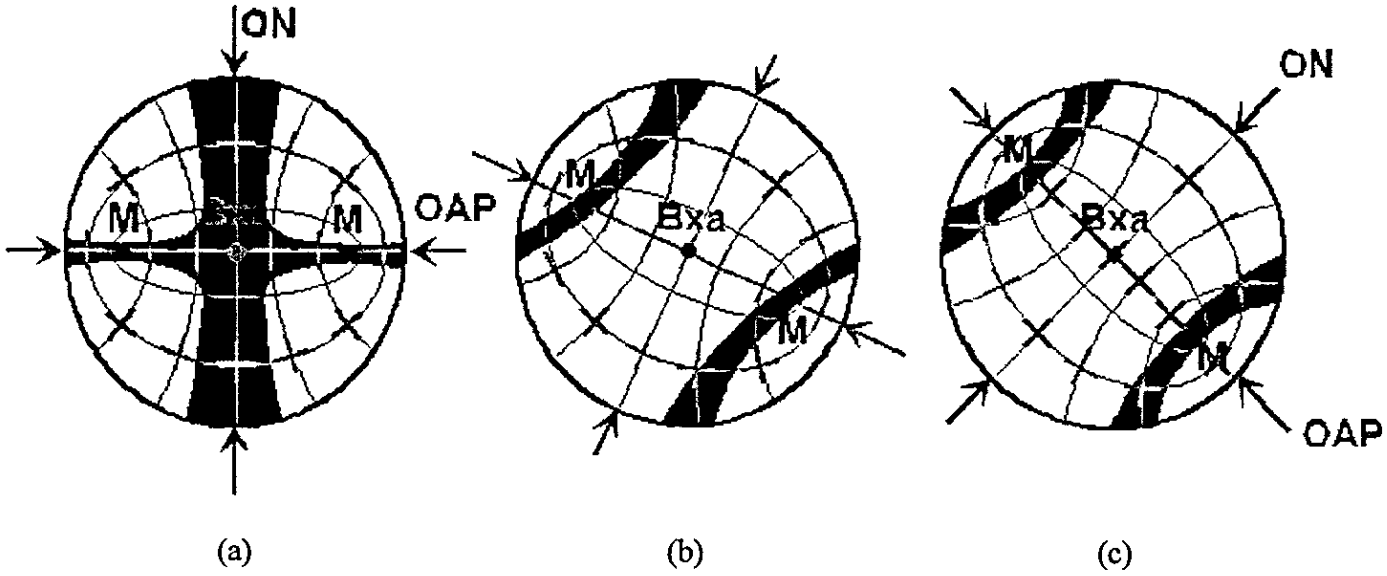

Figure 7.8: Interference patterns of a biaxial material with $2V < 40^{\circ}$ when (a) the melatopes are parallel, (b) the melatopes are in the angle $0 < x < 45^{\circ}$ and (c) the melatopes are 45° to the polarisation direction of the polariser. Picture taken from Reference 10.

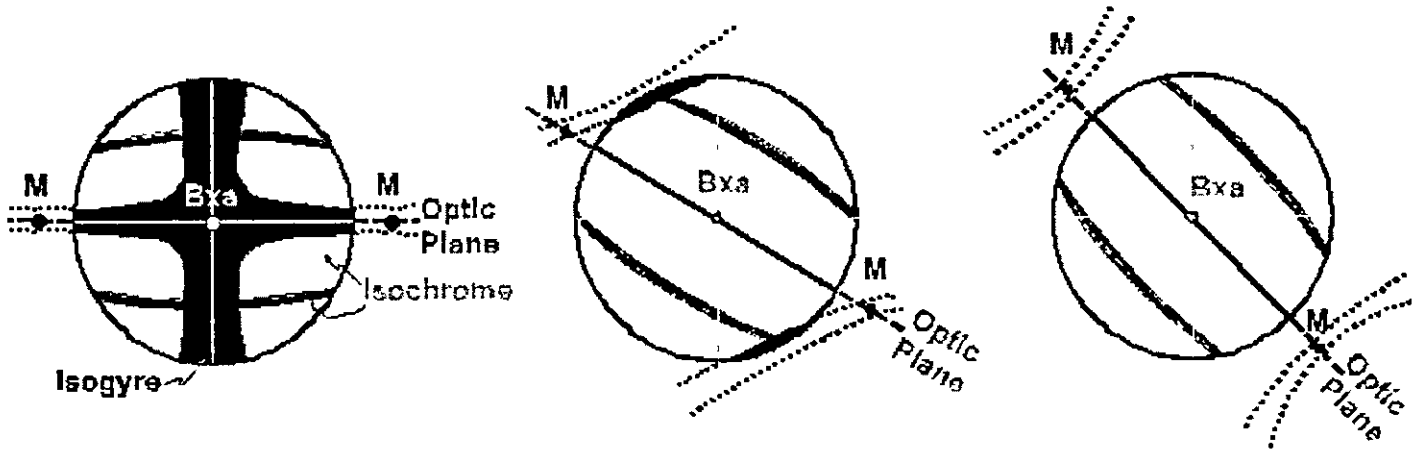

(a) (b) (c)

Figure 7.9: Interference patterns of a biaxial material with $2V > 40^{\circ}$ when (a) the melatopes are parallel, (b) the melatopes are in the angle $0 < x < 45^{\circ}$ and (c) the melatopes are 45° to the polarisation direction of the polariser Picture taken from Reference 10.

7.4 Measurement of Birefringence

The ordinary and the extraordinary rays after passing through an anisotropic material emerge with the planes of polarisation vibrating perpendicular to each other. Due to the difference of the refractive indices, there is an optical path difference, OPD (also called retardation, Γ) between the components that pass through the analyser. Thus, the birefringence, B is defined as a measure of the difference in refractive indices in two mutually perpendicular directions and can be calculated as

$$B = \left| n_{high} - n_{low} \right| = \frac{OPD}{t} \tag{7.1}$$

where t is the thickness of the sample. The optical path difference between the ordinary and extraordinary rays normally increases with increasing sample thickness.

7.5 Experimental

The Carl Zeiss 431 polarising microscope is used to measure the birefringence and to view the orientation of the compressed and uncompressed samples of PMMA and PS between two crossed polarisers.

The microscope stage is graduated in degrees around the edge. The sample mounted on a glass slide is laid on the stage. A layer of liquid with reflective index (n = 1.45), which is same as the sample reflective index, was put on the top and bottom surface of the sample to reduce refractions caused by the microcracks found on both surfaces of the sample. The microscope stage can be rotated in its own plane around the axis of the microscope so that the vibration directions of light in the sample under examination can be located at any desired angle to the planes of polarisation of the polariser and the analyser. The eyepiece (20x) and the objective lenses (1.25x) serve the purpose of magnifying the sample.

Two readings were taken from the Carl Zeiss 4894000 Erhinghaus compensator at two positions by turning the rotating drum to the left and to the right. Averaging of the two readings were made in order to reduce the error of the measurement. The path difference that corresponds to the reading taken was read off from the table provided

together with the compensator. Equation (7.1) was used to calculate the sample birefringence

7.6 Result and Discussion

A faint ring outside the sample is due to the solution put on the top and bottom surface of the sample to reduce the refraction caused by microcracks found on the surface of each sample.

It is essential to study the orientation of polymer chains as it has a greater effect on Young's modulus, tensile strength and elongation to break in the rigid polymers. For uniaxially oriented materials, tensile strength and Young's modulus are greater in the direction parallel to the orientation than that in the direction perpendicular to the orientation. Parallel to the orientation, stresses exerted are largely on the primary bonds of the polymer chains, while in the direction perpendicular to the orientation, forces act to a large extent on the weak secondary bonds between polymer chains.[4&5] Generally, the polymer chains tend to line up parallel to the direction of stretching Hence, by stretching a polymer in one direction at a temperature at which the polymer behaves as a rubber, uniaxial orientation is formed

For ductile polymers, the modulus and tensile strength are generally greater in the direction parallel than perpendicular to the orientation However, the elongations to break in ductile polymers are greater in the direction perpendicular to the direction of orientation. When the stress is applied perpendicular to the orientation of the chains, the chains first deorient, and then they become oriented parallel to the new stretching direction. Thus, in the perpendicular direction the polymer has the elongation to break characteristic of the parallel direction plus the elongation required to deorient the chains and reorient them again. This reorientation possibility gives rise to the differences between ductile and brittle polymers. Brittle polymers break before the reorientation process gets started.[6] However, the poor strength property in the uniaxial brittle polymers can be overcome if the polymer chains are oriented biaxially.[7]

All samples of PMMA and PS were of cylindrical shape. The compressed and uncompressed samples of PMMA and PS were put on the microscope stage with their z-axes parallel to the microscopic axis. The microscope stage was rotated in such a way so that the emergent light from the samples is at its maximum brightness. In this case, the samples were located at 45° to the polarisation direction of the polariser and the analyser.

A dark cross and a bright symmetrical interference on the four quadrants are seen for the uncompressed sample of PMMA viewed under the polarising microscope (Figure 7.10). This pattern is similar to the interference pattern of the biaxial orientation with its optic axis oriented vertically. The PMMA samples were cut from the rod produced by injection moulded process. The pattern indicates that the chains were oriented uniaxially during the flow of the molten polymer. When it cooled, the polymer chains remained in symmetrical uniaxial orientation. The birefringence of the uncompressed sample was difficult to measure as no ring formed on the edge of the uncompressed sample, unlike those shown in the compressed sample. Hence, the comparison of the birefringence is relative to the birefringence at 0.2 strain.

Figure 7.11, 7.12 and 7.13 show the interference patterns of PMMA samples compressed at 293 K, 323 K and 343 K using the Hounsfield machine Dark crosses are still found on the samples but became more distinct at the higher temperature. However, a new chain orientation was found near the edge of the compressed samples and became wider with strain. At higher temperature, the chain orientation near the edge displayed a higher birefringence. The accurary of the birefringence in Table 7.1 is determined based on the compensator table provided. For the scale less than 0.9°, the read-off path difference is in two decimal points, for the scale between 1.0° and 7.0°, it is in one decimal point and from 7.1° above, it is in integer

Graph 7.1 shows the birefringence against strain for PMMA tested at three different temperatures. For samples compressed at strain rate 0.0006 and 0.006 s^{-1} at temperature 323 K and 343 K, the birefringence obtained is almost constant with strain For compression at strain rates 0 006, 0 05 and 0.5 s^{-1} at 293 K, the birefringence increased almost in linear proportion with strain. However, for

compression at strain rates 0.05 and 0.5 s^{-1} at 323 K and 343 K, the sample birefringence increases with strain not in a linear proportion.

Graph 7.2 shows the birefringence against strain rate for PMMA tested at three different temperatures. For the samples tested below 0.05 s^{-1} at three test temperatures, no clear separation in birefringence as a function of strain rate is seen The variation in temperature might not give any effect to the chain orientation at strain rate below 0 05 s^{-1}. Overall, it can be seen that the samples tested at 293 K show birefringence lower than that observed at 323 K and 343 K Hence, it is worth reviewing the dependence of the birefringence on temperature for PMMA.

Graph 7.3 reveals that the PMMA samples tested had tendency to show a maximum birefringence at 323 K although at strain rates 0.05 and 0.5 s^{-1} the samples show maximum birefringence when they were compressed to 0.4 strain. An almost constant birefringence dependence on temperature is seen for the sample compressed to 0.8 strain at strain rate 0.006 s^{-1}.

The uncompressed sample of PS was visible when it was put between the polariser and the analyser. However, no dark cross is formed on the uncompressed PS sample (Figure 7.14). The polymer chains of the uncompressed PS sample is oriented, may be in uniaxial or biaxial. On compression at 293 K, 323 K and 353 K and at different strains (Figure 7.15, 7.16 and 7.17), a spectrum of interference colours was formed on the PS samples. The interference patterns were not regular but were speckled, this caused the birefringence to be difficult to measure using the compensator Hence, it is hard to relate the chain orientation with the stress applied in the case of PS. From Figure 7.15, 7.16 and 7.17, the interference patterns formed on the samples indicated that there were changes in the orientations of the polymer chains after stress was applied, however, the orientations of the chains did not show any clear sign of symmetry. The cracks on the PS surface seen in Figure 7.15(c) might be due to lack of lubricant applied during compression as the cracks are not observed in other samples.

7.7 Conclusion

The application of the stress changed the orientation of the polymer chains of PMMA and PS to certain degree. However, the pattern of the orientation at different strain rates can not give any clear link to the increase in the yield stress when the strain rate increases and the decrease in the yield stress when the temperature increases. Under the same strain rate (0.05 and 0.5 s^{-1}), the birefringence increased when strain increased.

T (K)	ε (s^{-1})	Birefringence at different strain (x 10^{-4})			
		0 8	0.6	0 4	0.2
293	0 0006	2.6	3.0	1.6	-
	0.006	2.4	1.3	0.03	-
	0 05	2.9	1.4	0 06	-
	0.5	4.5	3 3	2.2	-
323	0.0006	2.4	3 5	2.3	2.4
	0.006	2.0	2.6	2 5	2.1
	0.05	5.6	4 7	2.2	1.4
	0 5	5 8	4.4	2.5	0.1
343	0.0006	1.1	1.6	1.3	1.1
	0 006	1.9	1.8	1 6	2.3
	0 05	2.8	3.2	2.9	1 3
	0 5	4 6	3.9	3.5	0.7

Table 7.1: Birefringence of PMMA tested at different strain rates and at different temperatures using the Hounsfield Machine.

(a) T = 20 °C
(293 K)

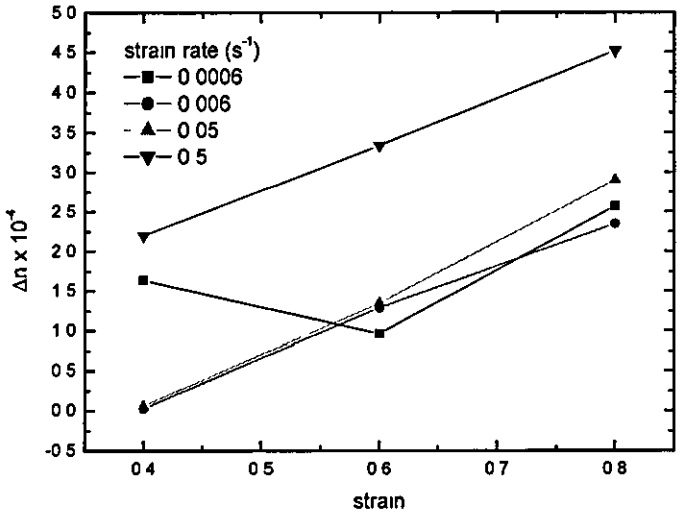

(b) T = 50 °C
(323 K)

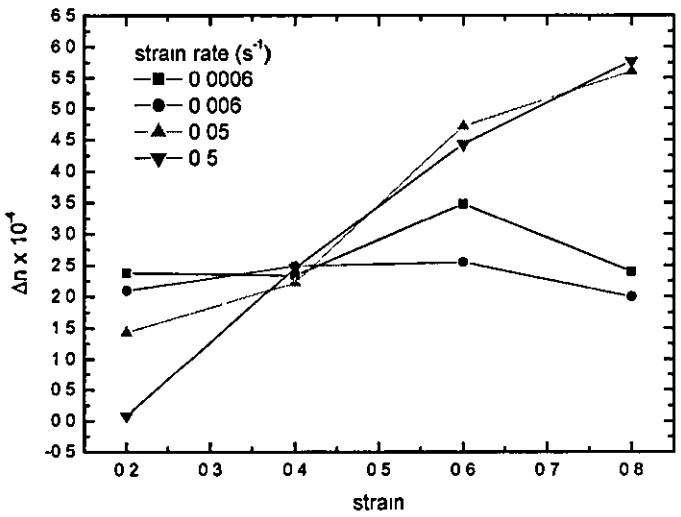

(c) T = 70 °C
(343 K)

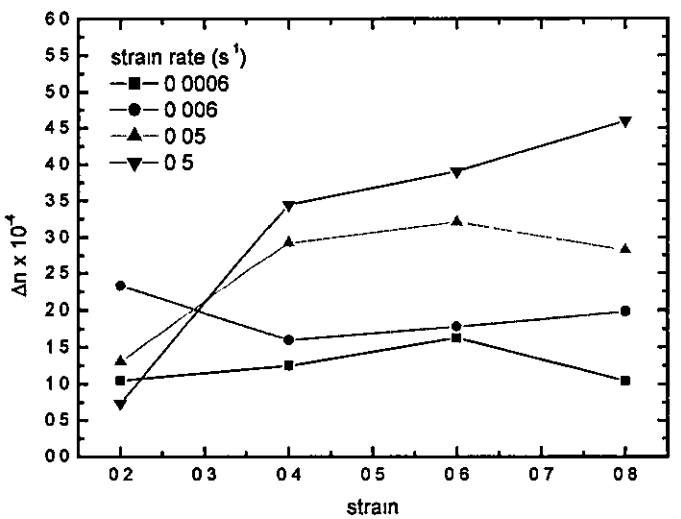

Graph 7.1: Birefringence against strain for PMMA tested at different strain rates at the temperatures (a) 293 K, (b) 323 K and (c) 343 K using the Hounsfield machine.

(a) Strain = 0.2

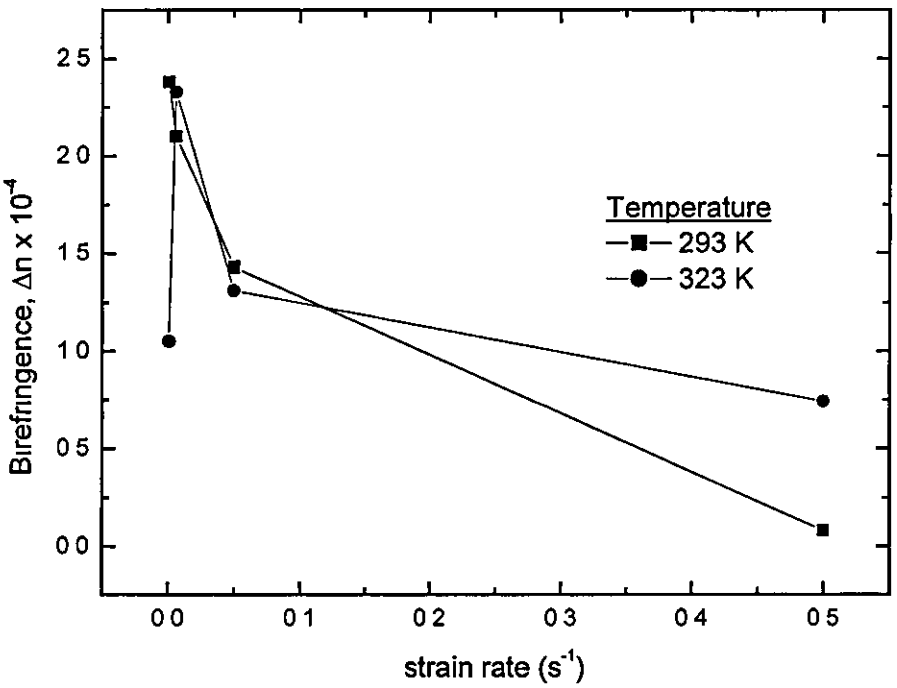

(b) Strain = 0 4

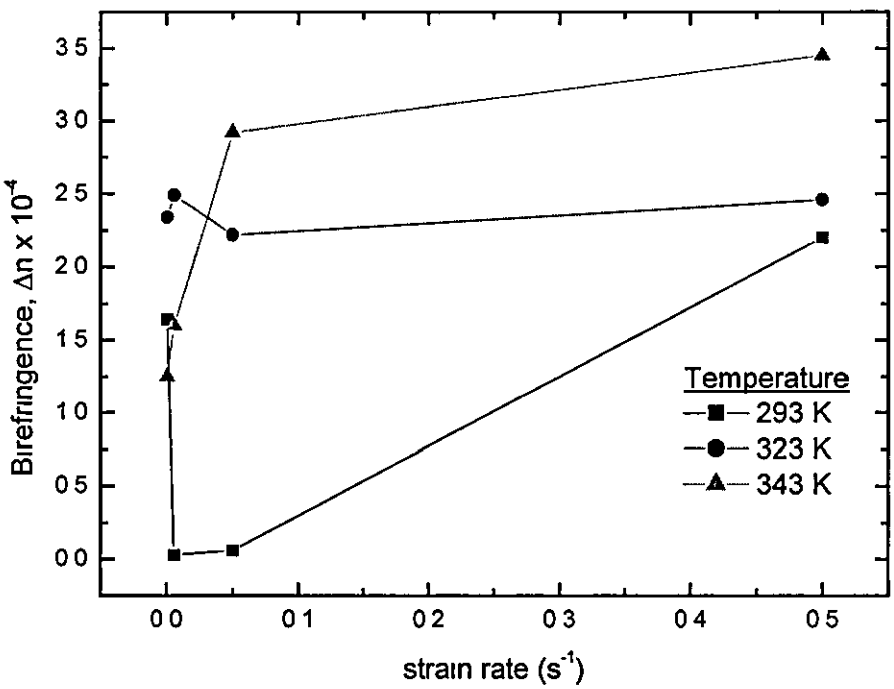

(c) Strain = 0 6

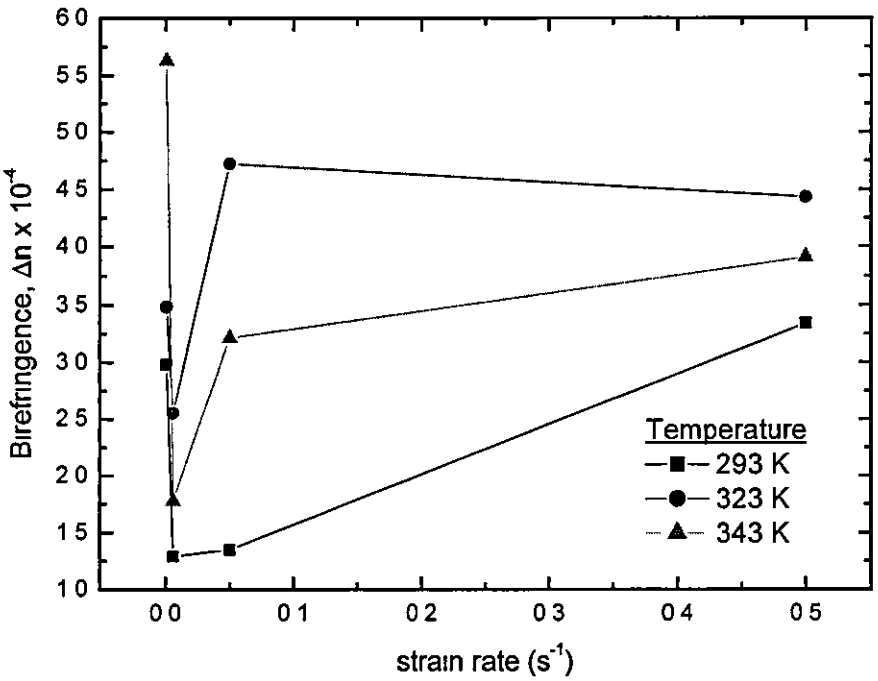

(d) Strain = 0.8

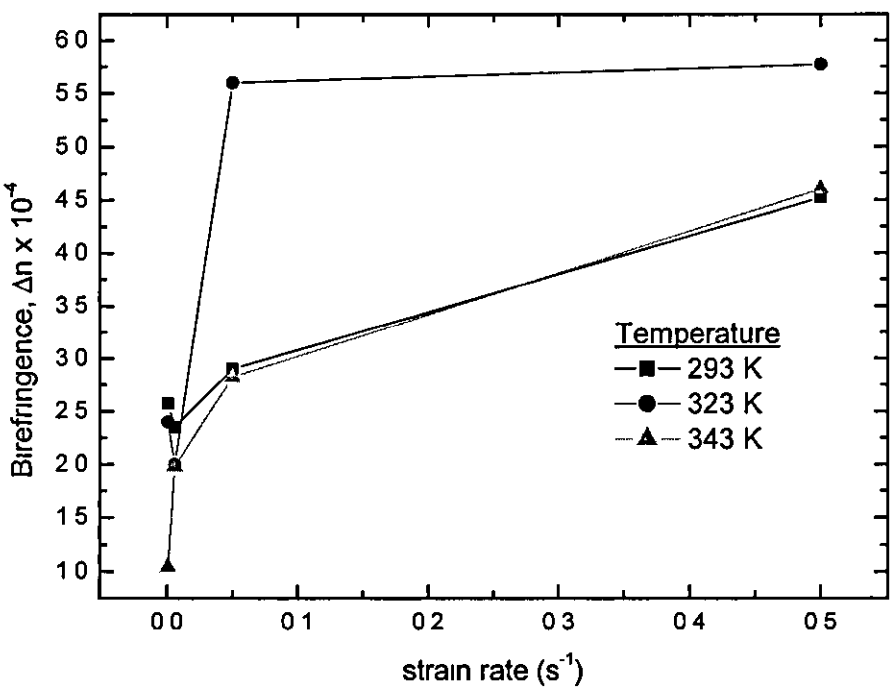

Graph 7.2: Birefringence against strain rate for PMMA tested at the different temperatures at the strain of (a) 0 2, (b) 0 4, (c) 0 6 and (d) 0 8 using the Hounsfield Machine

(a) strain = 0.8

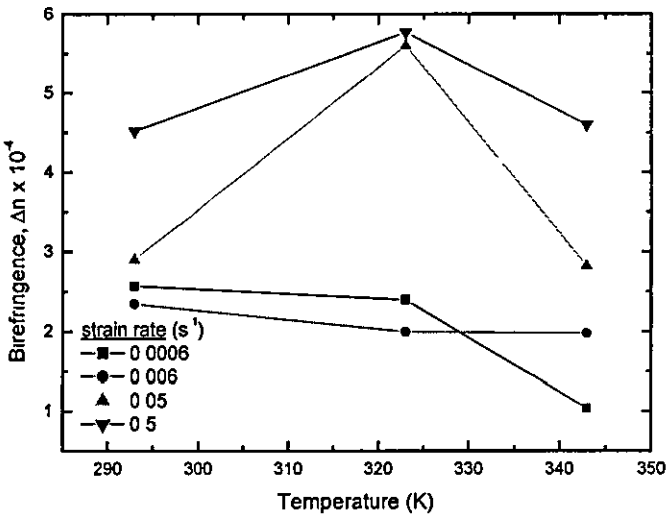

(b) strain = 0.6

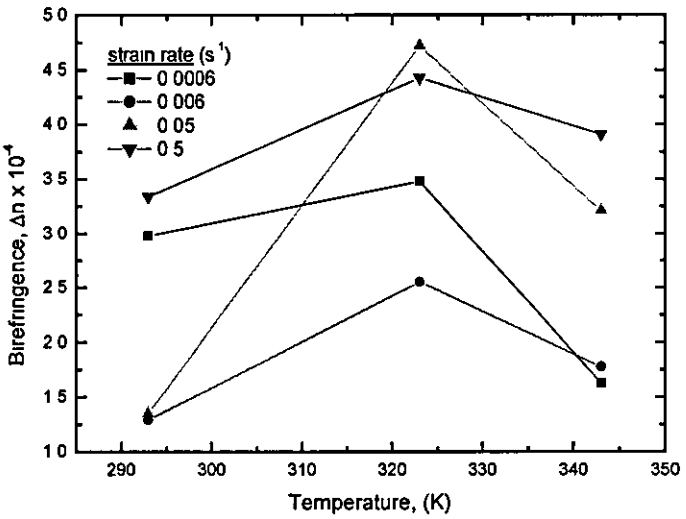

(c) strain = 0.4

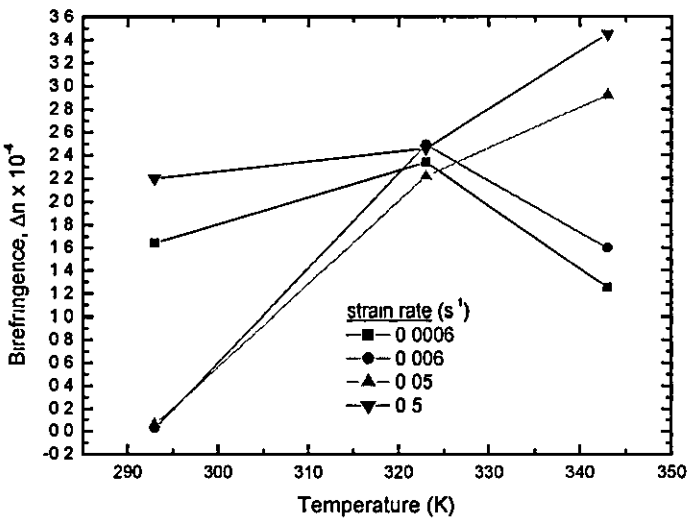

Graph 7.3: Birefringence versus temperature for PMMA compressed at different strain rates to the strain of (a) 0.8, (b) 0 6 and (c) 0 4.

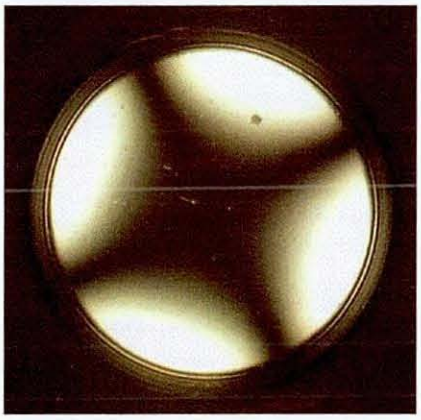

Figure 7.10: Interference pattern of the uncompressed PMMA sample put at 45° to the polarisation direction of the polariser and analyser viewed under the polarising microscope.

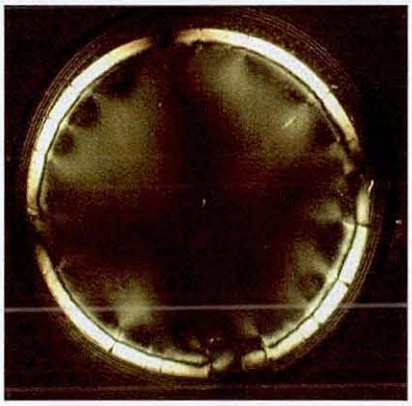

(a) Strain rate: 0.0006 s^{-1}
Strain: 0.8

(b) Strain rate: 0.0006 s^{-1}
Strain: 0.4

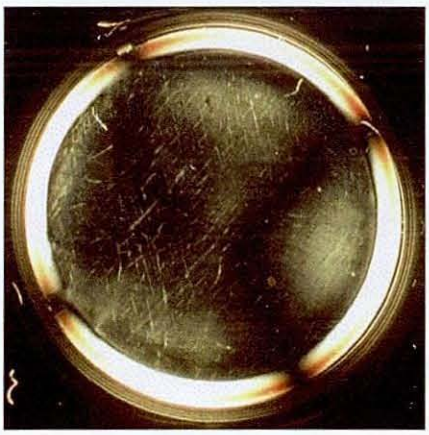

(c) Strain rate: 0.5 s^{-1}
Strain: 0.8

(d) Strain rate: 0.5 s^{-1}
Strain: 0.2

Figure 7.11: Interference patterns of the PMMA sample compressed at the temperature 293 K (20 °C) to 0.8, 0.4 and 0.2 strain with strain rate 0.0006 s^{-1} and 0.5 s^{-1} using the Hounsfield Machine.

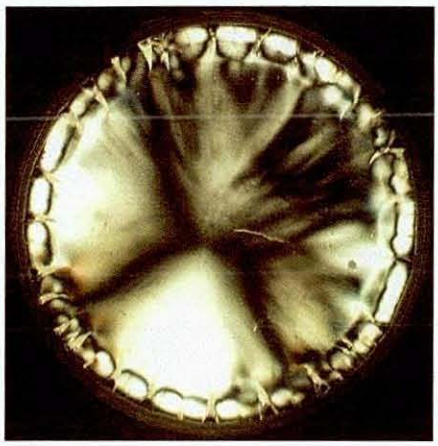

(a) Strain rate: 0.0006 s^{-1}
Strain: 0.8

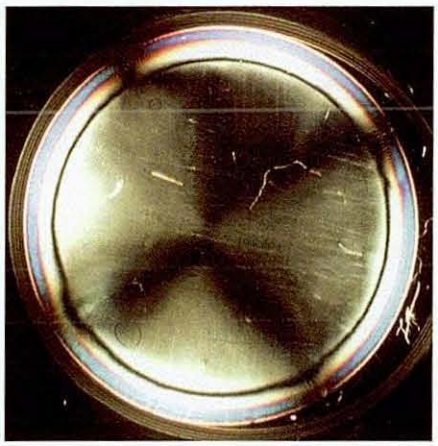

(b) Strain rate: 0.5 s^{-1}
Strain: 0.8

Figure 7.12: Interference patterns of the PMMA samples compressed at the temperature 323 K (50 °C) to 0.8 strain with strain rate 0.0006 s^{-1} and 0.5 s^{-1} using the Hounsfield Machine.

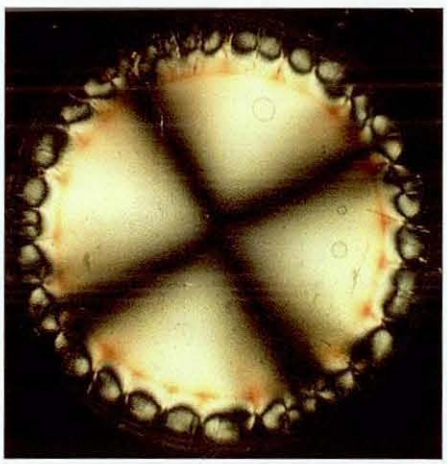

(a) Strain rate: 0.0006 s^{-1}
Strain: 0.8

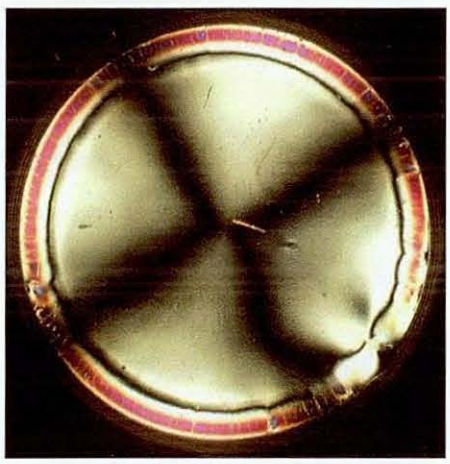

(b) Strain rate: 0.5 s^{-1}
Strain: 0.8

Figure 7.13: Interference patterns of the PMMA samples compressed at the temperature 343 K (70 °C) to 0.8 strain with strain rate 0.0006 s^{-1} and 0.5 s^{-1} using the Hounsfield Machine.

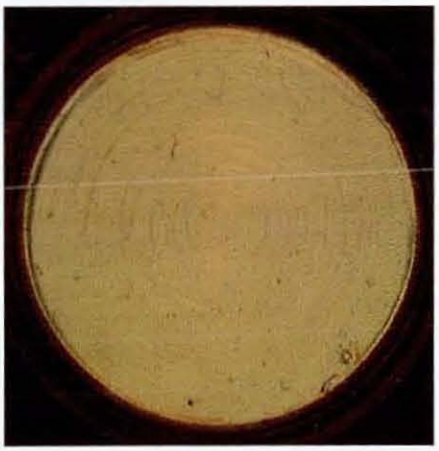

Figure 7.14: Interference pattern of the uncompressed PS sample put at 45° to the polarisation direction of the polariser and analyser viewed under the polarising microscope.

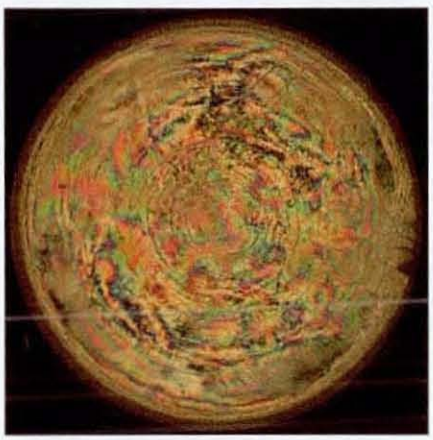

(a) Strain rate: 0.0006 s^{-1}
Strain: 0.8

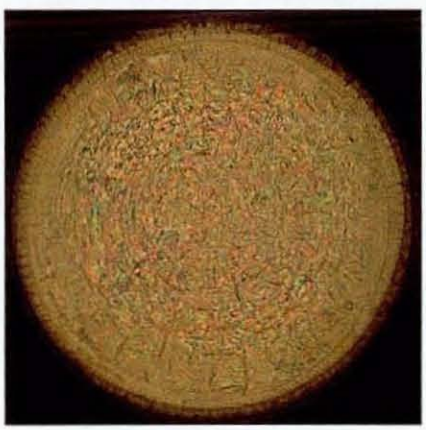

(b) Strain rate: 0.5 s^{-1}
Strain: 0.8

(c) Strain rate: 0.5 s^{-1}
Strain: 0.2

Figure 7.15: Interference patterns of the PS samples compressed at the temperature 293 K (20 °C) to 0.2 and 0.8 strain with strain rate 0.0006 s^{-1} and 0.5 s^{-1} using the Hounsfield Machine.

(a) Strain rate: 0.0006 s^{-1}
Strain: 0.8

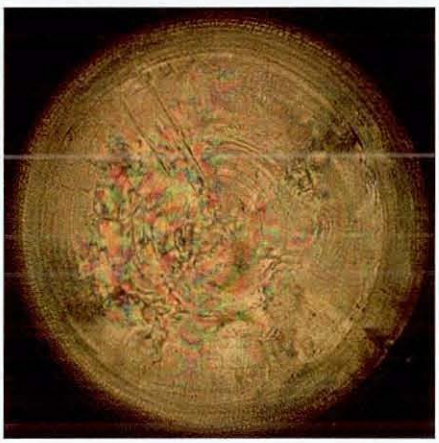

(b) Strain rate: 0.5 s^{-1}
Strain: 0.8

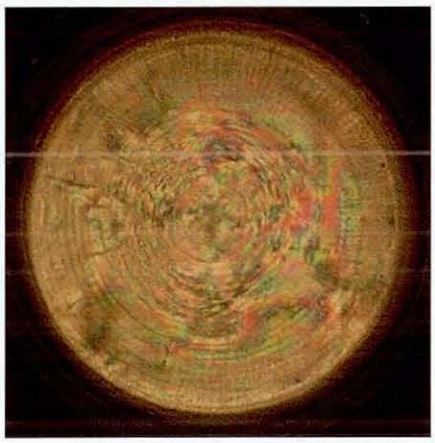

(c) Strain rate: 0.5 s^{-1}
Strain: 0.2

Figure 7.16: Interference patterns of the PS samples compressed at the temperature 323 K (50 °C) to 0.2 and 0.8 strain with strain rate 0.0006 s^{-1} and 0.5 s^{-1} using the Hounsfield Machine.

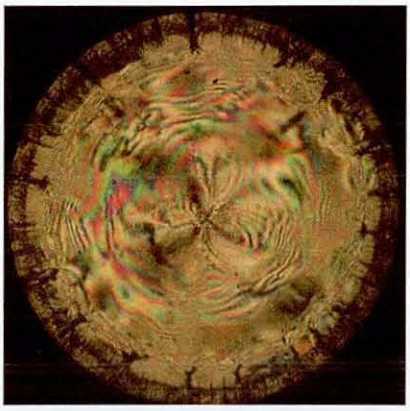

(a) Strain rate: 0.0006 s^{-1}
Strain: 0.8

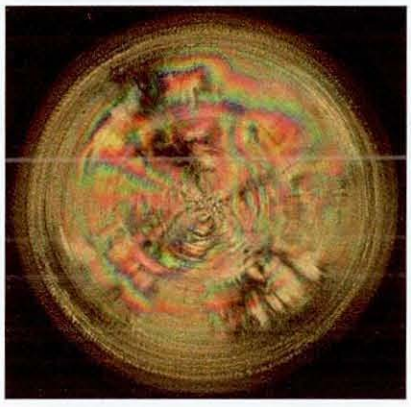

(b) Strain rate: 0.5 s^{-1}
Strain: 0.8

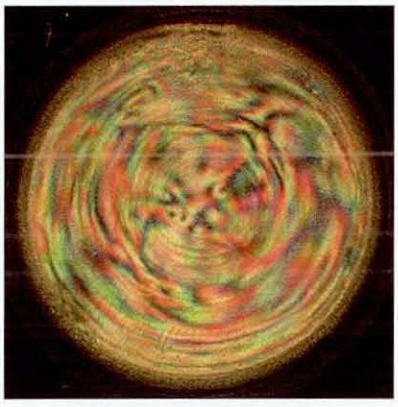

(c) Strain rate: 0.5 s^{-1}
Strain: 0.2

Figure 7.17: Interference patterns of the PS samples compressed at the temperature 353 K (80 °C) to 0.2 and 0.8 strain with strain rate 0.0006 s^{-1} and 0.5 s^{-1} using the Hounsfield Machine.

References

1. **I. M. Ward,** "Structure and Properties of Oriented Polymers", Applied Science Publishers Ltd., London, 1975

2. **L. E. Nielsen,** "Mechanical Properties of Polymers", Reinhold Publishing Corporation, London, 1967

3. **N. H. Hartshorne and A. Stuart,** "Crystals and the Polarising Microscope", Edward Arnold (Publishers) Ltd, London, 1970

4 **R. G. Cheatham and A. G. H. Dietz,** "Modern Physics", 29, 113 (Sept., 1951)

5. **L. E. Nielsen and R. J. Buchdahl,** Journal of Chemical Physics **21** (1950) 488

6. **B. Maxwell,** Journal of Applied Polymer Science **5** (1961) S11

7. **J. Bailey,** India Rubber World **118** (1948) 225

8. "Rotary Compensator by Ehringhaus Calcite Plates, Table of function", Carl Zeiss, 7082 Oberkochen, West Germany

9. http //www olympusmicro com/primer/lightandcolor/birefringence html

10. http://www.brocku.ca/earthsciences/people/gfinn/optical/bxarotat.htm

11 http //www brocku ca/earthsciences/people/gfinn/optical/unisogyr htm

12. http://www.brocku ca/earthsciences/people/gfinn/optical/uniflash htm

Chapter 8

Application of Eyring Theory

8.1 Introduction

The molecules in a condensed phase are in equilibrium positions and may vibrate about the minimum of a free energy well when no stress is acting. The structure of all condensed systems may be in a more or less regular lattice arrangement and is different from substance to substance. The regularities of the lattices in solid crystals are well-defined but incomplete because of dislocations and crystal imperfections, while liquids are less regular, having only short range order and have many empty places in the lattices, and thus, are readily deformable.

The application of a stress on a body induces molecules to displace from equilibrium along the various planes separating molecular layers. If the body is perfectly elastic, the stored potential energy is completely released when the stress is released and the molecular segments return to their original minimum positions in the energy wells. Hooke's law describes well the relation between the stress and the displacement when these quantities are relatively small. Thus, the elastic modulus, shear modulus, bulk modulus, and hardness are all functions of the steepness of the energy wells

If a relatively large stress acts constantly on a body, molecular segments on both sides of a shear plane jump with respect to each other over the energy barrier and take up the neighbouring new equilibrium position to release stress as thermal energy. This displacement of patches by jumping along shear planes to release stress in the direction of stress continues as long as the stress acts. In this way permanent deformation occurs. This relative displacement to new equilibrium positions along shear planes is called the relaxation theory of flow phenomena.[1]

8.2 Eyring's Model of Viscous Flow

Eyring et al.[2] study of the non-Newtonian visco-elastic behaviour from a molecular approach was closely allied to the attempt made to gain a molecular understanding of solution viscosities on the basis of the theory of thermally activated rate processes. Many of the investigations into the visco-elastic behaviour of yield point have chosen the Eyring viscosity equation as their starting points.[3] The effects of temperature and strain rate are encompassed in the Eyring viscosity equation.

It is assumed that deformation of the polymer involves the motion of chain molecules or parts of a chain molecule over potential energy barriers into empty spaces in the structure. The basis motion of molecules could be either intermolecular (e g chain sliding) or intramolecular (e g. change in the conformation of the chain).[4]

With no force acting, a dynamic equilibrium exists and the chain segments move over the potential barrier forwardly and backwardly with equal frequency, k'. Shear is considered to occur along sets of parallel layers and λ_1 is the distance between points of flow (Figure 8.1). The distance of two equilibrium positions in the direction of shear is λ (Figure 8 2). Let λ_2 and λ_3 be the distances between neighbouring chain segments and between two adjacent flowing chain segments in the moving layer respectively. If τ is the shear force per unit area, then on a single flow unit the shear force acting will be $\tau\lambda_2\lambda_3$, where $\lambda_2\lambda_3$ is the effective cross-sectional area. The shear force $\tau\lambda_2\lambda_3$ acts through a distance λ doing an amount of work $\tau\lambda_2\lambda_3\lambda$. Presumably as the unit moves forwardly, it will go through an intermediate state of higher energy at the distance $\lambda/2$, the amount of applied shear work needed to surmount the energy barrier is only $\tau(\lambda_2\lambda_3\lambda/2)^2$

As a result, the flow unit moves in the forward direction with frequency $k'\exp\{\tau\lambda_2\lambda_3\lambda/2kT\}$ and in the backward direction with $k'\exp\{-\tau\lambda_2\lambda_3\lambda/2kT\}$. The net frequency in the forward direction is thus

$$k'\exp\{\tau\lambda_2\lambda_3\lambda/2kT\}-k'\exp\{-\tau\lambda_2\lambda_3\lambda/2kT\} \qquad (8.1)$$

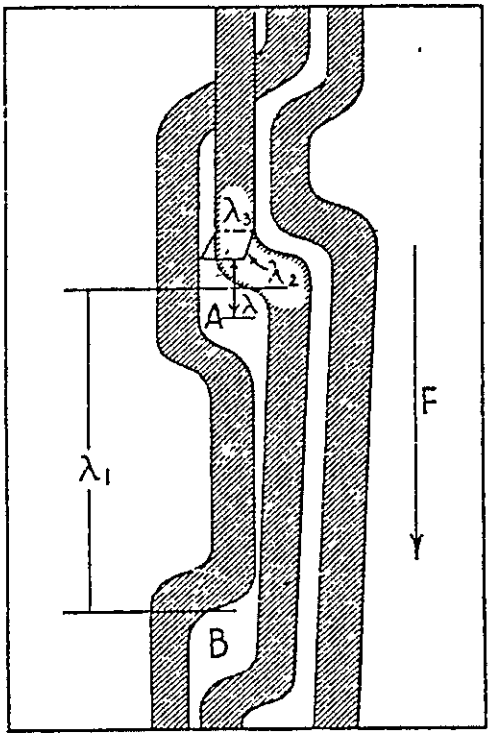

Figure 8 1: Simplified representation indicating voids or holes into which segments of molecules can jump, thus relaxing stress.[2]

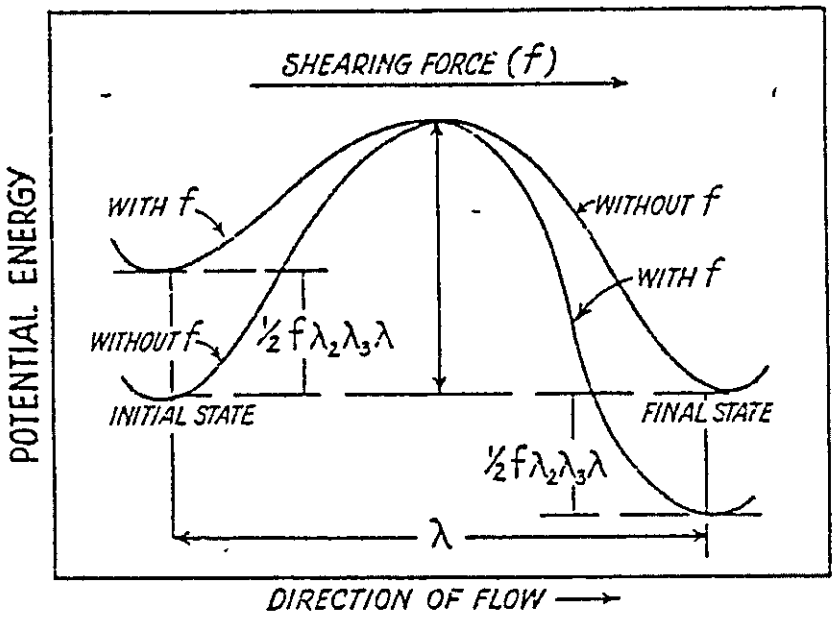

Figure 8.2: Diagram indicating how an applied stress alters the potential energy barrier a flowing molecular segment must surmount as it flows from one equilibrium position to the next.[2]

The net frequency in the forward direction times the distance λ is the forward velocity for the flow unit, that is

$$\lambda k'[\exp\{\tau\lambda_2\lambda_3\lambda/2kT\}-\exp\{-\tau\lambda_2\lambda_3\lambda/2kT)] \quad (8.2)$$

By dividing the forward velocity with λ_1 which is the distance between two points of flow in the flow direction, the shear rate, $\dot{\gamma}$ is

$$\dot{\gamma} = 2\frac{\lambda}{\lambda_1}k'\sinh\frac{\tau\lambda_2\lambda_3\lambda}{2kT} \quad (8.3)$$

with $\sinh x = \frac{e^x - e^{-x}}{2}$. The shear rate can be written as

$$\dot{\gamma} = 2\frac{\lambda}{\lambda_1}k'\sinh\frac{\tau\upsilon_a}{2kT} \quad (8\ 4)$$

where $\upsilon_a = \lambda_2\lambda_3\lambda$ is the activation volume for the molecular event

By the statistical thermodynamic theory of reaction rate[5]

$$k' = \frac{kT}{h}\exp\left(\frac{-\Delta G}{RT}\right) \quad (8\ 5)$$

where $\frac{kT}{h}$ is the universal frequency with k the Boltzmann's constant, T the temperature and h the Planck's constant. ΔG is the activation energy and R is the gas constant.

So the shear strain rate becomes

$$\dot{\gamma} = 2\frac{\lambda}{\lambda_1}\frac{kT}{h}\exp\left(\frac{-\Delta G}{RT}\right)\sinh\left(\frac{\tau\upsilon_a}{2kT}\right) \quad (8\ 6)$$

For higher value of stress (when $x >> 1$, $\sinh x = e^x/2$), the shear strain rate reduces to

$$\dot{\gamma} = \frac{\lambda}{\lambda_1}\frac{kT}{h}\exp\left(\frac{-\Delta G}{RT}\right)\exp\left(\frac{\tau\upsilon_a}{2kT}\right) \quad (8.7)$$

In order to convert the shear strain rate and shear force into uniaxial compression strain rate and stress, the following relationships are used,[6,7,8]

$$\tau = \frac{\sigma}{2} \tag{8 8}$$

$$\dot{\gamma} = \frac{3}{2}\varepsilon \tag{8.9}$$

By inserting Equations (8.8) & (8.9) into Equation (8.7) and taking the logarithm of the equation, the following equation is yielded,

$$\frac{\sigma}{T} = \frac{4k}{\upsilon_a}\left(\ln\varepsilon - \ln\frac{2}{3}\frac{\lambda}{\lambda_1}\frac{kT}{h} + \frac{\Delta G}{RT}\right) \tag{8.10}$$

8.3 Ree-Eyring's Model of Viscous Flow

Eyring's Theory of flow was derived under two assumptions which are (i) the flow system is homogeneous, being composed of only one kind of flow unit and (ii) the activated complex for flow is in complete equilibrium with the ambient temperature [1] For the system that has heterogeneous flow units, Ree-Eyring's theory is applied and it is merely a generalization of Eyring equation.

In the Ree-Eyring model,[9] it is assumed that

(a) There are n groups of flow units that differ in relaxation times and in geometrical dimensions. The flow units in each group have different relaxation times, but are sufficiently well described by an average value for the group.

(b) $x_1, x_2, \ldots, x_n$ are the fractional areas on a shear surface of the various units and $f_1, f_2, \ldots, f_n$ are the shear stresses per unit area acting on these areas.

(c) All the units on the same shear plane move at the same shear rate $\dot{\gamma}$.

Consider that a flow unit which belongs to the nth group of units, according to Eyring's equation of shear rate,

$$\gamma = 2\left(\frac{\lambda}{\lambda_1}\right)_n k_n' \sinh(\alpha_n \tau_n) \tag{8 11}$$

where $\alpha_n=(\upsilon_a/2kT)$ and k_n' is the rate constant for the flow processes of units belong to nth group. The force acting on the units of the nth group is $x_n\tau_n$, thus, the total stress is given as

$$\tau=\sum_{n=1}^{n} x_n\tau_n \tag{8.12}$$

where x_n is the fractional area on a shear surface occupied by a group of type i, where i = 1 or 2 or ..... or n

By introducing Equation (8.11) into Equation (8.12), the following equation results,

$$\tau=\sum_{n=1}^{n}\frac{x_n}{\alpha_n}\sinh^{-1}(\beta_n\dot{\gamma}) \tag{8.13}$$

where $\beta_n=1/\{(\lambda/\lambda_1)_n 2k_n'\}$, which is proportional to the relaxation time of the nth group. Consequently, a generalized viscosity η is given as follows,

$$\eta=\sum_{n=1}^{n}\frac{x_n\beta_n}{\alpha_n}\frac{\sinh^{-1}\beta_n\gamma}{\beta_n\dot{\gamma}} \tag{8.14}$$

The property of the function, $\frac{\sinh^{-1}X}{X}$, is as follows,

$$\lim_{\beta\gamma=0}\frac{\sinh^{-1}\beta\dot{\gamma}}{\beta\dot{\gamma}}=1, \tag{8.15}$$

and

$$\lim_{\beta\gamma\to\infty}\frac{\sinh^{-1}\beta\gamma}{\beta\dot{\gamma}}=0 \tag{8 16}$$

For non-Newtonian case, assuming there is no group 3 or greater, the viscosity is derived from Equation (8.14) as follows,

$$\eta=\frac{x_1\beta_1}{\alpha_1}\frac{\sinh^{-1}\beta_1\dot{\gamma}}{\beta_1\gamma}+\frac{x_2\beta_2}{\alpha_2}\frac{\sinh^{-1}\beta_2\dot{\gamma}}{\beta_2\gamma} \tag{8.17}$$

By introducing Equation (8.15) and the following relation

$$\sinh^{-1}\beta_2\dot{\gamma}\approx\ln 2\beta_2\dot{\gamma} \tag{8.18}$$

into Equation (8.17), the following equation obtained,

$$\tau = \frac{x_1\beta_1}{\alpha_1}\dot{\gamma} + \frac{x_2}{\alpha_2}\ln 2\dot{\gamma} + \frac{x_2}{\alpha_2}\ln\beta_2 \qquad (8.19)$$

Equation (8.18) holds only for large values of $\dot{\gamma}$, while Equation (8.15) holds for small values of γ. The subscripts 1 and 2 indicate a Newtonian-type and a non-Newtonian-type unit respectively However, in the higher range of γ, the Newtonian units became non-Newtonian units.[9,10]

8.4 Analysis on $\frac{\sigma}{T}$ versus Ln (ε)

Eyring's or Ree-Eyring's theory that relates the stress σ to the strain rate ε and temperature T has been widely used by researchers to study the molecular mechanism in polymers. Activation energy and volume could be calculated from the Eyring's or Ree-Eyring's equation by making a plot of σ/T against ln($\dot{\varepsilon}$) for polymers at a series of temperatures.

Bauwens-Crowet et al.[11] study of polycarbonate in tension, creep and impact tests revealed that a plot of σ/T against ln(ε) at a series of temperatures gave a series of parallel straight lines that fit well the Eyring equation of non-Newtonian viscous flow They calculated the Eyring's factors as explained in Appendix 8.1. In the calculation of Eyring's factors, they assumed that the change of activation energy and volume with temperature was negligible

Bauwen Crowet[12] carried out a study of the yield behaviour of PMMA in uniaxial compression over a wide range of temperature (-20 to 100°C) and discovered that a plot of σ/T against ln($\dot{\varepsilon}$) produced a set of parallel curves. He discovered that the set of curves can be looked upon as generated by the shift of one curve along a slanting straight line, locus of the intersections of the asymptotes of each curve. However, over a relatively wide region, the master curve exhibits an appreciable curvature and in this region $\left(\bar{1} \le \log\varepsilon \le 3\right)$, the data do not accurately fit the Ree-Eyring equation.

By assuming that two rate processes (α and β) are involved in the deformation at yield of PMMA, from the non-Newtonian type in Equation (8.19) of Ree-Eyring theory,

Bauwens' treatment predict that the asymptotes of a given curve could be expressed by

$$\frac{|\sigma_c|}{T} = A_{c\alpha}\left(\ln 2C_\alpha \varepsilon + \frac{Q_\alpha}{RT}\right) \text{ for } \dot{\varepsilon}_\alpha \le \varepsilon \le \dot{\varepsilon}_\beta \tag{8.20}$$

and

$$\frac{|\sigma_c|}{T} = A_{c\alpha}\left(\ln 2C_\alpha \dot{\varepsilon} + \frac{Q_\alpha}{RT}\right) + A_{c\beta}\left(\ln 2C_\beta \dot{\varepsilon} + \frac{Q_\beta}{RT}\right) \text{ for } \dot{\varepsilon} > \dot{\varepsilon}_\beta \tag{8.21}$$

where $A_{c\alpha}$, $A_{c\beta}$ are constants; C_α and C_β the constants containing a frequency factor; Q_α and Q_β the activation energies related to the α and β processes respectively and R the universal gas constant. $\dot{\varepsilon}_\beta$ is the value of the strain-rate corresponding to the intersection of the two asymptotes and $\dot{\varepsilon}_\alpha$ the value of the strain-rate obtained by extrapolating the curve to zero stress It follows that

$$\dot{\varepsilon}_\beta = \frac{1}{2C_\beta}\exp\left(-\frac{Q_\beta}{RT}\right) \tag{8 22}$$

and

$$\varepsilon_\alpha = \frac{1}{2C_\alpha}\exp\left(-\frac{Q_\alpha}{RT}\right) \tag{8.23}$$

The shift factor for the curves along d_c shown in Figure 8.3 has two components· horizontal component and vertical component as below,[13]

$$s_x(T_1, T_2) = \frac{Q_\beta}{2.303R}\left(\frac{1}{T_1} - \frac{1}{T_2}\right); \tag{8.24}$$

$$s_y(T_1, T_2) = \frac{-[A_\alpha(Q_\alpha - Q_\beta]}{R}\left(\frac{1}{T_1} - \frac{1}{T_2}\right) \tag{8.25}$$

The Ree-Eyring equation (Equation 8 21)may be written as follows·

$$\frac{|\sigma_c|}{T} = A_{c\alpha}\left(\ln 2C_\alpha \dot{\varepsilon} + \frac{Q_\alpha}{RT}\right) + A_{c\beta}\sinh^{-1}\left(C_\beta \dot{\varepsilon}\exp\frac{Q_\beta}{RT}\right) \tag{8.26}$$

The dashed curve in Figure 8.4 was calculated from Equation (8.26), using the values obtained: $A_{c\alpha} = 7.1 \times 10^{-4}$ kgmm^{-2}K^{-1}, $C_\alpha = 5 \times 10^{-52}$ sec, $Q_\alpha = 412.4$ kJmol^{-1} (98.5 kcalmol^{-1}), $A_{c\beta} = 3.74 \times 10^{-3}$ kgmm^{-2}K^{-1}, $C_\beta = 4.67 \times 10^{-17}$ sec and $Q_\beta = 107.2$ kJmol^{-1} (25.6 kcalmol^{-1}).

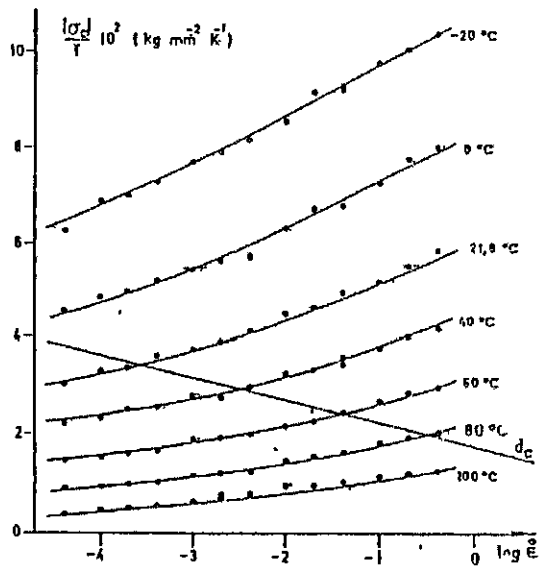

Figure 8.3. Ratio of compression yield stress to temperature as a function of logarithm of strain-rate The set of curves is generated by the shift of one curve along d_c, according to Equation (8.24). ($\dot{\varepsilon}$ in sec^{-1}).[12]

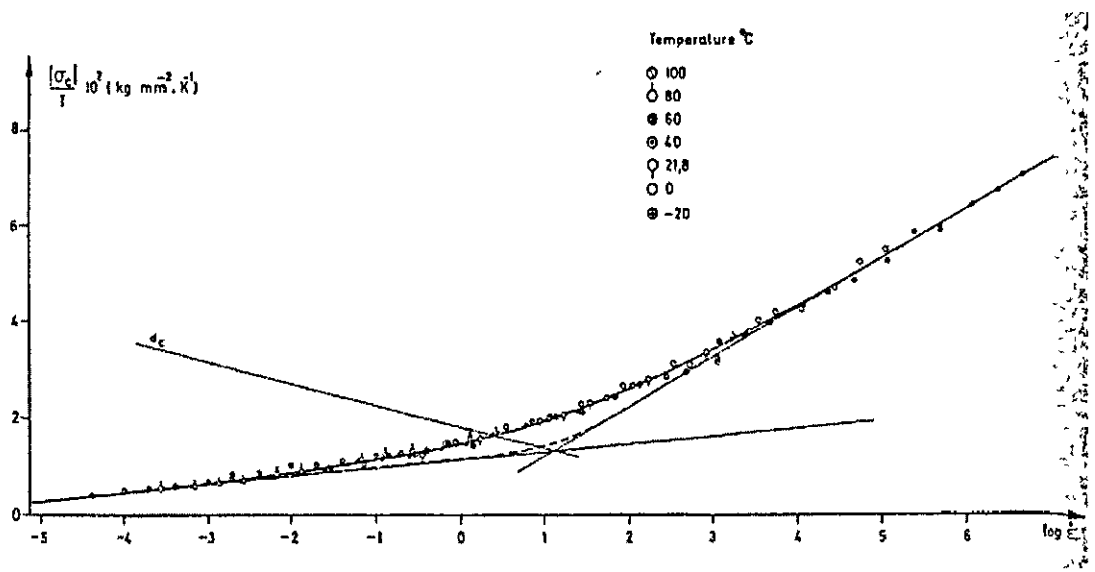

Figure 8.4: Master compression yield stress curve reduced to 100 °C (full curve). The asymptotes are expressed by Equations (8.20) & (8.21). The dashed curve is calculated from the Ree-Eyring Equation (8.26) [12]

polymer	volume of statistical link in solution ($Å^3$)	Eyring flow volume ($Å^3$)
polyvinylehloride	380	8600 23°C 5000 49°C 12600
polycarbonate	482	6440 25°C 6240 0°C 4300
poly(methyl methacrylate)	910	4660, 3900 3100 4100
polystyrene	1220	9600 2700
cellulose acetate	2060	8800 20300
cellulose trinitrate	2620	6070 23°C 6000 54°C
cellulose acetate	2060	17400 20°C 28000 33°C

Table 8.1: A comparison of the statistical segment volume for a polymer measured in solutions with the flow volumes derived from the Eyring theory.[14]

Nanzai[8] suggested that the non-linear curve between σ/T and $\ln(\dot{\varepsilon})$ of poly(methyl methacrylate) for the steady plastic flow can be analysed using the Eyring equation by segmentally fitting the curves with a group of straight lines. He assumed that the polymer glass structure in the lower yield range is continuously changeable depending on stress and temperature similar to that of the viscoelastic component at temperatures near T_g. In this case, the Eyring factors must be treated as continuously changeable in accordance with the structural change. However, the application of the Ree-Eyring equation to the plastic flow sets limits to the number of the elementary processes in plastic flow within the number of the multiple stages Hence, the Ree-Eyring equation may not be suitable for the plastic flow analysis.

Another suggestion by Zhu et al.[7] is taking partial differentials of Equation 8.10 with respect to $\ln(\dot{\varepsilon})$ under the condition that T is constant to calculate υ_a. This could be explained by taking tangents to the non-linear curve. In their study, ΔG was replaced with $(\Delta H - T\Delta S)$. To calculate ΔH, they took the partial differentials of the equation with respect to 1/T under the condition that $\dot{\varepsilon}$ is constant. In their first approximation, the parameters υ_a, ΔH and ΔS are assumed to be constants and do not change with T and ε. From the mathematical viewpoint, the approximation contained in their tangent method is equivalent to an iterative procedure from a first approximate value to a more exact result in second approximation. ΔS is then calculated by inserting the values of ΔH and υ_a into Equation (8.10).

8.5 Activation Energy and Activation Volume

The relaxation theory assumes that flow occurs only when there are holes present in the flow systems. The energy needed for the formation of the hole is a function of the bond strength between molecules and is called the activation energy.

The activation volume can be estimated from the size of the statistical link of the polymer chain in dilute solution This possible comparison to interpret the Eyring volume had been discussed by Haward and Thackray.[14] From Table 8.1, it can be seen that the activation volume varies from about two to ten times that of the

statistical link This suggests that yield involves the co-operative movement of a larger number of chain segments that would be required for a conformational chain in dilute solution.

In the recent studies of the activated rate process of yield behaviour, the activation energy was replaced with the following equation,

$$\Delta G = \Delta H - T\Delta S \tag{8.27}$$

where ΔH is the activation enthalpy and ΔS the activation entropy and T the temperature at which the activation takes place.

In thermodynamics, enthalpy H is the total energy of a body (e.g. a gas in a container) and can be written as

$$H = U + pV \tag{8 28}$$

where U is the internal energy and V is the volume of gas at pressure p. If the gas changes from state 1 to state 2, the difference in enthalpy is

$$\Delta H = \Delta U + p\Delta V \tag{8.29}$$

If $\Delta H>0$, which means H_{after} is larger than H_{before}, energy is added to the system This reaction is considered endothermic. If $\Delta H<0$, then the reaction is considered exothermic.[17]

Entropy is referred to the nature of system tends to go from an orderly state to a disorderly state. If a system goes from state 1 to state 2 undergoing a reversible change takes in a quantity of heat dQ at absolute temperature T, the change in entropy is defined as[18]

$$\Delta S_{1\to 2} = \int_1^2 \frac{dQ}{T} \tag{8.30}$$

A positive value of ΔS means an increase in the degree of disorder (e.g. ice melting); a negative value means a decrease in the degree of disorder (e.g. water freezing).

8.6 Application of Eyring's Theory to Experimental Data

The yield stress, defined as a point of the maximum stress on a stress-strain curve, is the stage a polymer exhibits pure viscous flow that is in agreement with Eyring's theory of non-Newtonian viscosity. It is also regarded as a state at which plastic flow begins. In the current analysis, Eyring's equation was applied on the yield point, 20% and 30% strain on the stress-strain curves of PMMA and PS.

Table 8.2(a, b & c) and 3(a, b & c) showed $\ln(\dot{\varepsilon})$ and σ/T at yield point, 20% and 30% strain obtained from the stress-strain curves of PMMA and PS tested at a temperature range of 293 to 363 K and at low strain rates 10^{-4} to 2 s^{-1} (Hounsfield Machine) and higher strain rates 10^{2} to 10^{3} s^{-1} (Dropweight Machine). The strain rates were calculated locally by taking tangent on the concerned strain in the strain versus time plot instead of that of crosshead and dropweight speed. Each data point in the Table 8.2 and 8.3 represents a single test.

Graph 8.1(a, b and c) showed σ/T against $\ln(\dot{\varepsilon})$ at yield point, 20% and 30% strain for PMMA tested at strain rates 10^{-4} to 10^{3} s^{-1} at 293 K and 363 K. It is found that σ/T at the higher strain rates do not fit in the polynomial second order curve produced for the data points of σ/T versus $\ln(\dot{\varepsilon})$ at low strain rates. Therefore, the activated analysis was only carried out on the low strain rate data of PMMA and PS shown in Graph 8 2(a, b & c) and Graph 8.3(a, b & c) respectively.

Graph 8.2(a, b & c) showed that plots of σ/T against $\ln(\dot{\varepsilon})$ for PMMA consisted of a set of curves In order to study the changeable Eyring's factors accurately, the method proposed by Zhu et al.[7] was adopted in this study In the current study, ΔG in Equation (8 10) was replaced with ΔH and ΔS (Equation 8.27). Therefore,

$$\frac{\sigma}{T} = \frac{4k}{\upsilon_a}\left(\ln\dot{\varepsilon} - \ln\frac{\upsilon_a}{\upsilon_m} - \ln\frac{2}{3}\frac{kT}{h} + \frac{\Delta H}{RT} - \frac{\Delta S}{R}\right) \qquad (8.31)$$

where υ_m is the molecular chain volume ($\lambda_1\lambda_2\lambda_3$) and υ_a is the activation volume ($\lambda\lambda_2\lambda_3$). Taking partial derivatives of σ/T with respect to $\ln(\dot{\varepsilon})$ under constant T by assuming that ΔH and ΔS do not change with $\dot{\varepsilon}$; σ/T with respect to 1/T under

constant $\dot{\varepsilon}$ by assuming υ_a and ΔS do not change with T, the following equations are obtained.

$$\left(\frac{\partial(\sigma/T)}{\partial \ln(\varepsilon)}\right)_T = \frac{4k}{\upsilon_a} \tag{8.32}$$

$$\left(\frac{\partial(\sigma/T)}{\partial(1/T)}\right)_\varepsilon = \frac{4k}{\upsilon_a}\left(\frac{\Delta H}{R} + T\right) \tag{8.33}$$

By taking tangents to the fitted curves in the graphs of σ/T versus $\ln(\varepsilon)$ and $1/T$ (Graph 8.2 and 8.4), υ_a and ΔH can be calculated from Equation (8.22) and (8 23). The calculated values of υ_a and ΔH are shown in Table 8.4a & 8.4b, 8.5a & 8.5b and 8.6a & 8.6b respectively. ΔS was then calculated by inserting these two values into Equation (8.31).

Table 8.4c, 8 5c and 8 6c showed the values of ΔS at yield point, 20% and 30% strain by assuming $\upsilon_m = \upsilon_a$ and $\upsilon_m = 284.24\ nm^3$ proposed by Zhu et al.[7] Graph 8 5 shows the plots of ΔS against $\ln(\dot{\varepsilon})$ for $\upsilon_m = \upsilon_a$ and $\upsilon_m = 284.24\ nm^3$ at yield point, 20% and 30% strain. It can be seen that the chosen value of υ_m only affects the magnitude of ΔS but not the trend of the plot, however, the effect on the magnitude of ΔS could be considered negligible. In the current study, $\upsilon_m = 284.24\ nm^3$ was chosen.

The activation energy ΔG was calculated from Equation (8 27) by inserting the values of ΔH, ΔS and T into the equation by assuming $\upsilon_m = 284\ 24\ nm^3$ (Table 8.4d, 8 5d and 8.6d).

Plots of σ/T against $\ln(\varepsilon)$ at yield point, 20% and 30% strain for PS showed a set of parallel lines (Graph 8.3). The flow process which occurred in PS is homogeneous. Thus, the method adopted by Bauwens-Crowet et al.[11] was used to calculate the Eyring's factors (Appendix 8 1). By rearranging Equation (8.10), the following equation is obtained,

$$\frac{\sigma}{T} = \frac{4k}{\upsilon_a}\left(\ln\dot{\varepsilon} - \ln CT + \frac{\Delta G}{RT}\right) \tag{8.34}$$

293 K		311 K		323 K		343 K		363 K	
$\ln(\dot{\varepsilon}_y)$	σ_y/T ($MPaK^{-1}$)	$\ln(\dot{\varepsilon}_y)$	σ_y/T ($MPaK^{-1}$)	$\ln(\dot{\varepsilon}_y)$	σ_y/T ($MPaK^{-1}$)	$\ln(\dot{\varepsilon}_y)$	σ_y/T ($MPaK^{-1}$)	$\ln(\dot{\varepsilon}_y)$	σ_y/T ($MPaK^{-1}$)
-7.311	0 333	-7.322	0 222	-7.332	0 170	-7.322	0 097	-7 346	0 058
-6 564	0 352	-6 790	0 228	-6 825	0 177	-6.790	0.102	-6 834	0 063
-6 190	0 363	-6 157	0 235	-6.281	0 187	-6 189	0 107	-6 293	0 070
-5.725	0 383	-5.769	0 251	-5.778	0 197	-5 797	0.110	-5 651	0.078
-5 483	0 378	-5.461	0.263	-5 548	0 207	-5 462	0.113	-5 477	0 083
-5 375	0.399	-5 270	0.263	-5.317	0 197	-5 327	0 121	-5 389	0 076
-4 706	0 421	-4.770	0.288	-4 771	0 207	-4 659	0.112	-4 646	0.084
-3.937	0.431	-3.946	0 293	-3.824	0 220	-3.854	0.133	-3 883	0.089
-3.496	0.447	-3.512	0 317	-3 443	0 235	-3.462	0.141	-3 407	0.101
-3.234	0.472	-3.120	0.325	-3.268	0 243	-3 255	0.141	-3 099	0.105
-2.458	0.530	-2.469	0.366	-2.342	0 255	-3 058	0.147	-3 089	0.095
-1.649	0.551	-1 965	0 371	-1.946	0 287	-2.468	0.176	-2 476	0.116
-1.279	0 559	-1 237	0.411	-1 659	0 298	-1.947	0.188	-1 890	0.131
-1 031	0 583	-0 844	0 413	-1.125	0 302	-1 689	0.179	-1 353	0.144
-0 777	0 590	-0 570	0 437	-0 960	0 314	-1 279	0.204	-1 054	0 150
-0 031	0 627	-0 178	0 460	-0 822	0 320	-0 857	0.215	-0 695	0 147
0 123	0 639	-0 099	0.459	-0 405	0 338	-0.755	0 219	-0 283	0.176
0 377	0 659	0 124	0 467	-0.146	0 332	-0.569	0 242	0 107	0.191
		0 269	0 478	0 102	0 355	-0 146	0.266	0 205	0.198
		0 457	0 499	0.294	0 361	0.135	0 268	0 406	0 200
				0 515	0 373	0 297	0.290	5 674*	0 285*
				5 296*	0.355*	0.506	0.300	6 332*	0 279*
				5.468*	0 395*			6 667*	0 280*
				6 268*	0.487*			6 677*	0 308*
				6.756*	0.394*			6 986*	0 290*
				6 711*	0.432*			7 082*	0 348*
				7 123*	0.379*				

Table 8.2a: Ln(ε) and σ/T at yield point for Poly(methyl methacrylate) tested at quasi-static and low strain rates 10^{-4} to 2 s^{-1} and high strain rate 10^2 to 10^3 s^{-1} (*) at various temperatures.

293 K		311 K		323 K		343 K		363 K	
$\ln(\dot{\varepsilon}_{20\%})$	$\sigma_{20\%}/T$ ($MPaK^{-1}$)	$\ln(\varepsilon_{20\%})$	$\sigma_{20\%}/T$ ($MPaK^{-1}$)	$\ln(\varepsilon_{20\%})$	$\sigma_{20\%}/T$ ($MPaK^{-1}$)	$\ln(\varepsilon_{20\%})$	$\sigma_{20\%}/T$ ($MPaK^{-1}$)	$\ln(\varepsilon_{20\%})$	$\sigma_{20\%}/T$ ($MPaK^{-1}$)
-7.165	0 308	-7.183	0.191	-7.197	0.128	-7 172	0 071	-7.147	0 0497
-6.571	0 323	-6 659	0 202	-6 542	0.154	-6 551	0 078	-6.541	0 042
-5.900	0 329	-6 076	0 200	-5.938	0 151	-6 017	0 078	-6.041	0 052
-5.570	0 344	-5 526	0 211	-5.496	0.166	-5 546	0.075	-5 541	0 058
-5 275	0.336	-5 274	0 220	-5 297	0.184	-5 265	0.089	-5.295	0 069
-5 133	0.363	-5 059	0 236	-5 020	0 167	-4.959	0.085	-5 026	0 053
-4 381	0.369	-4 293	0 234	-4 330	0 181	-4.344	0.095	-4.321	0 065
-3 695	0.397	-3 703	0 254	-3.626	0 199	-3.680	0 091	-3 719	0 065
-3 254	0.401	-3 357	0 263	-3 248	0.196	-3.255	0.105	-3 262	0 077
-3 003	0.419	-2 856	0 261	-2 941	0 201	-2.764	0.112	-3.014	0 083
-2 108	0.453	-2 206	0 278	-2 071	0 204	-2.153	0.127	-2.743	0 075
-1 428	0.482	-2 021	0 277	-1 686	0 233	-1.924	0.120	-2 070	0 084
-1 061	0.482	-1 768	0.301	-1 400	0 253	-1.750	0.129	-1.383	0.103
-0 712	0.490	-1.423	0 323	-0 945	0 264	-1.305	0.133	-0 945	0 097
-0 552	0.505	-0.996	0 320	-0 668	0 262	-1.066	0.160	-0 706	0 115
0.163	0 521	-0.559	0 346	-0 475	0 265	-0.727	0.168	-0 400	0 118
0 553	0 519	-0.097	0 360	-0 072	0 293	-0.524	0.177	0.240	0.138
0 836	0 546	0.196	0 350	0 215	0 282	-0 103	0.181	0 559	0 147
		0.532	0 382	0 563	0.311	0.176	0.188	0 867	0 150
		0.836	0 385	0 840	0.306	0 542	0.189	1 010	0 161
		1 030	0 399	1 026	0 312	0.876	0.214	5.236*	0 228*
				6 185*	0 405*	1 017	0.206	6.318*	0 244*
				6.775*	0 291*			6 667*	0.256*
				6 729*	0.341*			6.706*	0 237*
				7.139*	0.339*			7 069*	0 257*
								7 090*	0 301*

Table 8 2b· Ln($\dot{\varepsilon}$) and σ/T at 20% strain for Poly(methyl methacrylate) tested at quası-static and low strain rates 10^{-4} to 2 s^{-1} and high strain rate 10^{2} to 10^{3} s^{-1} (*) at various temperatures.

293 K		311 K		323 K		343 K		363 K	
$\ln(\dot{\varepsilon}_{30\%})$	$\sigma_{30\%}/T$ ($MPaK^{-1}$)	$\ln(\varepsilon_{30\%})$	$\sigma_{30\%}/T$ ($MPaK^{-1}$)	$\ln(\dot{\varepsilon}_{30\%})$	$\sigma_{30\%}/T$ ($MPaK^{-1}$)	$\ln(\dot{\varepsilon}_{30\%})$	$\sigma_{30\%}/T$ ($MPaK^{-1}$)	$\ln(\dot{\varepsilon}_{30\%})$	$\sigma_{30\%}/T$ ($MPaK^{-1}$)
-7.107	0 296	-7.087	0.193	-7 080	0.141	-7 074	0.083	-7 034	0.049
-6 488	0 310	- 6449	0.199	-6 480	0.161	-6 453	0 086	-6 467	0 050
-5.837	0 324	-5 924	0.207	-5 878	0.158	-5 913	0 091	-6 024	0 069
-5.497	0 336	-5.460	0.201	-5.444	0.169	-5 439	0 090	-5 466	0 056
-5.273	0.331	-5 251	0 222	-5.237	0 185	-5 243	0 090	-5 219	0 063
-5.029	0 358	-4 978	0 233	-4.921	0 172	-4 964	0 097	-4.941	0 066
-4.266	0 361	-4 229	0 238	-4.243	0 182	-4.239	0 088	-4 201	0 071
-3.609	0 394	-3 640	0 245	-3.572	0.182	-3 623	0 102	-3.688	0 065
-3.160	0.373	-3 189	0 245	-3.199	0 201	-3 208	0 100	-3 265	0 070
-2.896	0.387	-2.902	0 273	-2.880	0 197	-2 929	0 120	-3 011	0 083
-1.996	0 422	-1 957	0 270	-1.974	0 238	-1 982	0.128	-2 639	0 068
-1.302	0.438	-1 564	0 295	-1.580	0 223	-1 549	0.149	-1.976	0 081
-0 939	0.439	-1.286	0 309	-1.303	0 236	-1 290	0.135	-1 266	0 096
-0.598	0 449	-0 875	0 314	-0 829	0 238	-0 858	0 164	-0 806	0 135
-0 444	0.451	-0 590	0 310	-0.575	0 241	-0 596	0 150	-0 617	0.121
0 296	0 484	-0 398	0 317	-0.370	0 260	-0.380	0 170	-0 325	0.111
0 717	0 498	0 073	0 334	0 075	0 271	0 070	0.187	0 322	0 133
1 012	0.521	0 321	0.360	0 345	0 275	0 321	0 178	0 706	0.156
		0.728	0.355	0.745	0 284	0.722	0 197	1 028	0.152
		1 021	0.376	1.016	0 298	1.019	0 201	1 210	0.170
		1 207	0 379	1.211	0 312	1.198	0 223	6 279*	0 251*
				5.971*	0 439*			6 707*	0 247*
				6.745*	0 397*			6.735*	0 263*
				6.831*	0 252*			7.131*	0 229*
				7.178*	0 269*			7.153*	0 221*

Table 8.2c: Ln(ε) and σ/T at 30% strain for Poly(methyl methacrylate) tested at quasi-static and low strain rates 10^{-4} to 2 s^{-1} and high strain rate 10^{2} to 10^{3} s^{-1} (*) at various temperatures.

293 K		323 K		353 K	
$\ln(\dot{\varepsilon}_y)$	σ_y/T ($MPaK^{-1}$)	$\ln(\dot{\varepsilon}_y)$	σ_y/T ($MPaK^{-1}$)	$\ln(\dot{\varepsilon}_y)$	σ_y/T ($MPaK^{-1}$)
-7 684	0 313	-7.689	0 196	-7 571	0.117
-7 667	0 307	-7 053	0.211	-7 016	0.123
-7 002	0 314	-6.448	0 220	-6 475	0.141
-6 417	0 329	-6 067	0 214	-5 977	0.142
-5 967	0 332	-5 723	0.222	-5 937	0.146
-5 708	0 341	-5 530	0 231	-5 672	0.143
-5 449	0 343	-4 828	0 237	-4 865	0.152
-5.554	0 346	-4.129	0 247	-4 535	0 165
-4 820	0 345	-3.701	0 252	-4 342	0 173
-4.223	0 365	-3.455	0 259	-3.753	0 177
-3 739	0 370	-3.268	0 262	-3 493	0 185
-3 573	0 372	-2.573	0 261	-3 305	0 185
-3 352	0 372	-1 899	0 285	-2 610	0 192
-3 234	0 380	-1.555	0 290	-1 907	0.204
		-1.201	0.290	-1 590	0 203
		-1.110	0 288	-1 485	0 202
		-1 031	0 289	-1 074	0 208
		-0.684	0 295	-1 035	0 212
		-0 481	0.295	-0 714	0 209
		-0.227	0 303	-0 430	0 210
		-0.144	0.295	-0 119	0 212
		0 002	0 307	-0 085	0 219
		0 141	0 305	0 040	0 218
				0 190	0 220
				0.191	0 217

Table 8.3a: $\ln(\dot{\varepsilon})$ and σ/T at yield point for Polystyrene tested at quasi-static and low strain rates 10^{-4} to 2 s^{-1} at various temperatures

293 K		323 K		353 K	
$\ln(\dot{\varepsilon}_{20\%})$	$\sigma_{20\%}/T$ ($MPaK^{-1}$)	$\ln(\dot{\varepsilon}_{20\%})$	$\sigma_{20\%}/T$ ($MPaK^{-1}$)	$\ln(\varepsilon_{20\%})$	$\sigma_{20\%}/T$ ($MPaK^{-1}$)
-7 396	0 191	-7 296	0.114	-7 322	0 058
-6 718	0.190	-6 718	0 112	-6 688	0 058
-6 133	0 202	-6 099	0 115	-6 075	0 067
-5 705	0 202	-5 699	0 118	-5.704	0 065
-5 450	0 207	-5.481	0 122	-5.497	0 071
-5.207	0 211	-5 203	0.119	-5.351	0 073
-4 520	0 211	-4 514	0 125	-4.639	0 076
-3 826	0 222	-3 817	0.131	-4.163	0 079
-3.345	0 236	-3.374	0 132	-3.866	0 084
-3.112	0 233	-3 150	0.137	-3.454	0 081
-2.926	0 242	-2 918	0.140	-3.170	0 083
-2 864	0 234	-2 237	0 152	-2.936	0 092
		-1.543	0.164	-2.254	0 094
		-1 141	0 157	-1.575	0 103
		-0.743	0.140	-1.156	0 103
		-0 620	0.154	-0 963	0 098
		-0.234	0.157	-0 857	0 097
		0 037	0.147	-0 627	0 096
		0 279	0.158	-0 238	0 103
		0 442	0.169	0.068	0 105
		0 569	0 182	0.414	0 111
		0.718	0.166	0.550	0 113
				0.731	0.102
				0.835	0 109
				0.869	0.105

Table 8.3b: $\ln(\varepsilon)$ and σ/T at 20% strain for Polystyrene tested at quasi-static and low strain rates 10^{-4} to 2 s^{-1} at various temperatures.

293 K		323 K		353 K	
$\ln(\dot{\varepsilon}_{30\%})$	$\sigma_{30\%}/T$ ($MPaK^{-1}$)	$\ln(\dot{\varepsilon}_{30\%})$	$\sigma_{30\%}/T$ ($MPaK^{-1}$)	$\ln(\varepsilon_{30\%})$	$\sigma_{30\%}/T$ ($MPaK^{-1}$)
-7 282	0.184	-7 208	0.106	-7.215	0 061
-6 664	0 180	-6 661	0 113	-6.622	0 065
-6 052	0 193	-6 038	0.114	-5.983	0 064
-5 640	0 196	-5 648	0.115	-5.617	0 066
-5.376	0 200	-5 365	0 115	-5.355	0 073
-5.139	0.199	-5 143	0 116	-5.261	0 076
-4 476	0.199	-4 452	0 122	-4.527	0 072
-3.759	0 212	-3 779	0.121	-4 039	0 076
-3 256	0.209	-3 324	0 123	-3.745	0 079
-3 045	0 211	-3 094	0.131	-3.446	0.077
-2.754	0 207	-2 875	0 121	-3.110	0.084
		-2.188	0 130	-2.052	0 087
		-1 491	0 145	-1.487	0 089
		-1 074	0 144	-1 040	0 099
		-0 668	0.137	-0.862	0 097
		-0 543	0 138	-0.750	0 092
		-0.148	0.151	-0.539	0 087
		0 161	0.139	-0.141	0 101
		0 376	0 150	0 156	0 103
		0 554	0.150	0 525	0 101
		0 812	0 152	0 703	0 108
				0 826	0 098
				0 954	0.106
				1 039	0.103

Table 8 3c $\ln(\dot{\varepsilon})$ and σ/T at 30% strain for Polystyrene tested at quasi-static and low strain rates 10^{-4} to 2 s^{-1} and at various temperatures

(a)

$\ln(\dot{\varepsilon}_y)$	activation volume, υ_a (nm^3)				
	293 K	311 K	323 K	343 K	363K
-6 5	1.87	2.78	4 96	12.24	17 86
-5.5	1.64	2 24	3 54	5.59	7 22
-4.5	1.46	1 87	2.75	3 62	4 52
-3 5	1 31	1 61	2.25	2 68	3 29
-2 5	1 20	1 41	1 91	2.13	2 59
-1 5	1 10	1.26	1 65	1.76	2.13
-0 5	1 01	1.14	1.46	1 51	1.81
0 3	0 96	1.05	1.33	1.35	1.62

(b)

activation enthalpy, ΔH ($kJmol^{-1}$)				
293K	311 K	323 K	343 K	363 K
120 498	180 670	324.145	803 717	1174 207
116 169	159.708	253 923	402.471	519.927
112 281	144 929	213 987	282.396	352.782
108 704	133.735	187 807	223.908	275 394
105 354	124 803	169 027	188 845	230 199
102 176	117.390	154 686	165 176	200 185
99.130	111.047	143 217	147 904	178 533
96 770	106 546	135 487	137 007	164 979

(c)

$\ln(\varepsilon_y)$	activation entropy, ΔS ($kJmol^{-1}K^{-1}$) $\upsilon_m = \upsilon_a$					activation entropy, ΔS ($kJmol^{-1}K^{-1}$) $\upsilon_m = 284.24\ nm^3$				
	293 K	311 K	323 K	343 K	363K	293 K	311 K	323 K	343 K	363K
-6.5	0 016	0 292	0.752	2 351	3.686	0 058	0.294	0.682	1.976	2.935
-5 5	0 014	0 230	0.539	1 071	1.500	0 057	0 239	0.494	0 902	1.187
-4 5	0 012	0 185	0.416	0 680	0.936	0 056	0 198	0 386	0 575	0.737
-3 5	0 009	0.149	0 333	0 486	0.673	0 054	0 165	0 313	0 412	0.527
-2.5	0 006	0 119	0 272	0 366	0.517	0 052	0 138	0 259	0 311	0.402
-1 5	0 003	0 094	0.224	0 283	0.411	0 049	0 115	0 217	0 242	0 319
-0 5	0 0001	0.071	0.184	0 221	0.335	0 047	0 094	0 182	0 189	0.257
0 3	-0 002	0 054	0.157	0 180	0.286	0 045	0 079	0 158	0.155	0 218

(d)

activation energy, ΔG ($kJmol^{-1}$)				
293 K	311 K	323 K	343 K	363K
104	89	104	126	109
99	85	94	93	89
96	83	89	85	85
93	82	87	83	84
90	82	85	82	84
88	82	85	82	85
85	82	84	83	85
84	82	84	84	85

Table 8.4: The variation of (a) activation volume, (b) activation enthalpy, (c) activation entropy and (d) activation energy at yield point for Poly(methyl methacrylate) tested at various temperatures and low strain rates

(a)

$\ln(\varepsilon_{20\%})$	activation volume, υ_a (nm^3)				
	293 K	311 K	323 K	343 K	363K
-6 5	2 11	4 62	4.83	25.21	31.19
-5 5	2 02	3.53	3 86	8 51	11.02
-4 5	1.93	2.85	3 22	5.12	6 69
-3 5	1.85	2 39	2 76	3.66	4 80
-2 5	1.77	2 06	2 41	2.85	3 75
-1.5	1.70	1 81	2.15	2.33	3 07
-0 5	1 64	1 62	1.93	1.97	2 60
0.3	1 29	1 49	1.79	1.76	2 32

(b)

activation enthalpy, ΔH ($kJmol^{-1}$)				
293K	311 K	323 K	343 K	363 K
128.256	283 135	296 022	155.752	1927 613
132.978	234 330	256 762	568.812	737 520
136 422	202.900	229.145	365.843	479 189
138 750	180 483	208.182	276.907	364 394
140 096	163.339	191.377	226.140	298 417
140 573	149.547	177.344	192.756	254 854
140.279	138 017	165.252	168.745	223 432
139 545	129.968	156.613	153.700	203.704

(c)

$\ln(\dot{\varepsilon}_{20\%})$	activation entropy, ΔS ($kJmol^{-1}K^{-1}$) $\upsilon_m = \upsilon_a$					activation entropy, ΔS ($kJmol^{-1}K^{-1}$) $\upsilon_m = 284.24\ nm^3$				
	293 K	311 K	323 K	343 K	363K	293 K	311 K	323 K	343 K	363K
-6.5	0 041	0.546	0 605	4.052	5 041	0 082	0 581	0 639	4 072	5.059
-5.5	0 062	0 414	0.488	1.346	1.770	0 103	0 451	0 524	1 375	1.797
-4.5	0 078	0 327	0.405	0.783	1 059	0.120	0 365	0.442	0 816	1.090
-3.5	0 091	0 262	0.341	0.532	0.740	0 133	0 302	0.380	0 568	0.774
-2.5	0.100	0 212	0 289	0 386	0 556	0 143	0 252	0.328	0 424	0.592
-1.5	0.107	0 169	0 244	0 288	0 432	0 149	0.211	0 286	0 328	0 470
-0 5	0.110	0 133	0 205	0 216	0.342	0 153	0 176	0 246	0 257	0.381
0 3	0 111	0 107	0.176	0 170	0 285	0 154	0.151	0 218	0 212	0.325

(d)

activation energy, ΔG ($kJmol^{-1}$)				
293 K	311 K	323 K	343 K	363K
104	103	90	161	91
103	94	88	97	85
101	89	86	86	84
100	87	86	82	83
98	85	85	81	84
97	84	85	80	84
95	83	86	80	85
94	83	86	81	86

Table 8.5: The variation of (a) activation volume, (b) activation enthalpy, (c) activation entropy and (d) activation energy at 20% strain for Poly(methyl methacrylate) tested at various temperatures and low strain rates.

(a)

$\ln(\dot{\varepsilon}_{30\%})$	activation volume, υ_a (nm^3)				
	293 K	311 K	323 K	343 K	363K
-6 5	2.94	4 81	7 11	-	-
-5.5	2.67	3 82	5.19	13 21	22.17
-4.5	2.45	3 17	4 08	6 43	8.56
-3 5	2 26	2.71	3 37	4 25	5 30
-2.5	2 09	2.36	2.86	3 18	3 84
-1 5	1.95	2.09	2 49	2.53	3 01
-0 5	1.83	1.88	2.20	2.11	2 48
0.3	1.74	1.74	2.02	1.86	2 17

(b)

activation enthalpy, ΔH ($kJmol^{-1}$)				
293K	311 K	323 K	343 K	363 K
169 456	278.473	412.745	-	-
165 998	238 270	324 417	829 772	1394 719
161.830	210 137	271 556	429 287	571 827
157.118	188.786	235 479	298 064	372.188
151.979	171 625	208 663	231.601	280.545
146 499	157.234	187 497	190 649	226 903
140.744	144 919	170.283	162 761	191.591
135.976	135 820	157 940	145 032	169.507

(c)

$\ln(\varepsilon_{30\%})$	activation entropy, ΔS ($kJmol^{-1}K^{-1}$) $\upsilon_m = \upsilon_a$					activation entropy, ΔS ($kJmol^{-1}K^{-1}$) $\upsilon_m = 284.24\ nm^3$				
	293 K	311 K	323 K	343 K	363K	293 K	311 K	323 K	343 K	363K
-6.5	0.144	0 533	0 908	-	-	0 182	0 567	0.939	-	-
-5 5	0.146	0 424	0 665	2.046	3.517	0.184	0 460	0 698	2 071	3.538
-4 5	0.143	0.345	0 516	0.952	1.306	0 183	0.382	0 551	0 983	1 335
-3 5	0.138	0 283	0 412	0.587	0.761	0.178	0.322	0.449	0 622	0.794
-2 5	0.130	0.232	0 333	0.399	0.508	0 170	0.271	0 371	0 436	0 544
-1 5	0.120	0.187	0 269	0.281	0.358	0 161	0 228	0 308	0 320	0 396
-0 5	0 108	0.148	0 216	0.198	0.258	0 150	0 190	0 256	0 239	0.297
0.3	0 098	0 118	0 177	0 145	0.194	0 141	0 161	0.219	0 187	0 235

(d)

activation energy, ΔG ($kJmol^{-1}$)				
293 K	311 K	323 K	343 K	363K
116	102	109	-	-
112	95	99	119	111
108	91	94	92	87
105	89	91	85	84
102	87	89	82	83
99	86	88	81	83
97	86	87	81	84
95	86	87	81	84

Table 8.6: The variation of (a) activation volume, (b) activation enthalpy, (c) activation entropy and (d) activation energy at 30% strain for Poly(methyl methacrylate) tested at various temperatures and low strain rates.

(a) At yield point of Poly(methyl methacrylate)

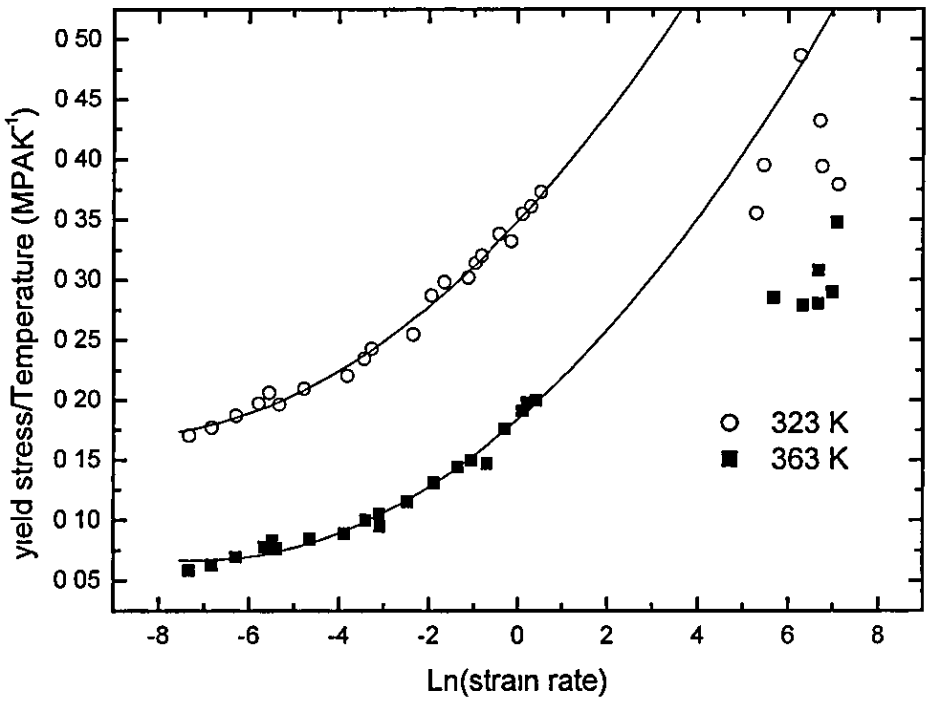

(b) At 20% strain of Poly(methyl methacrylate)

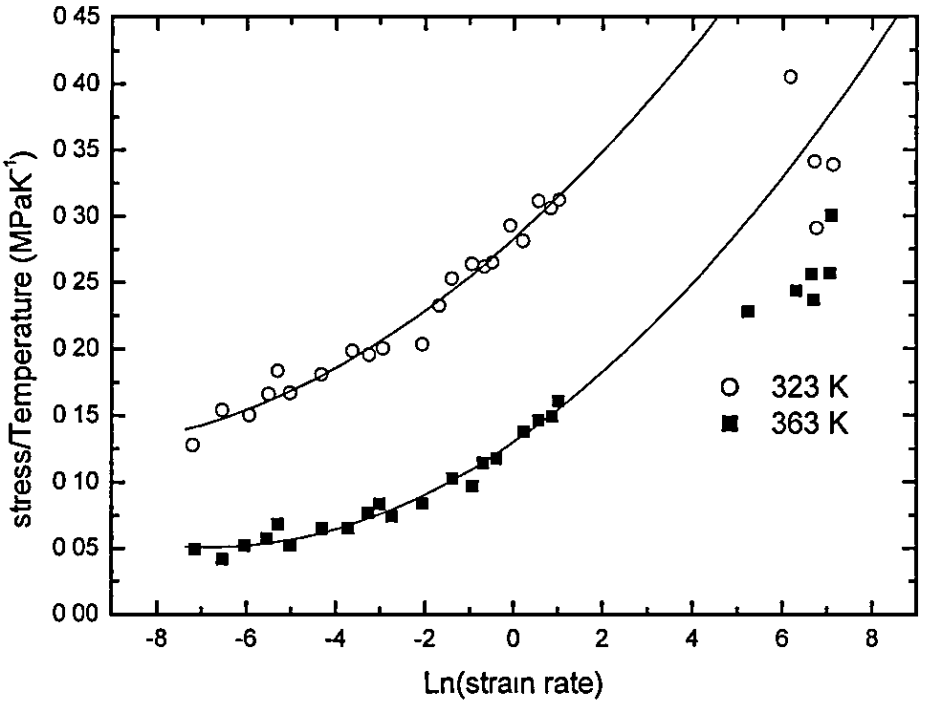

(c) At 30% strain of Poly(methyl methacrylate)

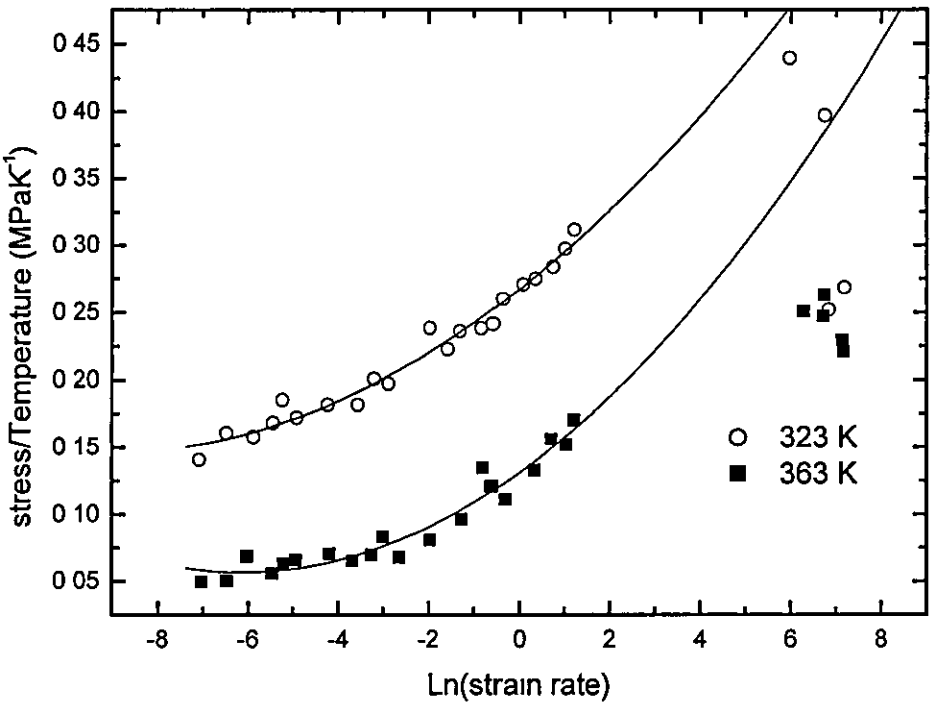

Graph 8.1: Stress/Temperature versus Ln(strain rate) at (a) yield point, (b) 20% strain and (c) 30% strain for Poly(methyl methacrylate) tested at strain rates 10^{-4} to 10^{3} s^{-1} at 323 K and 363 K.

(a) At yield point of Poly(methyl methacrylate)

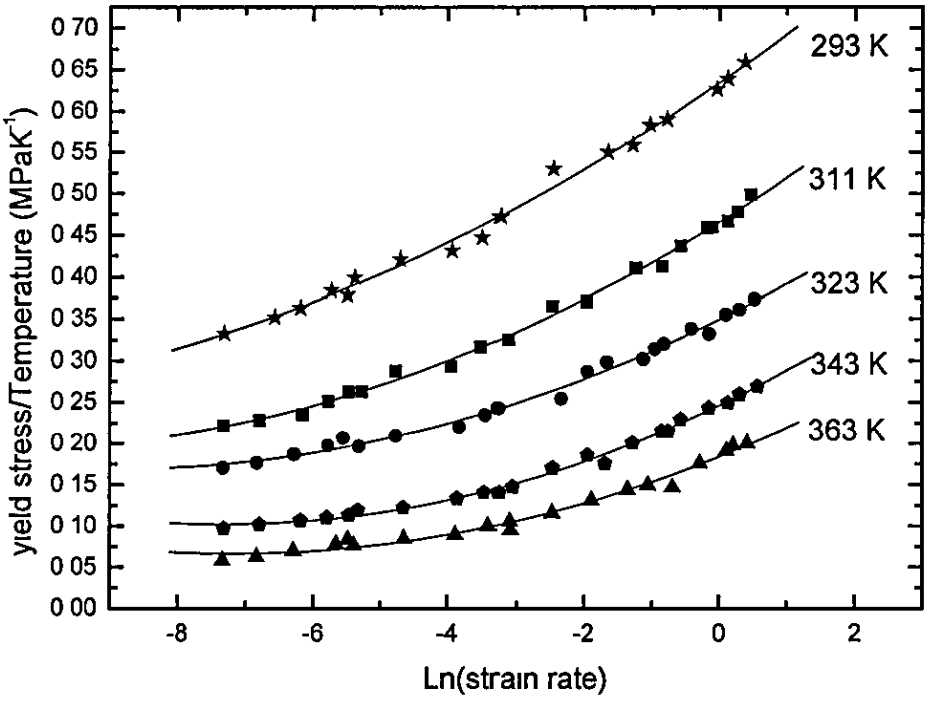

(b) At 20% strain of Poly(methyl methacrylate)

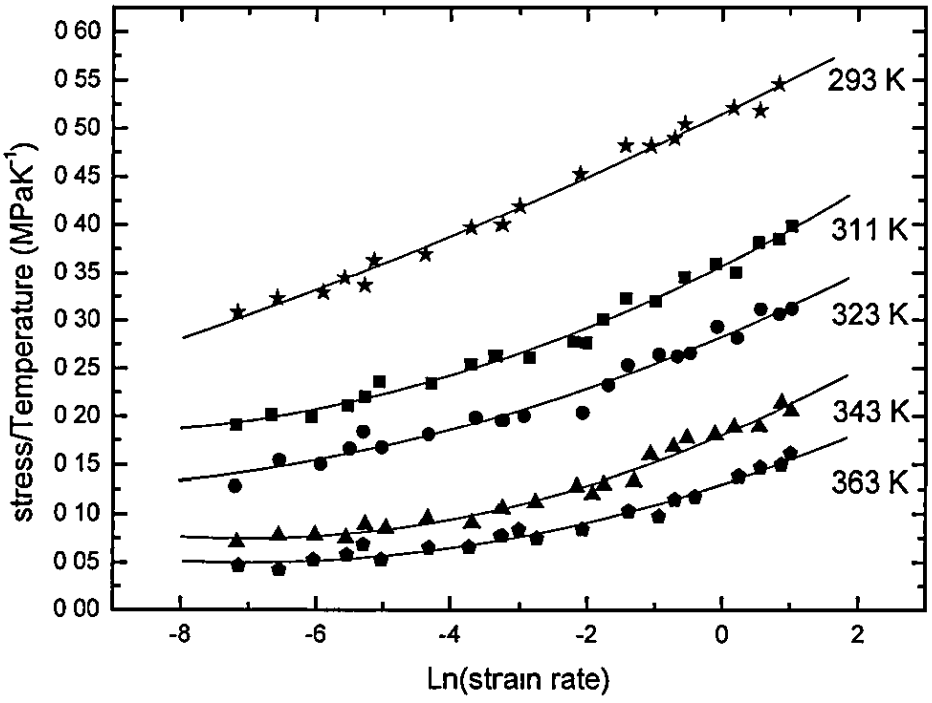

(c) At 30% strain of Poly(methyl methacrylate)

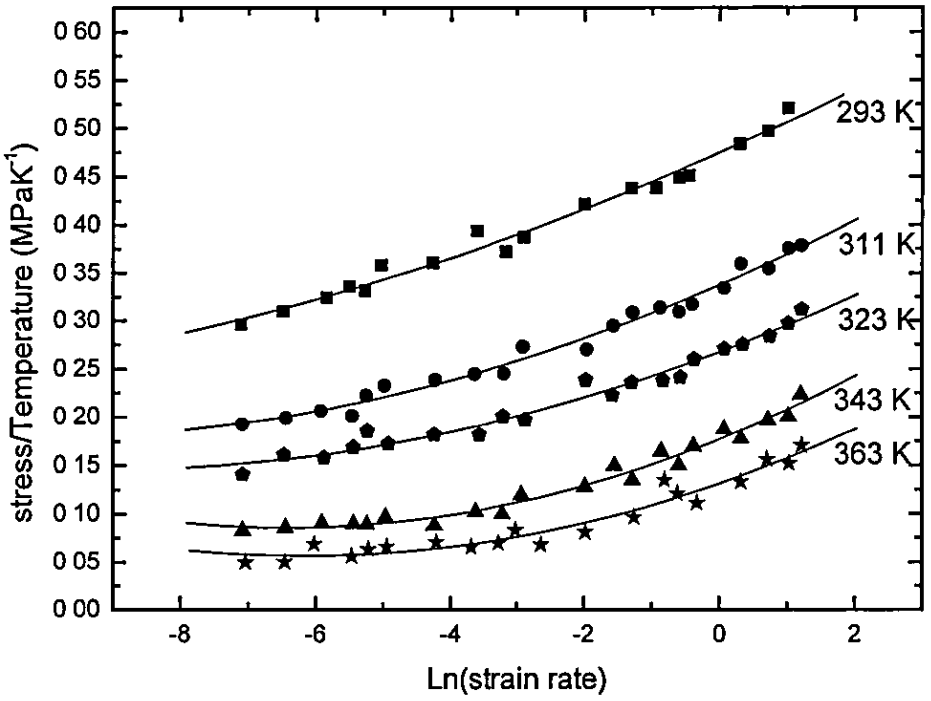

Graph 8.2: Stress/Temperature versus Ln(strain rate) at (a) yield point, (b) 20% strain and (c) 30% strain for Poly(methyl methacrylate) tested at low strain rates 10^{-4} to 2 s^{-1} at various temperatures.

(a) At yield point of Polystyrene

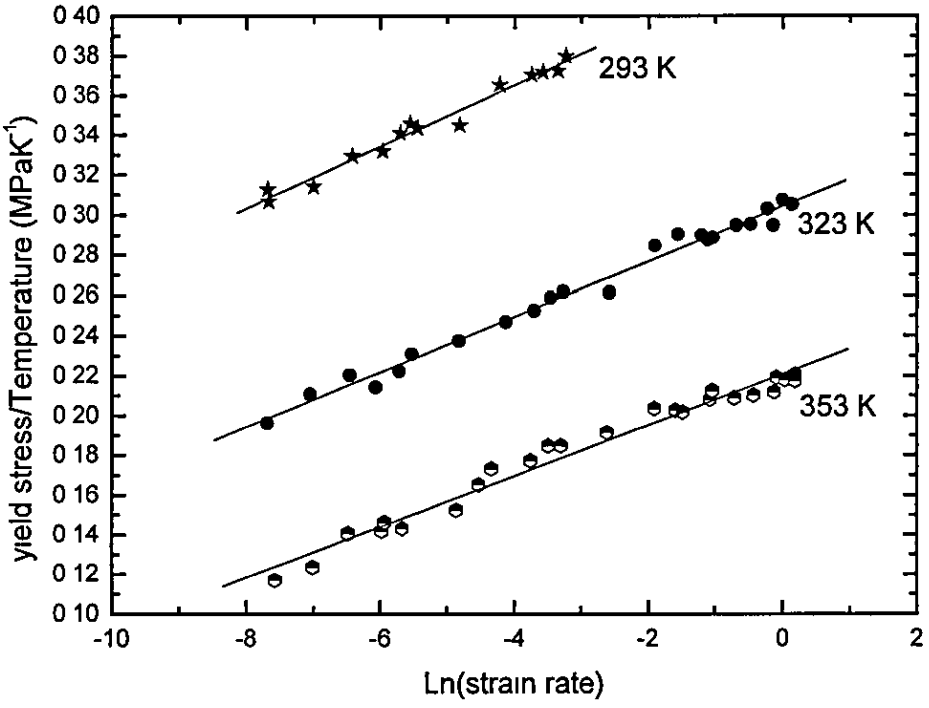

(b) At 20% strain of Polystyrene

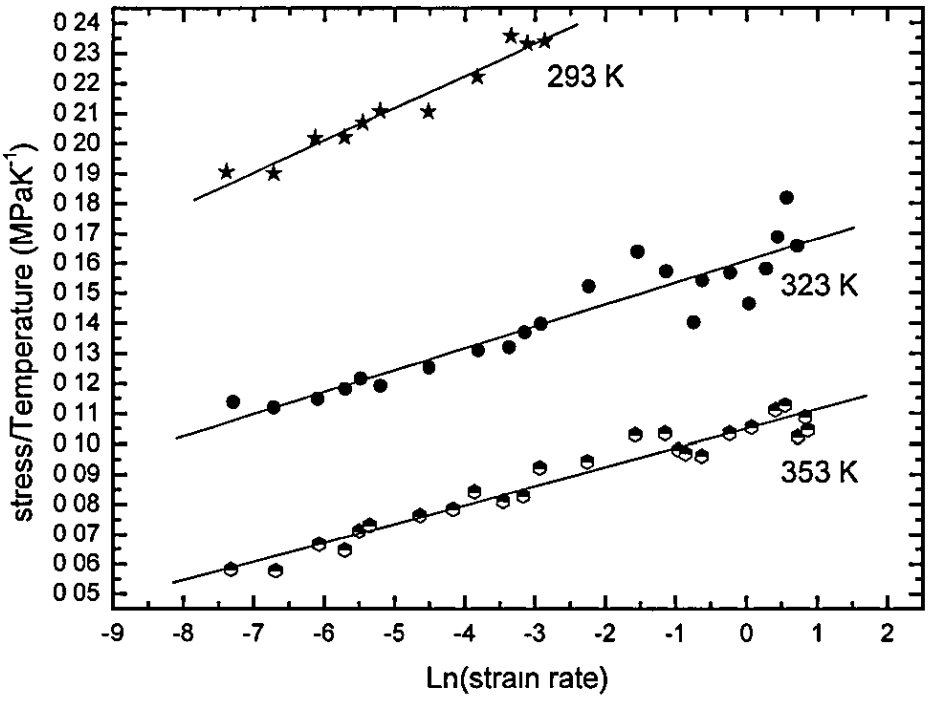

(c) At 30% of Polystyrene

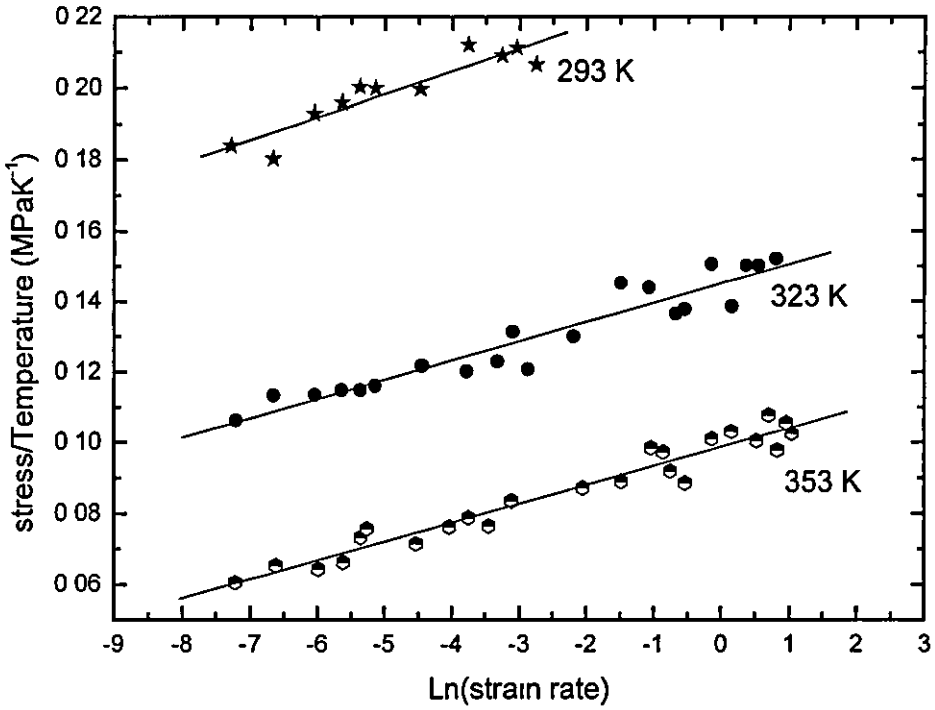

Graph 8.3: Stress/Temperature versus ln(strain rate) at (a) yield point, (b) 20% strain and (c) 30% strain for Polystyrene tested at low strain rates 10^{-4} to 2 s^{-1} at various temperatures.

(a) At yield point of Poly(methyl methacrylate)

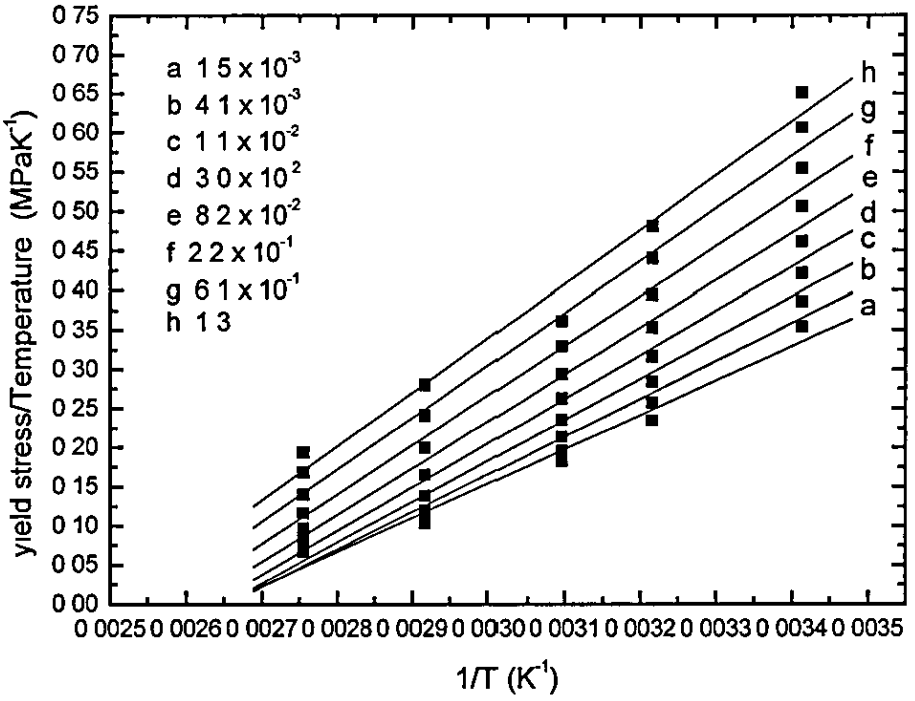

(b) At 20% strain of Poly(methyl methacrylate)

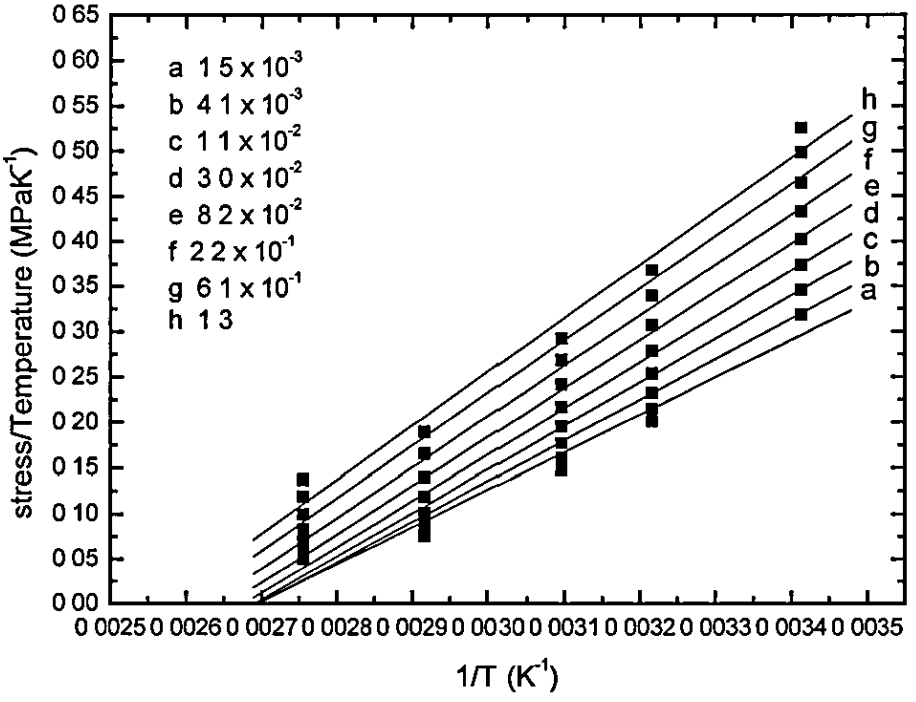

(c) At 30% strain of Poly(methyl methacrylate)

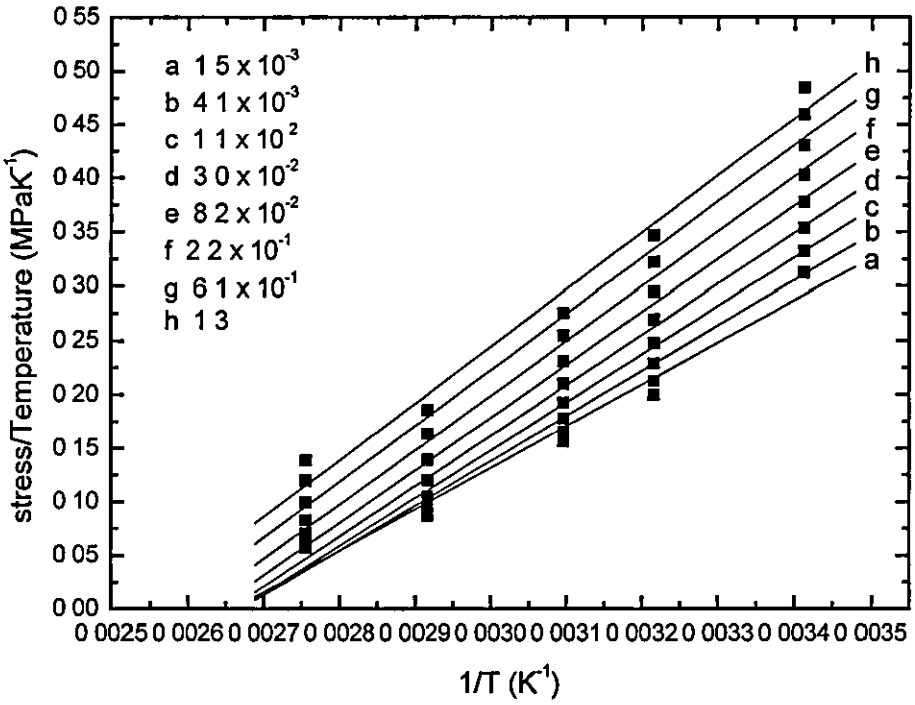

Graph 8.4: Stress/Temperature against 1/Temperature at (a) yield point, (b) 20% strain and (c) 30% strain for Poly(methyl methacrylate) tested at low strain rates 10^{-4} to 2 s^{-1} at various temperatures.

(a) At yield point of Poly(methyl methacrylate)

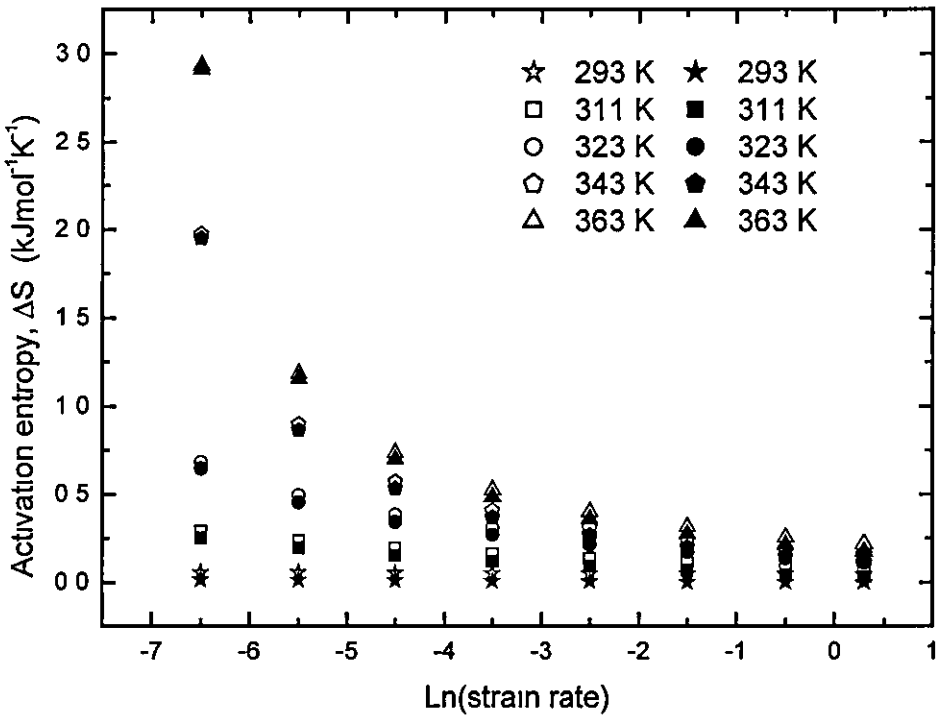

(b) At 20% strain of Poly(methyl methacrylate)

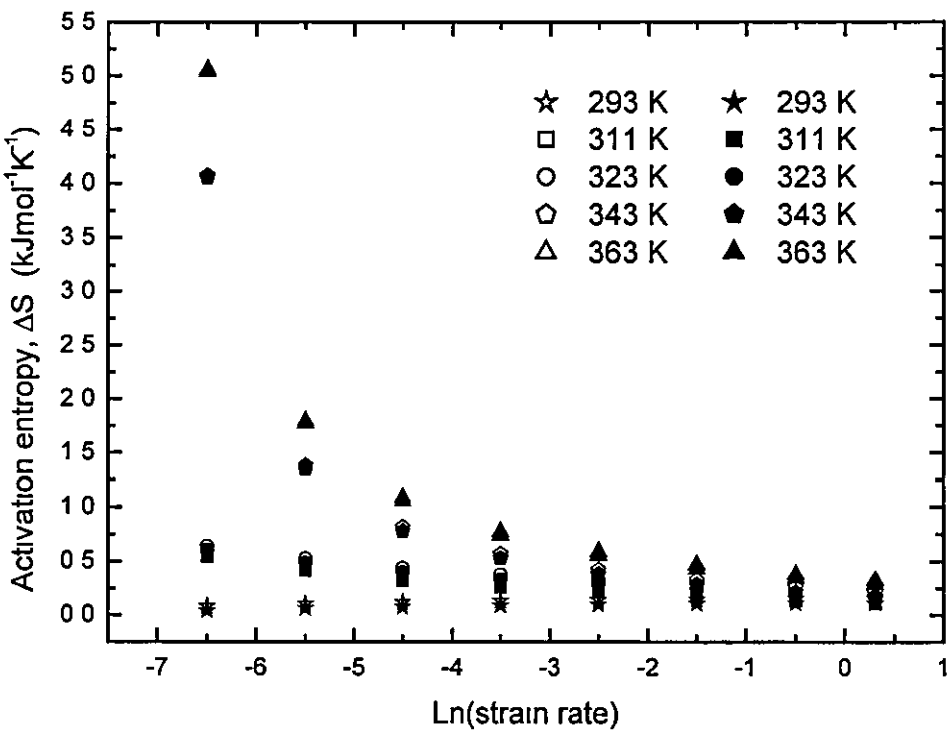

(c) At 30% strain of Poly(methyl methacrylate)

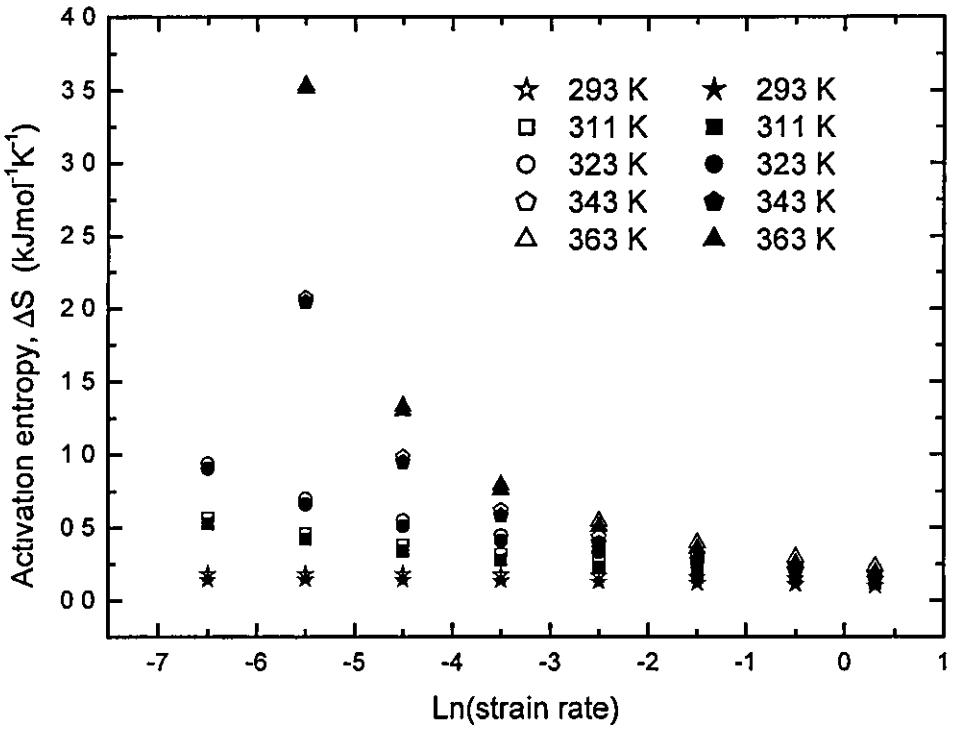

Graph 8.5: Activation entropy at (a) yield point, (b) 20% strain and (c) 30% strain for Poly(methyl methacrylate) tested at low strain rates 10^{-4} to 2 s^{-1} at various temperatures by assuming $\upsilon_m = \upsilon_a$ (filled symbols) and $\upsilon_m = 284.24$ nm^3 (unfilled symbols).

with $C = \frac{2}{3}\frac{\lambda}{\lambda_1}\frac{kT}{h}$.

8.7 High Strain Rate Analysis

When a material is subjected to compressive or tensile tests, some of the work done during deformation will appear as heat Temperature rise normally occurs in the material if the heat developed is not lost to the surrounding. In analysing the data for less temperature dependent materials such as metals, the resultant temperature rise can often be neglected. However, in polymeric materials which are very sensitive to strain rate and temperature, the heat developed during deformation can affect the stress-strain curve if the deformation does not take place isothermally.

Flow stress increases with increasing strain rate but decreases when temperature increases. At high strain rate, heat is generated during the polymer deformation too quickly to be lost to the surrounding. The deformation therefore takes place adiabatically and causes a rapid increase in the temperature of the sample tested. The temperature rise will produce strain softening and causes a change in the mechanical properties of polymers to occur.

The temperature rise, ΔT that occurs in the samples tested can be calculated using the following equation:[19]

$$\Delta T = \frac{\int \sigma d\varepsilon}{\rho C_p} \tag{8.35}$$

where the plastic work $\int \sigma d\varepsilon$ is calculated by measuring the area under the stress-strain curve. The density of PMMA (ρ) is taken to be 1190 kgm^{-3}. The heat of capacity of PMMA (C_p) is found from the DSC data which is 840 $Jkg^{-1}K^{-1}$ at 323 K and 970 $Jkg^{-1}K^{-1}$ at 343 K respectively.

8.8 Results and Discussion

8.8.1 Poly(methyl methacrylate)

Holt[15] studied the modulus and yield stress of poly(methyl methacrylate) and found that a plot of stress σ against strain rate ε at small strains (before yield) showed sigmoidal curves. At yield, the curve smoothed out. He suggested that the sigmoidal curves are due to the manifestation of the secondary (β) transition (the movement of the ester side group) in PMMA and this movement makes no major contribution to strain at yield. Instead the movement of molecular chain becomes more predominant at yield. He also suggested that at low strain rates the ester groups have time to readjust and relax the stress; at higher rates they are "frozen" and stress is higher for the same strain.

Bauwens-Crowet et al.[13] found that a plot of σ/T against $\log \varepsilon$ formed a set of parallel curves for PMMA and can be separated into two ranges. In the α range, below d_c, the molecular motions may correspond to the translational mode of the main chain and the β transition due to the local relaxation mode of chains can be neglected. In the range above d_c, the β mode is frozen and it is necessary first to liberate the local relaxation modes of the chains. Hence, larger stress is needed at the higher strain rates.

In this study to explain the behaviour of PMMA at yield, 20% and 30% strain from the molecular aspect, ΔG was replaced with ΔH and ΔS. The partial differential calculation method allowed a series of activation enthalpy, entropy and volume of the groups of flow units with respect to a range of strain rate to be found (Table 8 4, 8 5 and 8 6) by taking tangents to the fitted curves of σ/T versus $\ln(\dot{\varepsilon})$ and $1/T$ (Graph 8.2 and 8.4). Hence, the elementary processes occurred in PMMA during deformation could be calculated more explicitly using this method compared to the Ree-Eyring method adopted by some authors.[12,16] In the Ree-Eyring method, it is assumed that two rate processes occurred with α at the lower part of the curve and β at the upper part of the curve. In this case only two activation energies are calculated which are α activation energy ΔG_α and β activation energy ΔG_β. Bauwens-Crowet[12] found that ΔG_α and ΔG_β to be 412 and 107 kJmol^{-1} respectively; Roetling[16] 339 and 100 kJmol^{-1}

respectively using the Ree-Eyring method. Deutsch et al.[22] from tensile modulus measurements obtained a value of 334 $kJmol^{-1}$ for ΔG_α. From dielectric measurements, De Brouchere et al.[23] reported the values of ΔG_α and ΔG_β to be near 419 $kJmol^{-1}$ and about 84 to 96 $kJmol^{-1}$ respectively. From the calculations in this study, it is found that ΔG_y is around 82 ~ 126 $kJmol^{-1}$, $\Delta G_{20\%}$ around 81 ~161 $kJmol^{-1}$ and $\Delta G_{30\%}$ around 81 ~ 119 $kJmol^{-1}$ for the range of $\ln(\dot{\varepsilon})$ from –6.5 to 0 3 (strain rate: 0.002 to 1 3 s^{-1}). The values obtained are quite reasonable when compared with the values obtained using other methods. The advantage of this method is it allows ΔG at a particular strain rate to be obtained.

From Graph 8.8, the calculated values of activation energy do not show any clear trend, however, it can be seen that $\Delta G_{30\%} > \Delta G_{20\%} > \Delta G_{yield}$ Although $\Delta G_{30\%} > \Delta G_{20\%}$, $\Delta G_{30\%}$ at 311, 323, 343 and 363 K overlapped with $\Delta G_{20\%}$ at 293, 311, 323 and 343 K. This indicated that the difference between ΔG_{yield} and $\Delta G_{20\%}$ is bigger than that of $\Delta G_{20\%}$ and $\Delta G_{30\%}$. This may explained that in this plastic region before strain hardening, the flow of the system involved the break of Van der Waal's bonds between the molecular chains along the shearing plane. When the strain increases gradually in this plastic region before strain hardening, the magnitudes of the strength between molecular chains are getting weaker. By plotting ΔG and ΔH against $\ln(\dot{\varepsilon})$ under the same axes (Graph 8.9), it can be seen that the change of ΔG with temperatures is almost negligible when compared to the change of ΔH with temperatures. ΔG at the different temperatures formed almost a straight line. This is in agreement with the assumption made by Bauwens-Crowet et al.,[11,13] Roetling,[16] etc. that the activation energy is almost constant with temperature when calculating Eyring's factors.

8.8.2 High Strain Rate Analysis on Poly(methyl methacrylate)

Samples of PMMA were tested at high strain rate using a Dropweight Machine at the temperatures 323 K and 363 K with the difference of these two temperatures being 40 K. From Graph 8 1(a, b & c), it can be seen that most of the high strain rate data at 323 K fell below the extrapolated polynomial curve of 363 K. If it is assumed that the experimental data fall on the same curve as the isothermal data, then the temperature rises should be more than 40 K. However, the calculated temperature rises shown in Table 8.7a is less than 40 K.

Hall[20] study of yarns under extension showed that the deformation took place isothermally at strain rates below 0 04 s^{-1} and adiabatically at rates above 4 s^{-1}. He estimated that the temperature was likely to rise by 20 ~ 30 °C at strains above 10% during adiabatic extension. From the Table 8.7(a & b), the calculated values of temperature rise for 20% and 30% at 323 K are around 12 ~ 35 °C and are roughly in agreement with Hall's estimation. For strains at 20% and 30% at 363 K, the calculated values of temperature rise are less than 20 °C (Table 8.7b) and did not match Hall's estimation of the temperature rise. Detailed discussions and assumptions to explain the deviation from Hall's estimation and the excessive fall of experimental data on isothermal curve compared to the calculated temperature rises are done in Chapter 9.2.

The yield point occurs at strain around 8% to 11% and the calculated values of temperature rise were around 6 K to 20 K. This is in line with those computed and measured by Chou et al.[21] for PMMA compressed at strain rate 3 s^{-1} and 45 s^{-1}.

8.8.3 Polystyrene

A set of parallel lines shown in the plot of σ/T and $\ln(\varepsilon)$ revealed that the flow in polystyrene is homogeneous. The activation volumes at three different temperatures (293K, 323K and 363 K) were displayed in Table 8 8 as well as the mean values of activation volume, activation energy and constant C. The activation volume and energy increase at larger strain in the plastic region. The difference between $\Delta G_{20\%}$

and ΔG_y is 84 kJmol^{-1} and $\Delta G_{30\%}$ and $\Delta G_{20\%}$ is 33 kJmol^{-1}. The difference gets less when the strain increases gradually in the plastic region. It can be seen that the same phenomena that happen in the heterogeneous flow are found in the homogeneous flow.

8.8 Conclusion

The flow in PMMA is heterogeneous as plots of σ/T versus $\ln(\varepsilon)$ showed a set of parallel curves; in PS is homogeneous as plots of σ/T versus $\ln(\dot{\varepsilon})$ showed a set of parallel lines. The activation energy and volume increase when the strain increases. In the plastic region, the increase of the activation energy is not proportional to the increase in strain. The increase of the activation energy showed a gradual reduction in the difference of the following activation energy when strain increases. From the plots of activation energy and enthalpy versus $\ln(\dot{\varepsilon})$ under the same axes, the changes of the activation energy with temperatures could be considered constant For the high strain rate testing, crack propagated at the edge of the samples during deformation and affected the stress-strain curves obtained. Hence, this may caused the data of σ/T obtained lower than the actual values.

(a) At yield point of Poly(methyl methacrylate)

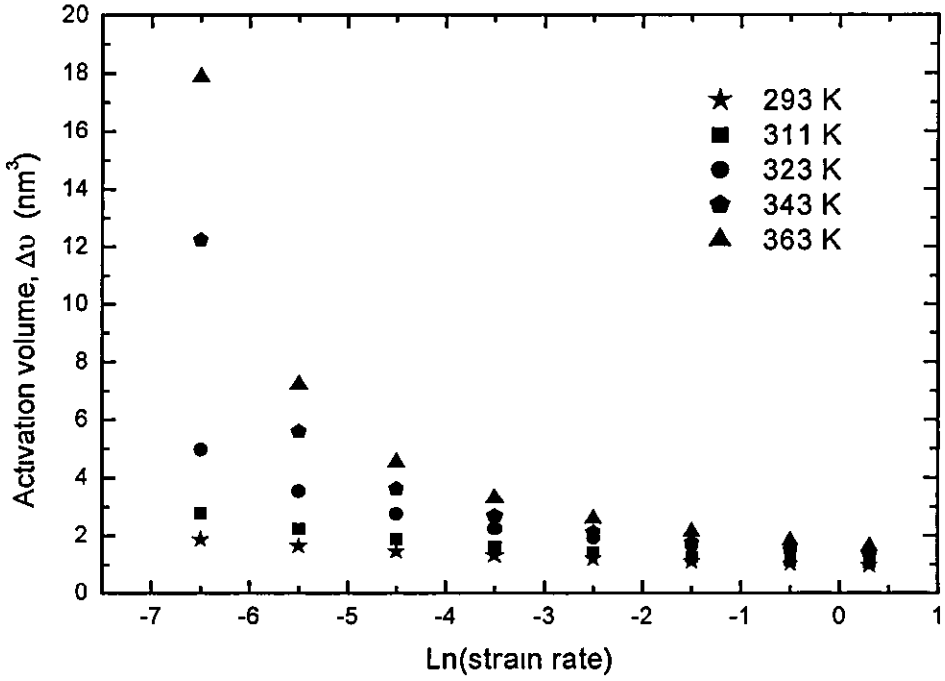

(b) At 20% strain of Poly(methyl methacrylate)

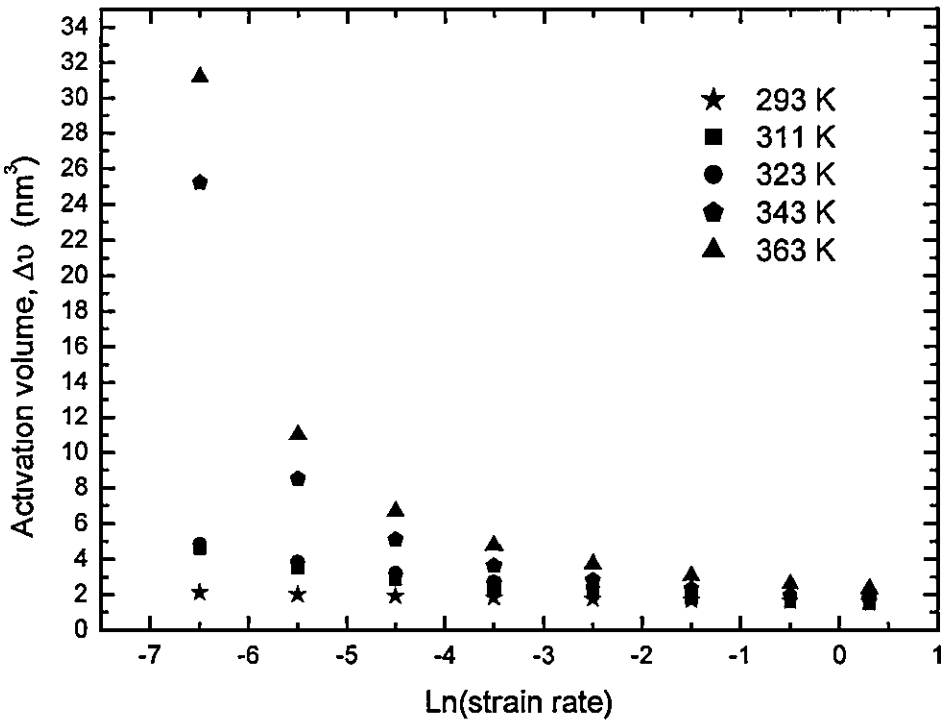

(c) At 30% strain of Poly(methyl methacrylate)

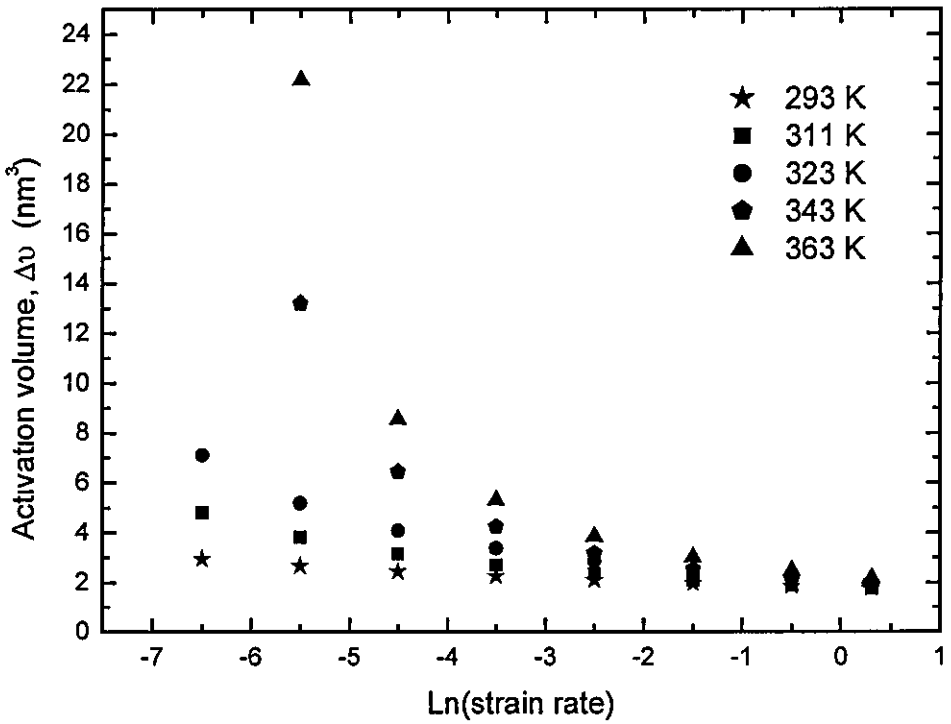

Graph 8.6: Activation volume at (a) yield point, (b) 20% strain and (c) 30% strain for Poly(methyl methacrylate) tested at low strain rates 10^{-4} to 2 s^{-1} at various temperatures.

(a) T = 293 K

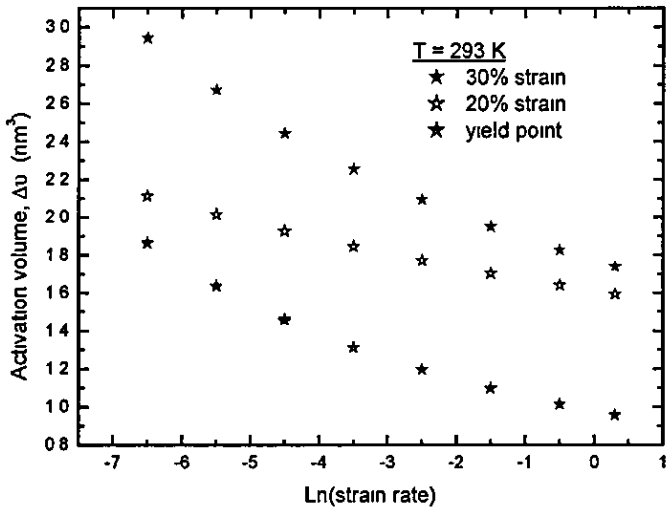

(b) 311 K

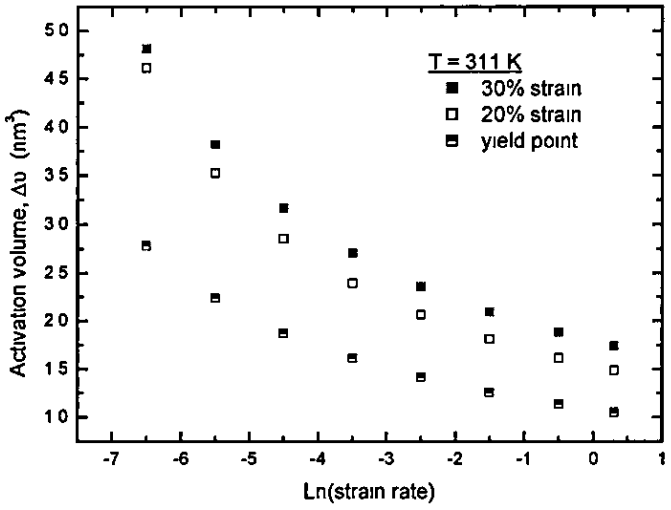

(c) T = 323 K

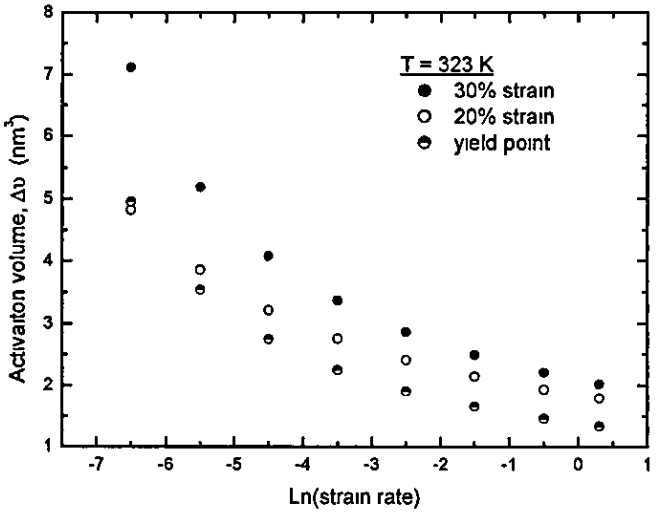

(d) T = 343 K

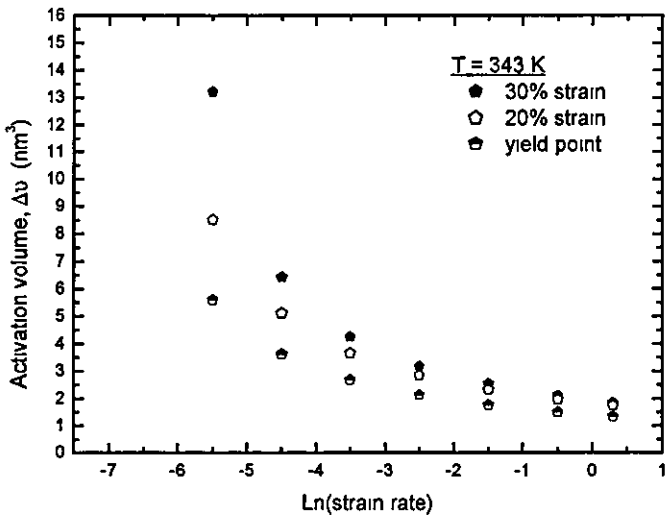

(e) T = 363 K

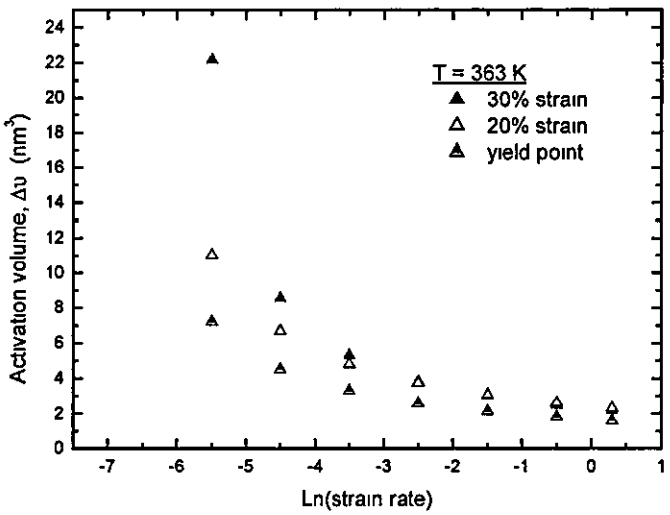

Graph 8.7: Comparison of the activation volume at yield point, 20% and 30% strain for Poly(methyl methacrylate) tested at low strain rates at (a) 293 K, (b) 311 K, (c) 323 K, (d) 343 K and (e) 363 K.

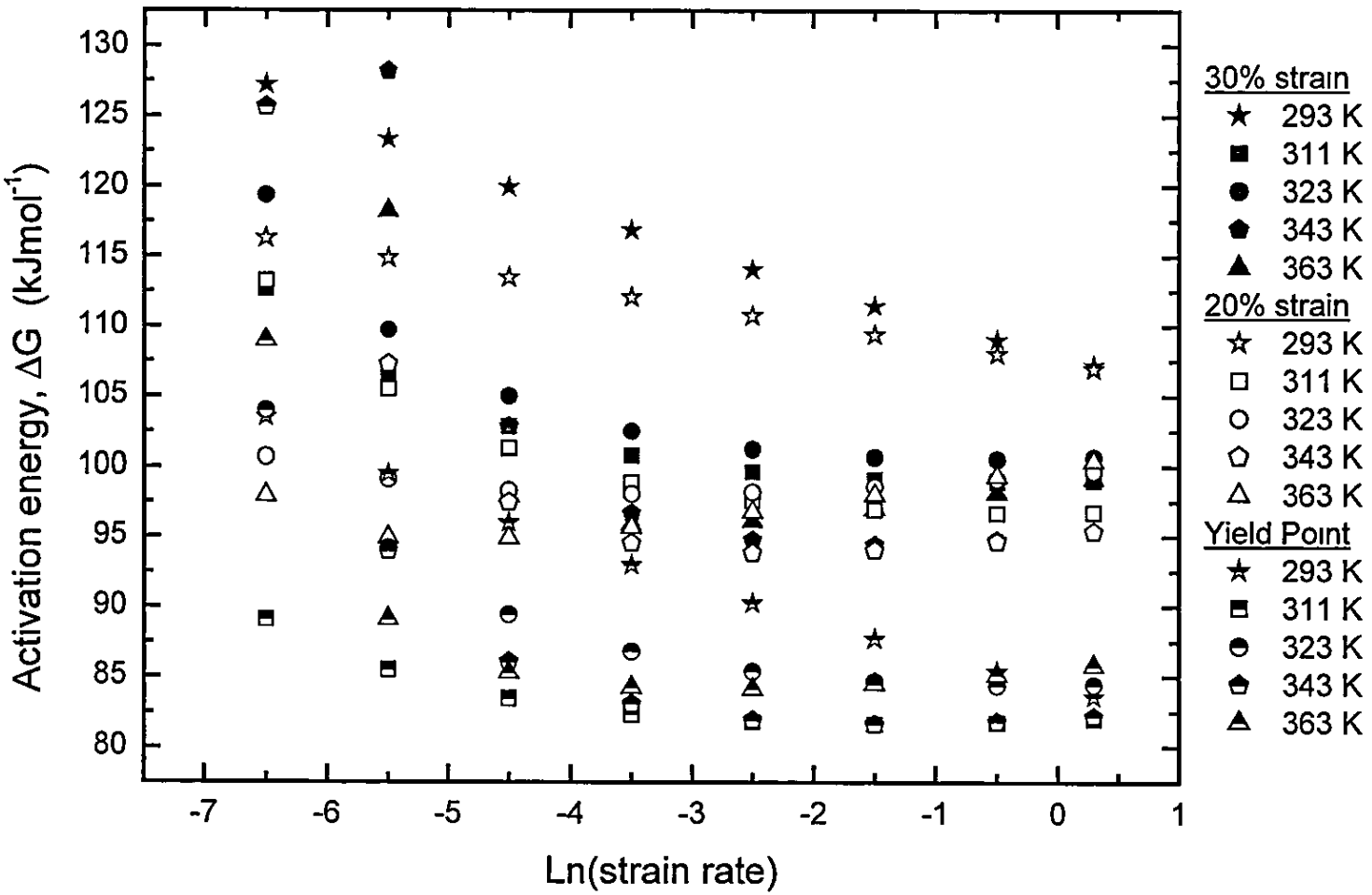

Graph 8.8: Activation energy at yield point, 20% and 30% strain for Poly(methyl methacrylate) tested at various temperatures and at quasi-static and low strain rates.

(a) At yield point of Poly(methyl methacrylate)

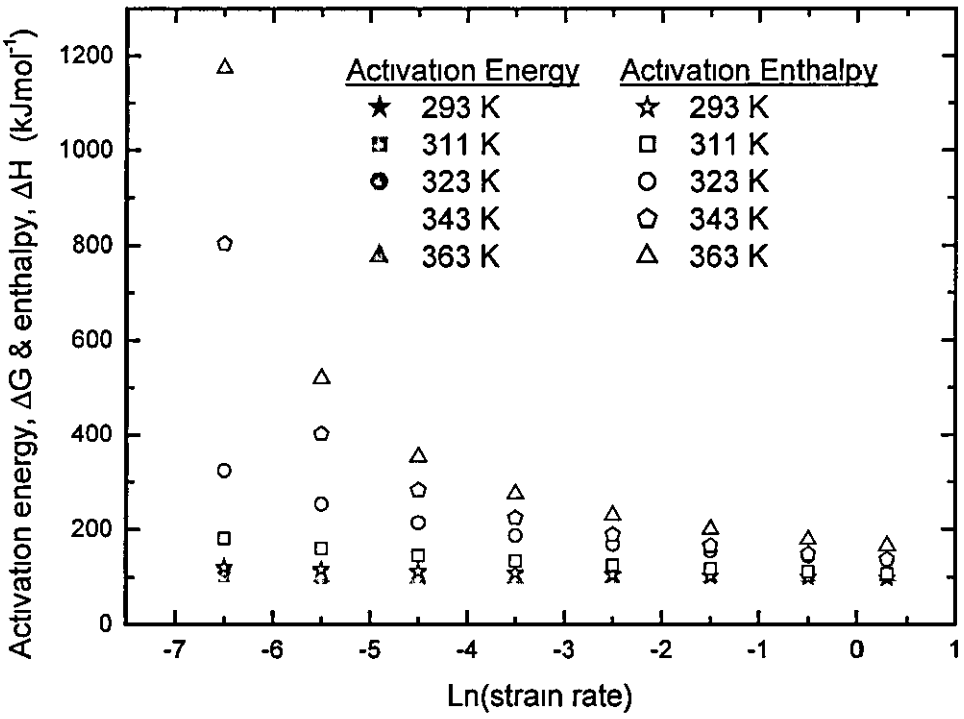

(b) At 20% strain of Poly(methyl methacrylate)

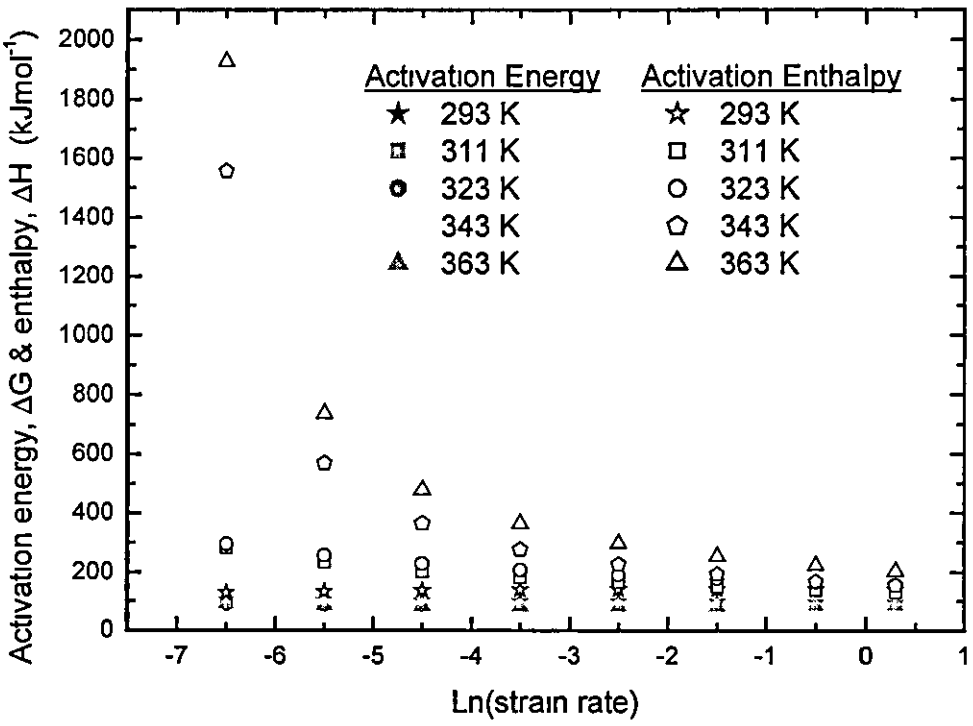

(c) At 30% strain of Poly(methyl methacrylate)

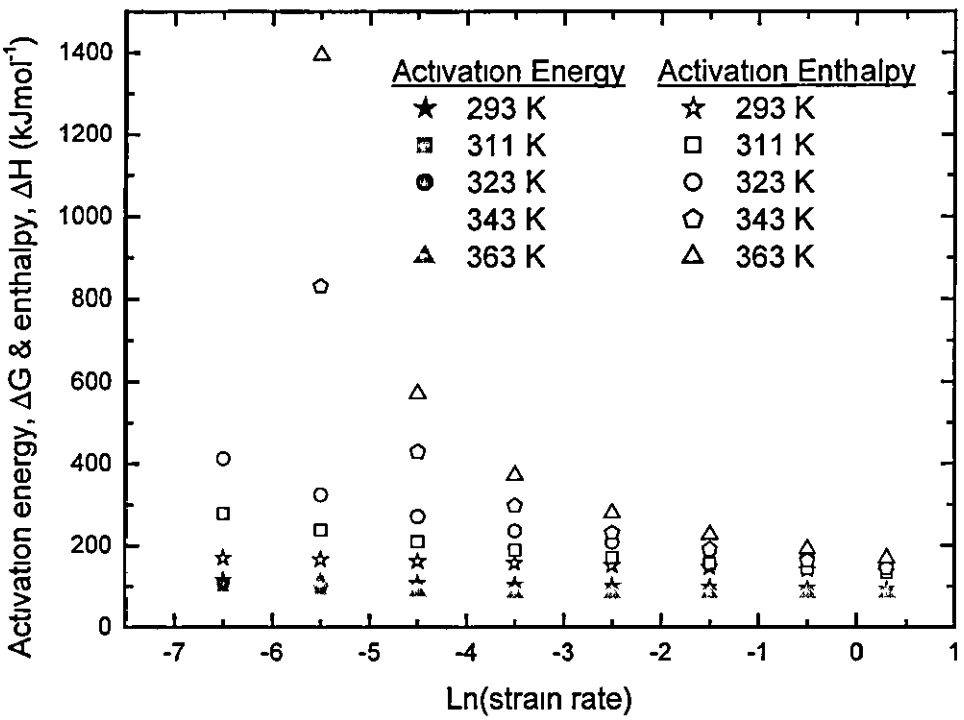

Graph 8.9: Activation energy and enthalpy at (a) yield point, (b) 20% strain and (c) 30% strain for Poly(methyl methacrylate) tested at low strain rates 10^{-4} to 2 s^{-1} at various temperatures under the same axes to see the variation of activation energy with temperatures.

Table 8.7a: Temperature rise (ΔT) for Poly(methyl methacrylate) tested at high strain rate (Dropweight Machine) at 323 K with specific heat = 840 $J/kg^{-1}K^{-1}$.

$\ln(\dot{\varepsilon}_y)$	ΔT_y	$\ln(\varepsilon_{20\%})$	$\Delta T_{20\%}$	$\ln(\dot{\varepsilon}_{30\%})$	$\Delta T_{30\%}$
5 296	4 1	6.185	20.9	5 971	34 6
5 468	4 6	6 775	12.3	6 745	31.2
6.268	9.4	6.729	19.4	6.831	20 7
6.756	8.9	7.139	14 6	7.178	23.4
6.711	8.4				
7.123	10.0				

Table 8.7b: Temperature rise (ΔT) for Poly(methyl methacrylate) tested at high strain rates (Dropweight Machine) at 363 K with specific heat = 1110 $J/kg^{-1}K^{-1}$.

$\ln(\varepsilon_y)$	ΔT_y	$\ln(\varepsilon_{20\%})$	$\Delta T_{20\%}$	$\ln(\dot{\varepsilon}_{30\%})$	$\Delta T_{30\%}$
5.674	3.8	5.236	9.7	6.279	16 3
6.332	5.6	6.318	9.9	6.707	16.1
6.667	9.7	6.667	9.7	6.735	18.0
6.677	4.7	6.706	10.9	7.131	17.1
6.986	6.8	7.069	8.5	7.153	15.3
7.082	7.5	7.090	10.7		

Table 8.8: The means of the activation volumes and activation energies at yield point, 20% and 30% strain for Polystyrene tested at various temperatures and at low strain rates.

	υ_a (nm^3)			$\overline{\Delta\upsilon}$ (nm^3)	$\overline{\Delta G}$ (kJmol-1)	$\overline{C}$ (s^{-1})
	293 K	323 K	353 K			
Yield Point	3.55	4.01	4.31	3.96	193	3.19×10^{18}
20% strain	5.17	7.56	8.76	7.16	277	$2\ 10 \times 10^{33}$
30% strain	8.64	10.11	10.38	9.71	310	1.24×10^{36}

Appendix 8.1: Calculation of Eyring's factors : Q, A and C[11,13]

Eyring's equation of viscous flow for compression can be expressed as below,

$$\frac{\sigma_c}{T} = A\left[\ln\dot{\varepsilon}_c - \ln CT + \frac{Q}{RT}\right]$$

with $A = \frac{4k}{\upsilon_a}$, $C = \frac{2\lambda\lambda}{3\lambda_1 h}$ and Q is the activation energy, k the Boltsmann's constant and h Plank's constant. To calculate the Eyring's factors of A, C and Q, data of σ_c/T against $\log(\varepsilon_c)$ are plotted and using the linear least-squares method, straight lines are calculated to fit the data related to each temperature. The mean slope of these straight lines is taken as A. The mean value of the activation energy, Q, is calculated from the horizontal/vertical distances between these lines. C is calculated from A and Q and the extrapolated value of the abscissa of each line for $\sigma_c/T = 0$.

References

1. **T. Ree and H. Eyring,** in "Rheology", Vol II, F. R. Eirich, Ed , Academic Press, New York, 1958, Chapter III

2. **G. Halsey, H. J. White, Jr. and H. Eyring,** Textile Research Journal **15** (1945) 295~311

3. **I. M. Ward,** Journal of Materials Science **6** (1971) 1397~1417

4. **I. M. Ward,** "Mechanical Properties of Solid Polymers", second edition, John Wiley and Sons, 1979

5. **S. Glasstone, K. J. Laidler, and H. Eyring,** "The Theory of Rate Processes", New York, McGraw-Hill Book Co , 1941

6. **S. P. Timoshenko and J. N. Goodier,** "Theory of Elasticity", McGraw Hill, New York, 1970

7. **X. X. Zhu and G. R. Zhu,** Polymer **33** (1992) 4968~4976

8. **Y. Nanzai,** Polymer Engineering and Science **30** (1990) 96~107

9. **T. Ree and H. Eyring,** Journal of Applied Physics **26** (1955) 793~800

10 **Shao-mu Ma,** Journal of the Korean Chemical Society **20** (1976) 173~184

11. **C. Bauwens-Crowet, J-M. Ots and J-C. Bauwens,** Journal of Material Science **9** (1974) 1197~1201

12. **C. Bauwens-Crowet,** Journal of Materials Science **8** (1973) 968~979

13. **C. Bauwens-Crowet, J. C. Bauwens and G. Homes,** Journal of Polymer Science A-2 **7** (1969) 735~742

14 **R. N. Haward and G. Thackray,** Proceedings. Royal Society of London **A 302** (1968) 453~472

15. **David L. Holt,** Journal of Applied Polymer Science **12** (1968) 1653~1659

16. **J. A. Roetling,** Polymer **6** (1965) 311~317

17. **Octave Levenspiel,** "Understanding Engineering Thermo", Prentice Hall PTR, London, 1996

18. **Evelyn Guha,** "Basic Thermodynamics", Alpha Science International, UK, 2000

19. **P. C. Dawson,** "The Mechanical and Thermal Behaviour of Polymers under High Strain Rate Compression", Department of Physics, Loughborough University, 1993

20. **H. Hall,** Journal of Applied Polymer Science **12** (1968) 739~750

21. **S. C. Chow, K. D. Robertson and J. H. Rainey,** Experimental Mechanics (1973) 422~432

22. **K. Deutsch, E. A. W. Hoff and W. Reddish,** Journal of Polymer Science **13** (1954) 565~582

23 **L. de Brouchere and G. Offergeld,** Journal of Polymer Science **30** (1958) 105~118

Chapter 9

Discussion, Conclusion and Suggestion for Future Work

9.1 Discussion

9.1.1 Introduction

This chapter discusses the results obtained from the mechanical tests, thermal analysis, density measurement and birefringence and relates them together to reveal some important features about the mechanical response of the samples to temperature and strain rate. High-speed photography helps in understanding the mechanisms occurring in the deformation and provides a clear insight about the fracture behaviour of the samples.

Molecular relaxation, the idea of localised stress, the structures of the polymers, the orientation of the polymer chains, the different energy state caused by heating and the transitions revealed in DMTA are used to explain the flow of polymer chains at low strain rates and high strain rates.

In the experiments, a few steps were taken to ensure the consistency of the data collected from the machines Petroleum jelly was used on both surfaces of samples throughout the experiments. The same aluminium-heating block and thermostat were used for all the mechanical tests carried out. Strain gauges were calibrated at the temperature of testing so that the thermal effect would be compensated when stress was calculated. The filtering circuit was tested for its output before used for filtering the output voltage.

This study first relates the chain orientation with temperature and strain, reveals the deformation mode, give possible explanations for the fracture and describes the flow mechanism of the polymer chains at a range of strain rates from the thermodynamic approach.

9.1.2 Low Strain Rate Test

The ductile-brittle transition temperatures for poly(methyl methacrylate) (PMMA) and polystyrene (PS) are at 45 °C and 90 °C respectively. However, PMMA and PS tested at quasi-static (0 0006~0.006 s^{-1}) and low strain rates (0 05~0.5 s^{-1}) showed ductile behaviour although they were tested at temperatures below their ductile-brittle transition temperatures (Graph 3.1 and 3.2). This could be because that at quasi-static and low strain rates, the polymer chains of PMMA and PS have enough time to relax the stress received.

For quasi-static and low strain rate tests, the stress-strain curves of PMMA and PS displayed yield point, strain softening and strain hardening before fracture. However, PS showed a sharp drop after the yield point compared to PMMA (Graph 3.1 & 3.2) The sharp drop might not be due to localised heating during compression as the tests were carried out at quasi-static and low strain rates. Any heat generated will have enough time to be transferred to the surrounding during compression. Thus, localised heating is unlikely to occur in the sample. It is suggested that the upper yield stress might initiate the movements of long-range chains and induce the yielding. PMMA and PS have different structures of side groups that might influence the yielding process and thus affect the shapes of stress-strain curves.

Samples were compressed up to or more than 70% strain in the tests. The applied stress became gradually greater than the yield stress when strain hardening started to take place in the sample. At strain rate 0.0006 s^{-1}, PMMA showed the commencement of strain hardening roughly after 25% strain and at a strain rate of 0.5 s^{-1}, the strain where the strain hardening commenced was roughly after 35% (Graph 3.1). For PS tested at strain rate 0.0006 s^{-1}, it was roughly after 30% of strain and at strain rate 0 5 s^{-1}, it was roughly after 40% of strain (Graph 3.2). It seemed that the strain rates influenced the point where the strain hardening commenced but the testing temperatures did not when samples were tested at quasi-static and low strain rates.

9.1.3 High Strain Rate Test

High strain rate tests were carried out using the in-house built Dropweight Machine and the C4-camera Dropweight system PMMA fractured before the yield point when tested at 20 °C and showed ductile behaviour when tested at temperatures 50 °C and 70 °C which are above its ductile-brittle transition temperature. PS shows brittle behaviour when tested at temperatures below the ductile-brittle transition temperature at high strain rates. The ductile-brittle phenomena observed in PMMA and PS when tested at high strain rates are the same as those reported by others. Generally, the motions of polymer chains are greatly dependent on temperature. When heated through a range of temperatures higher than room temperature, the mobility of the polymer chains is encouraged and this changes the polymer behaviour from brittle to ductile

At high strain rates, samples could only be compressed up to 25% strain for strain limited tests. In order to study the strain hardening, samples were compressed without the limitation of strain at high strain rate. From Graph 3.5, it is seen that the strain hardening at high strain rate occurred at a lower strain than that of the low strain rate tests. As the high strain rate and the low strain rate tests were carried out in different machines, this could cause the comparison to be invalid.

It is known that adiabatic heating is induced in a sample at high strain rates. In correlation with low strain rate data for analysis, it is essential that the data studied are under the same thermal condition. It is impossible to eliminate adiabatic heating at high strain rates by transferring the heat away through any kind of methods. Hence, temperature rises were calculated for each data at high strain rates with the assumption that the experimental data fall on the isothermal curves in Graph 8.1. The corrected temperatures (testing temperature + temperature rise) are smaller than the extrapolated isothermal temperature curve on which the experimental data is expected to fall, i.e. – a decrease in yield and flow stress is observed, below the extrapolation

For testing temperature 50 °C (323 K), the calculated temperature rises are in line with other researchers (Detailed explanations about the comparison are made in Chapter 8.8.2). However, it is worth mentioning that when a test takes place adiabatically,

some microstructures might change due to the localised heating and this is beyond the macroscopic perception This might affect the stress-strain curves obtained and the calculated temperature rises. For testing temperature 90 °C (363 K) which is close to the glass transition temperature range of PMMA (111 °C ~ 123 °C, obtained from DSC data), the calculated temperature rises at 20% and 30% strain (around 8 ~ 18 °C) are not in line with other researchers. This might be because during deformation the actual sample temperatures (testing temperature + temperature rise) reached close to the glass transition. This causes the phase of the structure to change and affects the stress-strain curves obtained, thus, limiting their validity for comparison with low rate date.

9.1.4 Temperature Test

Graph 5 3a and 5 3b shows the specific heat of PMMA and PS against temperature. From the dashed lines drawn on the curves, it can be seen that the specific heats of PMMA and PS are linearly increasing with temperature in the regions before and after the glass transition. The glass transition region is where the polymer changes from the glassy to rubbery state In the glass transition region, the specific heat shows an upswing with the slight increasing of temperature. This is reasonable, as in this region the onset of the movements of long-range segmental chains occur, thus, greater energy is needed to liberate them from the binding forces. However, in the glassy state, only the movements of the side groups and the short range of segmental chains are involved.

Dynamic Mechanical Thermal Analysis (DMTA) has been reported to be an unsuitable instrument to determine the glass transitions of polymers as they are influenced by the frequency at which they are subjected to. From the Graph 5.4(a & b) and 5.5(a & b), the glass transitions for PMMA tested at 0.1 Hz and 100 Hz are around 112 °C and 127 °C respectively; for PS at 0.1 Hz and 100 Hz are around 92 °C and 116 °C respectively. It can be seen that the glass transitions of PMMA and PS are greatly influenced by the frequency they subjected to when using DMTA. In addition, the broad peaks that related to β relaxation on the loss modulus curves of PMMA and PS moved to higher temperatures when tested at 100 Hz compared to 0.1 Hz. For PMMA tested at 0.1 Hz, the broad peak of β relaxation is around –50 °C to 25 °C

(Graph 5.4a), while at 100 Hz is around 35 °C to 70 °C (Graph 5.4b). For PS tested at 0.1 Hz, a very broad peak was observed at the temperature between –25 °C and 25 °C, however, at 100 Hz the peak seemed to appear on the shoulder of the glass transition as reported by other researchers From 0.1 Hz to 100 Hz involves an increase in frequency by a factor of 10^3. It can be said that the onset of the side group movement might contribute the reason to the ductile-brittle transition.

The storage and loss moduli of PMMA and PS obtained provide good information in revealing the dependence of the movement of polymer chains on temperature and are adopted in discussing the effect of chain orientations on strain, strain rate and temperature in Chapter 9.4.

9.1.5 Strain limited test and Density measurement

Strain limited tests were carried out with the purpose of studying how the morphology of a fully amorphous polymer changes with strain. The tests could provide important intermediate microstructural information on the state of a sample after compression to a certain strain. The densities of the PMMA samples after the strain limited tests were measured using a Six Column Density Apparatus. The PMMA samples were tested under the high strain rate deformation using the C4 Camera system. Since PMMA is fully amorphous, it is assumed that any changes in the density will be due to the compact arrangement of the polymer chains caused by compression.

The stress-strain curves of PMMA and PS compressed at four different strains (0 8, 0.6, 0.4 & 0.2) at different strain rates and temperatures were shown in Graph 3.3 and 3.4. It can be seen that compression to different strains did not much affect the stress-strain curves produced. For PMMA tested at 20 °C and 50 °C, the stress-strain curves show a deviation of ± 2 MPa at yield stress when tested at quasi-static rates (0 0006 and 0.006 s^{-1}). However, at low strain rates 0.05 and 0.5 s^{-1}, a deviation of ± 4~10 MPa is observed at yield stress that is bigger than that at quasi-static rates. PS tested at 20 °C and 50 °C displayed a deviation of around ± 2~5 MPa at quasi-static and low strain rates. For PMMA tested at 70 °C and PS at 80 °C, the stress-strain curves show almost the same deviation (± 4 MPa for PMMA and ± 2~7 MPa for PS) at yield stress at 0.0006, 0.006, 0.05 and 0.5 s^{-1} The response of equipment at higher rate may be

partially to blame. Temperature variations may have a little contribution to the deviation at yield stress as well. Samples were sat on the steel roller and encompassed in the aluminium-heating block during compression (Figure 3.2). The ambient temperature was hard to maintain at a constant value and this might cause the heat to be conducted away at different rates. The testing temperature was monitored to be within a deviation of ± 3 °C around the desired value by the use of a thermocouple thermometer. This deviation may explain the variation at yield stress.

From Table 6.1 and Graph 6.1, it can be seen that the difference of the sample density displayed at different strain is not great The accuracy of the density float is ± 0 00015 g/ml (0.15 kgm^{-3}). The purpose of measuring the sample densities after high rate compression is to see whether there is any density increase in the amorphous phase that may contribute to the increase in yield and flow stress. The error for the sample density before and after compression is ± 0.3 kgm^{-3}. The error for the difference in density is thus ± 0.6 kgm^{-3}. The density differences shown in Table 6.1 are too small to be treated as reliable when compared with the calculated error Appendix 6.2 shows the method used in calculating the error. The yield stress of PMMA and PS take place at around 0.1 strain in this study. In the case of the density measurements, PMMA was compressed to more than 0.4 strain and no density increase was observed. This implied that no change in the amorphous structure occurred during compression. Hence, density variations in the amorphous phase in semicrystalline polymers could not be the factor that causes the observed increase in yield stress. The positive difference observed in this work might be due to implantation of other materials during compression; the negative difference might be due to tiny crack during compression generating microvoids.

9.1.6 Dependence of Birefringence on Temperature, Strain and Strain Rate

It is worth reviewing the birefringence of the samples as it reveals the chain orientations in the samples tested. By relating the chain orientations to temperature, strain rate and strain, a pattern is revealed which gives an insight about how the morphology of the sample changes with temperature, strain rate and strain.

Graph 7.3 does not show any consistency in the variation of birefringence in PMMA with temperature. However, it can be seen that samples have tendencies to show higher birefringence at 323 K (50 °C). It may be argued that heating samples at 323 K has initiated side groups movement to new positions prior to compression. On compression, polymer chains relaxed the applied stress in such a way that the new structural arrangements of the chains and the side groups obtained showing maximum birefringence. Heating samples at 343 K (70 °C) certainly will initiate the movement of side groups to new position. From Graph 7.3, it can be observed that some curves showing maximum birefringence at 343 K. However, it is also found that at 343 K minimum birefringence is observed on some curves. Hence, it is difficult to understand the effect of the temperature on the chain orientation unless the movement of the chains is observed from a molecular point of view. In addition, there were only three temperatures adopted in this study. It is suggested that a range of temperatures should be used in order to see a clear pattern of how birefringence changes with temperature.

For PMMA, it is found that a bright ring was formed on the edge of each compressed sample. The width of the ring increased when samples were compressed from 0.2 to 0.8 strain. At 293 K, a diffused dark colour and two discrete cross bands were formed in the middle of the samples. This indicates that an unoriented structure was developed in the middle of the sample during compression when compared to the uncompressed sample. For samples tested at 323 K and 343 K and at the same strain rate of 0.0006 s^{-1}, it can be seen that granular cracks developed on the edges of the samples. The crack might be due to one surface expanding faster than the other surface during deformation. The dark diffused colour in the middle of the samples disappeared at higher temperature. Higher temperature encourages the mobility of molecules in the polymer prior to and after compression. On compression at higher temperature, the polymer chains can stretch in the radial direction easier than at lower temperature due to extra energy received from heating. In addition, polymer chains on the edges of the samples can move more freely than that in the centre. This might explain why birefringence is found on the edge rather than the centre of the sample

From Graph 7.1, it can be seen that birefringence does not increase in linear proportion with strain. Samples of PMMA were cut from a rod with most of the polymer chains aligned axially prior to compression. Birefringence is defined as

$$\Delta n = n_1 - n_2$$

where n_1 is the reflective index in vertical direction and n_2 is the reflective index in horizontal direction. On compression, polymer chains move radially outwards from the centre and gradually change from an axial to a radial position. The chains on the edge orient easier than those in the centre, hence, birefringence is greater on the edges of the samples. On increasing of strain, the degree of the radial alignment of polymer chains relative to the axial direction became greater. Hence, higher birefringence is found at higher strain.

The relationship between the chain orientation and strain rate is difficult to define. Graph 7.2 shows a random relationship between birefringence and strain rate. Graph 7.2(a) shows a drop at higher strain rate for compression up to 0.2 strain. At 0 4, 0.6 and 0.8 strain, not all the curves show maximum birefringence at strain rate 0 5 s^{-1}. In addition, maximum birefringence is observed at strain rate 0 006 s^{-1} on some of the curves. Hence, it can be said that the orientations of polymer chains in PMMA is not influenced by the applied strain rate.

9.1.7 High strain rate deformation

PMMA and PS are brittle at temperatures below their ductile-brittle transition temperatures when tested at high strain rates. Visualisation of the sample deformation through the high-speed photographic system enables the mechanisms involve in changing the brittle to ductile behaviour to be studied more explicitly.

Photo 4.1 and 4.2 show that PMMA and PS fractured into pieces without any shearing of the polymer when tested at temperatures below their ductile-brittle transition temperatures. The fracture is similar to the cleavage fracture as it involved the breaking of covalent bonds among carbon atoms. The cleavage fracture found in crystalline materials or metals is like a crack that propagates through the crystallographic plane. However, the fractures shown in PMMA and PS that are fully

amorphous are like an explosion. For PS, it can be seen that little energy was involved in the fracture as the sample failed before showing any expansion. However, for PMMA, it can be seen that the sample expanded before fractured. PS has a bulky side group that might cause the failure before much movement of the polymer chains.

Photo 4.3 and 4.4 show the deformations of PMMA tested at 50 °C and 70 °C. At 50 °C which is 5 °C above its ductile-brittle transition temperature 45 °C, cracks can be seen developing from the edge of the sample. For PMMA tested at 70 °C, cracks did not developed in the sample at the beginning of deformation. Instead a ring was formed in the sample. It can be seen that the ring developed faster than the expansion of the sample in the radial direction and cause the crack on the edge of the sample The developing of the cracks when tested at 50 °C and the developing of the ring at 70 °C may be relatively similar to the developing of necking observed in tension. In both cases, plastic deformation occurred before the failures took place. The slippage of the polymer chains is generally said to involve Van der Waal's forces between polymer chains rather than covalent force between two atoms.

9.1.8 Activation Enthalpy, Entropy, Energy and Activation Volume with Strain Rate and Temperature

The motions in polymers could be rotation of side groups, segmental chain motion involving 50~100 bonds, crankshaft motion involving 4~6 bonds, branch point motions and motion of crystallite. The presence of the motions depends on the temperature the polymer is subjected to. Heating a sample to higher temperature but less than T_g will encourage more types of motion.

Let assume that at the temperature close to 0 K, all the molecules in the sample are in standstill states with H_0 and S_0, which is position A in Figure 9.1. Molecules vibrate when the temperature is raised. Energy states of a molecule can be H_1 and S_1 or H_2 and S_2 depends on the temperature it is subjected to. Molecules will only surmount the potential barrier when they receive an amount of energy equal or more than the potential energy. In this case, the relaxation of stress is said to happen in the polymer chains The activation enthalpy ΔH and entropy ΔS are properties of the molecule and also functions of temperature. For a molecule vibrating to an energy state of H_1 and

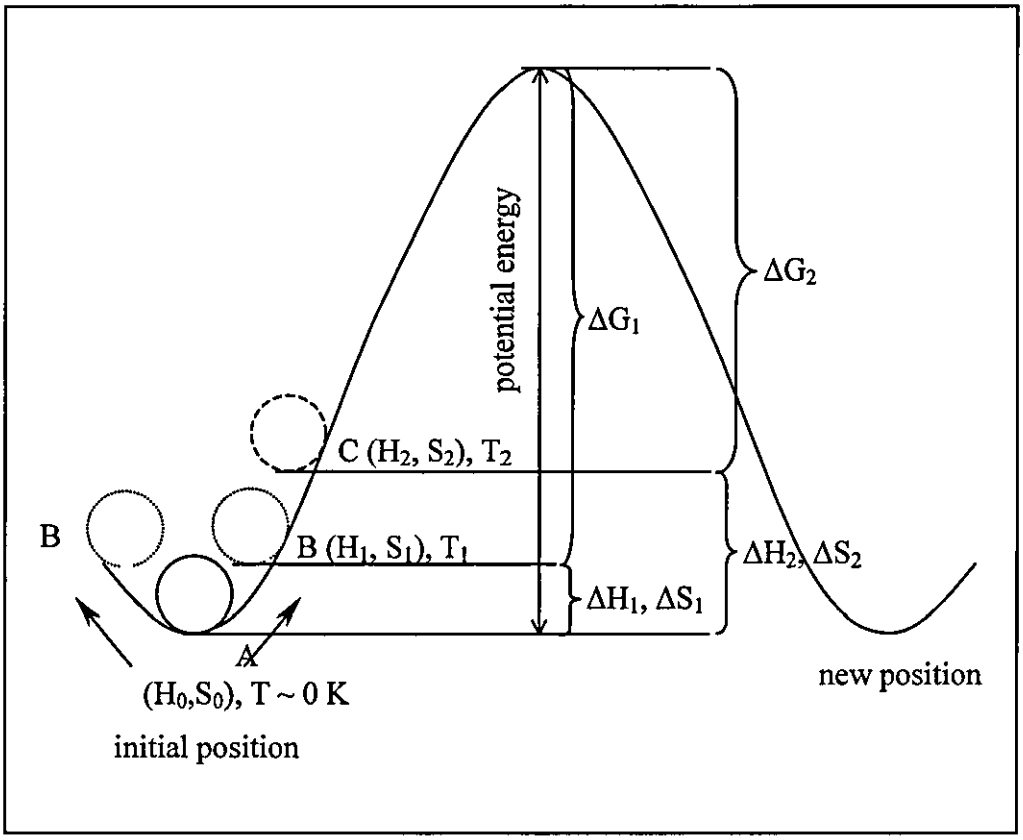

Figure 9.1: Diagram of the potential energy barrier of a molecule. When temperature close to 0 K, the molecule is in 'frozen' state. When temperature increases, the molecule starts to vibrate with amplitude depends on the temperature. $T_2 > T_1 > T_0$.

S_1 at T_1, the activation enthalpy and entropy are ΔH_1 and ΔS_1; for a molecule vibrating to an energy state of H_2 and S_2 at T_2, the activation enthalpy and entropy are ΔH_2 and ΔS_2, etc. $T_2 > T_1$, thus $\Delta H_2 > \Delta H_1$, $\Delta S_2 > \Delta S_1$ and $\Delta G_2 < \Delta G_1$ (Figure 9.1). By comparing the experimental data of ΔH, ΔS and ΔG of PMMA calculated at 293 K and 363 K (Table 8.4, 8.5, 8.6 and Graph 8.8), it can be seen that generally ΔG at 293 K is higher than ΔG at 363 K. While ΔH and ΔS of PMMA at 293 K are lower than ΔH and ΔS of PMMA at 363 K.

Graph 8.6 shows the activation volume against ln(strain rate) for PMMA. Activation volumes correspond to the empty spaces found in a sample and they vary in size. The molecules surrounding the activation volumes have different Van der Waal's forces depend on the sizes of the volumes. The application of stress initiates the flows of the molecules by providing energy to break the forces between the molecular chains/atoms in one plane, surmount the potential barrier and establish new bonds with molecular chains/atoms in the same plane. The energy is released when new bonds are formed. At quasi-static rates, it is suggested that the polymer chains have enough time to relax the stress in such a way that it starts from the space where the forces between molecules of adjacent chains are weaker, and the weaker forces are found at volumes with bigger sizes. At low strain rates, the polymer chains relax the stress in the sequence of ways different from those found at quasi-static rates. The relaxation of molecules at low strain rate might involve a group of activation volumes at one time rather than one followed by another as that happening at quasi-static rate. Thus, this might cause the mean volume to decrease as strain rate increases.

PMMA and PS fracture before any yielding of polymer chains occurs when tested at high strain rates and at temperatures below their ductile-brittle transition temperature This indicates that the polymer chains do not have enough time to relax the stress in the same way as that happening at quasi-static rates. However, by heating the samples at temperatures higher than their ductile-brittle transition temperatures, this put the molecules in 'ready to move' states rather than in 'frozen' state when the temperature is low. This indicates that when a sample is tested at high strain rates at temperatures above its ductile-brittle transition temperature, it shows ductile behaviour. Adiabatic heating occurring in the sample when tested at high strain rates can not be ignored This is since Eyring's theory is only applicable to the isothermal process. The

calculation of temperature rise is essential to put the corrected data on the isothermal data curve. It is suggested that the change of the structure due to adiabatic heating might affect the stress-strain curves obtained and thus reduces the accuracy of calculation. This makes inclusion of high strain rate data in the Eyring analysis difficult.

Graph 8.7 reveals that $\Delta v_{30\%} > \Delta v_{20\%} > \Delta v_y$. In addition, it can be seen that the sizes of the activation volumes are influenced by temperature. The activation volumes get larger with increasing temperature.

9.2 Conclusion

The objective of this research is to investigate possible causes of a change in yield and flow stress for PMMA and PS as a function of strain rate and temperature Generally, some polymers show a rapid increase in yield stress at strain rate > 10^2 s^{-1}, however, a decrease in yield stress has been reported sometimes.

Previous work on semicrystalline polymers discovered that the rapid increase in yield stress was not caused by the increase in crystallinity. This was because the crystallinity was only observed to increase after a high strain > 0.7 has been achieved. However, the contribution of the amorphous phase in semicrystalline polymer to the rapid increase in yield stress has not been fully studied. Thus, PMMA and PS, which are fully amorphous polymers, were chosen to complete the investigation of a rapid increase in yield stress at strain rates above 10^2 s^{-1}.

Stress-strain data of PMMA and PS at a range of temperatures and strain rates were obtained by compressing the samples in mechanical tests described in Chapter 3 and 4. The density, chain orientation and polymer transitions of the samples were studied to investigate their relationship with an increase in yield and flow stress. In addition, an application of Eyring's theory on the stress-strain data was made to explain the flow of the polymer from the thermodynamic point of view.

PS was only compressed at quasi-static and low strain rates in this study. The study of PS at high strain rates could not be made as it fractured before the yield point at temperatures below its ductile-brittle transition temperature 90 °C. For temperatures more than 90 °C, the PS samples deformed prior to compression. However, since the ductile-brittle transition temperature of PMMA is at 45 °C, the study of PMMA at high strain rates at temperatures above 45 °C was possible in this study.

From the DMTA data, the shift of the β transition from –25~25 °C at 0.1 Hz to the shoulder of the glass transition at 100 Hz might explain the brittle behaviour of PS at high strain rates. PMMA showed ductile behaviour at temperatures above 45 °C. The β transition of PMMA was around 35 °C to 70 °C at 100 Hz Thus, the onset of the side group movement seemed to have a great effect to the ductile-brittle transition.

Similarly to the case of semicrystalline polymers, the yield stress of PMMA and PS increased when the strain rate increased and decreased when the temperature increased. The densities of PMMA samples compressed to different strains under high strain rate deformation did not show any obvious increase. On the other hand, the assumption of the polymer chains of PMMA about compact arrangement after high rate deformation did not take place in the samples although it shows an increase in yield stress after high strain rate.

The chain orientations of PMMA and PS after being subjected to different limited compressive strains at different strain rates and temperatures were studied by means of optical birefringence. It was observed that the application of the stress changed the orientation of the polymer chains of PMMA and PS to a certain degree. The birefringence of the samples tested at the same strain rate increased with strain. It is known that the yield stress decreases when temperature increases. However, samples show greater tendency of maximum birefringence at 50 °C rather than at 20 °C or 70 °C. However, the pattern of birefringence at different strain rates does not give any clear link to the increase in the yield stress at higher strain rate. As maximum birefringence is not always observed for PMMA tested at higher strain rate. It can be said that the orientations of the polymer chains do not contribute any effect to the increase in yield stress at high strain rate.

The application of Eyring's theory on the PMMA and PS stress-strain curves managed to reveal some characteristics of the flow of the polymer chains in PMMA and PS. It can be seen that the flow in PMMA is heterogeneous as plots of σ/T versus $\ln(\dot{\varepsilon})$ showed a set of curves; in PS is homogeneous as plots of σ/T versus $\ln(\dot{\varepsilon})$ showed a set of lines. The activation volume increases when the strain increases. From the plots of activation energy and enthalpy versus $\ln(\dot{\varepsilon})$ under the same axes, the changes of the activation energy with temperatures and strains were considered constant For high strain rate tests, the calculated temperature rises for the samples tested at 50 °C were in agreement with the estimation value of other researchers, although the experiment data of σ/T fell on an extrapolated isothermal temperature curve that was different from the corrected temperatures (testing temperature + temperature rise). This may be due to some microstructural change caused by adiabatic heating during the tests.

9.3 Suggestion for Future Work

(i) It is recommended to investigate the deformation pattern of a wide range of polymers until fracture and relate it with the stress-strain curve obtain using the high-speed photographic system. Orientation of polymer chains during deformation probably can be viewed on the film if a polariser and analyser are put in the transmitted light path and coloured film is used. This will give more explicit explanation about the relationship between the stress-strain curve and the orientation of polymer chains as well.

(ii) Investigation into the ductile behaviour of polystyrene in the low rate region should be carried out in tensile tests using the Hounsfield H50KM Machine and compared the results with the compressive tests.

(iii) A suitable machine that can cover the range of strain rate from 10 to 500 s^{-1} should be adopted to study the validity of Ree-Eyring theory with the viscoelastic behaviours of polymers at higher rate.

(iv) DSC should be performed on a range of polymers to study their specific heats after the glass transition region and relate them with the structure of each polymer. The purpose is to see whether the specific heat is affected by the state which the polymers is in or the structure of the polymers

(v) The effect of temperature on the sample birefringence is an interesting area to study. Samples should be tested at a wide range of temperatures but subjected to the same strain and same strain rate to see a clearer trend of birefringence dependent on the temperature.

(vi) Ductile polymers should be adopted to visualise their deformations under the high-speed photographic system. The purpose is to examine whether the ductile polymers displays the same deformation mode as that displayed by the brittle polymers tested above their ductile-brittle transition temperature.